**University of Novi Sad
Serbia**

Acta Periodica Technologica

ACTA PERIODICA
TECHNOLOGICA

CONTENT

CITRULLUS COLOCYNTHIS FRUIT RESIN AND *CYPERUS ROTUNDUS* TUBER RESIN: ASSESSING THEIR ANALGESIC EFFECTS WITH HOT PLATE AND WRITHING TESTS

Anis BEN ALI[1,2]*, Atef CHOUIKH[2], Larbi HADDAD[3]

[1] Department of Cellular and Molecular Biology, Faculty of Life and Natural Science, El Oued University, PO Box 789, 39000 Algeria.
[2] Laboratory of Biology, Environment and Health, El Oued University, PO Box 789, 39000 Algeria.
[3] Faculty of Exact Sciences, El Oued University, PO Box 789, 39000 Algeria.

The hot plate test and writing test were both employed to investigate the analgesic effects of Citrullus colocynthis fruit resin and Cyperus rotundus tuber resin at varying concentrations and time intervals. The hot-plate test results revealed that Citrullus colocynthis fruit resin demonstrated significant dose-dependent and time-dependent analgesic effects. In contrast, Cyperus rotundus Tuber resin did not exhibit substantial analgesic effects in the hot-plate test.

In the writing test, Citrullus colocynthis fruit resin exhibited clear dose-dependent analgesic effects at higher concentrations. Cyperus rotundus Tuber resin demonstrated significant analgesic effects in reducing writing responses, although its efficacy was not as potent as the positive control indomethacin. These results offer insights into the potential use of these natural resins for pain management while also highlighting the importance of understanding the underlying mechanisms of their analgesic effects for further clinical applications

Keywords: analgesia, *Citrullus colocynthis*, *Cyperus rotundus*, hot plate test, pain management, writing test.

INTRODUCTION

Prioritizing pain management and reducing discomfort has been of great importance in both clinical and research settings. As a result, there have been many investigations into different natural sources that may possess analgesic properties (1). Plant-derived resins have attracted great interest due to their historical use in traditional medicine systems (2). The current research focuses on evaluating the analgesic properties of two different resins, namely the resin of *Citrullus colocynthis* fruit and the resin of *Cyperus rotundus* Tuber. This study seeks to examine the pain-modulating properties of plant-derived compounds by applying established experimental paradigms, namely the hot plate test and the torsion test. By implementing comprehensive evaluation methods, this research study makes a valuable contribution to the growing body of knowledge regarding the pharmacological properties of these resins. Thus, it provides valuable insights into the potential applications of these resins in the context of pain management strategies.

The historical and cultural use of plant resins as medicinal agents has been well documented, and these substances are often held in high regard for their purported therapeutic properties (3). The *Citrullus colocynthis* plant, which belongs to the Cucurbitaceae family, has been used historically in various traditional medicine practices due to its wide range of

pharmacological properties (4). Likewise, *Cyperus rotundus*, known for its powerful phyto-chemical composition, has received attention for its health-promoting properties (5). Both plant sources have shown analgesic effects, sparking interest in their potential application for the management of pain conditions (6,7).

The hot plate test and the writhing test are commonly employed methodologies for evaluating pain sensitivity and analgesic efficacy in preclinical research (8). The hot plate test is utilized to assess the central response to thermal stimuli, which indicates the capacity of substances to regulate the perception of pain (9). In contrast, the writhing test is utilized to evaluate abdominal discomfort by observing writhing responses, which serve as indicators of nociception (10).

This study aims to evaluate the analgesic efficacy of *Citrullus colocynthis* fruit resin and *Cyperus rotundus* Tuber resin, as well as to compare their efficacy with paracetamol and indomethacin, which are commonly used as standard analgesics. The study uses well-defined models for evaluation purposes. The investigations findings have the potential to reveal the magnitude of pain relief provided by these compounds derived from plants and can provide guidance for future research on their mechanisms of action. This study makes a valuable contribution to the ongoing investigation of natural resources in the context of therapeutic applications, and has potential implications for the advancement of innovative analgesic interventions.

EXPERIMENTAL

PLANT ATERIAL

Citrullus colocynthis fruits and *Cyperus rotundus* tubers were collected from the Oued Souf region, situated in the southeastern part of the Algerian Sahara.

EXTRACTION OF RESIN

The extraction process followed the guidelines outlined in the patent (11). First, a sample containing 100 grams of dried plant powder was prepared. Next, the powder was immersed in a 0.4 L solution of water, and maintained at ambient temperature, for 24 h. The water used in the infusion process showed a trace concentration of gallic acid and was subsequently adjusted to reach a pH level of 10. After completing this procedure, the resulting infusion was filtered, and the remaining plant residue was immersed in 0.4 L of ethanol. For a secondary soaking process. The ethanol solution, which contained a small amount of gallic acid and was adjusted to a pH of 10, was allowed to react with the plant remains for 24 h at ambient temperature. After the filtration process, the resulting material underwent a drying process, which resulted in the manufacture of the resin.

QUALITATIVE PHYTOCHEMICAL SCREENING

A thorough analysis was conducted on each resin in order to identify specific phytochemical groups, as described in previous studies (12-14). The evaluation encompassed the application of the subsequent reagents and chemicals: The identification of alkaloids was conducted utilizing Dragendorff's reagent, followed by confirmation using Bouchardat's reagent (I_2/MgI_2) and Meyer's reagent ($KI/MgCl_2$). The presence of coumarins was identi-

fied using a diluted sodium hydroxide and ultraviolet (U.V.) test. The quantification of flavonoids was achieved through a chemical reaction involving metallic magnesium and hydrochloric acid (HCl).

The identification of anthraquinones was conducted utilizing Borntrager's reagent. The screening of cardiac glycosides was first conducted using Kedde's reagent, followed by confirmation using Baljet's reagent. Iridoids were detected by employing a solution of hydrochloric acid that had been diluted. The suds-generating capacity of saponins was assessed. The detection of steroids was accomplished using the Liebermann reaction, which entails the utilization of acetic anhydride and concentrated sulfuric acid. Tannins were subjected to analysis using ferric chloride as a reagent, and their existence was subsequently verified through the application of concentrated hydrochloric acid, employing the Bath-Smith reaction. The identification of Gallic tannins was carried out using the Stiasny reagent.

ANIMALS

The study was carried out using male Wistar rats obtained from the Pasteur Institute of Algeria, with an average weight of 180 ± 20 g. The rats were housed in a controlled environment with a temperature of 22 ± 1 °C, a light-dark cycle of 12 hours, and a relative humidity of approximately 40%. The rats were administered a nutritionally balanced diet comprising proteins, lipids, carbohydrates, vitamins, and trace elements. Throughout the entire experimental period spanning 15 days, the animals were treated in accordance with established experimental procedures and protocols outlined in the European Communities Council Directive 2010/63/EU of 22 September 2010.

ACUTE TOXICITY

Thirty mice were subjected to a twenty-four-hour fasting period. After that, they were divided into eight groups, each group consisting of three mice. These groups were further classified into four groups based on the type of plant resin given. Each group received oral doses of *Citrullus colocynthis* fruit resin or *Cyperus rotundus* tuber resin, which were suspended in a 1% solution of carboxymethyl cellulose. The doses administered in this study were 300, 500 and 1000 mg/kg, with the aim of studying possible changes in behavior as well as neurological functions and independence. Furthermore, mortality was observed in mice 24 h and 72 h after drug administration, as determined by Whalum (15).

HOT-PLATE TEST

The hot-plate test was conducted following the procedure outlined by Ferreira et al, (16). Briefly, animals (n = 3) were intraperitoneally (i.p.) injected on the experimental day with 0.2 ml of normal saline (control group) or paracetamol (10 mg/kg) as a positive control, and the experimental groups were administered test samples (40 and 80 mg/kg) of the resin of *Citrullus colocynthis* fruits or *Cyperus rotundus tubers*. After 30 minutes, the animals were placed onto a heated plate maintained at 55 °C, and the time interval (in seconds) between placement and their hind paw licking or jumping response was recorded as the latency period. The maximum allowable time was set at 30 seconds. The measurement of reaction time was conducted at three time points: initially, as well as at the 60-minute and 90-minute intervals subsequent to the administration of the resin. (Figure1).
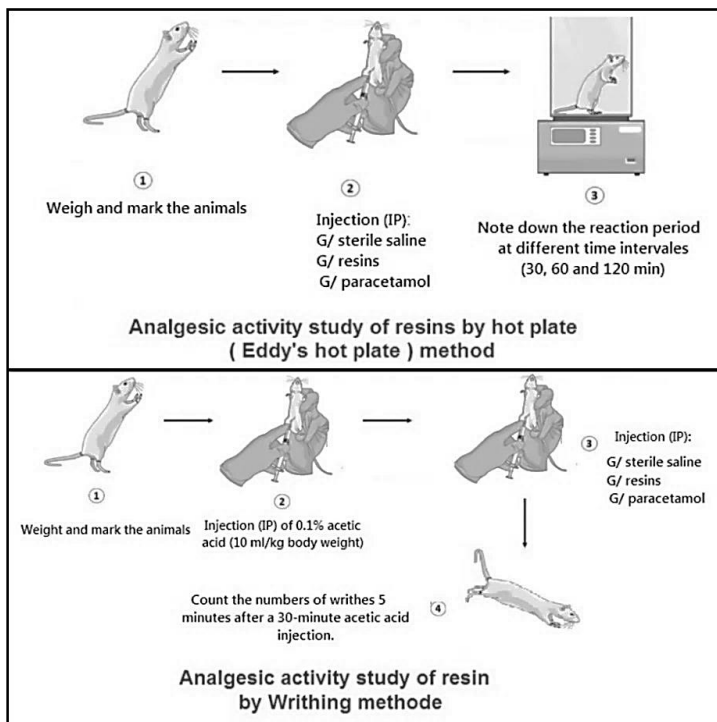
Figure 1. Methods of analgesic activity**.**

WRITHING TEST

The acetic acid writhing test was employed to assess the analgesic effects of the resin from either *Citrullus colocynthis* fruit or *Cyperus rotundus* tuber. Four sets of rat groups, each comprising three rats (n = 3 per group), were subjected to acetic acid injections (10 mL/kg body weight). The degree of nociception was quantified by tallying the total instances of writhing observed over a 30-minute duration. Prior to acetic acid injection, the animals were administered a dose of plant resin (at 40 and 80 mg/kg body weight) or sterile saline (control group, 0.9%, w/v) with a 30-minute time lapse.

Indomethacin was employed as a reference substance for the purpose of establishing a benchmark (positive control), with a dosage of 10 mg per kilogram of body weight. The count of writhing episodes was recorded 5 minutes after acetic acid injection and continued for 30 minutes, following the methodology outlined by Koster (17) (Figure 1).

The extent of writhing inhibition was computed using the subsequent formula (18):

$$\text{Inhibition of writhing (\%)} = \frac{\text{Mean number of control- Mean number of test}}{\text{Mean number of control}} \times 100$$

DATA ANALYSIS

The results obtained are expressed as the mean ± SEM. Data analysis was performed by using Student's t test using SPSS Statistics (version 23.0) at a significance level of $p < 0.05$.

RESULTS AND DISCUSSION

EXTRACTION YIELDS

The results presented in (Table 1). clearly demonstrate a marked disparity in the extraction yields between Cyperus rotundus tuber resin and *Citrullus colocynthis* fruit resin. Specifically, *Cyperus rotundus* tuber resin exhibits a notably superior extraction yield compared to that of Citrullus colocynthis fruit resin.

The variation in extraction yields observed when applying the same extraction method to *Cyperus rotundus* Tuber and *Citrullus colocynthis* Fruit can be ascribed to a multifaceted interplay of factors encompassing plant material characteristics, phytochemical composition, cellular structure, extraction parameters, sample preparation techniques, genetic diversity, and environmental influences (19). This accounts for the superiority of *Cyperus rotundus* Tuber in comparison to *Citrullus colocynthis* fruit.

The results presented in (Table 1). The results of the experiment clearly illustrate a significant difference in the extraction yields between the resin obtained from the tubers of *Cyperus rotundus* and the resin obtained from the fruits of *Citrullus colocynthis*. The extraction yield of *Cyperus rotundus* tuber resin is significantly higher than that of *Citrullus colocynthis* fruit resin.The variation in extraction yields observed when applying the same extraction method to *Cyperus rotundus* Tuber and *Citrullus colocynthis* Fruit can be ascribed to a multifaceted interplay of factors encompassing plant material characteristics, phytochemical composition, cellular structure, extraction parameters, sample preparation techniques, genetic diversity, and environmental influences(19). This accounts for the superiority of *Cyperus rotundus* Tuber in comparison to *Citrullus colocynthis* fruit.

QUALITATIVE PHYTOCHEMICAL SCREENING

During the process of phytochemical screening, it became evident that *Cyperus rotundus* tuber resin surpassed *Citrullus colocynthis* fruit resin in terms of the richness and diversity of secondary metabolites (Table 1).

Table 1. Extraction yields and phytochemical screening of secondary metabolites from *Citrullus colocynthis* fruit resin and *Cyperus rotundus* tuber resin.

Resin	Extraction yields	Phytochemical screening							
		Alkaloids	*Coumarins*	*Flavonoids*	*Anthraq.*	*Cardiac glyc*	*Saponids*	*Steroids*	*Gallic tanins*
C. colocynthis	4.36%	+	-	+	-	-	-	+	-
C. rotundus	10.57%	+	-	+	-	+	+	+	+

Antraq. - anthraquinones; cardiac glyc. - cardiac glycosides; + - presence; − - absence

Furthermore, it is noteworthy that the outcomes of the phytochemical screening for both the aqueous and alcoholic extracts (20, 21) exhibit a remarkable consistency with the findings for the respective resins, The uniformity observed also applies to the occurrence of identical secondary metabolite compounds, suggesting that the nature and makeup of these compounds are comparable in both the extracts and resins. This suggests a strong correlation in the phytochemical profiles between the different forms of the plant material, affirming the reliability and reproducibility of the analytical results across various extraction methods.

ACUTE TOXICITY

In the evaluation of acute toxicity, it was observed that both resins exhibited safety across all concentrations tested, including the maximum dosage of 1000 mg/kg, leading to no deaths among the subjects under investigation (Table 2). These data also made it possible to select therapeutic doses from 40 mg/kg to 80 mg/kg.

Table 2. Result of toxicological testing of Wistar rats.

Resin	Dose (mg/kg)	Activity disorder	Reaction disorder	Undernutrition	Coma	Dead
C. colocynthis	300	-	-	-	-	-
	500	-	-	-	-	-
	1000	-	-	-	-	-
C. rotundus	300	-	-	-	-	-
	500	-	-	-	-	-
	1000	-	-	-	-	-

(-): Nothing to report.

HOT-PLATE TEST

The hot-plate test outcomes offer crucial insights into the analgesic properties of *Citrullus colocynthis* fruit resin and *Cyperus rotundus* Tuber resin, highlighting their distinct effects compared to a positive control, paracetamol.

The statistical analysis using a T test yielded statistically significant results, which led to extensive scholarly discourse.

Citullus colocynthis Fruit Resin Results

Animals administered injections of *Citrullus colocynthis* fruit resin at different concentrations (80 mg/kg and 40 mg/kg) and time intervals displayed notable outcomes (Figure 2). Significantly, the group administered with the higher concentration (80 mg/kg) demonstrated superior outcomes in comparison to the group administered with the lower concentration (40 mg/kg) at 30 minutes, 60 minutes, and 90 minutes. This observation indicates that there is a relationship between the dosage and duration of administration, where higher concentrations and longer intervals result in more noticeable analgesic effects. Significantly, both concentrations of *Citrullus colocynthis* fruit resin exhibited analgesic effects that were superior to the positive control, paracetamol (10 mg/kg). The statistical significance of these differences ($p < 0.05$) underscores their credibility.

Cyperus rotundus Tuber Resin Results

In contrast, the administration of *Cyperus rotundus* Tuber resin failed to elicit noticeable analgesic effects, regardless of the concentration and time intervals (Figure 3). The lack of statistically significant differences, as evidenced by p-values greater than 0.05, between the experimental group and the control group suggests that there is no observable effect on pain response.

The findings of this study underscore the significant analgesic properties of *Citrullus colocynthis* fruit resin, particularly when administered at higher concentrations and longer intervals. This is evident from its superior efficacy compared to the lower concentration and

its efficacy even exceeding that of the positive control. Conversely, *Cyperus rotundus* Tuber resin did not demonstrate significant changes in pain response, suggesting its limited or nonexistent role in pain modulation within the parameters of this experiment.

The T test outcomes underscore the substantial analgesic potential of *Citrullus colocynthis* fruit resin, especially at higher concentrations and longer intervals, in contrast to the limited effects of *Cyperus rotundus* Tuber resin.

	control	paracetamol (10 mg/kg)	C. colocynthis Resin (80mg/kg)	C. colocynthis Resin (40mg/kg)
■ 30 Min	8,66	13,66	16	13,66
■ 60 Min	9	14,33	23,66	19
■ 90 Min	10	17,66	27,33	19
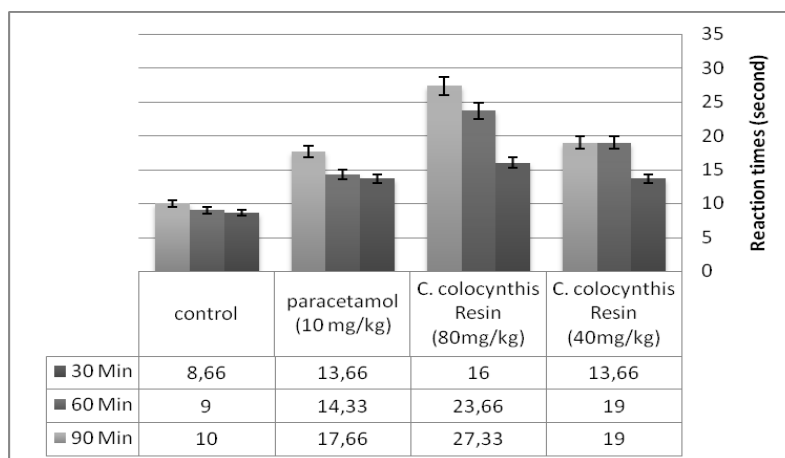
Figure 2. Impact of the resin derivatives sourced from *Citrullus colocynthis* fruit as well as paracetamol, on thermal pain sensitivity induced by a hot plate in rat subjects.

	control	paracetamol (10 mg/kg)	C. Rotundus Resin (80mg/kg)	C. rotundus Resin (40mg/kg)
■ 30 Min	8,66	13,66	12	8,66
■ 60 Min	9	14,33	13	8
■ 90 Min	10	17,66	13	12,33
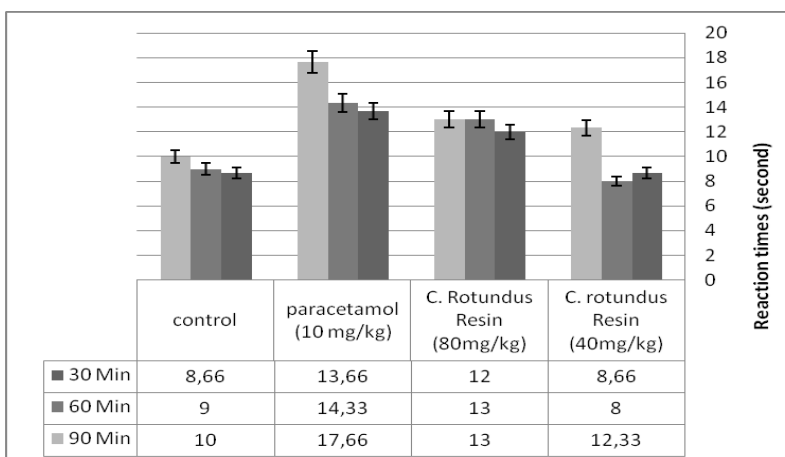
Figure 3. Impact of the resin derivatives sourced from *Cyperus rotundus* Tuber as well as paracetamol on thermal pain sensitivity induced by a hot plate in rat subjects.

Pain and inflammation are pivotal components in the pathology of numerous clinical conditions, including arthritis, cancer, and vascular diseases (22).

The hot-plate test serves as a widely accepted model for neurologic pain assessment. Central analgesic agents can extend reaction times in this test, acting primarily at the spinal cord level (23). In our study, we observed distinct effects of *Citrullus colocynthis* fruit resin compared to a positive control, paracetamol.

At a concentration of 80 mg/kg, the highest recorded reaction time was observed at 90 minutes, with *Citrullus colocynthis* fruit resin exhibiting a reaction time of 27.33 seconds and *Cyperus rotundus* tuber resin displaying a reaction time of 13 seconds. Comparison of both with *Cyperus rotundus* was made due to limited previous studies on *Citrullus colocynthis*.

According to the research conducted by Rajamanickam and Rajamanickam (24), the study on *Cyperus rotundus* revealed that the administration of two distinct doses (250 and 500 mg/kg body weight) led to the observation of peak reaction times at the 90-minute time interval. The methanol extract demonstrated reaction times of 6.42 ± 1.11 seconds and 8.60 ± 1.00 seconds for the lower and higher doses, respectively measurement of maximum reaction times at the 90-minute time interval. Specifically, the methanol extract exhibited reaction times of 6.42 ± 1.11 seconds and 8.60 ± 1.00 seconds for the lower and higher doses, respectively. Conversely, the chloroform extract demonstrated reaction times of 8.89 ± 1.12 seconds and 10.67 ± 1.10 seconds for the same respective doses. Additionally, the ethyl acetate extract, when administered at equivalent dosage levels, produced maximum reaction times of 10.34 ± 1.14 seconds and 12.72 ± 1.15 seconds. It is worth noting that the control group displayed a reaction time of 4.62 ± 0.6 seconds at the 90-minute time point.

These observations emphasize the substantial efficacy *of Citrullus colocynthis* fruit resin when compared to the outcomes observed with various extracts of *Cyperus rotundus*, which closely resemble the results obtained for *Cyperus rotundus* tuber resin.

WRITHING TEST

The results of the writhing test offer significant insights into the analgesic effects of *Citrullus colocynthis* fruit resin and *Cyperus rotundus* Tuber resin at varying concentrations.

The subsequent T test analysis generated compelling findings, prompting a comprehensive scientific discussion.

Citrullus colocynthis Fruit Resin Results

Animals subjected to injections of *Citrullus colocynthis* fruit resin at different concentrations (80 mg/kg and 40 mg/kg) displayed notable outcomes (Table 3). Notably, the cohort administered with the higher concentration (80 mg/kg) demonstrated superior outcomes in terms of mitigating writhing responses in comparison to the cohort administered with the lower concentration (40 mg/kg).

The observed dose-dependent effect highlights the significance of concentration in determining the effectiveness of analgesics. Moreover, both concentrations of *Citrullus colocynthis* fruit resin outperformed the positive control, indomethacin (10 mg/kg), in terms of reducing writhing responses.

The statistical significance of these differences ($p < 0.05$) solidifies their credibility.

Cyperus rotundus Tuber Resin Results

Interestingly, the administration of *Cyperus rotundus* Tuber resin elicited a notable analgesic effect, which was observed at both concentrations (Table 4). Importantly, the observed effect was significant when compared to the control group ($p < 0.05$), underscoring the resin's impact on reducing writhing responses.

However, when contrasted with the positive control indomethacin (10 mg/kg), the resin did not exhibit statistically significant differences ($p > 0.05$), indicating that while it dis-

played an analgesic effect, the observed potency of the substance was comparatively lower than that of the positive control.

These results collectively highlight the robust analgesic potential of *Citrullus colocynthis* fruit resin, particularly at a higher concentration, and the notable effects of *Cyperus rotundus* Tuber resin in reducing writhing responses. The differences between the resin concentrations and the comparison with indomethacin underscore the varying degrees of efficacy among the substances tested.

The T test outcomes underscore the substantial analgesic potential of *Citrullus colocynthis* fruit resin, especially at higher concentrations, and indicate a significant analgesic effect of *Cyperus rotundus* Tuber resin.

While these findings provide significant insights, it is important to acknowledge certain limitations. Factors such as individual variations, potential interactions with physiological systems, and the specific mechanisms of action require further investigation.

Additionally, the biochemical pathways through which these resins induce analgesia warrant in-depth exploration.

Table 3. Effect of the resin of *Citrullus colocynthis* fruit and indomethacin on abdominal writhings induced by acetic acid in rats.

Treatment	Dose	Number of abdominal cramps	Inhibition (%)
Control (acetic acid 0.1%)	10 mL/kg	16.33 ± 1.52**	/
Normal control (distilled water)	5 mL/kg	16.33 ± 1.52**	/
Indomethacin	10 mg/kg	5 ± 0.00	69.39
C. colocynthis **Resin**	80 mg/kg	$3 + 1.73$**	81.63
C. colocynthis **Resin**	40 mg/kg	4 ± 1.00*	75.51

Values represented as the mean ± SEM (n = 3); *: $p \leq 0.05$; **: $p \leq 0.01$ compared to indomethacin**.**

Table 4. Effect of the resin of *Cyperus rotundus* Tuber and indomethacin on abdominal writhings induced by acetic acid in rats.

Treatment	Dose	Number of abdominal cramps	Inhibition (%)
Control (acetic acid 0.1%)	10 mL/kg	16.33 ± 1.52**	/
Normal control (distilled water)	5 mL/kg	16.33 ± 1.52**	/
Indomethacin	10 mg/kg	5 ± 0.00	69.39
C. rotundus **Resin**	80 mg/kg	$6.33 + 1.15$	61.22
C. rotundus **Resin**	40 mg/kg	7.33 ± 1.5	55.1

Values represented as the mean ± SEM (n = 3); *: $p \leq 0.05$; **: $p \leq 0.01$ compared to indomethacin.

The writhing test, induced by acetic acid, is employed to evaluate peripherally acting analgesics. Pain is generated indirectly through endogenous mediators such as prostaglandin, which stimulates peripheral nociceptive neurons (25). The increase in prostaglandin levels within the peritoneal cavity enhances inflammatory pain by increasing capillary permeability (26). The identification of alkaloids in the botanical extract indicates a potential for central stimulatory effects (27), whereas the presence of flavonoids in all seed extracts is associated with their recognized analgesic and anti-inflammatory properties (28).

The resin derived from the fruit of Citrullus colocynthis demonstrated a significant inhibitory effect on writhing at a concentration of 80 mg/kg, resulting in an observed percen-

tage inhibition of 81.63. Inhibition of writhing in aqueous extract of fruits was estimated at 54.93 percent at a concentration of 8 mg/kg according to Marzouk et al, (29). The analgesic effects of immature fruits were found to be dependent on the dosage, with the most potent activity observed in polar extracts of immature seeds and fruits (specifically, acetone and methanol extracts). The analgesic effect was found to be positively correlated with the polarity of the extract (30). The most potent analgesic effects were observed when using polar extracts derived from immature seeds and fruits, specifically those obtained through the utilization of acetone and methanol. These extracts, whether sourced from seeds or fruits, exhibited a closely related property. In both cases, the analgesic effectiveness displayed an upward trend with increasing extract polarity. The efficacy of seed extracts varied between 91.56% (chloroform extract) and 95.68% (methanol extract). Similarly, the efficacy of fruit extracts ranged from 82.96% (petroleum ether extract) to 95.74% (methanol extract), except for the petroleum ether seed extract, which demonstrated a noteworthy efficacy of 93.42% (30).

Cyperus rotundus tuber resin showed a writhing inhibition percentage of 61.22% at a concentration of 80 mg/kg. Methanol extract administration at doses of 250 and 500 mg/kg resulted in percentage inhibitions of 45.73% and 55.38%, respectively. Chloroform and ethyl acetate extracts displayed higher writhing inhibition percentages, with values such as 58.64% and 66.17% and 64.5%, respectively (24). This proves the superiority of the resin over other extracts.

CONCLUSION

The present study emphasizes the potential of *Citrullus colocynthis* fruit resin and *Cyperus rotundus* tuber resin as natural analgesic agents. The hot plate test and writhing test provide valuable insights into the distinct impacts they have on thermal and visceral pain responses. Additional investigation is necessary to elucidate the exact mechanisms that contribute to their analgesic properties, establishing a basis for potential therapeutic utilization in strategies for pain management.

Acknowledgements

REFERENCES

1. Sevcikova, Z.; Pour, M.; Novak, D.; Ulrichova, J.; Vacek, J. Chemical properties and biological activities of cyclopentenediones: a review. *Mini reviews in medicinal chemistry*. **2014**, *14*(4), 322-331.
2. Kokoska, L.; Kloucek, P.; Leuner, O.; Novy, P. Plant-derived products as antibacterial and antifungal agents in human health care. Current medicinal chemistry **2019**, *26*(29), 5501-5541. https://doi.org/10.2174/0929867325666180831144344
3. Sen, S.; Chakraborty, R. Revival, modernization and integration of Indian traditional herbal medicine in clinical practice: Importance, challenges and future. *J of traditional and complementary medicine*. **2017**, *7*(2), 234-244. https://doi.org/10.1016/j.jtcme.2016.05.006

4. Hussain, A.I.; Rathore, H.A.; Sattar, M.Z.; Chatha, S.A.; Sarker, S.D.; Gilani, A.H. *Citrullus colocynthis* (L.) Schrad (bitter apple fruit): A review of its phytochemistry, pharmacology, traditional uses and nutritional potential. *J of ethnopharmacology*. **2014**, *155*(1), 54-66. https://doi.org/10.1016/j.jep.2014.06.011

5. Meena, A.; Yadav, A; Niranjan, U.; Singh, B.; Nagariya, A.; Verma, M. Review on *Cyperus rotundus*-A potential herb. *International Journal of Pharmaceutical and Clinical Research.* **2010**, *2*(1), 20-22.

6. Gurudeeban, S.; Satyavani, K.; Ramanathan, T. Bitter apple (*Citrullus colocynthis*): An overview of chemical composition and biomedical potentials. *Asian Journal of plant sciences*. **2010**, *9*(7), 394.

7. Mohammed, G.F. The effectiveness of *Cyperus rotundus* essential oil in reducing the side effects of laser hair removal. *J of Cosmetic Dermatology*. **2022**, *21*(4), 1501-1505. https://doi.org/10.1111/jocd.14301

8. Berge, O.G. Predictive validity of behavioural animal models for chronic pain. *British journal of pharmacology*. **2011**, *164*(4), 1195-1206. https://doi.org/10.1111/j.1476-5381.2011.01300.x

9. Menéndez, L.; Lastra, A.; Hidalgo, A; Baamonde, A. Unilateral hot plate test: a simple and sensitive method for detecting central and peripheral hyperalgesia in mice. *J of neuroscience methods*. **2002**, *113*(1), 91-97. https://doi.org/10.1016/S0165-0270(01)00483-6

10. Muley, M.M.; Krustev, E.; McDougall, J.J. Preclinical assessment of inflammatory pain. *CNS neuroscience & therapeutics*. **2016**, *22*(2), 88-101. https://doi.org/10.1111/cns.12486

11. Querci, C.; Del Seppia, A.; Oliosi, M.; Prando T. U.S. Patent No. 10,654,945. *Washington, DC: U.S. Patent and Trademark Office.* **2020**.

12. Sakar, M.K.; Tanker, M. Fitokimyasal analizler. *Ankara Üniversitesi Eczacılık Fakültesi Yayınları,* **1991**, 67.

13. Trim, A.; Hill, R. The preparation and properties of aucubin, asperuloside and some related glycosides. *Biochemical journal*. **1952**, *50*(3), 310. https://doi.org/10.1042/bj0500310

14. Tijjani, A.; Sallau, M.; Sunus, I. Synergistic activity of methanolic extract of *Adenium obesum* (Apocynaceae) stem-bark and oxytetracycline against some clinical bacterial isolates. *Bayero Journal of Pure and Applied Sciences*. **2011**, *4*(1), 79-82. https://doi.org/10.4314/bajopas.v4i1.18

15. Walum, E. Acute oral toxicity. *Environmental health perspectives*. **1998**, *106*(2), 497-503. https://doi.org/10.1289/ehp.98106497

16. Ferreira, J.; Campos M.M.; Araújo, R.; Bader, M.; Pesquero, J.B.; Calixto, J.B. The use of kinin B1 and B2 receptor knockout mice and selective antagonists to characterize the nociceptive responses caused by kinins at the spinal level. *Neuropharmacology*. **2002**, *43*(7), 1188-1197. https://doi.org/10.1016/S0028-3908(02)00311-8

17. Koster, R. Proceedings of the Acetic acid for analgesics screening. *In Fed proc.* **1959**, *18*, 412-417.

18. Chouikh, A. Phytochemical profile, antioxidant, analgesic and hypolipidaemic effects of *ephedra alata* decne. female cones extract. *Farmacia.* **2020**, *68*(6), 1011-1020. https://doi.org/10.31925/farmacia.2020.6.7

19. Oumar, Y.S.; Nathalie, G.K.; Karamoko, O.; Alexis, B.G.; Adama, C. In vitro antioxidant activity of extracts of the root *Cochlospermum planchonii* Hook. f. ex. Planch (Cochlospermaceae). *J of Pharmacognosy and Phytochemistry*. **2014**, *3*(4), 164-170.

20. Marzouk, B.; Marzouk, Z.; Décor, R.; Edziri, H.; Haloui, E.; Fenina, N.; Aouni, M. Antibacterial and anticandidal screening of Tunisian *Citrullus colocynthis* Schrad. from Medenine. *J of ethnopharmacology*. **2009**, *125*(2), 344-349. https://doi.org/10.1016/j.jep.2009.04.025

21. Karzan, K.; Shnawa, B.; Gorony, S. Antimicrobial activity of *Cyperus rotundus* Linn. extracts and phytochemical screening. *Eurasian Journal of Science and Engineering*. **2017**, *312*, 82. https://doi.org/10.23918/eajse.v3i2p82

22. Weitzman, S.A.; Gordon, L.I. Inflammation and cancer: role of phagocyte-generated oxidants in carcinogenesis. *Blood*. **1990**, *76*(4), 655-663. https://doi.org/10.1182/blood.V76.4.655.655

23. Wigdor, S.; Wilcox, G.L. Central and systemic morphine-induced antinociception in mice: contribution of descending serotonergic and noradrenergic pathways. *J of pharmacology and Experimental Therapeutics*. **1987**, *242*(1), 90-95.

24. Rajamanickam, M.; Rajamanickam, A. Analgesic and anti-inflammatory activity of the extracts from Cyperus rotundus Linn rhizomes. *J of Applied Pharmaceutical Science*. **2016**, *6*(9), 197-203. https://doi.org/10.7324/JAPS.2016.60929

25. Collier, H.; Dinneen, L.; Johnson, C.A.; Schneider, C. The abdominal constriction response and its suppression by analgesic drugs in the mouse. *British journal of pharmacology and chemotherapy*. **1968**, *32*(2), 295-310. https://doi.org/10.1111/j.1476-5381.1968.tb00973.x

26. Zakaria, Z. A.; Abdul Ghani, Z. D. F.; Raden Mohd. Nor, R. N. S.; Gopalan, H. K.; Sulaiman, M. R.; Mat Jais, A. M.; Ripin, J. Antinociceptive, anti-inflammatory, and antipyretic properties of an aqueous extract of Dicranopteris linearis leaves in experimental animal models. *J of natural medicines*. **2008**, *62*, 179-187.

27. Davis, J.M.; Zhao. Z.; Stock, H.S.; Mehl, K.A.; Buggy, J.; Hand, G.A. Central nervous system effects of caffeine and adenosine on fatigue. *American Journal of Physiology-Regulatory, Integrative and Comparative Physiology*. **2003,** *284*(2), 399-404.
https://doi.org/10.1152/ ajpregu.00386.2002

28. Borgi, W.; Recio, M.C.; Ríos, J.; Chouchane, N. Anti-inflammatory and analgesic activities of flavonoid and saponin fractions from *Zizyphus lotus* (L.) Lam. *South African Journal of Botany*. **2008**, *74*(2), 320-324. https://doi.org/10.1016/j.sajb.2008.01.009

29. Marzouk, B.; Marzouk, Z.; Haloui, E.; Fenina, N.; Bouraoui, A.; Aouni, M. Screening of analgesic and anti-inflammatory activities of *Citrullus colocynthis* from southern Tunisia. *J of ethnopharmacology*. **2010**, *128*(1), 15-19. https://doi.org/10.1016/j.jep.2009.11.027

30. Marzouk, B.; Marzouk, Z.; Fenina, N.; Bouraoui, A.; Aouni, M. Anti-inflammatory and analgesic activities of Tunisian *Citrullus colocynthis* Schrad. immature fruit and seed organic extracts. *European Review for Medical and Pharmacological Sciences*. **2011**, *15*(6), 665-672.

BIOCONTROL AND PLANT GROWTH PROMOTING PROPERTIES OF *Bacillus* sp. BioSol021 GROWN ON MEAT AND DAIRY INDUSTRY EFFLUENTS

Borislav M. DULOVIĆ[1] ID, Tatjana D. DUJKOVIĆ[1] ID, Ivana S. DANILOV[1] ID,*
Vanja R. VLAJKOV[1] ID, Marta Č. LOC[2] ID, Mila S. GRAHOVAC[2] ID, Jovana A. GRAHOVAC[1] ID

[1] University of Novi Sad, Faculty of Technology Novi Sad, Bulevar cara Lazara 1, 21000 Novi Sad, Serbia.
[2] University of Novi Sad, Faculty of Agriculture, Trg Dositeja Obradovića 8, 21000 Novi Sad, Serbia.

The valorization of industrial waste streams generated in vast quantities is becoming an increasingly prominent priority in line with the principles of circular economy. One potential avenue for utilizing food industry waste streams lies in the production of microbial agents with biocontrol and PGP (plant-growth promotion) properties. Bacillus species, given their broad spectrum of bioactive metabolites, exhibit significant potential in the production of such bioagents. The aim of this study was to investigate the circular economy approach by utilizing whey from dairy industry, meat processing wastewater and digestate obtained from biogas production using solid meat industry effluents, as potential bases for media used to cultivate Bacillus sp. BioSol021 and to investigate their biocontrol activity against pepper black spot causal agent, Xanthomonas euvesicatoria, as well as their PGP effects in the pepper seed germination phase. The highest antimicrobial activity, tested using the disc diffusion method, was observed in the whey-based cultivation broth sample after 96 hours of cultivation. Pepper seeds treated with cultivation broth of Bacillus sp. BioSol021 based on meat industry wastewater exhibited the best results in terms of germination rate (80%), root length (10.40 mm) and shoot length (6.20 mm). The results of this study confirm the suitability of whey, meat industry wastewater, and biogas production digestate as the potential cultivation media components for producing Bacillus-based biocontrol and PGP agents for a more sustainable agricultural practice.

Keywords: whey, meat industry wastewater, digestate, *Xanthomonas euvesicatoria*, bacterial spot.

INTRODUCTION

The global demand for dairy products, supported by growing approximately 270 million cows worldwide, not only comes after the fact that dairy products are among the vital nutritional sources for billions of people, but also creates income opportunities for various stakeholders in the dairy industry (1). The European dairy sector, in particular, stands out as a leading market, annually consuming around 45 million metric tons of fresh milk (2). The dairy industry involves the transformation of raw milk into a diverse range of products, such as pasteurized and sour milk, yoghurt, cheese, cream, butter, and various desserts, making it a significant contributor to the European agricultural output (3). However, the rapid industrialization of the dairy sector, coupled with the increasing rate of milk production, has positioned dairy processing as a major contributor to industrial food wastewater generation, particularly in Europe. Water plays a crucial role in milk processing, with significant water requirements for various activities, including cleaning, washing, disinfection, heating, and cooling (3). Each year, the dairy industry generates millions of tons of by-products, with cheese whey being the primary constituent. Cheese whey is the residual fraction remaining after milk coagulation. Approximately 9-10 liters of whey are produced per 1 kg of

cheese (4). The dairy industry, on an average, generates 2.5–10.0 L of wastewater per liter of milk processed. The wastewater generated in dairy plants is characterized by fluctuations in quality and quantity, presenting challenges for wastewater treatment plants due to the requirement for diverse technological lines for different milk products. Dairy wastewater, on average, is characterized by a high biological oxygen demand (BOD: 40-8240 mg/L), chemical oxygen demand (COD: 430–18045 mg/L), high suspended solids (SS: 24-4500 mg/L) and nutrients content, such as total nitrogen (TN: 14–830 mg/L), and total phosphorus content (TP: 9-280 mg/L) (1).

The European slaughterhouse industry, specifically meat processing, was reported to consume clean water in the amount of 2.5 m^3 up to 40 m^3 per metric ton of meat products, hence resulting in a total of 145 million cubic meters every year (5). The water footprint of meat processing increases from chicken meat (4300 m^3/t), goat meat (5500 m^3/t), pig meat (6000 m^3/t) and sheep meat (10400 m^3/t) to beef (15400 m^3/t) (6). The freshwater used turns into significant volumes of slaughterhouse wastewater (SWW) with a complex composition. The composition of SWW includes organic loads, microbial pathogens, pharmaceuticals, detergents, and disinfectants, highlighting the need for specialized treatment due to its detrimental effects globally (7). SWW is typically rich in suspended organic particles (0.28-0.34 kg/t), nitrogen (0.23-1.4 kg N/t) due to the presence of animal proteins, and phosphorus (0.012-0.09 kg P/t), while COD values go up to 40 kg O_2/t (8). Effluents from slaughterhouses constitute one of the most serious causes of environmental pollution, bad odors and health hazards in almost all of the developing countries.

Appropriate raw material for production of biogas must contain organic material that is suitable for anaerobic digestion, therefore dairy and slaughterhouse effluents are fit candidates for biogas production. In Serbia, 73500 t of slaughterhouse waste can be treated for biogas production, with the potential of biogas production estimated at 19.11 million m^3 per year (9). Biogas digestate, the by-product of biogas production, often contains nutrients such as nitrogen, phosphorus, and potassium, making it a potentially valuable organic fertilizer, but also an adequate candidate as a medium for microbial cultivations (10). According to Kefalew and Lami (11), the estimated production of biogas digestate was found to be in ratio 1:16 (solid to solid) compared to slaughterhouse waste generated, with excellent nutritional properties, i.e. sufficient levels of phosphorus, potassium, calcium, magnesium, manganese, iron, and zinc.

As the human population continues to expand and natural resources deplete due to excessive consumption, researchers and policymakers are increasingly focusing on sustainability principles. The idea of sustainable development proposes that people should be able to fulfill their current requirements without compromising the capacity of future generations to satisfy their own needs. In parallel, circular economy proposes an industrial system that is restorative by design, with the end goal to enable economic growth without impacting the environment (12). Certain industries can valorize waste in order to affordably provide substrates for their production processes and one of them is the relatively novel industry of biocontrol agents (13). Considering the substantial concentration of both organic and inorganic nutrients found in wastewater originating from the meat and dairy industries conducive to microbial growth, a viable approach to wastewater treatment involves the microbial bioconversion of these nutrients into microbial biocontrol agents (14). The synergy of multiple industries and establishing an industrial symbiosis network for circular economy can prove to be beneficial to each stakeholder involved, with local or regional interests at the central point of the circular network design (15).

On the other hand, several factors influence rising demand for eco-friendly product to maintain and improve agricultural outputs for food production. The estimated potential yield losses caused by the bacterial plant pathogens are up to 16% globally and most research in plant pathology aims to reduce yield loss directly or indirectly (16). Bacterial spot, alongside various other bacterial diseases affecting crops, stands as a primary contributor to significant global yield losses. This impact extends to both human nutrition and the economies of the countries engaged in the affected crops' production. Worldwide, bacterial spot specifically affects two crucial crops, namely tomato and pepper, and is attributed to the presence of four distinct phytopathogenic bacterial species, of which one is *Xanthomonas euvesicatoria* (17). This pathogen causes lesions on the leaves, stems, and fruits. Leaf infection results in blight, necrosis, and early leaf fall. These cause a reduction in photosynthesis and further fruit infection, resulting in direct economic loss. Contaminated seeds and plant debris are common inoculum sources, and the disease is also transmitted by rain splash (18). Control measures are predominantly confined to chemical bactericides, particularly copper-based compounds. Nevertheless, the rise of copper-tolerant *Xanthomonas* strains has become widespread, rendering chemical control alone inadequate for managing the disease, especially in favorable weather conditions. Moreover, the application of copper compounds has resulted in soil contamination in certain cases and fast pathogen resistance development (19). Microbial biocontrol agents offer promising alternatives for the management of plant diseases due to their selective efficacy, diverse mechanisms of action, reduced likelihood of antimicrobial resistance development, and specific biocontrol activity. Among these agents, bacteria from the *Bacillus* genus are widely preferred as active components. This preference is attributed to their numerous beneficial biocontrol traits, including the production of a broad spectrum of volatile and diffusible antimicrobial agents, superior competitive advantages in terms of occupying growth space and acquiring nutrients, as well as their capabilities in promoting plant growth and enhancing plant immunity against various plant pathogens (14). Several studies have confirmed the biocontrol activity of various *Bacillus* strains against *Xanthomonas euvesicatoria*, commonly associated with diseases of tomato and pepper. Research conducted by Hernández-Huerta et al. (20) demonstrated significant antagonistic activity of *Bacillus* isolates against *Xanthomonas euvesicatoria* as well as promotion of seedling growth and crop development. The strain B10(3) investigated by Zhan et al. (21), identified as *Bacillus amyloliquefaciens* showed the best biocontrol effect on *Xanthomonas euvesicatoria* among all the tested isolates due to ability for production of lipopeptides. It has also been demonstrated that treating bacterial spot with *Bacillus subtilis* CBR05 induces a defense-related enzyme response in tomatoes (22). Hence the aim of this study was to investigate the circular economy approach by utilizing whey from dairy industry, meat processing wastewater and digestate obtained from biogas production using solid meat industry effluents, as potential bases for media used to cultivate *Bacillus* sp. BioSol021 and to investigate its biocontrol activity against the pepper black spot causal agent, *Xanthomonas euvesicatoria*, as well as its PGP effects in the pepper seed germination phase.

EXPERIMENTAL

ORIGIN AND IDENTIFICATION OF MICROORGANISMS

The producing microorganism used in this study was *Bacillus* sp. BioSol021, isolated from the rhizosphere of common beans or kidney beans (*Phaseolus vulgaris*) and previously identified by 16S rRNA sequencing and biochemically characterized by the VITEK2

Compact System identification as a member of the operational group *Bacillus amyloliquefaciens*. The 16S rRNA gene sequence has been deposited in the NCBI GenBank database under accession number ON569805 (23). Pepper bacterial spot pathogen, *Xanthomonas euvesicatoria* PL1, isolated from diseased pepper plants, was used as a test microorganism (14).

STORAGE AND ACTIVATION OF MICROORGANISMS

Both microorganisms were stored at the Laboratory for Biochemical Engineering, Faculty of Technology Novi Sad, and refreshed under the following conditions (medium, temperature): nutrient agar (Himedia Laboratories, India), 28 °C for the producing microorganism, and YMA (yeast maltose agar, (24)), 26 °C for the test microorganism.

INOCULUM PREPARATION

The preparation of the *Bacillus* sp. BioSol021 inoculum involved transferring a loopful of bacterial biomass to a synthetic liquid medium, nutrient broth (Himedia Laboratories, India), and cultivation on a laboratory rotary shaker at 28 °C, 170 rpm, with spontaneous aeration for 48 hours. Ten percent (v/v) of the inoculum was used for inoculation of the cultivation medium.

CULTIVATION MEDIA AND PARAMETERS

Cultivation of the producing microorganism was performed using the following media: nutrient broth (Himedia Laboratories, India) as the referent commercial medium (CM), meat industry wastewater (MIW), whey (W), and digestate from biogas production (BPD). Meat industry wastewater and whey were utilized in their original form, without any treatment or dilution, while digestate from biogas production was dissolved in distilled water (1:9 solid to liquid ratio). All cultivation media were sterilized by autoclaving at 121 °C and 2.1 bar for 20 min. Cultivation of the producing microorganism was carried out on a laboratory shaker at 28 °C, with an external agitation rate of 170 rpm and spontaneous aeration for 96 hours. Daily sampling was conducted to evaluate antimicrobial activity against *Xanthomonas euvesicatoria* PL1.

IN VITRO BIOCONTROL EXPERIMENTS

The suspension of the test microorganism *Xanthomonas euvesicatoria* PL1 was prepared by adding the bacterial biomass in sterile saline to achieve the final concentration of 10^6 CFU/mL. YMA medium was melted, tempered (50±1 °C) and inoculated with 1 mL of the previously prepared bacterial suspension before pouring into Petri plates. The disc diffusion method in triplicate tests was employed to evaluate the antimicrobial activity of the cultivation broth samples (3x10 µL) collected at different cultivation time points. The incubation was carried out at 26 °C for 72 h and had been followed by the inhibition zone diameter measurement.

IN VITRO PGP EXPERIMENTS

The impact of *Bacillus* sp. BioSol021 on plant germination was assessed using pepper seeds (*Capsicum annuum*). For this assay, pepper seeds underwent surface sterilization with a chlorine bleach solution (6% (v/v), 1 min) and were thoroughly washed with sterile distilled water for 5 min. Following drying, the seeds were placed in Petri plates containing sterile filter paper at the bottom. Seeds were treated with 1 mL of *Bacillus* sp. BioSol021 cultivation broth samples and 5 mL of sterile tap water. Incubation was carried out at 25 °C for 7 days. After the incubation period, the percentage of germination for pepper seeds was determined, and the lengths of both roots and shoots were measured. The results obtained from treating seeds with these cultivation samples were compared with a negative control that used tap water, as well as with the cultivation broth produced using nutrient broth as the cultivation medium.

EXPERIMENTAL DATA ANALYSIS

Statistica 13.3 software (Dell Technologies, TX, USA) was used for statistical analysis of the experimental data. Levene's test and ANOVA (analysis of variance, data not shown) were performed before the Duncan's multiple range test, which was conducted to determine homogeneous groups of the independent variables at the same level of statistical significance. This test has shown to be superior over the Fisher's Least Significance Difference (LSD) method when taking into account requirements for larger differences between means that had been compared. All statistical analyses were carried out at a significance level of 95%.

RESULTS AND DISCUSSION

BIOCONTROL ACTIVITY OF *Bacillus* sp. BIOSOL021 AGAINST *Xanthomonas euvesicatoria*

To investigate the possibility of using effluents from the meat and dairy industry as a media for the production of biocontrol agents based on *Bacillus* sp. BioSol021, antimicrobial activity was tested against the phytopathogen *Xanthomonas euvesicatoria* PL1 using the cultivation broth samples obtained at different cultivation time points. Figure 1 shows the mean values of the inhibition zone diameters, which serve as a direct indicator of the suppressive effect of the cultivation broth samples. To explore differences between commercial media and waste-based media and their impact on the biocontrol activity of the investigated isolate, nutrient broth as a common medium for bacterial cultivation was also included in the screening process.

Based on the results presented in Figure 1, it can be concluded that the whey-based cultivation broth of *Bacillus* sp. BioSol021 is the most suitable medium in terms of expressing the antimicrobial effects against the investigated bacterial spot pathogen. The highest antimicrobial activity, indicated by the inhibition zone diameter of 72.33 mm, was observed in the whey-based cultivation broth sample after 96 hours of cultivation. A significant increase in the inhibitory effect of the same cultivation broth was observed between 72 and 96 hours of cultivation, where the diameter of the inhibition zones increased from 52.33 to 72.33 mm, suggesting intensified secondary metabolite synthesis in the stationary growth phase usually observed after 48 h of cultivation for majority of *Bacillus* strains (14).

Figure 1. Biocontrol activity of *Bacillus* sp. BioSol021 grown on whey (W), meat industry wastewater (MIW), digestate from biogas production (BPD) and nutrient broth (CM) against *Xanthomonas euvesicatoria PL1*

Previous studies have demonstrated the ability of *Bacillus amyloliquefaciens* strains to produce antimicrobial metabolities such as cyclic lipopeptides surfactin, iturin A and fengycin as well as the iron-siderophore bacillibactin (25). In addition to these non-ribosomally synthesized peptides, three additional gene clusters directing the synthesis of the antibacterial polyketides macrolactin, bacillaene and difficidin were identified (26). On the other hand, cultivation broths based on wastewater from the meat industry, digestate from biogas production and nutrient broth showed approximately similar level of antimicrobial activity, significantly lower compared to the value achieved by using whey as a cultivation medium. The changes in the level of antagonistic activity of the cultivation broth samples during cultivation might be related to the multiplication intensity of the investigated isolate at the exponential phase and to secondary metabolism in the stationary phase. Only in the case of cultivation broth based on biogas production digestate, the antimicrobial activity achieved at 48 hours of cultivation remained at approximately the same level in the following two samplings. Taking into account the observed antimicrobial assay results, it is clear that whey, as a cultivation medium for the production of biocontrol agents based on the isolate *Bacillus* sp. BioSol021, has great potential, demonstrating much better efficacy compared even to the commercial medium. According to the research conducted by Pajčin et al. (27), whey and meat processing wastewater have already been investigated as a potential medium for a *Bacillus*-based biocontrol agent. In that study, the inhibition zones, measured after 72 hours of cultivation, achieved by *Bacillus velezensis* IP22 whey-based cultivation broth samples against *Xanthomonas euvesicatoria* PL1 were 25.83 mm, while

the inhibition zones achieved by the MPW (meat processing wastewater) medium were 27 mm, suggesting higher potential of the isolate *Bacillus* sp. BioSol021 in terms of biocontrol activity against pepper bacterial spot. Dmitrović et al. (28) have also demonstrated the successful utilization of whey and winery flotation effluent in producing biocontrol agents based on *Bacillus amyloliquefaciens*. The antimicrobial effect of *Bacillus clausii* cultivation broth based on a whey medium has also been demonstrated against human pathogens, including *Salmonella typhimurium*, *Escherichia coli*, *Shigella flexneri*, *Staphylococcus aureus, Listeria monocytogenes*, and *Enterococcus faecalis* (29).

THE EFFECTS OF *BACILLUS* SP. BIOSOL021 TO PEPPER SEED GERMINATION

The efficiency of *Bacillus* sp. BioSol021 cultivation broths in pepper seed germination was investigated for cultivation broth samples based on different waste streams in comparison to nutrient broth as a commercial medium and tap water as negative control. The germination percentage of pepper seeds treated with the aforementioned cultivation broth samples, as well as homogenous groups of independent variables according to Duncan's multiple test, are given in Figure 2.
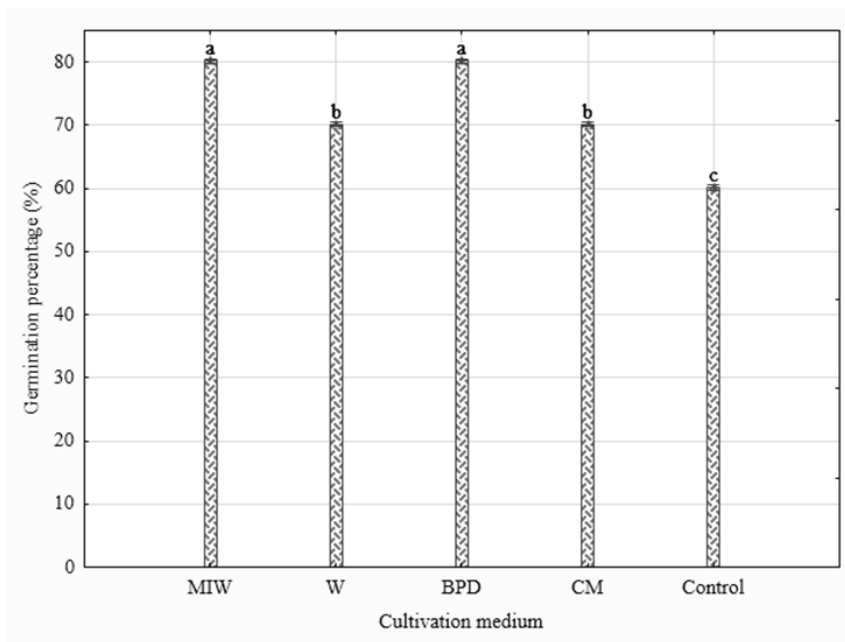
Figure 2. The effects of *Bacillus* sp. BioSol021 grown on whey (W), meat industry wastewater (MIW), digestate from biogas production (BPD) and nutrient broth (CM) on pepper seed germination. The designations a, b and c represent different homogeneous groups according to the Duncan's multiple range test, performed at the significance level of 95%.

Duncan's multiple range test was employed to identify homogenous groups of the independent variables. The results reveal two distinct groups: cultivation broth samples based on meat industry wastewater (MIW) and biogas production digestate (BPD) form one

group, while those based on whey and nutrient broth constitute another. The highest germination percentage (80%) was observed when using MIW- and BPD-based cultivation broth samples. Seeds treated with whey and nutrient broth-based cultivation broth exhibited a germination rate of 70%, whereas germination with tap water as a control reached 60%. The increased germination rate with *Bacillus* sp. BioSol021 cultivation broths compared to the negative control confirms the beneficial impact of bacteria on promoting pepper germination. Moreover, the higher germination success achieved by using media based on meat industry wastewater and digestate from biogas production than commercial media indicates the significant potential of utilizing these waste streams for biofertilizer or seed coating agents' production.

Mean values and standard deviations of pepper root and shoot lengths are presented in Figures 3 and 4. Notably, the seeds treated with MIW-based cultivation broth exhibited the highest root length, reaching 10.40 mm, indicating superior results in terms of root development. According to Duncan's multiple range tests, all of the tested waste streams formed separate groups, while cultivation broth based on nutrient broth and tap water were grouped together, suggesting similar effects on root length. In contrast, when considering shoot length, a significant difference was observed between MIW-based cultivation broth samples and the other tested cultivation broth samples which were in the same group as negative control. The maximum shoot length was observed in seeds treated with MIW-based cultivation broth, reaching approximately 6.20 mm. In contrast, the seeds treated with other cultivation broth samples exhibited slightly over 3 mm in length. This suggests that while the other cultivation broth samples exhibited similarities in their effects on shoot length, MIW-based cultivation broth had a distinct impact, deviating from the observed patterns.
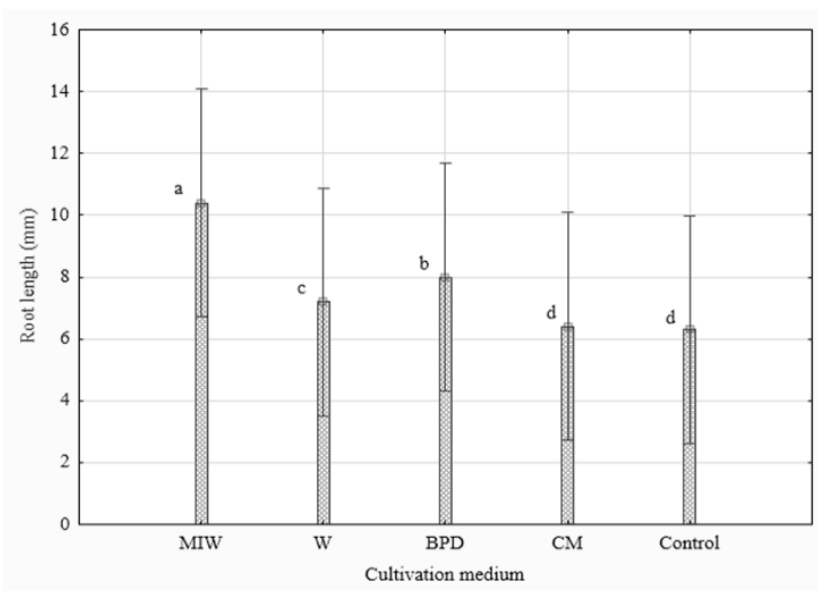
Figure 3. The effects of *Bacillus* sp. BioSol021 grown on whey (W), meat industry wastewater (MIW), digestate from biogas production (BPD) and nutrient broth (CM) on pepper root length. The designations a, b, c and d represent different homogeneous groups according to the Duncan's multiple range test, performed at the significance level of 95%.

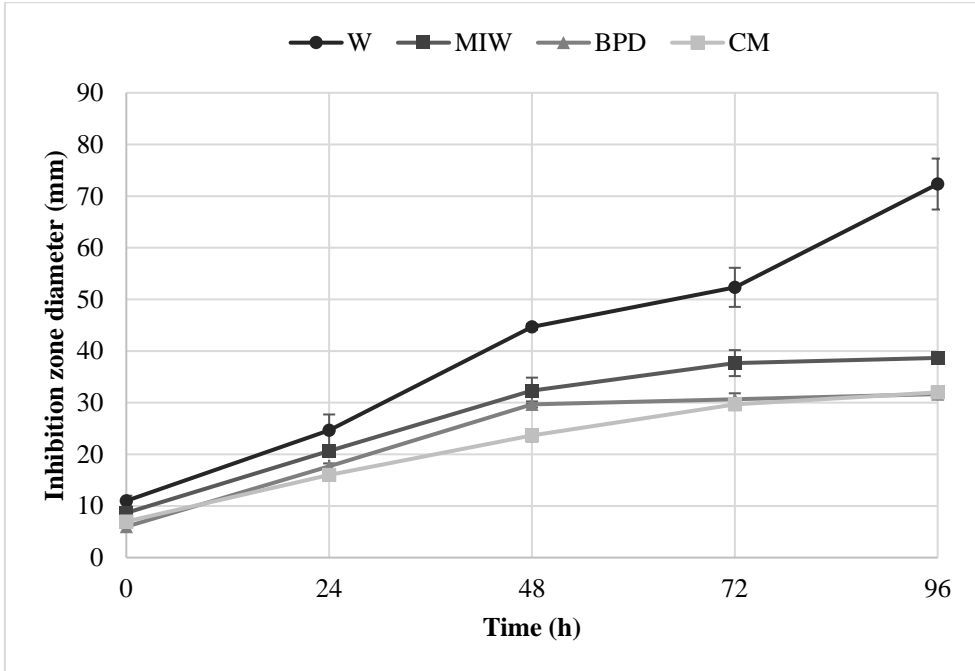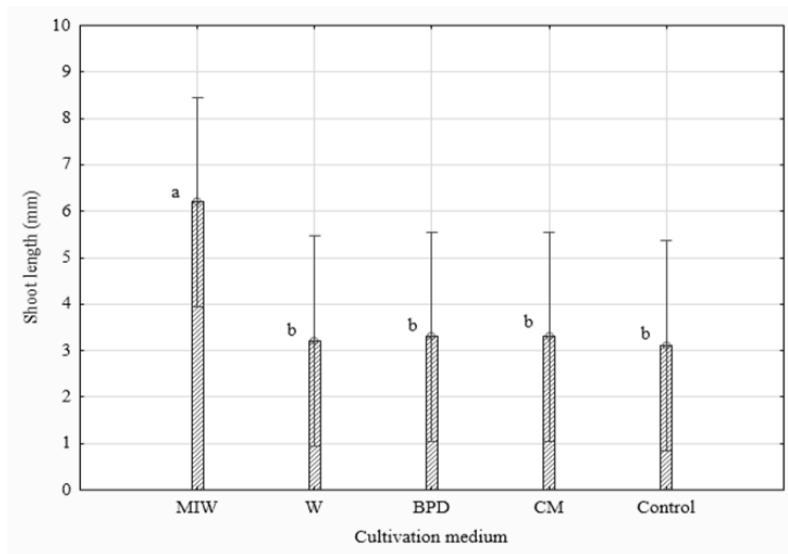**Figure 4.** The effects of *Bacillus* sp. BioSol021 grown on whey (W), meat industry wastewater (MIW), digestate from biogas production (BPD) and nutrient broth (CM) on pepper shoot length. The designations a and b represent different homogeneous groups according to the Duncan's multiple range test, performed at the significance level of 95%.

The advantageous characteristics of *Bacillus* strains in facilitating seed germination and seedling growth involve several beneficial mechanisms. These include enhancing nutrient availability by enzymatic actions like solubilizing phosphorus, zinc, and potassium, along with nitrogen fixation. Additionally, *Bacillus* strains promote plant growth through the production of plant hormones such as auxins (including IAA) and cytokinins, the synthesis of siderophores, and the creation of antibacterial and antifungal compounds. These actions collectively improve seedling vigor and fortify the plant against both biotic and abiotic stresses (30). Some of the mentioned PGP traits have been proven for *Bacillus amyloliquefaciens* in the study conducted by Vlajkov et al. (30) where seed germination performance was investigated on maize. According to Joo et al. (31), among all tested rhizobacteria, *Bacillus pumilus* led to the most significant enhancements in both seedling height and root fresh weight of red pepper, with a 12% increase in height and a 20% increase in root fresh weight. The study by Meng et al. (32) demonstrated that *Bacillus velezensis* BAC03 enhanced the growth of certain tested plants across different plant parts and at various levels. *Bacillus cereus* and *Bacillus thuringiensis* strains investigated by Hernández-Huerta et al. (20) have shown great potential for use as a biofertilizer, as well as a biocontrol agent, significantly promoting pepper seedling growth and crop development while also demonstrating antagonistic potential against *Xanthomonas euvesicatoria*.

Significant improvement in the root and shoot growth of pepper seedlings observed when using cultivation broth of *Bacillus* sp. BioSol021 based on meat industry wastewater makes it a promising medium for the production of microbial fertilizers or biostimulants. Such results indicating a better growth stimulation of plants through the application of meat industry wastewater as a cultivation medium may be attributed to the superior nutritional composition of this wastewater compared to whey and biogas production digestate. MIW

usually contain considerable amounts of total phosphorus, total nitrogen, total organic carbon, together with higher chemical oxygen demand, biochemical oxygen demand and total suspended solids content (33). Although BDP is also effluent from meat industry, it contains significantly fewer nutrients due to being a waste from secondary production/valorization cycle that has already undergone digestion during biogas production process, during which microorganisms had already used part of its organic and inorganic compounds (33). On the other hand, when targeting maximal antibacterial activity, whey-based medium has shown supremacy compared to both commercial medium and other waste-based media. This fact points out that the nutritional requirements of the producing microorganism should be thoroughly considered when developing biocontrol and PGP-aimed products for agricultural applications, especially when considering multi-beneficial products from the perspective of agricultural production efficiency. Generally, besides nutritional differences, lower pH value of the whey (4) compared to other effluents could represent a benefit for improved antibacterial activity, without compromising effects on the growth of the sporogenous *Bacillus* isolate.

Although the possibility of cultivating biocontrol agents based on *Bacillus* species has been demonstrated on other waste streams such as molasses, brewery effluents, starch industry wastewater and others, production process development usually remains at the laboratory level (34, 35, 36). These bioprocess solutions that would utilize food industry effluents as raw materials for producing biocontrol agents offer effective alternatives to chemical pesticides including also economic and environmental added value. This circular economy-based initiative aims to foster a more environmentally friendly agricultural production system while promoting the adoption of greener technologies. By extracting/utilizing effluents from industrial processes and transforming them into value-added products the alignment with the principles of circular economy has been greatly achieved, and by fostering industrial symbiosis beyond individual industrial facilities, the pressing issue of industrial waste generation and disposal could be effectively addressed (37).

However, for the successful implementation of such a production method, additional research is necessary regarding the complete composition of waste streams and further medium composition optimization, together with optimization of bioprocess parameters, techno-economic analysis, and the formulation of the final product itself.

CONCLUSION

The presented study confirms the suitability of whey, meat industry wastewater, and biogas production digestate as cultivation media for producing biocontrol and PGP agents utilizing the *Bacillus* sp. isolate BioSol021. The medium based on whey demonstrated superior antimicrobial activity against *Xanthomonas euvesicatoria* PL1, whereas the wastewater from the meat industry exhibited a more favorable influence on pepper plant growth. However, in both cases, superior outcomes are attained when utilizing waste streams as a medium compared to a commercial medium (nutrient broth). This suggests the potential for cost reduction in the overall production process and supports the feasibility of implementing the circular economy principles by repurposing waste from one industry as a substrate in another. Further research will focus on evaluating the viability of the proposed valorization routes and optimizing the bioprocess to maximize biocontrol and plant growth-promoting characteristics of the investigated bacterial isolate. Additionally, there is a need for identification and characterization of the components produced by the tested isolate in

terms of antimicrobial activity and PGP activity. The following steps will also include estimating and validating the product efficiency under real conditions through the conduction of field trials. This research has also paved the path for investigation of other industrial effluents as possible nutrient sources for microbial bioconversion, with the rising necessity of further identification and characterization of microbial catalysts suitable for transformation of waste-based nutrients to other types of industrially important biotechnological products.

Acknowledgement

REFERENCES

1. Ekka, B.; Dejus, S.; Juhna, T. Case study on the dairy processing industries and their wastewater generation in Latvia. *J. Dairy Res.* **2021**, *88*(4), 425–428.
2. Burrell, A. The future of dairy policy in the European Union. *Advances in Dairy Technology.* **2000**, *12*, 313-322.
3. Slavov, AK. General Characteristics and Treatment Possibilities of Dairy Wastewater - A Review. *Food Technol Biotechnol.* **2017**, *55*(1), 14-28.
4. Pires, AF.; Marnotes, NG.; Rubio, OD.; Garcia, AC.; Pereira, CD. Dairy By-Products: A Review on the Valorization of Whey and Second Cheese Whey. *Foods.* **2021**, *10*(5), 1067.
5. Ahmad Latiff, N.A.; Radin Mohamed, R.M.S.; Shanmugan, V.A.; Mohd Apandi, N.; Mohd Tajuddin, R.; Mohd Kassim, A.H. Characteristics of Water Quality from Meat Processing Wastewater. *J. Adv. Res. App. Sc. Eng. Tech.* **2020**, *17*(1), 78-84.
6. Mekonnen, M.; Hoekstra, A. A Global Assessment of the Water Footprint of Farm Animal Products. *Ecosystems.* **2012**, *15*(3), 401–415.
7. Bustillo-Lecompte, C.F.; Mehrvar, M. Slaughterhouse wastewater characteristics, treatment, and management in the meat processing industry: A review on trends and advances. *J. Environ. Manage.* **2015**, *161*, 287-302.
8. Botiş, M. Purification of the wastewater from meat industry. *J. Process. Energy Agric.* **2015,** *19*(1), 21-23.
9. Cvetković, S.; Radoičić, T.; Vukadinović, B.; Kijevčanin, M. Potentials and status of biogas as energy source in the Republic of Serbia. *Renewable Sustainable Energy Rev.* **2014**, *31*, 407-16.
10. Roopnarain, A.; Akindolire, M.A.; Rama, H.; Ndaba, B. Casting Light on the Micro-Organisms in Digestate: Diversity and Untapped Potential. *Fermentation.* **2023**, *9*(2), 160.
11. Kefalew, T.; Lami, M. Biogas and bio-fertilizer production potential of abattoir waste: implication in sustainable waste management in Shashemene City, Ethiopia. *Heliyon*, **2021**, *7*(11).
12. Lamba, H.; Kumar, N.; Dhir, S. Circular economy and sustainable development: a review and research agenda. *Int. J. Product. Perform. Manag.* **2023**, *73*(2), 497-522.
13. Tripti; Kumar, A.; Kumar, V.; Anshumali; Bruno, L.B.; Rajkumar, M. Synergism of Industrial and Agricultural Waste as a Suitable Carrier Material for Developing Potential Biofertilizer for Sustainable Agricultural Production of Eggplant. *Horticulturae.* **2022**, *8*(5), 444.
14. Pajčin, I.; Vlajkov, V.; Frohme, M.; Grebinyk, S.; Grahovac, M.; Mojićević, M.; Grahovac, J. Pepper bacterial spot control by *Bacillus velezensis*: Bioprocess solution. *Microorganisms*, **2020**, *8*(10), 1463.

15. Oughton, C.; Kurup, B.; Anda, M.; Ho, G. Industrial Symbiosis to Circular Economy: What Does the Literature Reveal for a Successful Complex Industrial Area?. *Circ. Econ. Sust.* **2022**, *2*(4), 1317–1344.

16. Ficke, A.; Cowger, C.; Bergstrom, G.; Brodal, G. Understanding Yield Loss and Pathogen Biology to Improve Disease Management: Septoria Nodorum Blotch - A Case Study in Wheat. *Plant Dis.* **2018**, *102*(4), 696-707.

17. Shopova, E.; Brankova, L.; Ivanov, S.; Urshev, Z.; Dimitrova, L.; Dimitrova, M.; Hristova, P.; Kizheva, Y. *Xanthomonas euvesicatoria*-Specific Bacteriophage BsXeu269p/3 Reduces the Spread of Bacterial Spot Disease in Pepper Plants. *Plants*, **2023**, *12*(9), 3348.

18. Kyeon, M.; Son, S.; Noh, Y.; Kim, Y.; Lee, H.; Cha, J. *Xanthomonas euvesicatoria* Causes Bacterial Spot Disease on Pepper Plant in Korea. *Plant Pathol. J.* **2016**, *32*(5), 431-440.

19. Hert, A.; Marutani, M.; Momol, M.; Roberts, P.; Olson, S.; Jones, J. Suppression of the bacterial spot pathogen *Xanthomonas euvesicatoria* on tomato leaves by an attenuated mutant of *Xanthomonas perforans*. *Appl Environ. Microbiol.* **2009**, *75*(10), 3323-30.

20. Hernández-Huerta, J.; Tamez-Guerra, P.; Gomez-Flores, R.; Delgado-Gardea, M. C. E.; Robles-Hernández, L.; Gonzalez-Franco, A. C.; Infante-Ramirez, R. Pepper growth promotion and biocontrol against *Xanthomonas euvesicatoria* by *Bacillus cereus* and *Bacillus thuringiensis* formulations. *PeerJ.* **2023**, *11*, e14633.

21. Zhan, M. L.; Chen, C. J.; Luo, X. H.; Hu, F. P.; Cai, X. Q. Identification of a biocontrol strain against *Xanthomonas euvesicatoria* and its biological control mechanism. *J. South. Agric.* **2020**, *51*(12), 2945-2951.

22. Chandrasekaran, M.; Chun, S. C. Induction of defence-related enzymes in tomato (*Solanum lycopersicum*) plants treated with *Bacillus subtilis* CBR05 against *Xanthomonas campestris* pv. *vesicatoria*. *Biocontrol Sci. Technol.* **2016**, *26*(10), 1366-1378.

23. Dmitrović, S.; Pajčin, I.; Lukić, N.; Vlajkov, V.; Grahovac, M.; Grahovac, J.; Jokić, A. Taguchi grey relational analysis for multi-response optimization of *Bacillus* bacteria flocculation recovery from fermented broth by chitosan to enhance biocontrol efficiency. *Polymers*, **2022**, *14*(16), 3282.

24. Grahovac, J.; Pajčin, I.; Vlajkov, V.; Rončević, Z.; Dodić, J.; Cvetković, D.; Jokić, A. *Xanthomonas campestris* biocontrol agent:selection, medium formulation and bioprocess kinetic analysis. *Chem. Ind. Chem. Eng. Q.* **2021**, *27*(2), 131-142.

25. Luo, L.; Zhao, C.; Wang, E.; Raza, A.; Yin, C. *Bacillus amyloliquefaciens* as an excellent agent for biofertilizer and biocontrol in agriculture: An overview for its mechanisms. *Microbiol. Res.* **2022**, 259, 127016.

26. Arguelles-Arias, A.; Ongena, M.; Halimi, B.; Lara, Y.; Brans, A.; Joris, B.; Fickers, P. *Bacillus amyloliquefaciens* GA1 as a source of potent antibiotics and other secondary metabolites for biocontrol of plant pathogens. *Microb. Cell Fact.* **2009**, 8(63).

27. Pajčin, I.; Vlajkov, V.; Dujković, T.; Grahovac, J. Effluents from industrial processing of the food of animal origin as media for biocontrol agents production. *J. Process. Energy Agric.* **2023**, *27*(1), 16-21.

28. Dmitrović, S.; Pajčin, I.; Vlajkov, V.; Grahovac, M.; Jokić, A.; Grahovac, J. Dairy and wine industry effluents as alternative media for the production of *Bacillus*-based biocontrol agents. *Bioengineering.* **2022**, *9*(11), 663.

29. Rochín-Medina, J. J.; Ramírez-Medina, H. K.; Rangel-Peraza, J. G.; Pineda-Hidalgo, K. V.; Iribe-Arellano, P. Use of whey as a culture medium for *Bacillus clausii* for the production of protein hydrolysates with antimicrobial and antioxidant activity. *Food Sci. Technol. Int.* **2018**, *24*(1), 35-42.

30. Vlajkov, V.; Pajčin, I.; Loc, M.; Budakov, D.; Dodić, J.; Grahovac, M.; Grahovac, J. The Effect of Cultivation Conditions on Antifungal and Maize Seed Germination Activity of *Bacillus*-Based Biocontrol Agent. *Bioengineering*, **2022**, *9*(12), 797.

31. Joo, G. J.; Kim, Y. M.; Lee, I. J.; Song, K. S.; Rhee, I. K. Growth promotion of red pepper plug seedlings and the production of gibberellins by *Bacillus cereus*, *Bacillus macroides* and *Bacillus pumilus*. *Biotechnol. Lett.* **2004**, *26*, 487-491.

32. Meng, Q.; Jiang, H.; Hao, J. J. Effects of *Bacillus velezensis* strain BAC03 in promoting plant growth. *Biol. Control.* **2023**, *98*, 18-26.

33. Bustillo-Lecompte, C. F.; Mehrvar, M. Slaughterhouse wastewater characteristics, treatment, and management in the meat processing industry: A review on trends and advances. *J. Environ. Manage*. **2015**, *161*, 287-302.

34. Płaza, G. A.; Król, E.; Pacwa-Płociniczak, M. M.; Piotrowska-Seget, Z.; Brigmon, R. L. Study of antifungal activity of *Bacilli* species cultured on agro-industrial wastes. *Acta Sci. Pol. Hortorum Cultus*. **2012**, *11*(5), 169-182.

35. Yezza, A.; Tyagi, R. D.; Valero, J. R.; Surampalli, R. Y. Bioconversion of industrial wastewater and wastewater sludge into *Bacillus thuringiensis* based biopesticides in pilot fermentor. *Bioresour. Technol*. **2006**, *97*(15), 1850-1857.

36. Kumar, L. R.; Ndao, A.; Valéro, J.; Tyagi, R. D. Production of Bacillus thuringiensis based biopesticide formulation using starch industry wastewater (SIW) as substrate: a techno-economic evaluation. Bioresour. Technol. **2019**, *294*, 122144.

37. Neves, A.; Godina, R.; Azevedo, S. G.; Matias, J. C. A comprehensive review of industrial symbiosis. *J. Cleaner Prod*. **2020**, *247*, 119113.

PREDICTION OF HARDNESS OF PALM INTER-FRUITLET MEMBRANE REINFORCED HIGH-DENSITY POLYETHYLENE-WASTE (HDPEw) COMPOSITES

Agha Inya NDUKWE[1]*   , Nelson Ogadi AZOLIBE[1], Kooffreh OKON[1,2], Promise C. CHRISTOPHER[1], Michael C. COLLINS[1], Chibuike C. OZOH[1], Paul Osondu OBASI[1], Collins Kenechukwu EZE[1], Augustus C. EZEM[1], Chidiebere Bright THOMAS[1], Chijioke Sydney OGBODO[1]

[1] Department of Materials & Metallurgical Engineering, Federal University of Technology,
P. M. B. 1526, Owerri, Imo State, Nigeria.
[2] African Centre of Excellence in Future Energies and Electrochemical Systems,
Federal University of Technology, Owerri (ACE-FUELS, FUTO), Imo State, Nigeria.

    This study concerns the prediction of the hardness of reinforced high-density polyethylene waste (HDPEw) composites. The locally sourced palm inter-fruitlet membrane served as the reinforcing (filler) material while the Yoghurt Can wastes constituted the polymer matrix. The palm inter-fruitlet membrane, used for the study were pulverized and sieved to fine particle sizes. All filler particles passed through a mesh of 250 μm. Consequently, the filler sample was characterized using DTA, TGA, and FTIR techniques whereas SEM was used to study the morphology of the produced composite. Different weight-percentage compositions of the filler were used to produce the examined samples with the following formulations: 100 % LDPEw, 6wt.%, 12wt.%, 18wt.%, and 24wt.% filler composites using the compression moulding method. On the other hand, hardness, flexural, tensile, and impact strengths were conducted to understand the mechanical behaviour of the produced composites. Multiple regression and artificial neural networks were used to predict the experimental hardness values in consideration of other independent variables like composite formulations, tensile, flexural, and impact strengths. The result of the TGA analysis showed the weight loss and degradation of the organic constituents in the filler while the DTA study revealed a variety of thermal occurrences and transitions indicating dehydration, phase change, and filler disintegration. The maximum hardness value of 76.67 HV was recorded for the composite with 24 wt.% filler while the composite formulation with 12 wt.% filler had the highest flexural and impact strengths of 41.87 MPa and 0.4979 J/mm² respectively. The composite composition with 18 wt.% filler gave the highest tensile strength of 39.04 MPa. The unequal distribution of the filler within the HDPEw matrix was revealed by the SEM micrographs. The more uniformly dispersed composites with 12 and 18 wt.% fillers were seen to have improved mechanical properties whereas the reverse was the case for the 24 wt.% filler composite formulation which was found to exhibit directional reinforcement zones. The mean squared error assessment of the predicted hardness values indicated that predictions by multiple regression were more accurate than those that were obtained by ANN. This outcome could be caused by the relative linearity of the examined variables.

Keywords: Polymer-matrix composites (PMCs), hardness, polyethylene waste composites, palm inter-fruitlet membrane, mechanical properties, compression moulding.

INTRODUCTION

    Polyethylene, which has been reported as the most common and readily available plastic in recent times (1) possesses some endearing characteristics such as affordability, and profound insulation to electricity over a large span of frequencies (2). It has been discovered

that plastics are very difficult to degrade (3), and invariably top the priority of concerns for waste management (4). The number of polyethylene materials that are polluting the environment is very alarming (5,6), and it is a threat to every living thing (7). Currently, the world is being faced with the rigour of managing plastic waste (8). Interestingly, the sky-rocketing use of polyethylene materials may be attributed to mere convenience (9). While it has been reported that the littered polyethylene materials could have resulted in unconscious behaviour towards their disposal (10), a counterclaim argues that polyethylene materials are widely used and disposed of indiscriminately even though it is obvious that they cause environmental pollution (11). Studies have shown that reinforcing the high-density polyethylene matrix with the empty palm fruit bunch can improve the mechanical behaviour of the new product (12-14).

The palm inter-fruitlet membrane (PIFM) is obtained from the empty palm fruit bunch, which is usually marked for disposal during the processing of palm oil (15), and serves as a veritable source of fuel (16). This empty palm fruit bunch is produced in large quantities in Malaysia (17), and Indonesia (18). Utilizing agricultural by-products, such as palm inter-fruitlet membranes (PIFMs), is a potential strategy in the search for sustainable materials. Large amounts of PIFM waste are produced by the palm oil industry, and if they are not properly handled, they may contribute to environmental damage. The high mechanical strength, low density, and renewability of PIFM, a fibrous material rich in cellulose and lignin (19-21), suggest that it has potential as a reinforcing agent for polymer composites. The empty palm fruit bunch has been reported as a source of fertilizer (22), and energy (23). As part of its usefulness in agriculture, about a 49.2 % increase in plant yield and growth was recorded when the empty palm fruit bunch was used for mulching and as compost in the cultivated soil (24).

There is limited work on the production of palm inter-fruitlet membrane-reinforced high-density polyethylene-waste (HDPEw) composites. However, studies have been done using the entire empty palm fruit bunch to reinforce plastic materials. Hashim et al. (25) explored epoxy resin-reinforced natural fibre of palm empty fruit bunches (PEFB) as polymer composites. The main goal of the study was to determine the best mixture of LDPE plastic waste and PEFB fibres to attain the requisite characteristics for deck panel applications. According to the research findings, the polymer composites with the best mechanical qualities had a PEFB/epoxy resin ratio of 30% PEFB fibres and 70% epoxy resin. It demonstrated greater flexural, tensile, compression, and impact strengths when compared with other tested composite formulations. In another study, Amir et al. (26) investigated how gamma radiation influenced the compressive qualities of hybrid materials made of kevlar and oil palm empty fruit bunches. The outcomes showed that gamma radiation improved the compressive capabilities of the hybrid composites made of Kevlar fibre, oil palm empty fruit bunch (EFB) fibre, and epoxy. This study points to the possibility that gamma radiation may be an effective way to improve the mechanical qualities of these hybrid composite materials, possibly enabling their usage in a variety of applications where increased compressive strength is required.

This experimental study seeks to predict the experimental hardness values of the produced composites using artificial neural networks and multiple regression. Since there is limited knowledge about PIFM-reinforced HDPEw composites, TGA, DTA, and FTIR will be used to characterize the PIFM filler while the morphology of the produced composites will be studied by SEM. Nonetheless, the production of palm inter-fruitlet membrane reinforced high-density polyethylene waste (i.e., Disposed Yoghurt Can) composites prepared with filler particles of 250 μm and compositions (6 wt.%, 12 wt.%, 18 wt.%, and 24 wt.%)

will be done using a two-mill roll and compression moulding. The water absorption behaviour and mechanical properties (hardness, flexural, impact, and tensile strengths) of the produced composite will be examined.

MATERIALS AND METHODS

The high-density polyethylene waste (HDPEw), in the form of Yogurt can waste, was obtained from Zaria, in Kaduna State, Nigeria. On the other hand, the empty palm inter-fruitlet membrane filler was obtained from the palm fruit processing plant in Eziobodo, Owerri West, Imo State, Nigeria. The filler was directly taken from the dried empty palm fruit bunch. Furthermore, the palm inter-fruitlet membrane filler was fed into the grinding burr mill and pulverized repeatedly up to five different times to achieve the desired fineness. Subsequently, the filler particles were sieved, and all particle sizes passed through a mesh size of 250 microns.

PRODUCTION OF THE COMPOSITE

The mixing and hot pressing, leading to the production of the composites (specimens) were achieved following the earlier reported methods (6).

CHARACTERIZATION OF FILER

FTIR analysis

The FTIR analysis of the palm inter-fruitlet membrane filler was conducted using the Agilent Technologies FTIR spectrometer that employed the transmittance method. The filler sample used for the FTIR test was provided in a particle size of 250 microns. In addition to the 30 sample scans, 16 background scans were performed to account for any environmental influences. The resolution was set to 8, and the spectral range was defined as 4000 to 650 cm^{-1}. For processing the data, the Happ-Genzel apodization function was applied.

Thermal analysis

The thermogravimetric and differential thermal analyses of the filler were studied using the PerkinElmer Analyzer. The initial quantity of the filler sample used for the TGA test was 18.338 mg. Before the commencement of the TGA analysis, the sample was put in the machine's sample holder which was situated in a platinum pan. The temperature was maintained between 30 and 950 °C at the rate of 10 °C/min. The thermal behaviour of the filler was recorded by the TGA machine as the temperature varied throughout the test. To avoid any unintended responses or impacts, the material was treated in a controlled environment during the study. On the other hand, the differential thermal analysis was carried out using the PerkinElmer Analyzer. The palm inter-fruitlet membrane filler sample of 18.302 mg, was heated in an alumina crucible under controlled conditions from 30 °C to 95 °C at a rate of 10 °C/min.

SEM OF COMPOSITES

The study of composite materials was conducted through electron microscopic scanning, following the requirements outlined in ASTM E986. To carry out this analysis, the

Pro: X: Phenom world 800-07334 model was used. A 0.5g cross-sectional slice of the sample was carefully inserted into the sample holder to initiate the examination process. The sample holder was then accurately positioned under the magnification screen of the machine, after which the chamber was gradually closed. The samples underwent electron microscopy examination and were zoomed in on areas of interest for clearer identification.

MECHANICAL CHARACTERIZATION

The impact test was rigorously carried out following the established standards specified by the ASTM D-156 standard. Each specimen had a 45° incision at the middle and was cut to exact measurements of 64 mm x 12.7 mm x 3.2 mm. An Izod Impact Tester (also known as a Resil impactor testing equipment) was used to quantify the impact energy. A hammer weighing 1500 N was launched at a 150° inclined angle after being tightly clamped onto the machine's jaw and arranged on the specimen in a vertical configuration (IZOD). The tested specimen's impact energy was measured and recorded, allowing the impact strength to be computed using the proper equation:

$$\text{Impact Strength} = \frac{\text{Average Impact Energy}}{\text{Sample thickness}^*} \quad (\text{J/mm}^2) \qquad [1]$$

* Sample thickness = 3.2 mm

The composite material's flexural strength test was carried out in line with ASTM D-790 requirements. A carefully constructed specimen with dimensions of 100 mm × 25 mm x 3.2 mm was laid out horizontally on a support span while retaining a gauge length of 80 mm. A three-point bending situation was maintained until the specimen eventually failed by employing a loading nose to impart a controlled and constant stress to the specimen's core. The highest load (in Newtons, N) and the associated deflection (in millimetres, mm) were painstakingly monitored and recorded throughout the testing process. The flexural strength and flexural modulus were then precisely computed for thorough study using the relevant formulae:

$$\text{Flexural Strength} = 3FL/2bd^2 \qquad [2]$$

$$\text{Flexural Modulus} = FL^3/4bd^3D \qquad [3]$$

where:
F = Maximum Load at break
L = Distance between the support spans at both edges of the specimen = 80 mm
b = Sample width = 25 mm
d = Sample thickness = 3.2 mm

The Vickers microhardness tester was used to perform the hardness tests. The mounting stage was used to hold the 1 x 2 x 0.3 cm specimen, and the indenter was lowered until it contacted the specimen at a constant pressure. All of the studied specimens had readings taken, and the process was repeated three (3) times at various locations on the specimen.

The universal testing machine (model no. D-100KN, SN:190536) was used to perform the tensile strength test by ASTM D-638 requirements. Samples in the shape of dumbbells, with gauge measurements of 50 mm x 10 mm x 3.2 mm, were pulled apart under a regulated tensile stress. Key tensile characteristics, including tensile strength, percentage of elon-

gation, and modulus, were automatically calculated for each unique sample using the Universal Testing Machine.

WATER ABSORPTION TEST

The water absorption test was carried out by the ASTM D570 standard. For the assessment, carefully chosen specimens with exact preparation and 50 mm x 50 mm x 3.2 mm measurements were used. The test protocol involved completely submerging the samples in distilled water at room temperature for seven days. The samples were rigorously weighed using an accurate digital weighing scale every 24 hours to determine the rate of water absorption. The given equation was then used to precisely compute the % water absorption of the composite samples for thorough examination.

$$\% \text{ Water Absorbed} = \frac{w_2 - w_1}{w_1} \; x \; 100 \qquad [4]$$

where:
w_2 = final weight of composite
w_1 = initial weight of composite

IBM SPSS

In this study, the multilayer perceptron (MLP) network was used to predict the hardness values of the examined composites using neural networks and multiple regression predictive protocols. IBM SPSS (Statistical Package for the Social Sciences) (27) is a very robust statistical software with an interface that is user-friendly. The neural network and multiple regression are fully integrated into the SPSS application. IBM SPSS technology is utilized by commercial establishments, government, and academic institutions all around the world (28).

Multiple regression (MR)

Multiple regression is a powerful and versatile method that enables the modelling of the effects of several independent variables on a dependent variable simultaneously. This method allows for the modelling of main, interacting, or curvilinear effects, and also provides the ability to determine the incremental effect on the model by adding or removing independent variables (29). In social and behavioural research, multiple regression is used to deduce the amount of variance in a criterion variable that can be explained by two or more predictor variables. It is important to note that predictor variables in multiple regression analysis are usually correlated, which can make it difficult to interpret results (30). The most common objectives of multiple regression analysis include: 1) developing a model to describe the relationship between explanatory variables and the response variable, 2) using sample data to make predictions, and 3) confirming theories about individual variables by determining which variables or combination of variables should be included in the model (31). Whether the objective of the analysis is to estimate the effect of a covariate or to predict the value of the response based on the covariate values, a regression model is used to make the prediction (32). In regression analysis, we can determine the relationship between the independent variables $x = [x_1, x_2, ..., x_n]$ and dependent variables $y = [y_1, y_2, ..., y_m]$, where n is the number of independent variables present in each observation and m is the number of dependent variables. The regression model is expressed as follows:

$$y = f(x) + \varepsilon \qquad [5]$$

where f(x) is a vector function [$f_1(x)$,…, $f_m(x)$] and $\varepsilon = [\varepsilon_1,…, \varepsilon_m]$ is a vector of random error of functional approximation. The general model is frequently simplified by assuming a linear relationship between the independent and dependent variables. The multiple dependent variables x and y are considered separately to give m-independent regression models. In the simplest case of a single dependent variable, the regression models are given as:

$$y = a_0 + a_{1x} + \varepsilon \qquad [6a]$$

or

$$y = a_0 + a_{1x1} + \cdots + a_{mxm} + \varepsilon \qquad [6b]$$

The above expressions are called simple linear regression and multiple linear regression, respectively (33).

For the current study, the following relationships are relevant, thus:

$$\text{Hardness-Value }_{(PREDICTED)} = T_P + Q_T \text{ (quantity of HDPEw) +}$$
$$P_H \text{ (tensile strength of composite) + FN (flexural strength of composite) +}$$
$$I_S \text{ (impact strength of composite)} \qquad [7]$$

where:

$T_P =$ Intercept on Hardness-Value $_{(PREDICTED)}$ axis.

$Q_T =$ Change in Hardness-Value $_{(PREDICTED)}$ for each increment change in quantity of HDPEw.

$P_H =$ Change in Hardness-Value $_{(PREDICTED)}$ for each increment change in tensile strength of composite.

$F_N =$ Change in Hardness-Value $_{(PREDICTED)}$ for each increment change in flexural strength of composite.

$I_S =$ Change in Hardness-Value $_{(PREDICTED)}$ for each increment change in impact strength of composite.

ANN$_S$ (Artificial Neural Networks)

ANN is a modelling approach inspired by the human nervous system that allows for learning by example from representative data describing a physical phenomenon or decision process (34). Artificial neural networks (ANN) are computational modelling methods that are rooted in statistics and imitate the ability of the human brain to acknowledge patterns profoundly (35). An ANN is made up of basic processing elements (called neurons), which are connected via synaptic weights (coefficients) and can learn a task by adjusting weights. These connections constitute the neuronal structure wherein the training and recall algorithms are linked (36). The sizes of ANNs, for instance, the number of artificial neurons can range from tens of thousands to only as little as less than ten [1-3] (37), while the structure of an artificial neural network consists of three interconnected layers namely: an input layer; a hidden layer; and an output layer (35). The interconnection of the various neurons in the network is referred to as the topology, architecture, or graph of an artificial neural network. The different interconnections lead to diverse possible topologies which can be broadly divided into two basic classes: Feed-forward (FNN) and Recurrent (RNN) topology (38). One unique feature of all ANN methods is their ability to work best when

dealing with non-linear dependence between the inputs and outputs (the ANN is capable of handling complex data sets with non-linear relationships and multiple variables (i.e., ≥ 3 variables) (35, 37). Artificial Neural Networks (ANN) have proven to be a versatile tool, successfully applied in various fields such as control engineering, medicine, industry, economics, biology, software engineering, environment and social studies (38). The ANN is trained to predict the output response based on the input values of the training data. With ANN, data collection is flexible, and the values can be chosen arbitrarily without specific criteria. The ANN will then train and discover non-linear patterns among the elements with one or a few specific responses (39). ANN's ability to establish empirical correlations between independent and dependent variables, and to extract delicate information and complicated knowledge from representative datasets, is a distinguishing characteristic. The ANN models provide several advantages over regression-based models, including the ability to handle noisy data, without making any assumptions about any mathematical representation of the phenomenon. The present study focused on the hardness of composite materials as the dependent variable. The independent variables included the filler and HDPEw compositions, as well as the tensile, flexural, and impact strengths of the composites being examined. To forecast the experimental hardness values of the produced composites, artificial neural networks were used, as shown in Figure 1 with the parameter estimates as presented in Table 1.
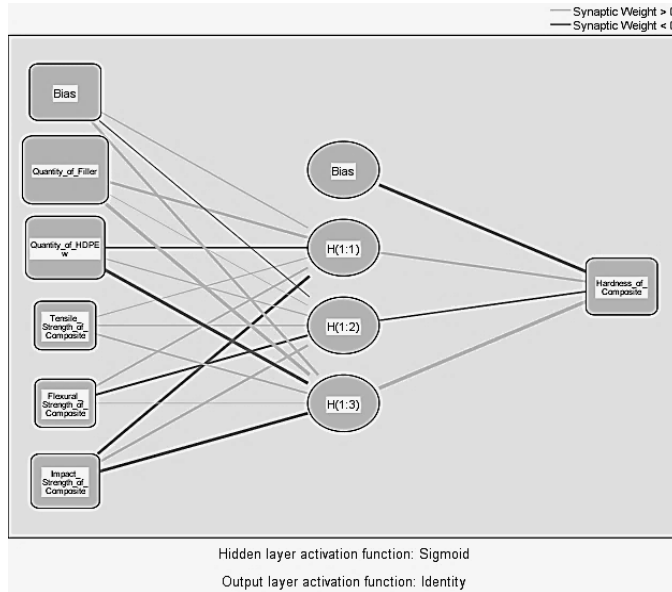
Figure 1. Diagram of artificial neural networks for forecasting the experimental hardness values of the produced composites.

With a unit, z in the output or hidden layer, the input (net), Iz, relating to the unit, z may be given thus (40–45):

$$Iz = \sum_i w_{iz} O_i + \emptyset_z \qquad [8]$$

where:

w_{iz} = the weight that connects unit i, in the previous layer to unit z.

O_i = unit i's output from the previous layer.

$\emptyset_z$ = the unit's bias. This moderates the unit's activity *(46)*.

Based on the net input Iz to unit z, the output of unit z can be obtained with the relationship below:

$$O_z = \frac{1}{1+e^{Iz}}$$ [9]

Table 1. Prediction of hardness values of the produced composites by artificial neural network

Independent Variable Importance			
Independent variables	**Importance**		
Quantity of Filler	0.414		
Quantity of HDPEw	0.316		
Tensile Strength of Composite	0.059		
Flexural Strength of Composite	0.049		
Impact Strength of Composite	0.162		
Parameter estimates for prediction			
Predictor		Predicted	
		Hidden Layer 1	Output Layer
		H(1:1) H(1:2) H(1:3)	Hardness of Composite
Input Layer	(Bias)	0.192 -0.118 0.418	
	Quantity of Filler	0.447 0.069 1.418	
	Quantity of HDPEw	-0.248 0.186 -1.104	
	Tensile Strength of Composite	0.140 0.210 0.285	
	Flexural Strength of Composite	0.314 -0.316 0.079	
	Impact Strength of Composite	-0.488 0.399 -0.571	
Hidden Layer 1	(Bias)		-1.061
	H(1:1)		0.348
	H(1:2)		-0.220
	H(1:3)		1.817

Error in prediction assessment

The mean squared error (MSE_{RR}) is often used to evaluate how close the predicted value is to the experimental value. It is expressed in mathematical form as:

$$MSE_{RR} = \frac{1}{N}\sum(S_i - T_i)^2$$ [10]

where:
N = the total number of samples tested.
T_i = the experimental value.
S_i = the predicted experimental value.

RESULTS AND DISCUSSION

CHARACTERIZATION OF SAMPLES

FTIR

The FTIR spectra obtained from the filler sample of the palm inter-fruitlet membrane showed distinctive peaks corresponding to various functional groups. The peaks at 1319.5, 1371.7, 1420.1, 1505.8, 1595.3, 2113.5, 2217.8, 2918.5, and 3336.0 cm^{-1} were the most noti-

ceable as shown in Figure 2. Specific functional groupings in the sample are represented by each peak. The peak at 1319.5 cm^{-1} is an indication that aromatic amines (C-N), alcohols, esters, and carboxylic acids (C-O) are present. This peak can also be used to infer medium stretching vibrations of nitro compounds (N-O). The spectrum at 1420.1 cm^{-1} indicates that the material contains medium-stretching vibrations of C-C aromatic rings while the peak at 1505.8 cm^{-1} suggests that (N-O) nitro compounds are responsible for significant stretching vibrations. The peaks at 1595.3 cm^{-1} show stretching vibrations of C-C aromatic rings, indicating the existence of aromatic chemicals in the palm inter-fruitlet membrane.
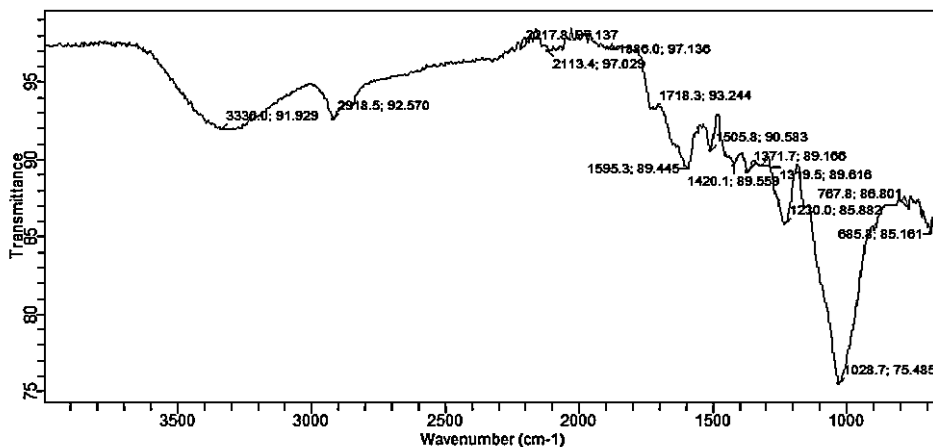
Figure 2. FTIR result of palm inter-fruitlet membrane filler.

Weak stretching vibrations indicating the existence of alkynes were identified to be linked to wavenumbers 2113.5 and 2217.8 cm^{-1}. The presence of the filler's (O-H) carboxylic acids, alcohols, and phenols exhibit stretching vibrations, as seen by the peaks at 2918.5 cm^{-1} and 3336.0 cm^{-1}. Also, the presence of functional groups, such as the hydroxyl, carbonyl, and carboxylic groups, which are significant structural properties of lignin (47), confirmed the existence of lignin in the filler. The discovery of lignin compounds in the filler sample points to their potential use as a renewable resource for a variety of applications, including the production of paper, and bio-based composites. The inter-fruitlet membrane fillers from palm trees need to be completely explored to maximize their use.

TGA result of palm inter-fruitlet membrane filler

The result of the weight loss behaviour of the palm inter-fruitlet membrane filler sample under-regulated heating conditions is shown in Figure 3. The sample was observed to gradually lose weight when it was heated from room temperature to around 200 °C. The first weight loss may be due to the moisture and volatile substances that were present in the sample evaporating.
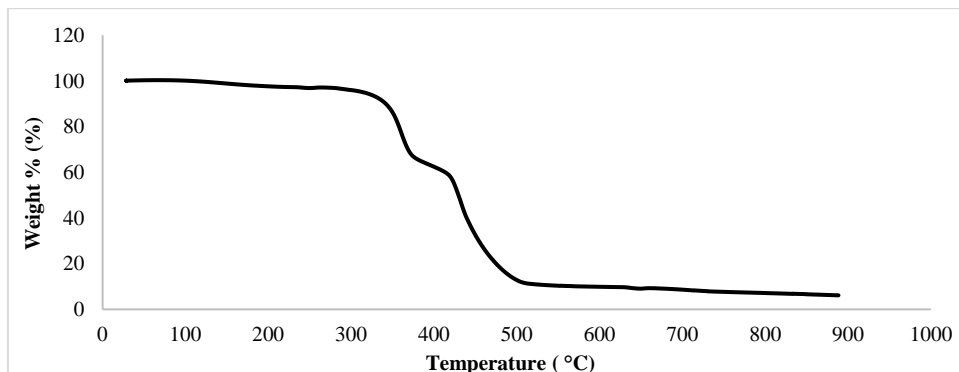
Figure 3. TGA result of the palm inter-fruitlet membrane filler

Noticeable weight loss was observed as the temperature increased from 250 °C to 550 °C, indicating that the organic components in the palm inter-fruitlet membrane filler have begun to decompose. Further breakdown of any lingering organic components was noticed after 550 °C. However, in comparison with the preceding breakdown stage, the weight loss after 550 °C weight loss was rather insignificant.

DTA RESULT OF PALM INTER-FRUITLET MEMBRANE FILLER

The DTA conducted on the palm inter-fruitlet membrane filler revealed a variety of thermal occurrences and transitions. A slight endothermic disposition was observed from the commencement of the DTA till the dip was reached at about 130 °C. The initial endothermic reaction may have led to the dehydration of the palm fruitlet membrane. Between 130 and 142 °C, the temperature of the filler was observed to be similar to that of the reference substance (alpha–alumina). This further denotes that both substances are being heated approximately under a commensurate condition. Furthermore, as the temperature increased from 140 to 220 °C, a slight exothermic effect was recorded as shown in Figure 4.
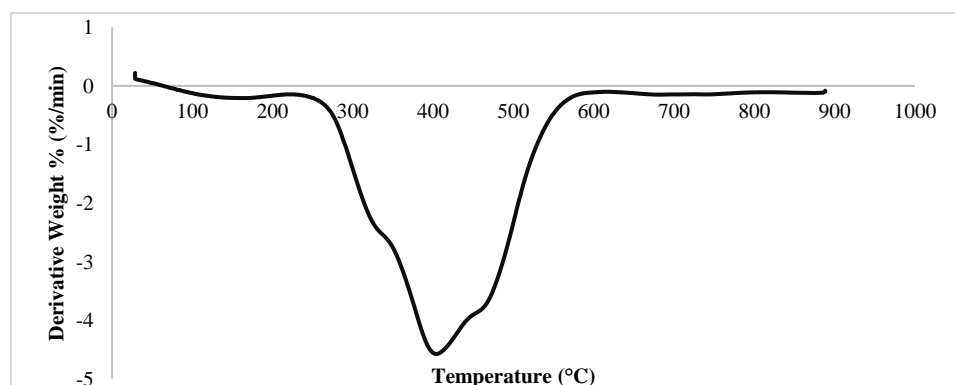
Figure 4. DTA result of the palm inter-fruitlet membrane filler

As the temperature increased from 220 °C to 400 °C the second endothermic reaction, which was noticeable was observed, with its dip reaching at about 401 °C. The endothermic effect may depict further dehydration, phase transformation, and possible decomposition of

the filler. A progressive exhibition of an exothermic reaction was observed as the temperature increased. Additional heating revealed a wide exothermic peak with a peak at around 600 °C indicating a phase change or breakdown process. Finally, a little exothermic peak was noticed at about 770 °C, signifying denoting that the breakdown process had reached its conclusion. In essence, the profile revealed that between 600 and 900 °C, both endothermic and exothermic reactions interchangeably occurred.

RESULTS OF MECHANICAL BEHAVIOUR, EXPERIMENTAL AND PREDICTED HARDNESS VALUES OF PALM INTER-FRUITLET MEMBRANE REINFORCED HDPEW COMPOSITES

Results of the mechanical performance of the examined composite samples and the predicted hardness values are presented in Tables 1-4 and shown in Figures 5 and 6. The mechanical characteristics of the examined composites were found to steadily increase in hardness values as the weight percentage of the reinforcing material increased. The composite formulation with 24 wt.% filler had the maximum hardness value, measuring 76.67 HV as shown in Figure 5, indicating exceptional mechanical qualities. On the other hand, 100 % HDPEw (control) recorded the least hardness value of 60.83 HV.

Table 2. Results of mechanical behaviour, experimental and predicted hardness values of palm inter-fruitlet membrane reinforced HDPEw composites

Formulation of composites (Test pieces)		Mechanical properties of specimens				Prediction of Composite's Hardness by ANN		Prediction of Composite's Hardness by MR	
Inter-fruitlet membrane filler (wt.%)	HDPEw (wt.%)	Tensile strength (MPa)	Flexural strength (MPa)	Impact strength (J/mm^2)	Hardness (HV)	ANN (HV)	Error	R (HV)	Error
0	100	18.56	36.59	0.4217	60.83	62.75	-1.92	60.83	0
6	94	21.31	36.87	0.4778	66.7	65.25	1.45	66.70	0
12	88	25.38	41.87	0.4979	72.73	71.58	1.15	72.73	0
18	82	39.04	40.00	0.2539	75.3	75.66	-0.36	75.30	0
24	76	17.65	36.88	0.2023	76.67	75.86	0.81	76.67	0
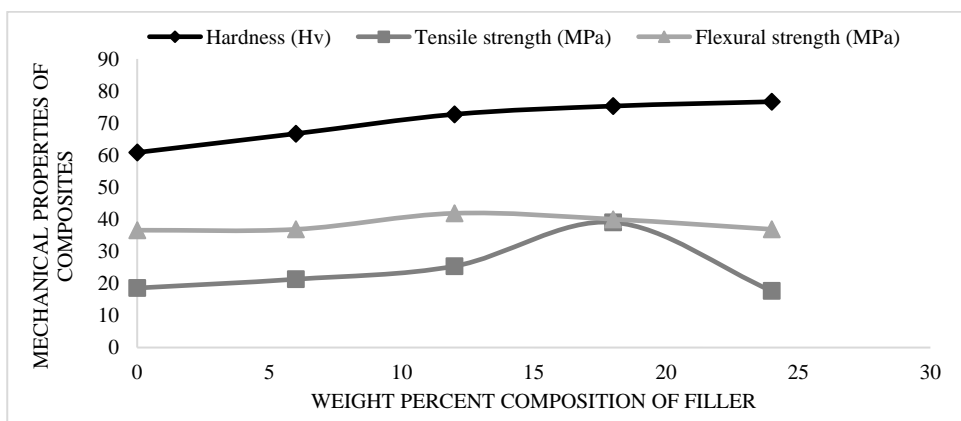
Figure 5. Effect of weight per cent composition of filler on the hardness value, tensile, flexural, and impact strengths of the produced composites

Both tensile and flexural strengths of the composite samples exhibited a similar trend by increasing as the weight per cent composition of the filler increased in the first instance, but started to decrease after a certain quantity of the filler was added. For the flexural strength, the highest value of 41.87 MPa was recorded for the composite formulation of 12 wt.% filler. Subsequently, the flexural strengths were further reduced to 40 MPa and 36.88 MPa as the content of the filler in the composite increased from 18 wt.% to 24 wt.%. The same trend was also recorded for the flexural modulus.

For the tensile strengths of the produced composites, a gradual increase in strength was observed until the composite formulation of 12 wt.% filler gave a strength of 25.38 MPa. The highest tensile strength of 39.04 MPa was exhibited by the composite with 18 wt.% filler content. However, a noticeable decrease in strength to 17.65 MPa was observed for the composite formulation having 24 wt.% filler. It was later discovered from the SEM micrograph that the arrangement of the reinforcement filler was directional within the HDPEw matrix. This development may have been the cause of the decline in tensile strength.

Furthermore, the impact strength of the produced composite showed a slight increase from 0.4217 J/mm^2 when no filler was added, through 0.4778 J/mm^2 at 6 wt.% filler to the maximum impact strength of 0.4979 J/mm^2 for the composite formulation of 12 wt.% filler as shown in Figure 6.
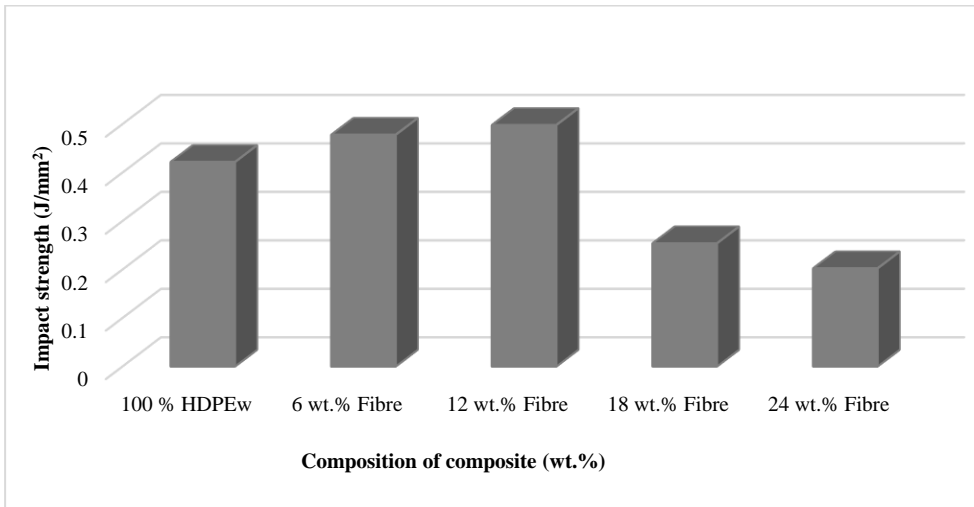
Figure 6. Effect of the addition of the palm inter-fruitlet membrane filler on the impact strength of the produced composites

Further addition of the filler drastically reduced the impact strength to 0.2539 J/mm^2 for the composite with 18 wt.% filler content. Consequently, the composite composition with the highest quantity of filler (24 wt.% filler) gave the lowest impact strength.

PREDICTION OF HARDNESS VALUE OF COMPOSITE BY ANN AND MR

The prediction of experimental hardness values of the produced composites was achieved by MR and ANN. The hardness values that were predicted are presented in Table 2. In essence, the use of multiple regression led to the establishment modelling (Table 3) of the predictive equation:

Hardness value (PREDICTED) = 127.947 – 0.792 (Quantity of HDPEw) +   [11]
0.108 (Tensile Strength of Composite) + 0.112 (Flexural Strength of Composite) +
4.406 (Impact Strength of Composite)

The prediction of the experimental hardness value was found to be majorly influenced by the filler quantity (41.4%), followed by the polymer-matrix composition (31.6%), impact strength (16.2%), tensile strength (5.9%), and flexural strength (4.9%) of the produced composite according to the artificial network modelling protocol as presented in Table 1.

Table 3. Predictive model for the hardness of the produced composite

Predicted composite behaviour	Constant	Model coefficients			
		Quantity of HDPEw (wt.%)	Tensile Strength of Composite (MPa)	Flexural Strength of Composite (MPa)	Impact Strength of Composite (J/mm²)
Hardness	127.947	- 0.792	0.108	0.112	4.406

The analysis to unravel how close the predicted value was to the experimental value was achieved by the mean squared error [MSE_{RR}] (Table 4 and Figure 7). Figure 6 shows the error observed in predicting the experimental hardness value of the produced composite by ANN and MR.

Table 4. Error assessment of predicted hardness values of the produced composites using mean squared error (MSE_{RR})

Error assessment method	Prediction of composite's hardness by ANN	Prediction of composite's hardness by MR
MSE_{RR}	0.2554	0
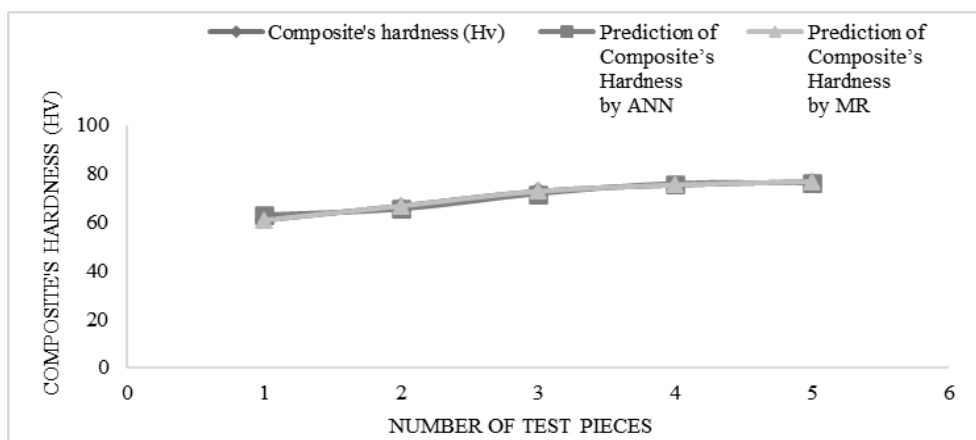
Figure 7. Comparison in error for predicting the experimental hardness values of the produced composites.

The results of the mean squared error as shown in Figure 6 indicated that the composite's hardness predictions by multiple regression were more accurate than those that were obtained by ANN. This outcome could be occasioned by the relative linearity of the examined variables. It can be deduced that multiple linear regression can accurately predict linear relationships better than artificial neural networks. However, artificial neural networks have been reported to be amenable to accurately predicting complex and nonlinear relationships (35, 37).

<div align="center">

RESULT OF WATER ABSORPTION TEST ON TEST SPECIMENS

</div>

Results of the water absorption tests conducted on the produced palm inter-fruitlet membrane filler-reinforced composites are presented in Table 5 and shown in Figure 8. Water absorption was observed to increase with the increase in the quantity of the composite's filler content. The HDPEw (control) sample was observed to absorb the least water.

Table 5. A summary of water absorption of palm inter-fruitlet membrane reinforced HDPEw composites

Time of immersion (h)	Water absorption (%)				
	100 % HDPEw	6 wt.% Filler	12 wt.% Filler	18 wt.% Filler	24 wt.% Filler
24	0	0.0347102	0.1023367	0.4989677	0.489083
48	0	0.1387925	0.1022321	0.1198425	0.1390579
72	0	0.1905752	0.2893617	0.0341997	0.2256553
96	0.0688231	0.0864603	0	0.3931624	0.3117423
120	0.0343879	0	0	0.0170271	0.086326
144	0.017188	0	0.0169722	0	0
168	0	0	0	0	0.0172503
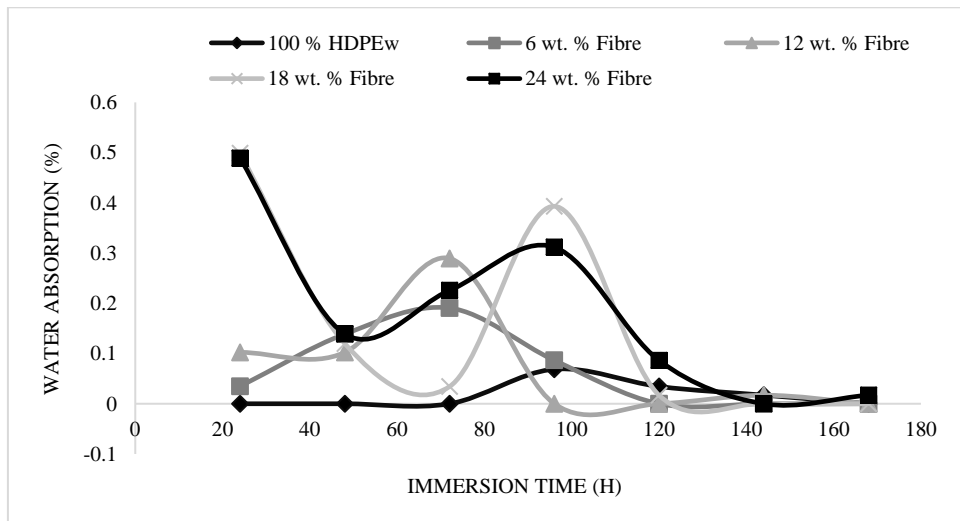
Figure 8. Result of water absorption of palm inter fruitlet membrane reinforced HDPEw composites

The water absorption of the composites was observed to be higher in comparison with the HDPEw matrix after 24 hours with approximately 0.499 % and 0.489 % values for composites containing 18 wt.% and 24 wt.% filler contents respectively. From the commencement of the test to about 72h, the HDPEw (control) showed insignificant per cent water absorption. However, the water absorption of other composites continued to increase. After 96 h, the absorption of water by the composites was found to decline as shown in Figure 8.

This observation of an increase in water absorption by the composites suggests that they can be suitably used for household ceilings and tabletops. The improved hardness of the composite is a favourable attribute for a wider application of the composite. Hence the conversion of the so-called wastes to useful products.

SEM MORPHOLOGY OF THE PALM INTER FRUITLET MEMBRANE REINFORCED HDPEw COMPOSITES

The SEM micrographs of all the examined composites are represented in Figure 9. The HDPEw [control] (Figure 9a) was observed to be blank without showing any presence of the filler material. The introduction of the reinforcing material led to the uneven distribution of the palm inter-fruitlet membrane filler within the HDPEw matrix as shown in Figure 9b.
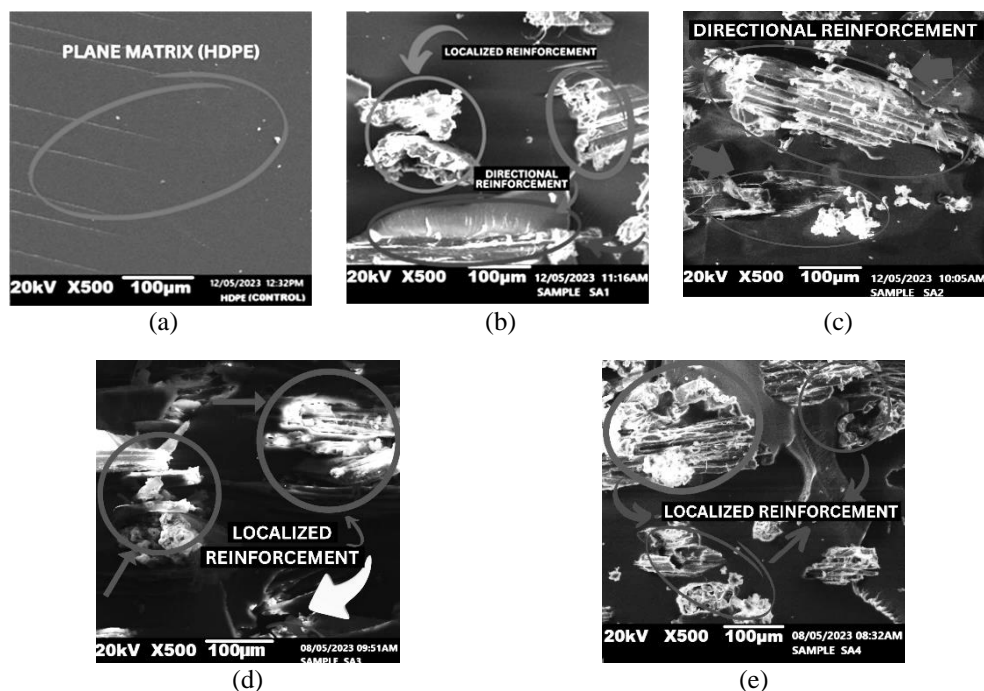
Figure 9. SEM micrographs of the produced composites: (a) 100wt.% HDPEw [control] (Yogurt Can wastes); (b) 6 wt.% filler and 94 wt.% matrix; (c) 12 wt.% filler and 88 wt.% matrix; (d) 18 wt.% filler and 82 wt.% matrix; (e) 24 wt.% filler and 76 wt.% matrix

The filler compositions in the composite with 12 wt.% (Figure 9c) and 18 wt.% (Figure 9d) filler materials were found to be relatively directionally and locally distributed across

the matrixes. This development may have been the cause of the increased tensile and flexural strength values that were recorded by the two sets of composites. On the other hand, the SEM image of the composite formulation with 24 wt.% filler (Figure 9e) showed a combination of minimal directional and localized arrangements of the reinforcement material along certain parts of the composite. This arrangement of the palm inter-fruitlet membrane filler within the HDPEw matrix may have led to a decrease in the mechanical behaviour of the composite.

CONCLUSIONS

The following conclusions can be drawn from the current study on the prediction of hardness of palm inter-fruitlet membrane reinforced high-density polyethylene-waste (HDPEw) composites:

1. The presence of substantial functional groups, such as alcohol hydroxyl, phenolic hydroxyl, and carbonyl groups, as determined by the FTIR analysis, indicated the existence of lignin in the reinforcing material.
2. Weight loss from moisture and degradation of the filler's organic components were discovered by the TGA analysis. The DTA study revealed a variety of thermal occurrences and transitions that suggested dehydration, phase change, and filler disintegration.
3. The hardness values of the mechanical properties of the composite specimens were observed to steadily rise as the weight per cent filler in the produced composites increased. The composite with the highest hardness value of 76.67 HV was obtained by the composite with 24 wt.% filler. According to other findings, the addition of the palm inter-fruitlet membrane filler increased flexural, impact, and tensile strengths up to a certain wt.% filler composition, above which a decline in strength was recorded. The composite formulation with 12 wt.% filler produced the highest flexural and impact strengths of 41.87 MPa and 0.4979 J/mm respectively. On the other hand, the composite composition with 18 wt.% filler yielded the maximum tensile strength of 39.04 MPa. Despite having the maximum hardness value, the composite with 24 weight per cent filler had the lowest tensile and impact strengths.
4. The composites' water absorption behaviour was observed to increase with an increase in the filler content. The composite containing 24 wt.% filler was observed to have the maximum water uptake after 24 hours.
5. SEM micrographs demonstrated the filler's uneven dispersion inside the HDPEw matrix. The rather equal dispersion of the filler in the composites with 12 and 18 wt.% fillers improved their mechanical characteristics. However, the 24 wt.% filler composites' flexural, tensile and impact strengths declined due to their directional reinforcing disposition.
6. Based on the mean squared error results, it can be concluded that the predictions of the examined composite's hardness values were more precise when obtained through multiple regression than when obtained through ANN. This outcome is likely because the examined variables were relatively linear. Therefore, it can be inferred that multiple linear regression is better suited for predicting linear relationships in comparison with artificial neural networks.

KEY APPLICATION AREAS OF THE PRODUCED COMPOSITES

Previous studies have identified a possible application of fibre reinforced composites in the acoustic industry. Furthermore, the interaction between additives in the polymer matrix

is critical in defining mechanical, thermal, and acoustic characteristics, according to research on polymer additives and interfacial adhesion. In particular, the reduction in interfacial adhesion between the polymer matrix and natural fibers should be addressed in future study aimed at better understanding and managing this connection. It has been proposed that combining several natural fiber kinds to produce hybrid composites improves their tensile and flexural qualities (48). The development of hybrid composites to maximize sound absorption qualities should be the main focus of future research.

Automobile parts can be made using the composites that were produced. Natural fiber reinforced composites (NFRCs) are typically employed in interior automobile components due to their inherent susceptibility to moisture and their comparatively poor mechanical characteristics. NFRCs may be found in a variety of nonstructural interior components, including indoor panels, dashboards, floor mats, package shelves, and storage bins (49).

Multilayer ballistic armor can be made from the composites which were produced. According to Haro et al. (50), the bio-composite with microparticles of chonta palm wood showed the best mechanical performance under both quasi-static tensile and dynamic compression loading, as well as the maximum ballistic impact resistance. These findings imply that the mechanical characteristics and ballistic resistance of the polymer are enhanced by the deposition of wood palm microparticles in a polymeric matrix (HDPE), producing biocomposites that perform better than unreinforced HDPE.

RECOMMENDATION

Following the observed reduction in flexural and tensile strengths of the composite with 24 wt.% filler composition which invariably was as a result of the directional filler arrangement within the HDPEw matrix, it is recommended that further studies be conducted to checkmate directional filler arrangement within the polymer matrix.

REFERENCES

1. Patel, R. M. 2 - Polyethylene. In *Multilayer Flexible Packaging (Second Edition)*. Wagner, J. R., Ed.; Plastics Design Library; William Andrew Publishing, 2016; pp 17–34. doi:10.1016/B978-0-323-37100-1.00002-8.

2. Ronca, S. Chapter 10 - Polyethylene. In *Brydson's Plastics Materials (Eighth Edition)*. Gilbert, M., Ed.; Butterworth-Heinemann, 2017; pp 247–278. doi:10.1016/B978-0-323-35824-8.00010-4.

3. Ghatge, S.; Yang, Y.; Ahn, J.-H.; Hur, H.-G. Biodegradation of polyethylene: a brief review. *Applied Biological Chemistry* **2020**, *63*(1), 27. doi:10.1186/s13765-020-00511-3.

4. Babayemi, J. O.; Nnorom, I. C.; Osibanjo, O.; Weber, R. Ensuring sustainability in plastics use in Africa: consumption, waste generation, and projections. *Environmental Sciences Europe* **2019**, *31*(1), 60. doi:10.1186/s12302-019-0254-5.

5. Chamas, A.; Moon, H.; Zheng, J.; Qiu, Y.; Tabassum, T.; Jang, J. H.; et al. Degradation Rates of Plastics in the Environment. *ACS Sustainable Chemistry & Engineering* **2020**, *8*(9), 3494–3511. doi:10.1021/acssuschemeng.9b06635.

6. Ndukwe, A. I.; Umoh, S.; Ugwochi, C.; Ogbuji, C.; Ngolube, C.; Aliegu, F.; et al. Prediction of compression strength of bamboo reinforced low-density polyethylene waste (LDPEw) composites. *Composites theory and practice* **2022**, *22*(3).

7. Kumar, R.; Verma, A.; Shome, A.; Sinha, R.; Sinha, S.; Jha, P. K.; et al. Impacts of Plastic Pollution on Ecosystem Services, Sustainable Development Goals, and Need to Focus on Circular Economy and Policy Interventions. *Sustainability* **2021**, *13*(17), 9963. doi:10.3390/su13179963.

8. Kibria, Md. G.; Masuk, N. I.; Safayet, R.; Nguyen, H. Q.; Mourshed, M. Plastic Waste: Challenges and Opportunities to Mitigate Pollution and Effective Management. *International Journal of Environmental Research* **2023**, *17*(1), 20. doi:10.1007/s41742-023-00507-z.

9. Yao, Z.; Seong, H. J.; Jang, Y.-S. Environmental toxicity and decomposition of polyethylene. *Ecotoxicology and Environmental Safety* **2022**, *242*, 113933. doi:10.1016/j.ecoenv.2022.113933.

10. Ncube, L. K.; Ude, A. U.; Ogunmuyiwa, E. N.; Zulkifli, R.; Beas, I. N. An Overview of Plastic Waste Generation and Management in Food Packaging Industries. *Recycling* **2021**, *6*(1), 12. doi:10.3390/recycling6010012.

11. Uje. *The negative environmental effects of plastic shopping bags*. <https://www.ibanet.org/article/ 76F8D2A9-1A1D-4A2F-8A6F-0A70149FD4D5> Accessed 23.07.21.

12. Arif, M. F.; Yusoff, P. S. M. M.; Eng, K. K. Effect of Reinforcement Shape and Fiber Treatment on the Mechanical Properties of Oil Palm Empty Fruit Bunch-Polyethylene Composites. *AIP Conference Proceedings* **2010**, *1217*(1), 335–340. doi:10.1063/1.3377839.

13. Kakou, C. A.; Arrakhiz, F. Z.; Trokourey, A.; Bouhfid, R.; Qaiss, A.; Rodrigue, D. Influence of coupling agent content on the properties of high density polyethylene composites reinforced with oil palm fibers. *Materials & Design* **2014**, *63*, 641–649. doi:10.1016/j.matdes.2014.06.044.

14. 14. ZULNAZRI; SURYATI; AZHARI; Wirjosentono, B.; Dahliana, H. High density polyetylene (HDPE) - oil palm empty fruit bunch filled micro composites using melt blending process. *Proceedings of The Annual International Conference, Syiah Kuala University - Life Sciences & Engineering Chapter* **2014**, *4*(1), 65–71.

15. Noah, A. S. Oil Palm Empty Fruit Bunches (OPEFB) – Alternative Fibre Source for Paper-making. In *Elaeis guineensis*; IntechOpen, 2022. doi:10.5772/intechopen.98256.

16. Han, J.; Kim, J. Process Simulation and Optimization of 10-MW EFB Power Plant. In *Computer Aided Chemical Engineering*. Friedl, A., Klemeš, J. J., Radl, S., Varbanov, P. S., Wallek, T., Eds.; 28 European Symposium on Computer Aided Process Engineering; Elsevier, 2018; Vol. 43, pp 723–729. doi:10.1016/B978-0-444-64235-6.50128-5.

17. Foo, D. C. Y.; Tan, R. R.; Lam, H. L.; Kamal, M.; Klemeš, J. J. Synthesis of Flexible Palm Oil-Based Regional Energy Supply Chain. In *Computer Aided Chemical Engineering*. Pistikopoulos, E. N., Georgiadis, M. C., Kokossis, A. C., Eds.; 21 European Symposium on Computer Aided Process Engineering; Elsevier, 2011; Vol. 29, pp 2014–2018. doi:10.1016/B978-0-444-54298-4.50181-1.

18. Majesty, K. I.; Herdiansyah, H. The Empty Palm Oil Fruit Bunch as the Potential Source of Biomass in Furfural Production in Indonesia: Preliminary Process Design and Environmental Perspective. *Journal of Physics: Conference Series* **2019**, *1363*(1), 012096. doi:10.1088/1742-6596/1363/1/012096.

19. Yiin, C. L.; Ho, S.; Yusup, S.; Quitain, A. T.; Chan, Y. H.; Loy, A. C. M.; et al. Recovery of cellulose fibers from oil palm empty fruit bunch for pulp and paper using green delignification approach. *Bioresource Technology* **2019**, *290*, 121797. doi:10.1016/j.biortech.2019.121797.

20. Kresnowati, M.; Mardawati, E.; Setiadi, T. Production of Xylitol from Oil Palm Empty Friuts Bunch: A Case Study on Bioinefinery Concept. *Modern Applied Science* **2015**, *9*(7), p206. doi:10.5539/mas.v9n7p206.

21. Susi, S.; Ainuri, M.; Wagiman, W.; Falah, M. A. F. High-Yield Alpha-Cellulose from Oil Palm Empty Fruit Bunches by Optimizing Thermochemical Delignification Processes for Use as Microcrystalline Cellulose. *International Journal of Biomaterials* **2023**, *2023*, e9169431. doi:10.1155/2023/9169431.

22. Rosenani, A. B.; Hoe, S. F. Decomposition of oil palm empty fruit bunches in the field and mineralization of nitrogen. In *Progress in Nitrogen Cycling Studies: Proceedings of the 8th Nitrogen Workshop held at the University of Ghent, 5–8 September, 1994*. Van Cleemput, O., Hofman, G., Vermoesen, A., Eds.; Developments in Plant and Soil Sciences; Springer Netherlands: Dordrecht, 1996; pp 127–132. doi:10.1007/978-94-011-5450-5_20.

23. Januari, A. D.; Agustina, H. Palm Oil Empty Fruit Bunches and The Implementation of Zero Waste and Renewable Energy Technologies. *IOP Conference Series: Earth and Environmental Science* **2022**, *1034*(1), 012004. doi:10.1088/1755-1315/1034/1/012004.

24. Adu, M. O.; Atia, K.; Arthur, E.; Asare, P. A.; Obour, P. B.; Danso, E. O.; et al. The use of oil palm empty fruit bunches as a soil amendmentto improve growth and yield of crops. A meta-analysis. *Agronomy for Sustainable Development* **2022**, *42*(2), 13. doi:10.1007/s13593-022-00753-z.

25. Hashim, M. M.; Marsi, N.; Rus, A. Z. M.; Sharom, N. S. M.; Said, A. M. Natural Fiber of Palm Empty Fruit Bunches (PEFB) Reinforced Epoxy Resin as Polymer Composites. In *Structural Integrity and Monitoring for Composite Materials*. Ariffin, A. H., Latif, N. A., Mahmod, M. F. bin, Mohamad, Z. B., Eds.; Composites Science and Technology; Springer Nature: Singapore, 2023; pp 213–242. doi:10.1007/978-981-19-6282-0_14.

26. Amir, S. M. M.; Sultan, M. T. H.; Jawaid, M.; Ariffin, A. H.; Ishak, M. R.; Yusof, M. R.; et al. Effect of Gamma Radiation on Compressive Properties of Kevlar/Oil Palm Empty Fruit Bunch Hybrid Composites. *BioResources* **2018**, *13*(4), 7628–7639.

27. Čaplová, Z.; Švábová, P. Chapter 7.1 - IBM SPSS statistics. In *Statistics and Probability in Forensic Anthropology*. Obertová, Z., Stewart, A., Cattaneo, C., Eds.; Academic Press, 2020; pp 343-352. doi:10.1016/B978-0-12-815764-0.00027-7.

28. Software?, W. I. S. *IBM SPSS Statistics | IBM*. <https://www.ibm.com/products/spss-statistics> Accessed 23.08.12.

29. Orme, J. G.; Buehler, C. Introduction to multiple regression for categorical and limited dependent variables. *Social Work Research* **2001**, *25*(1), 49–61. doi:10.1093/swr/25.1.49.

30. 30. Nimon, K.; Lewis, M.; Kane, R.; Haynes, R. M. An R package to compute commonality coefficients in the multiple regression case: An introduction to the package and a practical example. *Behavior Research Methods* **2008**, *40*(2), 457–466. doi:10.3758/BRM.40.2.457.

31. Kuiper, S. Introduction to Multiple Regression: How Much Is Your Car Worth? *Journal of Statistics Education* **2008**, *16*(3), 10. doi:10.1080/10691898.2008.11889579.

32. Gareen, I. F.; Gatsonis, C. Primer on Multiple Regression Models for Diagnostic Imaging Research. *Radiology* **2003**, *229*(2), 305–310. doi:10.1148/radiol.2292030324.

33. Bargiela, A.; Pedrycz, W.; Nakashima, T. Multiple regression with fuzzy data. *Fuzzy Sets and Systems* **2007**, *158*(19), 2169–2188. doi:10.1016/j.fss.2007.04.011.

34. Sadiq, R.; Rodriguez, M. J.; Mian, H. R. Empirical Models to Predict Disinfection By-Products (DBPs) in Drinking Water: An Updated Review☆. In *Encyclopedia of Environmental Health (Second Edition)*. Nriagu, J., Ed.; Elsevier: Oxford, 2019; pp 324–338. doi:10.1016/B978-0-12-409548-9.11193-5.

35. Xia, X.; Nie, J. F.; Davies, C. H. J.; Tang, W. N.; Xu, S. W.; Birbilis, N. An artificial neural network for predicting corrosion rate and hardness of magnesium alloys. *Materials & Design* **2016**, *90*, 1034–1043. doi:10.1016/j.matdes.2015.11.040.

36. Shanmuganathan, S. Artificial Neural Network Modelling: An Introduction. In *Artificial Neural Network Modelling*. Shanmuganathan, S., Samarasinghe, S., Eds.; Studies in Computational Intelligence; Springer International Publishing: Cham, 2016; Vol. 628, pp 1–14. doi:10.1007/978-3-319-28495-8_1.

37. Zupan, J. Introduction to Artificial Neural Network (ANN) Methods: What They Are and How to Use Them. *Acta Chimica Slovenica* **1994**, 327–352.

38. Suzuki, K. *Artificial Neural Networks - Mthodological Advances and Biomedical Applications*; InTech, 2011.

39. Chung, N. T.; Choi, S.-R.; Kim, J.-G. Comparison of Response Surface Methodologies and Artificial Neural Network Approaches to Predict the Corrosion Rate of Carbon Steel in Soil. *Journal of The Electrochemical Society* **2022**, *169*(5), 051503. doi:10.1149/1945-7111/ac700d.

40. Ndukwe, A. I.; Anyakwo, C. N. Modelling of corrosion inhibition of mild steel in hydrochloric acid by crushed leaves of sida acuta (malvaceae). *The International Journal Of Engineering And Science* **2017**, *6*(1), 22–33.

41. Ndukwe, A. I.; Anyakwo, C. N. Predictive model for corrosion inhibition of mild steel in HCl by crushed leaves of clerodendrum splendens. *International Research Journal of Engineering and Technology* **2017**, *4*(2), 679–688.

42. Ndukwe, A. I.; Anyakwo, C. N. Modelling of corrosion inhibition of mild steel in sulphuric acid by thoroughly crushed leaves of voacanga Africana (apocynaceae). *American Journal of Engineering Research* **2017**, *6*(1), 344–356.

43. Ndukwe, A. I.; Anyakwo, C. N. Predictive Corrosion-Inhibition Model for Mild Steel in Sulphuric Acid (H₂SO₄) by Leaf-Pastes of Sida Acuta Plant. *Journal of civil, construction and environmental engineering* **2017**, *2*(5), 123–133. doi:10.11648/j.jccee.20170205.11.

44. Ndukwe, A. I.; Ihuoma, S. O.; Akuwudike, C.; Oluehi, D. O.; Akaneme, F. A.; Chibiko, E. U. Predictive model for the corrosion inhibition of mild steel in 1.5 m HCl by the leaf-juice of Carica papaya. *Zastita materijala,* **2023**, *64*(4), 413-423.

45. Anyakwo, C. N.; Ndukwe, A. I. Mathematical model for corrosion inhibition of mild steel in hydrochloric acid by crushed leaves of tridaxprocumbens (asteraceae). *International Journal of Science and Engineering Investigations* **2017**, *6*(65), 81–89.

46. Han, J.; Kamber, M.; Pei, J. *Data Mining: Concepts and Techniques - 3rd Edition*. https://shop.elsevier.com/books/data-mining-concepts-and-techniques/han/978-0-12-381479-1 Accessed 23.09.10.

47. El Mansouri, N.-E.; Salvadó, J. Analytical methods for determining functional groups in various technical lignins. *Industrial Crops and Products* **2007**, *26*(2), 116–124. doi:10.1016/j.indcrop.2007.02.006.

48. Mohammadi, M.; Taban, E.; Tan, W. H.; Che Din, N. B.; Putra, A.; Berardi, U. Recent progress in natural fiber reinforced composite as sound absorber material. *Journal of Building Engineering* **2024**, *84*, 108514. doi:10.1016/j.jobe.2024.108514.

49. Li, M.; Pu, Y.; Thomas, V. M.; Yoo, C. G.; Ozcan, S.; Deng, Y.; et al. Recent advancements of plant-based natural fiber–reinforced composites and their applications. *Composites Part B: Engineering* **2020**, *200*, 108254. doi:10.1016/j.compositesb.2020.108254.

50. Haro, E. E.; Szpunar, J. A.; Odeshi, A. G. Dynamic and ballistic impact behavior of biocomposite armors made of HDPE reinforced with chonta palm wood (Bactris gasipaes) microparticles. *Defence Technology* **2018**, *14*(3), 238–249. doi:10.1016/j.dt.2018.03.005.

SYNTHESIS, STRUCTURAL AND ELECTRICAL STUDIES OF Li-Ni-Zn FERRITES SYNTHESIZED BY SOLID STATE REACTION METHOD

S. U. DURGADSIMI[1] [ID]*, V. R. KATTIMANI[2]* [ID]*, N. S. MARUTI[3]* [ID]*, A. B. KULKARNI[4]** [ID]*,
K. A. KULKARNI[4] [ID]*, S. N. MATHAD[5]* [ID]*, V. G. HIREMATH[6]* [ID]

[1] Department of Physics, Basaveshwar Engineering College, Bagalkot, Karnataka, India.
[2] Department of Chemistry, Basaveshwar Engineering College, Bagalkot, Karnataka, India.
[3] Department of Physics, KRCES GGD Arts BMP Commerce and SVS Science college,
Bailhongal, Karnataka, India.
[4] Department of Physics, SKE Society's Govindram Seksaria Science College, Belagavi, Karnataka, India.
[5] Department of Physics, K.L.E Institute of Technology, Hubballi, Karnataka, India.
[6] Department of Mathematics, K.L.E Institute of Technology, Hubballi, Karnataka, India.

The $Li_{0.5}Ni_{0.6}Zn_{0.15}Fe_2O_4$ (Q), $Li_{0.5}Ni_{0.5}Zn_{0.25}Fe_2O_4$ (R) ferrite samples have been synthesized by solid state reaction method. X-ray diffraction (XRD) pattern confirms the formation of cubic spinel structure with lattice constants 8.378, 8.397 Å respectively. The scanning electron microscopy (SEM) images show grain size in the range of few micrometres with variety of structures. The Fourier transform infrared spectroscopy (FTIR) spectrum of both samples show two (v_1 and v_2) significant absorption bands, corresponding to metal oxygen vibration at tetrahedral (A) and octahedral (B) interstitial sites respectively. The Cole-Cole plots show the electrical conductivity is mainly due to grains in both samples.

Keywords: XRD, SEM, FTIR, Cole-Cole plot.

INTRODUCTION

Ferrites having a general chemical formula of AB_2O_4 with spinel structure are having wide range of applications in the field of material science due to their versatile properties (1). Structural, electrical and magnetic properties of ferrites are dependent on synthesis conditions, size of particles, cation distribution at tetrahedral and octahedral sites and metal ions in composition (2). The nickel ferrite composites are having large number of applications due to its very high stability, good resistivity, good retentivity, good coercivity, optimum saturation magnetization (3-4). The nickel ferrite composites are found to be good material in applications like catalytic activity (5), magnetic shielding (6), magnetic core, memory storage devices (7), gas sensor (8), microwave devices (9) etc. Nickel ferrites with Zn substitution show better saturation magnetization; improvising magnetic properties in terms of storage of energy (10). Lithium substitution reduces magnetic losses (11). The present work is an attempt to synthesize using low cost and environment friendly solid-state reaction method (12-13) and conduct structural and electrical studies of $Li_{0.5}Ni_{0.6}Zn_{0.15}Fe_2O_4$ (Q), $Li_{0.5}Ni_{0.5}Zn_{0.25}Fe_2O_4$ (R) ferrite composites.

EXPERIMENTAL

High-purity AR grade Li_2O_3, NiO, ZnO, and Fe_2O_3 powders are used as starting materials. The oxides were taken in adequate amounts and ground for 4 h in an agate mortar in

---

* Corresponding author: Akshay B. Kulkarni, e-mail: akshayk.kud@gmail.com

acetone medium. The above mixtures were sintered at 900 °C for 10 h. Resultant fine pow-
ders were milled again in an agate mortar for 2–3 h, mixed with 2–3 drops of poly-vinyl al-
cohol as a binder, and compacted into pellets 10 mm under a pressure of about 7 ton/inch^2.
The schematic diagram of synthesis is shown in Fig. 1.
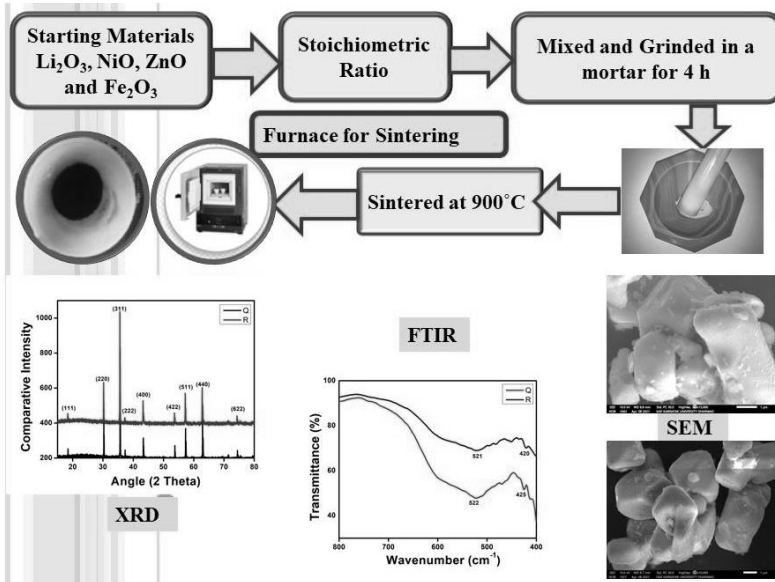
Figure 1: Schematic diagram of synthesis and characterization of $Li_{0.5}Ni_{0.6}Zn_{0.15}Fe_2O_4$ (Q),
$Li_{0.5}Ni_{0.5}Zn_{0.25}Fe_2O_4$ (R) ferrite samples.

RESULT AND DISCUSSION
X-RAY DIFFRACTION ANALYSIS
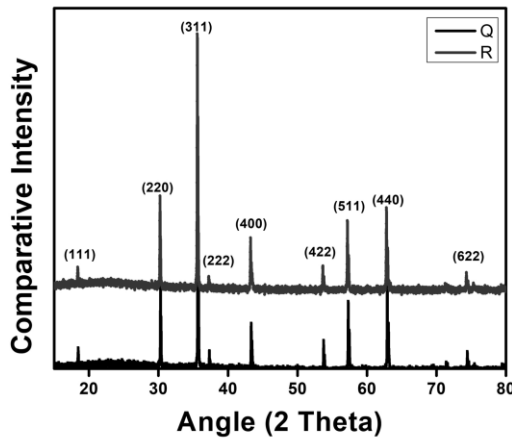
Figure 2: XRD pattern of $Li_{0.5}Ni_{0.6}Zn_{0.15}Fe_2O_4$ (Q), $Li_{0.5}Ni_{0.5}Zn_{0.25}Fe_2O_4$ (R) ferrite
samples.

XRD pattern of synthesized $Li_{0.5}Ni_{0.6}Zn_{0.15}Fe_2O_4$ (Q), $Li_{0.5}Ni_{0.5}Zn_{0.25}Fe_2O_4$ (R) ferrite samples is shown in Figure 2. Indexing of the peaks in XRD pattern is done by JCPDS (Joint Committee on Powder Diffraction Standards) card no. 10-0325. Analysis of XRD pattern using Bragg's reflection planes (111), (220), (311), (222), (400), (422), (511), (440) and (622) indicates the formation of cubic spinel structure. Interplanar spacing is calculated using Bragg's equation (12-13) given by equation [1].

$$n\lambda = 2d\sin\theta \tag{1}$$

where 'n' is order of diffraction, λ wavelength of x rays (0.154nm) and 'd' is interplanar spacing. For cubic spinel structure, interplanar spacing in terms of Miller indices is given by the equation:

$$d = \frac{a}{\sqrt{h^2 + k^2 + l^2}} \tag{2}$$

In X-ray diffraction the formula which relates the crystallite size to the broadening of a peak in diffraction pattern is Debye-Scherrer's formula which is given by the equation:

$$D = \frac{0.9\lambda}{\beta\cos\theta} \tag{3}$$

where D is average crystallite size, λ wavelength of incident X-ray and β angular line width of half maximum intensity (FWHM).

Dislocation density (δ) represents the amount of defects in the sample and is calculated using equation [4]:

$$\delta = \frac{1}{D^2} \tag{4}$$

The micro-strain is defined as the deformation of an object divided by its effective length and is represented by 'ε':

$$\varepsilon = \frac{\beta\cos\theta}{4} \tag{5}$$

The distance between magnetic ions (hopping length) in tetrahedral A site (L_A) and octahedral B site (L_B) were calculated using the following relations:

$$L_A = \frac{a\sqrt{3}}{4} \text{ and } L_B = \frac{a\sqrt{2}}{4} \tag{6}$$

where 'a' is lattice constant.

The calculated values of crystallite size (D), lattice constant (a), unit cell volume (V), dislocation density (δ), micro-strain (ε) and hopping lengths LA and LB of Q and R samples are tabulated in Table 1.

Table 1. Crystallite size, lattice constant, unit cell volume, dislocation density, microstrain (ε) and hopping lengths (L_A and L_B) of Q and R samples

Sample	$Li_{0.5}Ni_{0.6}Zn_{0.15}Fe_2O_4$ (Q)		$Li_{0.5}Ni_{0.5}Zn_{0.25}Fe_2O_4$ (R)	
Crystallite Size (D) (nm)	118.38		111.83	
Lattice constant (a) (Å)	8.378		8.397	
Volume (a^3) ($Å^3$)	588		591	
Dislocation density (δ) (m^{-2})	$9.01 \times 10^{+13}$		$8.85 \times 10^{+13}$	
Microstrain (ε)	3.15×10^{-4}		3.2×10^{-4}	
Hopping Length (Å)	$L_A = 3.627$	$L_B = 2.962$	$L_A = 3.636$	$L_B = 2.967$

SCANNING ELECTRON MICROSCOPE (SEM) ANALYSIS

The SEM image of Q and R ferrite sample particles are shown in Figure 3. The particles are observed to be various shapes like granular, cubic, cuboidal and regular octahedron. Sizes of particles observed in the range of few micrometres. The size of particles is smaller for R sample compared to Q. The sharpness of the edges of particles increased in R sample.

(a)   (b)
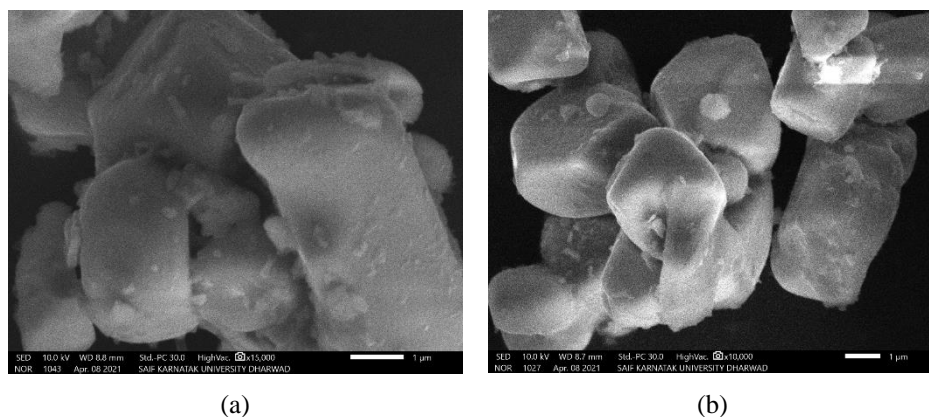
Figure 3: SEM image of (a) $Li_{0.5}Ni_{0.6}Zn_{0.15}Fe_2O_4$ (Q), and (b) $Li_{0.5}Ni_{0.5}Zn_{0.25}Fe_2O_4$ (R) ferrite samples

FOURIER TRANSFORM INFRARED (FT-IR) STUDIES

Figure 4 shows the Fourier Transform Infrared (FTIR) spectrum of $Li_{0.5}Ni_{0.6}Zn_{0.15}Fe_2O_4$ (Q), $Li_{0.5}Ni_{0.5}Zn_{0.25}Fe_2O_4$ (R) ferrite samples. Waldron (14) observed that both absorption bands of ferrites are due to the familiar tetrahedral octahedral M-O stretching vibration modes. The spectrum of Q and R ferrites under investigation reveals the formation of a cubic spinel structure showing two significant absorption bands, at 520 cm^{-1} and around 420 cm^{-1} corresponding to high frequency band ν_1 and low frequency band ν_2 arising from tetrahedral (A) and octahedral (B) interstitial sites respectively (15).
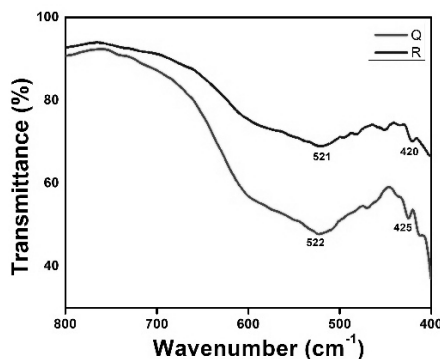
Figure 4. FTIR spectra of $Li_{0.5}Ni_{0.6}Zn_{0.15}Fe_2O_4$ (Q), $Li_{0.5}Ni_{0.5}Zn_{0.25}Fe_2O_4$ (R) ferrite samples

COLE-COLE PLOT

(a)   (b)
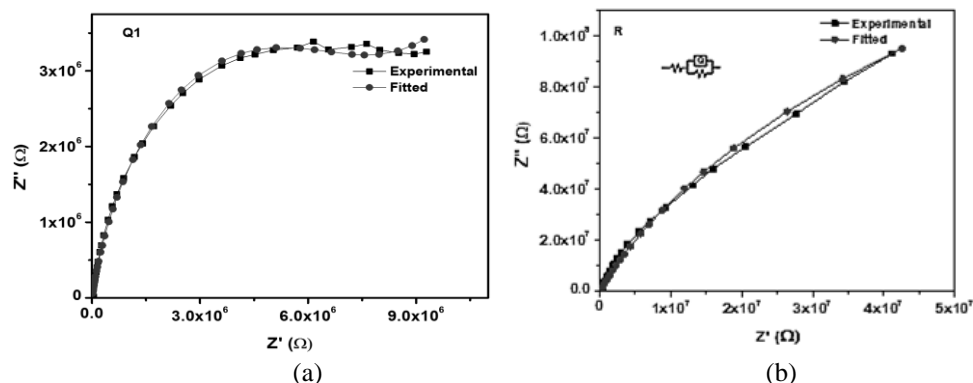
Figure 5. Cole-Cole plot of (a) $Li_{0.5}Ni_{0.6}Zn_{0.15}Fe_2O_4$ (Q), (b) $Li_{0.5}Ni_{0.5}Zn_{0.25}Fe_2O_4$ (R) ferrite samples

Complex impedance graphs also known as Cole-Cole plots cater a detailed image of the microstructural resistances involved in particle interactions. The Cole-Cole plot of Q & R ferrite samples are shown in Figures 5(a) & 5(b) respectively. In Cole-Cole plots, maxima of the arc point towards resonance condition corresponding contribution from grain boundary and grain. This is usually observed in oxide ceramics, where low frequency arc is assigned to grain boundary contribution and high frequency arc is assigned to grain contribution (16).

Single semicircle behaviour is usually due to the contribution from the grain or intrinsic bulk contribution (R1, C1), whereas, two or more successive semicircles are account of contributions from grain boundary (R2, C2) and/or electrodes (R3, C3) in a polycrystalline material. In our $Li_{0.5}Ni_{0.6}Zn_{0.15}Fe_2O_4$ (Q), $Li_{0.5}Ni_{0.5}Zn_{0.25}Fe_2O_4$ (R) ferrite samples a single semicircle is found to lie below the real axis thus suggests a non-Debye type of relaxation process due to the contribution from the grain or intrinsic bulk contribution (R1, C1). The diameter of the semicircles corresponds to the resistance of the grain and grain boundaries. The plot shows that as the zinc concentration increases, the diameter of the semicircle varies imposing direction on the change in resistance of the grain interior and grain boundary.

CONCLUSIONS

The spinel $Li_{0.5}Ni_{0.6}Zn_{0.15}Fe_2O_4$ (Q), $Li_{0.5}Ni_{0.5}Zn_{0.25}Fe_2O_4$ (R) ferrite samples have been synthesized by solid state reaction method. X-ray diffraction (XRD) pattern show lattice constant 8.378 Å (Q), 8.379Å (R). The crystallite size of the samples is observed to be in the range of 110-120 nm (Debye-Scherrer method). The two bands in FTIR spectra are observed in the range of 520 cm^{-1} and 420 cm^{-1} for both samples confirming the tetrahedral and octahedral interstitial sites. The XRD and FTIR analysis confirms the formation of cubic spinel structure. The SEM images show variety of structures with size in the range few micrometres. The Cole-Cole plots show the contribution to electrical conductivity only due to grain boundary in both samples.

REFERENCES

1. Soohoo, R. F. *Theory and Application of Ferrites*, Englewood Cliffs, NJ: Prentice-Hall, 1960.
2. Goldman, A. *Modern ferrite technology*, 2nd edition. Springer New York, NY, 2005.
3. Ranganathan, R.; Ray, A. Ferrites - what is new? *Pramana*, **2002**, *58*(5-6), 995-1002.
4. Sugimoto, M. The Past, Present, and Future of Ferrites, *J. Am. Cer. Soc.,* **2004**, *82*(2), 269-280.
5. Tsuji, M; Kato, H.; Kodama, T.; Chang, S.G.; Hesegawa, N.; Tamaura, Y. Methanation of CO_2 on H_2-reduced Ni(II)-or Co(II)-bearing ferrites at 200 ºC", *J. Mater. Sci.*, **1994**, *29*(23), 6227-6230.
6. Dar, M. A.; Majid, K.; Najar, M. H.; Kotnala, R. K.; Shah, J.; Dhawan, S. K.; Farukh, M. Surfactant assisted synthesis of Polythiophene/$Ni_{0.5}Zn_{0.5}Fe_{2-x}Ce_xO_4$ ferrite composites: Study of structural, dielectric and magnetic properties for EMI shielding applications, *Phy. Che. Che. Phy.* **2017**, *19*(16), 1-35.
7. Bahadur, D.; Giri, J.; Nayak, B. B.; Sriharsha, T.; Pradhan, P.; Prasad, N. K.; Barick, R. C.; Ambashta, R. D. Processing, properties and some novel applications of magnetic nanoparticles, *Pramana*, **2005**, *65*(4), 663-679.
8. Kamble, R. B.; Mathe, V. L. Nanocrystalline nickel ferrite thick film as an efficient gas sensor at room temperature", *Sens. Actuators B: Chemical*, **2008**, *131*(1), 205-209.
9. Bi, K.; Zhu, W.; Lei, M.; Zhou, J. Magnetically tunable wideband microwave filter using ferrite-based metamaterials, *Appl. Phys. Lett.*, **2015**, *106*(17), 173507.
10. Tehrani, F. S., Daadmehr, V.; Rezakhani, A. T.; Akbarneja, R. H.; Gholipour, S. Structural, magnetic, and optical properties of zinc- and copper- substituted nickel ferrite nanocrystals, *J. Supercond. Novel Magn.*, **2012**, *25*, 2443-2455.
11. Assar, S. T.; Abosheiasha, H. F.; Saafan, S. A.; El Nimr, M. K. Preparation, characterization and magnetization of nano and bulk $Ni_{0.5}Co_{0.5-2x}Li_xFe_{2+x}O_4$ samples, *J. Mol. Str.*, **2015**, *1084*, 128-134.
12. Kulkarni, A. B.; Mathad, S. N. Synthesis and Structural Analysis of Co–Zn–Cd Ferrite by Williamson–Hall and Size–Strain Plot Methods, *Int. J. Self-Prop. High-Temp. Synth.*, **2018**, *27*(1), 37-43.
13. Kulkarni, A. B.; Mathad, S. N. Variation in structural and mechanical properties of Cd-doped Co-Zn ferrites, *Mater. Sci. Energy Tech.*, **2019**, *2*, 455-462.
14. Waldron, R. D. Infrared spectra of ferrites, *Phys. Rev.*, **1955**, *99*(6), 1727-1765.
15. Rendale, M. K.; Mathad, S. N.; Puri, V. Structural, mechanical and elastic properties of $Ni_{0.7-x}Co_xZn_{0.3}Fe_2O_4$ nano-ferrite thick films, *Microelectronics Int.*, **2017**, *34*(2), 57-63.
16. Maurya, J. C.; Bhoraskar, S. V.; Mathe, V. L. Effect of manganese substitution on magnetoimpedance and magnetostriction of cobalt ferrites, *Physica B: Condensed Matter*, **2014**, *436*, 220-226.

TOTAL QUALITY INDEX APPROACH APPLIED TO CHAGA EXTRACTS OBTAINED BY GREEN EXTRACTION TECHNIQUES

Vesna LAZIĆ[1]* ⓘ, *Ana DOROŠKI*[1] ⓘ, *Ilija DJEKIĆ*[1] ⓘ, *Jovana VUNDUK*[2] ⓘ,
Maja KOZARSKI[1] ⓘ, *Anita KLAUS*[1] ⓘ

[1] Institute for Food Technology and Biochemistry, Faculty of Agriculture, University of Belgrade, Nemanjina 6, 11080 Belgrade, Serbia.
[2] Institute of General and Physical Chemistry, Studentski trg 12/V, 11158 Belgrade, Serbia.

This study aimed to develop a single quality index of Serbian (IS) and Mongolian (IM) Chaga (Inonotus obliquus) extracts obtained by different types of extraction. Microwave-assisted extraction (MW), ultrasonic-assisted extraction (VAE), and supercritical water extraction (SWE) were used to prepare the extracts. Seven quality parameters of a mushroom extract were considered, including the free radical scavenging capability determined by the 1,1-diphenyl-2-picrylhydrazyl ($DPPH^\bullet$) and 2,2'-azino-bis (3-ethylbenzothiazoline-6-sulfonic acid) ($ABTS^{\bullet+}$) assays, the ability to chelate ferrous ions (Fe^{2+}), as well as the total amount of phenolic compounds, proteins, polysaccharides, and glucans. The mentioned parameters were used to define the total quality index (TQI). Based on TQI scores SWE can be recommended as the most effective type of extraction (favors the yield) of total phenolic compounds (TPC), total extracted proteins (TEP), total polysaccharides (TPS), total glucans (TG), and antioxidant assays. Finally, TQI results for seven quality parameters, derived from six Chaga samples using SWE at 200 °C, showed the best overall quality for both the IS and IM extracts.

Keywords: antioxidant activity, Chaga, *Inonotus obliquus*, quality index, quality parameters.

INTRODUCTION

I. obliquus, also known as Chaga, is a parasitic species most often found on birches and other trees in the forests of the Circumboreal Region of the Northern Hemisphere. Although well-known in traditional medicine, chemical analysis revealed that *I. obliquus* produces diverse secondary metabolites, including phenolic compounds, melanins, and triterpenes (1, 2), thus represents a source of valuable antibacterial, anti-inflammatory, anti-tumor, antioxidant, and immunostimulating components (3).

Today, with the growing nutraceutical sector, the industry is competing on several levels including production technology (such as green extraction techniques), sustainability, as well as the final product's quality (4). Managing these processes can be optimized by applying quality tools like TQI. This approach in production management enables the selection of the desired parameters (of importance) without the restriction on their number (5). Based on the TQI score, the production can be modified to achieve the highest quality taking into consideration the previously set requirements.

This study aimed to determine the quality of Serbian and Mongolian Chaga extracts obtained by different green types of extraction (subcritical water extraction, ultrasonic, and microwave extraction). To compare the quality of six mushroom extracts, a single total quality index (TQI) was calculated using seven quality parameters. These parameters included the ability to scavenge free radicals as determined by $ABTS^{\bullet+}$, $DPPH^\bullet$ and Fe^{2+} assays, as well as the total amount of phenolic compounds, proteins, polysaccharides, and glucans.

EXPERIMENTAL

MUSHROOM MATERIAL

Two strains of the mushroom *I. obliquus* (Chaga) originating from the Vlasina mountain, Republic of Serbia (IS), and from the forest area of Mongolia (IM) were used. The mushrooms were identified based on taxonomic characteristics and descriptions that can be found in monographs. After identification, carpophores were air-dried at 40 °C to constant mass (Heratherm IGS60 incubator, Germany) and ground to fine particles in a Ciclotech mill (Tecator, Hoganas, Sweden) using a 0.5 mm sieve and then stored in the dark until analysis. Representative fruiting body specimens are deposited in the herbarium in the collection of the Department of Industrial Microbiology, University of Belgrade - Faculty of Agriculture.

EXTRACTION TECHNIQUES

MW was performed using a modified home microwave (NN-E201W, Panasonic, Japan) and appropriate glass apparatus with a round flask and condenser. Microwave frequency (50 Hz) was applied, and the extract was obtained by treating Chaga powder (10g) + with water (100mL) using microwave power of 470 W for 30 min as described by Vladić et al. (6). Additionally, VAE was conducted in a sonication water bath (EUP540A, Euinstruments, France) to obtain an extract from Chaga powder (10g) mixed with water (100mL) at a frequency of 40 kHz and ultrasonic power (60 W/L) for 60 min as described by Vladić et al. (6). SWE was carried out using a batch-type high-pressure extractor (Parr Instrument Company, Moline, IL, USA). The extraction procedure and apparatus details have been previously described by Vladić et al. (7). The extraction was conducted at the temperature of 200 °C (SWE 200 °C), while the pressure (30 bar) was kept constant during the 20 minutes extraction time.

Table 1. Extract codes of Serbian and Mongolian I. obliquus obtained by different types of extraction

No.	Extraction codes	Type of extraction
1	IS MW H$_2$O	microwave-assisted extraction Chaga from Serbia
2	IS VAE H$_2$O	ultrasound-assisted extraction Chaga from Serbia
3	IS SWE 200 °C	subcritical water extraction Chaga from Serbia
4	IM MW H$_2$O	microwave-assisted extraction Chaga from Mongolia
5	IM VAE H$_2$O	ultrasound-assisted extraction Chaga from Mongolia
6	IM SWE 200 °C	subcritical water extraction Chaga from Mongolia

DETERMINATION OF POLYSACCHARIDE, PROTEIN, AND PHENOL CONTENT

TPS was determined by the phenol-sulfur acid method with D-glucose as a standard (8). Protein concentrations were determined using the method of Bradford (9) and a standard calibration curve was constructed using bovine serum albumin (BSA) in the concentration range of 0.1-1.0 mg/mL. TEP in the extracts were expressed as g BSA equivalents per 100 g

dry weight of the extracts. TPC was measured according to the method described by Petrović et al. (10). The results were expressed as gallic acid equivalents (GAE) per dry weight of the extracts (11).

DETERMINATION OF TOTAL GLUCANS CONTENT (TG)

TG was determined in the extracts using the Mushroom and Yeast β-glucan Assay K-YBGL09/2009 (Megazyme Int., Wicklow, Ireland). The β-glucan content was calculated by subtracting the α-glucan from the total glucan content. All values of glucans content were expressed as g of D-glucose equivalents per 100 g of dry matter.

ANTIOXIDATIVE POTENTIAL *IN VITRO*

Different methods corresponding to different mechanisms of antioxidant activity were used to measure the antioxidant properties of the tested samples *in vitro*. The DPPH$^\bullet$ and ABTS$^{\bullet+}$ scavenging activity assays were done according to the modified method of Doroški et al. (12). The results were expressed using the standard curve equation and the difference between the absorbance of the control and extract samples. The ability of mushroom samples to chelate ferrous ions (Fe^{2+}) was tested based on the microplate assay described by Vunduk et al. (13).

TOTAL QUALITY INDEX OF MUSHROOM EXTRACTS

To calculate the quality index, the following quality parameters have been selected: TPS (mg Glu/g DW of extract); TEP (mg BSA/g of extract); TPC (mg GAE/g of extract); TC (100 mg Glu/g DW of extract); DPPH$^\bullet$ (1.25 mg/mL); Fe^{2+} chelating ability (1.25 mg/mL); ABTS$^{\bullet+}$ (1 mg/mL).

To calculate the TQI of mushroom extracts, the following rule was applied for all selected quality parameters: "the higher value, the better quality" rule using the following formula:

$$QI_j = \left| \frac{x_{max} - x_i}{x_{max} - x_{min}} \right|, \ x_i \le x_{max}$$

where X_i is the measured value; x_{max} is the maximal value and x_{min} is the minimal value in the subset of values for the unique QI.

To evaluate all samples to identify the one with the best overall characteristics, the total quality index approach, based on the investigations of Horn and Johnson (14) and Djekić et al. (15, 16) was used. The result is interpreted as „the lower the TQI value, the better the overall quality". All QI$_N$ indices as components of the Euclidean norm vector were used to represent the total quality index (TQI):

$$TQI = \sqrt{\sum_{j=1}^{N} (QI_j)^2}$$

SPSS Statistics 17.0 and Microsoft Excel 2010 were used for statistical data analysis. One-way analysis of variance (ANOVA), Tukey's post hoc test, least significant difference (LSD) was applied with statistical significance at the $p < 0.05$ level.

RESULTS AND DISCUSSION

Quality indices for quality parameters - TPC, TPS, TEP, and TG are presented in Table 2. The best QI for the TPC parameter was achieved by the sample IS SWE 200 °C. No statistically significant difference was found in the quality of samples IS MW H_2O and IM SWE 200 °C. This study revealed that the type of extraction has an impact on the QI for TPC, while the effect of the solvent is negligible. In recent years, subcritical extraction, due to its many advantages, has become a useful substitute for conventional extraction methods. This environmentally friendly method that ensures higher yields of nutritional compounds was used by Seo and Lee (17). They reported that the amount of TPC in SWE extracts was affected by temperature and duration of extraction. Thus, it was found that the amount of TPC was 18 times higher in the extracts obtained at 250 °C for 30 min compared to extracts obtained at 50 °C for 10 minutes.

Table 2. The quality indices (QI) for total phenolic compounds, total polysaccharides, total extracted proteins, and total glucans of *I. obliquus* extracts

QI					
IS MW H_2O	IS VAE H_2O	IS SWE 200°C	IM MW H_2O	IM VAE H_2O	IM SWE 200°C
0.28±0.01[b]	0.7±0.05[d]	0[a]	0.6±0.01[c]	1[e]	0.28±0.03[b]
0.8±0.02[c]	0.81±0.01[c]	0.50±0.08[b]	0.96±0.04[d]	0.99±0.02[d]	0[a]
0.49±0.25	0.64±0.32	0.65±0.36	0	0.49±0.41	0.16±0.17
0.84±0.01[c]	0.84±0.02[c]	0.03±0.02[b]	0.93±0.00d	1[e]	0[a]

Note: Mean of three replicates ± standard deviation. Means in the same row with different lowercase letters are significantly different ($p < 0.05$). Abbreviations: IS - Serbian Chaga, IM - Mongolian Chaga, MW H_2O - microwave-assisted extraction, VAE H_2O - ultrasound-assisted extraction, SWE 200 °C - subcritical water extraction. TPC - total phenolic compounds; TPS - total polysaccharides; TEP - total extracted proteins; TG - total glucans.

Polysaccharides attract a lot of attention in medicine and the food industry due to their numerous biological activities. Previously published data indicate that polysaccharides obtained from *I. obliquus* have a wide range of properties such as anti-microbial (18), antioxidant (19), antitumor (20), etc. IM SWE 200 °C showed the best quality for TPS and TG which can be attributed to the fact that the optimum temperature for the extraction of water-soluble polysaccharides is around 200 °C (21). In a study conducted by Xi et al. (22), it was shown that increasing the temperature from 160 to 190 °C resulted in an increase in the content of polysaccharides from 85 mg/g to 132 mg/g. Similar to TPC, IM VAE H_2O had the worst quality index for TPS and TPC, while IS Chaga samples obtained by microwave and ultrasonic extraction showed no statistically significant difference between these two chemical parameters. According to the previous work of Chen et al. (23), ultrasonic and microwave extraction shorten the extraction time and improve the yield of polysaccharides but not enough in comparison to SWE. These researchers claimed that the glucan content was lowest in VAE because the low temperature prevented efficient glucan extraction. The

best quality index value for proteins was achieved by the IM VAE H$_2$O sample while a statistically significant difference for this parameter was not determined in other samples.

Mushrooms are rich nutritional and medicinal resources with various pharmacological functions and are attractive for study as a highly valuable functional food ingredient (24). Chaga known for its strong antioxidant effect, is primarily associated with phenolic compounds, which are key molecules capable of scavenging free radicals (20). Antioxidant activity was tested using various methods. To better understand the antioxidant potential of different extracts. The quality indices for ABTS$^{\bullet+}$ scavenging ability were significantly different for the tested extracts at a concentration of 1 mg/ml. Thus, IM SWE 200 °C showed the best quality in this case. The tested extracts showed higher or comparable ABTS$^{\bullet+}$ scavenging activities than the synthetic antioxidant catechin. Previously, Seo and Lee (17) found that the highest ABTS$^{\bullet+}$ value of 97.8% was detected in the SWE extract obtained at 250 °C for 30 minutes, which was 6 times higher than the value reached by the extract obtained at 50 °C for 60 minutes.

This research showed that the IM MW H$_2$O sample exhibited the highest quality, while on the other hand the IS MW H$_2$O and IS VAE H$_2$O samples had the lowest (Table 3).

Table 3. The quality indices (QI) for antioxidant properties of *I. obliquus* extracts

	QI					
	IS MW H$_2$O	IS VAE H$_2$O	IS SWE 200°C	IM MW H$_2$O	IM VAE H$_2$O	IM SWE 200°C
ABTS$^{\bullet+}$	0.07±0.02[ab]	0.94±0.07[d]	0.48±0.00[c]	0.11±0.06[b]	0.99±0.02[d]	0[a]
DPPH$^{\bullet}$	0.96±0.06[c]	0.97±0.05[c]	0.44±0.19[ab]	0.09±0.16[a]	0.27±0.32[ab]	0.59±0.09[bc]
Fe^{2+}	0.27±0.17[b]	0[a]	0.20±0.14[ab]	1[c]	0.23±0.06[ab]	0.77±0.01[c]

Note: Mean of three replicates ± standard deviation. Means in the same row with different lowercase letters are significantly different (p<0.05). Abbreviations: IS - Serbian Chaga, IM - Mongolian Chaga, MW H$_2$O – microwave-assisted extraction, VAE H$_2$O - ultrasound-assisted extraction, SWE 200°C - subcritical water extraction.

Extracts obtained using SWE did not show statistically significant differences in the ability to reduce free DPPH$^{\bullet}$ radicals. The difference compared to the ABTS$^{\bullet+}$ scavenging ability can be explained by the different reactivity of the tested samples with the selected radical species. For example, while the ABTS$^{\bullet+}$ test can show specificity towards a certain structure of the examined compounds, the DPPH$^{\bullet}$ test specifically recognizes functional groups such as –OH and –NH^{3+} (25). Xu et al. (21) reported that active substances extracted using ultrasound-assisted technique showed higher antioxidant activity than those extracted using conventional extraction methods. Regarding the evaluation of the chelating ability of ferrous ions, the IS VAE H$_2$O sample reached the best quality. Additionally, no statistically significant difference was between IS VAE H$_2$O, IS SWE 200 °C, and IM VAE H$_2$O samples for this assay.

Samples IM SWE 200 °C and IS SWE 200 °C showed the best overall quality based on the seven selected parameters, as represented in Figure 1. On the contrary, the samples IS VAE H2O and IM VAE H2O received the highest points, but their overall quality was the worst. These results suggest that SWE is an effective method for the extraction of polysaccharides and phenolic compounds from Chaga. A significant improvement in the yield of these compounds was observed using SWE at high temperature. This model was previously applied in the evaluation of the quality of Pleurotus ostreatus mushroom extracts (5). The authors reported that the quality of mushroom extracts increased with increasing pomace in the substrate, as pomace content affected the extract's chemical composition and antioxidant potential.
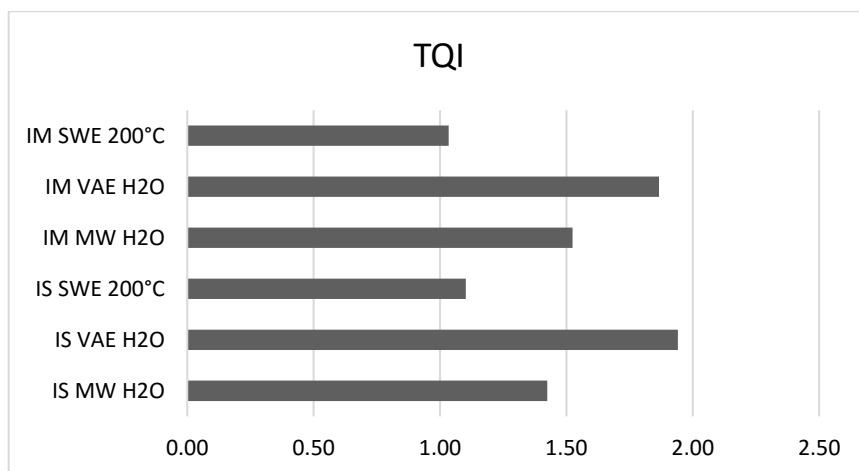
Figure 1. Total quality index (TQI) of parameters derived from the analyzed parameters of mushroom extract.

Note: IS - Serbian Chaga, IM - Mongolian Chaga, MW H_2O - microwave-assisted extraction, VAE H_2O - ultrasound-assisted extraction, SWE 200 °C - subcritical water extraction.

CONCLUSION

TQI is stated as a benchmark tool for providing cost-effective management in organizations and production. Depending on the production requirements a specific set of parameters of interest can be selected to reflect the needs of the specific industry or consumers. When it comes to mushroom-based nutraceuticals and functional food, the amounts of polysaccharides, proteins, phenolics, etc. are often listed as of the utmost importance. Hereby, we demonstrated the application of TQI when deciding upon the use and selection of green extraction techniques applied to medicinal Chaga mushrooms. When the extraction yield of bioactive compounds is the goal, SWE could be recommended as the best technique.

REFERENCES

1. Hwang, B. S.; Lee, I. K.; Yun, B. S. Phenolic compounds from the fungus *Inonotus obliquus* and their antioxidant properties. *J. Antibiot*. **2016**, *69*(2), 108–110.
2. Géry, A.; Dubreule, C.; André, V.; Rioult, J. P.; Bouchart, V.; Heutte, N.; Eldin de Pécoulas, P.; Krivomaz, T.; Garon, D. Chaga (*Inonotus obliquus*), a Future Potential Medicinal Fungus in Oncology? A Chemical Study and a Comparison of the Cytotoxicity Against Human Lung Adenocarcinoma Cells (A549) and Human Bronchial Epithelial Cells (BEAS-2B). *Integr. Cancer Ther*. **2018**, *17*(3), 832–843.
3. Shashkina, M. Y.; Shashkin, P. N.; Sergeev, A. V. Chemical and medicobiological properties of chaga (review). *Pharm. Chem. J*. **2006**, *40*(10), 560–568.
4. Chemat, F.; Vian, M. A.; Cravotto, G. Green extraction of natural products: Concept and principles. Int. J. Mol. Sci. **2012**, *13*(7), 8615–8627.
5. Doroški, A.; Klaus, A.; Kozarski, M.; Cvetković, S.; Nikolić, B.; Jakovljević, D.; Tomasevic, I.; Vunduk, J.; Lazić, V.; Djekic, I. The influence of grape pomace substrate on quality characteriza-

tion of Pleurotus ostreatus—Total quality index approach. *J. Food Process. Preserv.* **2021**, *45*(1), 1–15.

6. Vladić, J.; Janković, T.; Živković, J.; Tomić, M.; Zdunić, G.; Šavikin, K.; Vidović, S. Comparative Study of Subcritical Water and Microwave-Assisted Extraction Techniques Impact on the Phenolic Compounds and 5-Hydroxymethylfurfural Content in Pomegranate Peel. *Plant Foods Hum. Nutr*. **2020**, *75*(4), 553–560.

7. Vladic, J.; Nastic, N.; Stanojkovic, T.; Zizak, Z.; Cakarevic, J.; Popovic, L.; Vidovic, S. Subcritical water for recovery of polyphenols from comfrey root and biological activities of extracts. *Acta Chim. Slov.* **2019**, *66*(2), 473–483.

8. Du Bois, M.; Gilles, K. A.; Hamilton, J. K.; Rebers, P. A.; Smith, F. Colorimetric method for determination of sugars and related substances. *Anal. Chem.* **1956**, *28*, 350–356.

9. Bradford, M. M. A refined and sensitive method for the quantitation of microgram quantities of protein using the principle of protein-dye binding. *Anal. Biochem.* **1976**, *72*, 248–255.

10. Petrović, P.; Ivanović, K.; Octrue, C.; Tumara, M.; Jovanović, A.; Vunduk, J.; Nikšić, M.; Pjanović, R.; Bugarski, B.; Klaus, A. Immobilization of chaga extract in alginate beads for modified release: Simplicity meets efficiency. *Hem. Ind.* **2019**, *73*(5), 325–335.

11. Lazić, V.; Klaus, A.; Kozarski, M.; Doroški, A.; Tosti, T.; Simić, S.; Vunduk, J. The Effect of Green Extraction Technologies on the Chemical Composition of Medicinal Chaga Mushroom Extracts. *J. Fungi* **2024**, 10(3), 225.

12. Doroški, A.; Klaus, A.; Kozarski, M.; Nikolić, B.; Vunduk, J.; Lazić, V.; Djekic, I. Impact of grape pomace as a cultivation substrate on the *Pleurotus ostreatus* chemical and biological properties. *Acta Period. Technol.* **2021**, 52, 25–32.

13. Vunduk, J.; Kozarski, M.; Djekic, I.; Tomašević, I.; Klaus, A. Effect of modified atmosphere packaging on selected functional characteristics of *Agaricus bisporus*. *Eur. Food Res. Technol.* **2021**, 247(4), 829–838.

14. Horn, R. A.; Johnson, C. R. Matrix Analysis, Cambridge University Press, Cambridge, UK, 1985, pp 257-342.

15. Djekic, I.; Tomic, N.; Bourdoux, S.; Spilimbergo, S.; Smigic, N.; Udovicki, B.; Hofland, G.; Devlieghere, F.; Rajkovic, A. Comparison of three types of drying (supercritical CO2, air and freeze) on the quality of dried apple – Quality index approach. *LWT.* **2018**, *94*, 64-72.

16. Djekic, I.; Vunduk, J.; Tomašević, I.; Kozarski, M.; Petrovic, P.; Niksic, M.; Pudja, P.; Klaus, A. Total quality index of *Agaricus bisporus* mushrooms packed in modified atmosphere. *J. Sci. Food Agric*., **2017**, *97*(9), 3013-3021.

17. Seo, H. K.; Lee, S. C. Antioxidant activity of subcritical water extracts from chaga mushroom (*Inonotus obliquus*). *Sep. Sci. Technol.* **2010**, *45*(2), 198–203.

18. Martins, S.; Mussatto, S. I.; Martínez-Avila, G.; Montañez-Saenz, J.; Aguilar, C. N.; Teixeira, J. A. Bioactive phenolic compounds: Production and extraction by solid-state fermentation. A review. *Biotechnol. Adv.* **2011**, *29*(3), 365–373.

19. Abu-Reidah, I. M.; Critch, A. L.; Manful, C. F.; Rajakaruna, A.; Vidal, N. P.; Pham, T. H.; Cheema, M.; Thomas, R. Effects of pH and temperature on water under pressurized conditions in the extraction of nutraceuticals from chaga (*Inonotus obliquus*) mushroom. *Antioxidants,* **2021**, *10*(8), 1322.

20. Balandaykin, M. E.; Zmitrovich, I. V. Review on chaga medicinal mushroom, *Inonotus obliquus* (Higher Basidiomycetes): Realm of medicinal applications and approaches on estimating its resource potential. *Int. J. Med. Mushrooms,* **2015**, *17*(2), 95–104.

21. Xu, S. Y.; Liu, J. P.; Huang, X.; Du, L. P.; Shi, F. L.; Dong, R.; Huang, X. T.; Zheng, K.; Liu,Y.; Cheong, K. L. Ultrasonic-microwave assisted extraction, characterization and biological activity of pectin from jackfruit peel. *LWT.* **2018**, *90*, 577–582.

22. Yuan, X. Subcritical Water Extraction and Characterization of Polysaccharides and Phenolic Compounds from *Inonotus Obliquus*. Ph.D. Thesis, University of Tsukuba, Tsukuba, Japan, **2017**.

23. Chen, Y.; Gu, X.; Huang, S.; quan Li, J.; Wang, X.; Tang, J. Optimization of ultrasonic/microwave assisted extraction (UMAE) of polysaccharides from *Inonotus obliquus* and evaluation of its anti-tumor activities. *Int. J. Biol. Macromol.* **2010**, *46*(4), 429–435.

24. Matsugo, S.; Sakamoto, T.; Wakame, K.; Nakamura, Y.; Watanabe, K.; Konishi, T. Mushrooms as a Resource for Mibyou-Care Functional Food; The Role of Basidiomycetes-X (Shirayukidake) and Its Major Components. *Nutraceuticals*, **2022**, *2*(3), 132–149.

25. Platzer, M.; Kiese, S.; Herfellner, T.; Schweiggert-Weisz, U.; Miesbauer, O.; Eisner, P. Common trends and differences in antioxidant activity analysis of phenolic substances using single electron transfer based assays. *Molecules,* **2021**, *26*(5) 1244.

ENHANCING THERMAL EFFICIENCY OF EARTH-AIR TUNNEL HEAT EXCHANGERS (EATHE) THROUGH RESPONSE SURFACE METHODOLOGY

Mohamed Amine KHORCHEF[1]*, *Mohamed SERIER[2]*,
Aboubakeur BENARIBA[3], *Sheymaa ALAZZAWI[4]*

[1] GIDD Industrial Engineering and Sustainable Development Laboratory, Faculty of Engineering and Technology, University of Ahmed Zabana, 48000 Relizane, Algeria.
[2] LMPM, Department of Mechanical Engineering, University of SidiBel Abbes, BP 89 Cité Ben M'hidi 22000, SidiBel Abbes, Algeria.
[3] Laboratory of Industrial Technologies, University of Tiaret, Tiaret, Algeria.
[4] Materials laboratory Engineering Department University of Diyala, Iraq.

This study investigates the optimization of Earth-Air Tunnel Heat Exchanger (EATHE) systems for maximizing air temperature reduction in Algeria's Timimoun region. Employing a Response Surface Methodology approach and Ansys Fluent 16.2 software, we meticulously analyze the influence of critical parameters on air temperature reduction: pipe depth, length, air velocity, and thermal conductivity of PVC and high-density polyethylene (HDPE) pipes. twenty-six simulations were conducted to optimize these parameters. The results reveal a significant influence of all investigated factors on air temperature reduction. Pipe depth emerged as the most influential factor, accounting for (56.22 %) of the temperature variance. This was followed by pipe length (28.26 %), air velocity (4.88 %), and pipe thermal conductivity (4.21 %). Based on these findings, we recommend prioritizing deeper placements (4 m), longer pipes (18 to 20 m), and air velocities below 3 m/s. For moderate-temperature applications, HDPE pipes offer a favorable choice.

Keywords: Earth-Air Tunnel Heat Exchanger (EATHE), Response Surface Methodology, Thermal Efficiency, Timimoun Region

INTRODUCTION

Buildings are responsible for approximately 40% of global energy consumption and contribute to one-third of energy-related greenhouse gas emissions (1). This heightened energy demand stems from population growth, economic expansion, and rising living standards (1). Space heating and cooling account for a significant portion of this usage, with 32–33 % of building sector energy consumption and 39 % of its energy-related CO_2 emissions when considering upstream power generation (2, 3). Therefore, improving energy efficiency and integrating renewable energy sources (RES) in both new and existing buildings presents a critical opportunity to reduce energy consumption and greenhouse gas emissions, while simultaneously driving advancements in research and technology (4). The scientific community has diligently explored energy-efficient solutions for space conditioning using RES over recent decades, with the aim of promoting energy conservation and environmental protection (5, 6). Among these alternative energy sources, geothermal energy stands out for its sustainability and versatility in applications like space heating and cooling, district heating systems, and industrial processes (7). Specifically, Earth-Air Heat Exchangers (EAHEs) represent a promising technology within Earth-source heat exchange. Their ability to preheat

incoming air in winter and facilitate cooling in summer makes them highly effective in reducing building heating and cooling loads (8).

Figure 1 illustrates the operating principle of the EATHE system. A blower at the inlet controls the airflow speed. The buried pipes, situated 1 to 6 meters below the surface, carry the forced airflow. In colder seasons, the incoming air is preheated by the warmer subsurface soil through convection and conduction. Conversely, during warmer seasons, the air is cooled by the cooler subsurface soil. This conditioned air then facilitates energy-efficient building cooling.
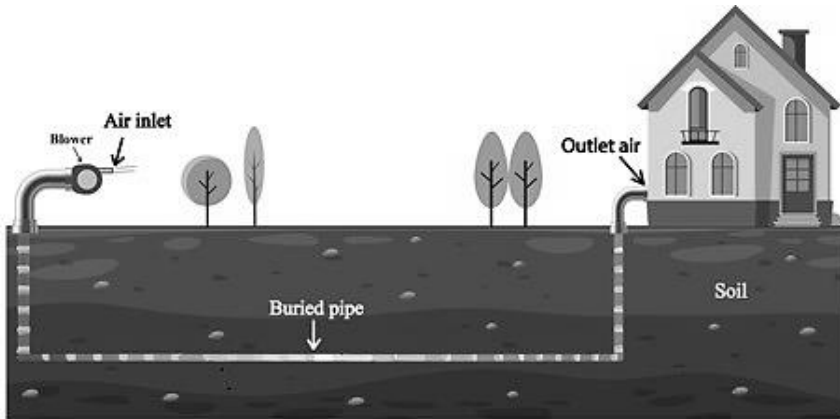
Figure 1. Schematic of (EATHE) System.

Several previous studies have investigated the thermal performance of (EAHE) using various modelling approaches. Benhammou and Draoui (9) developed a transient one-dimensional model for summer cooling in the Algerian Sahara, validating it against experimental data and showing good agreement. Their sensitivity analysis revealed that pipe length positively affects daily mean efficiency, while pipe cross-section and air velocity have negative impacts. Similarly, Papakostas et al. (10) compared two one-dimensional models, finding deviations of less than 10% compared to measurements and highlighting the simplicity and accuracy of this approach. Su et al. (11) constructed a one-dimensional numerical sub-model for air temperature and moisture content calculations, while Ni et al. (12) developed a validated one-dimensional steady-state model for performance analysis and regression modelling. Li et al. (13) presented a novel 1D-2D hybrid model for both shallow and deep EAHE systems, concluding that the optimal pipe depth depends solely on depth. Xamán et al. (14) employed a pseudo-transient conjugate heat transfer model in two dimensions to evaluate the thermal behavior of an EAHE under various climatic conditions.

The application of Statistical (DoE) as a powerful tool for process optimization is well-established (15, 16). Within DoE methods, FFD, (RSM), and the Taguchi method offer distinct approaches to planning and conducting experiments. Both RSM have been utilized to evaluate, model, and optimize the impact of process parameters on product quality characteristics (17). The Taguchi method is particularly attractive due to its effectiveness, simplicity, and systematic approach (18). Full factorial design, on the other hand, excels at unravelling complex interactions and pinpointing key parameters for optimization (19).

Numerous researchers have employed various DoE approaches to investigate factors influencing ground-to-air heat exchangers. This review highlights a selection of these studies,

emphasizing the importance of optimization in EAHE systems for achieving distinct optimal conditions in both winter and summer. For instance, one study employed a full factorial design to identify key factors influencing temperature regulation within an EAHE system (19). This experimental approach validated the predictive model and suggested future research directions for enhancing sustainable heating and cooling technologies.

Another study, focusing on optimizing an EAHE in Peshawar, Pakistan, utilized the Response Surface Method (RSM) (20). This research established the significance of pipe parameters through analysis of variance (ANOVA) and demonstrated the EAHE's effectiveness in reducing temperatures by 15–18 °C for livestock building cooling. The study also introduced a novel regression model to predict temperature variations (ΔT_{i-o}) and cooling capacity (CC) based on critical factors, ultimately delineating optimal design configurations for the EAHE to enhance animal comfort through parametric analysis (20, 21).

Similarly, another investigation employed the Taguchi method to optimize EAHE performance through a validated Computational Fluid Dynamics (CFD) model (22). The study explored four parameters: pipe diameter, length, inlet air velocity, and temperature. This analysis led to the derivation of optimal parameter combinations for maximizing temperature reduction and heat transfer efficiency. The subsequent statistical analysis revealed the significant influence of inlet air temperature on temperature reduction and pipe diameter on heat transfer rate (22).

Furthermore, research has extended to developing and validating TRNSYS models, which were subsequently, optimized using the Taguchi methodology (23). This culminated in a refined design configuration encompassing specific values for window-to-wall ratio, glazing type, insulation thickness, and earth tube dimensions, ultimately aiming to optimize solar radiation absorption and heat transfer within the system (23).

Motivated by the growing interest in (EATHE) systems under diverse conditions and modelling techniques, this study investigates performance improvement for air conditioning buildings in Timimoun, Algeria. Our primary objective is to reduce reliance on fossil fuels and promote environmental sustainability. To achieve this, a mathematical model is developed using (RSM) to predict the outlet air temperature. This model allows us to analyze the impact of various factors on the EATHE's cooling performance. Subsequently, recommendations are formulated for optimizing parameter values to maximize the system's performance in this specific region.

This paper presents a three-part investigation of (EATHE) system. The first part, "Building and Validating the Model" utilizes ANSYS Fluent to simulate the system. This section details the physical model, mesh distribution, governing equations, assumptions, boundary conditions, solution technique, convergence analysis, and validation of the simulation model. The second part, "Methodology," outlines the (RSM) approach and data analysis procedures. Here, the focus is on establishing the statistical significance of factors through analysis of variance (ANOVA) and method to determining the percentage contribution of parameters. Finally, the "Simulation and Analysis" part presents simulations for the Timimoun region, Algeria. This section encompasses parametric analysis, simulation results, exploration of factor combinations, single-factor experiments, optimization using a Response Surface Methodology, and the analysis of each parameter's contribution.

BUILDING AND VALIDATING THE MODEL

PHYSICAL MODEL AND MESH DISTRIBUTION

The study employs Ansys Fluent 16.2 software to simulate the EATHE system, focusing on the physical model. The methodology involves:

- Utilizing ANSYS Workbench's DESIGN MODELER for constructing and refining the simulation model.
- The computational domain was divided into three sub-domains: "domain-air," "domain-soil," and "domain-pipe," as illustrated in figure 2 and 3. This division facilitates a detailed analysis of heat transfer within each individual sub-domain.
- Tube length: 20m; inner diameter: 0.1 m; tube wall thickness: 0.01 m.
- The surrounding soil was modelled with a thickness of 0.49 m, as informed by the observational study of (24). The air's influence extended to a depth of 0.25 m within three hours, expanding to 0.3 m and 0.45 m after five and eight hours, respectively.
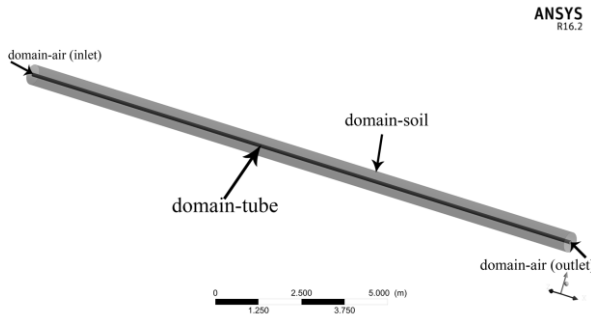
Figure 2. Physical Model of (EATHE) System.
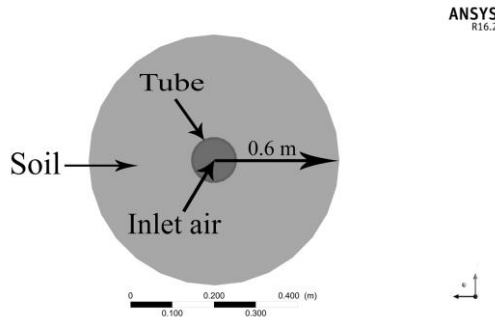
Figure 3. Sectional View of the (EATHE).

REGARDING MESH DISTRIBUTION

- Employing hybrid 3D meshing (hexahedral and tetrahedral), Figure 4 shows mesh results.
- Choosing element sizes of 0.02 m.
- All input parameters in the validation case were set precisely to match the field experiment conditions, as shown Table 1.
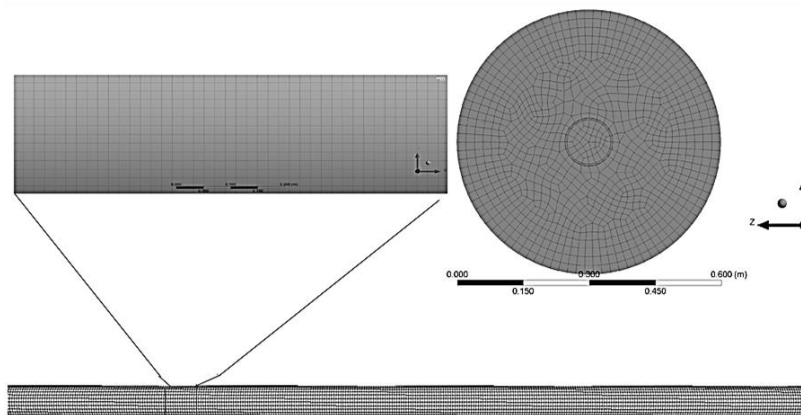
Figure 4. Meshing Model for EATHE with Hybrid 3D Meshing (Hexahedral and Tetrahedral).

Table 1. Input Parameters for Validation Matching Field Experiment Conditions

Parameter	Units	Values
Outer diameter	m	0.11
Inner diameter	m	0.1
Length	m	20
PVC pipe (25)		
Thermal conductivity	W/m·K	0.16
Specific heat	J/kg·K	900
Density	Kg/m^3	1380
Soil (25)		
Thermal conductivity	W/m·K	0.52
Specific heat	J/kg·K	1840
Density	kg/m^3	2050
Air (25)		
Thermal conductivity	W/m·K	0.02
Specific heat	J/kg·K	1006
Density	kg/m^3	1.22
Operating conditions		
inlet temperature for validation (21)	K	313.15
inlet temperature for Grid-Independence Study (22)	K	319.15
soil temperatures at depths of 3 m (21)	K	300.2
Initial air velocity (21)	m/s	5

GOVERNING EQUATIONS

This study employed ANSYS Fluent 16.2 to develop a 3D numerical model simulating heat transfer within the fluid flow. The model incorporates constant, turbulent, and incompressible airflow conditions. Thermal energy equations were employed to determine the

temperature distribution within both the pipe and the surrounding soil. Furthermore, the model solved the continuity, momentum, and energy conservation equations for the steady-state fluid domain inside the pipe.

Continuity equation (26):

$$\frac{\partial u}{\partial x} + \frac{\partial v}{\partial y} + \frac{\partial w}{\partial z} = 0 \qquad [1]$$

Law of energy conservation (22):

$$u\frac{\partial T}{\partial x} + v\frac{\partial T}{\partial y} + w\frac{\partial T}{\partial z} = \alpha \left[\frac{\partial^2 T}{\partial x^2} + \frac{\partial^2 T}{\partial y^2} + \frac{\partial^2 T}{\partial z^2}\right] \qquad [2]$$

X-momentum equation (27):

$$u\frac{\partial u}{\partial x} + v\frac{\partial u}{\partial y} + w\frac{\partial u}{\partial z} = -\frac{1}{\rho}\frac{\partial p}{\partial x} + \vartheta \left[\frac{\partial^2 u}{\partial x^2} + \frac{\partial^2 u}{\partial y^2} + \frac{\partial^2 u}{\partial z^2}\right] \qquad [3]$$

Y-momentum equation:

$$u\frac{\partial v}{\partial x} + v\frac{\partial v}{\partial y} + w\frac{\partial v}{\partial z} = -\frac{1}{\rho}\frac{\partial p}{\partial y} + \vartheta \left[\frac{\partial^2 v}{\partial x^2} + \frac{\partial^2 v}{\partial y^2} + \frac{\partial^2 v}{\partial z^2}\right] \qquad [4]$$

Z-momentum equation:

$$u\frac{\partial w}{\partial x} + v\frac{\partial w}{\partial y} + w\frac{\partial w}{\partial z} = -\frac{1}{\rho}\frac{\partial p}{\partial z} + \vartheta \left[\frac{\partial^2 w}{\partial x^2} + \frac{\partial^2 w}{\partial y^2} + \frac{\partial^2 w}{\partial z^2}\right] \qquad [5]$$

In Equations [1]-[5], p and T represent the pressure and temperature of the flowing air, and u, v, and w represent the velocity components in the x, y, and z directions.
Equations for transport in the realizable k-epsilon model (26).

$$\frac{\partial}{\partial t}(\rho k) + \frac{\partial}{\partial x_j}(\rho k u_j) = \frac{\partial}{\partial x_j}\left[\left(\mu \frac{\mu_t}{\sigma_k}\right)\frac{\partial k}{\partial x_j}\right] + G_k + G_b - \rho\epsilon - Y_M + S_k \qquad [6]$$

$$\frac{\partial}{\partial t}(\rho\epsilon) + \frac{\partial}{\partial x_j}(\rho\epsilon u_j) = \frac{\partial}{\partial x_j}\left[\left(\mu \frac{\mu_t}{\sigma_\epsilon}\right)\frac{\partial \epsilon}{\partial x_j}\right] + \rho C_1 S\epsilon - \rho C_2 \times \frac{\epsilon^2}{k+\sqrt{v\epsilon}} + C_{1\epsilon}\frac{\epsilon}{k}C_{3\epsilon}G_b + S_\epsilon \qquad [7]$$

$$C_1 = max\left[0.43, \frac{\eta}{\eta+5}\right], \eta = S\frac{k}{\epsilon}, S = \sqrt{2S_{ij}S_{ij}} \qquad [8]$$

The formulation Equations [6]-[8] comprises essential components: ρ represents the density of the fluid in kg/m³. G_k and G_b represent the generation of turbulence kinetic energy due to mean velocity gradients and buoyancy effects, respectively. Y_M accounts for the role of fluctuating dilatation in compressible turbulence on dissipation. Constants C_1 and C_2 shape the equations. Turbulent Prandtl numbers, σ_k for k and σ_ϵ for ϵ, relate molecular diffusion to turbulent transport. S_k and S_ϵ are user-defined source terms, allowing model customization. η is a variable related to turbulence quantities and is used in the definition of C_1.
Eddy viscosity is calculated using data from Equation [9]:

$$\mu_t = \rho C_\mu \frac{k^2}{\epsilon} \qquad [9]$$

The model constants are:

$$C_{1\epsilon} = 1.44, \sigma_\epsilon = 1.2, C_2 = 1.9 \qquad [10]$$

ASSUMPTIONS

In order to streamline the analysis, the numerical model incorporates several key assumptions:

- The soil properties are assumed to be isotropic and constant, including attributes such as heat capacity and thermal conductivity.
- The airflow within the system is considered incompressible, and its thermal properties are assumed to be constant.
- The model incorporates both convective and conductive heat transfer processes. However, it neglects radiative and latent heat transfer effects.
- The model assumes perfect thermal contact between the pipe and the surrounding soil, eliminating interfacial thermal resistance. Additionally, the temperature of the adjacent soil is presumed to be identical to the external surface temperature of the pipe.

BOUNDARY CONDITIONS

The simulation incorporates various boundary conditions. At the EATHE inlet, the air velocity follows a perpendicular "Velocity Inlet" condition with a uniform velocity and 5% turbulence intensity, mimicking real airflow conditions (24). A zero-heat flux boundary condition is enforced on the inlet and exit faces of the EATHE to ensure consistent temperatures within the system. The upper and lower walls of the soil domain maintain isothermal states corresponding to the buried depth, accurately representing the surrounding soil's thermal behavior. Sidewalls remain adiabatic, reflecting their minimal influence on heat transfer processes within the EATHE. Distant boundaries in the soil domain have fixed temperatures, treating the soil conditions as constant in deeper layers to optimize computational efficiency while capturing essential heat transfer aspects. This approach aligns with the findings of numerous simulations (28, 29). A coupled heat transfer condition, with no-slip conditions controlling velocity and temperature on duct surfaces, prevails at the soil-pipe interface. This boundary condition plays a crucial role in capturing the interaction between the soil and air within the EATHE.

SOLUTION TECHNIQUE AND CONVERGENCE ANALYSIS

The simulation employed the pressure-based Navier-Stokes algorithm with the (SIMPLE) pressure-velocity coupling technique. The (LSCB) methodology and second-order schemes were used to solve pressure gradients. Second-order upwind techniques were employed for calculating kinetic energy and turbulent momentum. The model utilized the viscous (k-ε) realizable turbulence model with a standard wall function and focused on the flow of incompressible fluids. The convergence criteria for continuity, velocities, (k-ε) (10^{-3}), and the energy equation (10^{-3}) were satisfied at each time step. A time step of 60 seconds was utilized.

GRID-INDEPENDENCE STUDY

To establish grid independence in the simulations, we conducted a study by varying element sizes (0.12 m, 0.10 m, 0.06 m, and 0.02 m). The resulting EATHE outlet temperatures (presented in Table 2) showed minimal variations (305.038 K, 305.190 K, 305.290 K, and 305.042 K). Compared to the finest grid (0.02 m), the largest temperature change was only 0.082%, confirming grid independence. While all grids produced similar results, the 0.02 m element size was chosen for subsequent simulations to prioritize accuracy. This selection acknowledges the trade-off between computational efficiency and capturing potentially influential details within the EATHE system.

Table 2. Outlet Temperature Fluctuations Across Different Grid Sizes in the Grid-Independence Study

Grid Size (m)	Number of elements	Outlet Temperature (K)	Percentage Difference from Baseline
0.02	1048773	305.042	-
0.06	189159	305.290	0.0081%
0.1	175456	305.190	0.0015%
0.12	173732	305.038	0.0014%

SIMULATION MODEL VALIDATION

To ensure the accuracy and reliability of our EATHE simulation model, a thorough validation process was undertaken. This process involved comparing our computational results with experimental data obtained by Misra et al. (30). As illustrated in Figures 5 and 6, the comparison revealed excellent agreement between the two models, with a relative error of only 0.2%. This close agreement confirms the credibility and validity of our simulation approach.
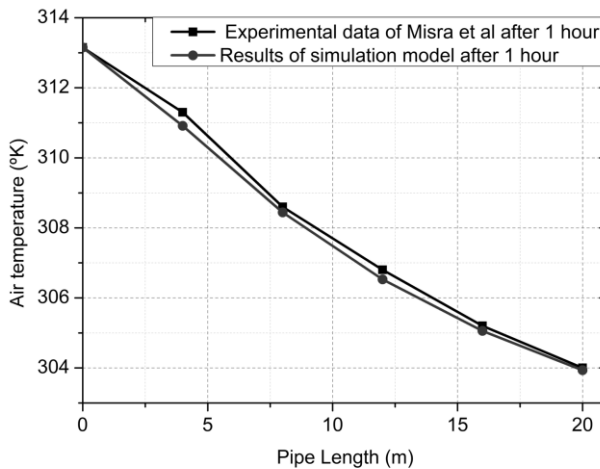
Figure 5. Comparison of the present (CFD) results with experimental data from (30).
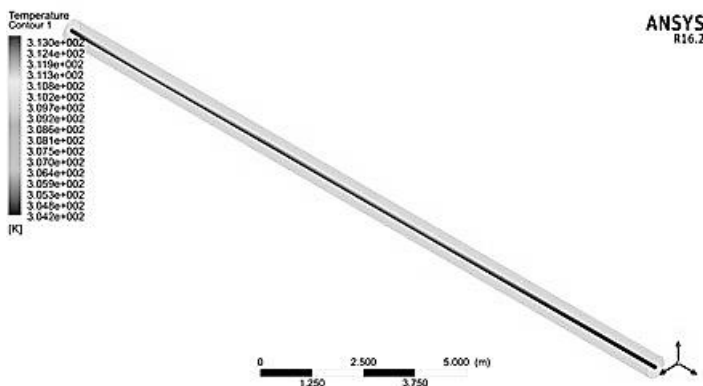
Figure 6. Temperature distribution within (EATHE) system after 1 hour of operation simulated using ANSYS Fluent software.

METHODOLOGY

RESPONSE SURFACE METHODOLOGY

This study employed (RSM), a collection of statistical techniques ideal for optimizing processes influenced by multiple variables (31). RSM utilizes central composite design (CCD), which offers advantages like reduced experimental runs compared to full factorial designs, minimizing resource consumption (time, cost, materials) (32, 33). Here, CCD explores the influence of four key factors on Earth Air Thermal Heat Exchanger (EATHE) performance during summer:

- X_1 (Pipe Depth): Depth of underground pipes within the EATHE system.
- X_2 (Pipe Length): Length of pipes used within the EATHE system.
- X_3 (Air Velocity): Velocity of air flow through the system.
- X_4 (Pipe Thermal Conductivity): Thermal conductivity of the pipes, considering both PVC and HDPE materials.

The real values of the independent variables (X_i) ranged from 2 to 5 m (X_1), 10 to 20 m (X_2), 3 to 6 m/s (X_3), and 0.16 to 0.461 W/m·K (X_4), as detailed in Table 3. To facilitate a comprehensive analysis of their combined effects, these real values were transformed into dimensionless independent variables (z_i) using Equation [11]. This transformation assigns -1 and +1 to the lowest and highest real values for each variable, respectively. In this context, X_0 represents the real value at the center point, and ΔX_i signifies the step change (34).

$$z_i = \frac{x_i - x_0}{\Delta x_i} \tag{11}$$

In CCD, the total number of unique runs in this study is as follows in Equation [12]:

$$Runs = 2^k + 2k + n_c = 2^4 + 2(4) + 2 = 26 \tag{12}$$

- K represents the number of factors.
- n_c number of central points.

Table 3. Range of Independent Variables and Corresponding Dimensionless Values in CCD Approach

Factor	Parameter	Units	Low level (-1)	Medium level (0)	High level (+1)
X_1	Pipe depth	m	2	3.5	5
X_2	Pipe length	m	10	15	20
X_3	Air velocity	m/s	3	4.5	6
X_4	Pipe thermal conductivity	W/m·K	0.16	0.31	0.461

A second-order polynomial equation [13] incorporating linear, quadratic, and interaction terms for the selected factors was used to predict the temperature response (y) in Kelvin. This approach enabled effective modelling and analysis of the experimental data (35).

$$T = \beta_0 + \sum_{i=1}^{k} \beta_i x_i + \sum_{i=1}^{k} \beta_{ii} x_i^2 + \sum_{i<j} \sum \beta_{ij} x_i x_j \qquad [13]$$

In this equation:

- The intercept term β_0 represents the overall mean score.
- β_i, β_{ii}, and β_{ij} are the regression coefficients for the linear, quadratic, and interaction terms, respectively.
- x_i and x_j denote the levels of the factors.

DATA ANALYSIS

The statistical significance of each factor was assessed through an analysis of variance (ANOVA), with the p-value serving as the metric. This p-value represents the probability that observed effects in the model arise by chance alone (36). A lower *p*-value (<0.05) indicates a higher degree of statistical significance for the associated term. To visualize the factorial design and its effects, several graphical tools were employed, including examining individual factor effects and creating contour plots. All data analysis procedures were performed using STATISTICA software (Stat Soft, Inc., USA) version 10, ensuring a rigorous and comprehensive assessment of the experimental results.

THE PERCENTAGE CONTRIBUTION

Within the field of RSM, (CCD) is a widely used technique. However, even when employing a CCD design with its additional axial or star points to capture curvature and interaction effects, assessing the individual percentage contributions of factors remains crucial for understanding their influence on the response variable. Equation [14] details the calculation for these contributions, where the sum of squares due to each factor is divided by the total sum of squares.

$$Percentage\ contribution = \left(\frac{SS_{due\ to\ factor}}{SS_{total}} \right) * 100 \qquad [14]$$

RESULTS AND DISCUSSION

PARAMETRIC ANALYSIS OF EATHE IN TIMIMOUN REGIONS, ALGERIA

This study investigated the thermal efficiency of (EATHE) within the Timimoun region of southern Algeria. The aim was to identify influential parameters and optimize them for improved performance. Using ANSYS Fluent software, 26 simulations were conducted. Table 4 summarizes the operating conditions and material properties. Soil properties for this region, along with ambient air temperature and soil temperatures at depths of 2 m, 3.5 m and 5 m for August, were adopted from (37).

Table 4. Input Parameters and Environmental Conditions for EATHE Simulation in the Timimoun Region, Algeria.

Component	Parameter	Units	Value
PVC pipe	Density	Kg/m^3	1380
	Specific heat	J/kg·K	900
	Thermal conductivity	W/m·K	0.16
HDPE pipe	Density	Kg/m^3	955
	Specific heat	J/kg·K	2300
	Thermal conductivity	W/m·K	0.461
Sandy Clay Soil	Density	Kg/m^3	1800
	Specific heat	J/kg·K	1340
	Thermal conductivity	W/m·K	1.55
Operating conditions	inlet temperature	K	310.05
	soil temperatures at depths of 2 m	K	303.65
	soil temperatures at depths of 3.5 m	K	302.47
	soil temperatures at depths of 5 m	K	298.95

SIMULATION RESULTS AND FACTOR COMBINATIONS FOR (EATHE) SYSTEM

Table 5 presents the simulation results of the (EATHE) system. It provides a detailed overview of temperature variations across different combinations of factors (pipe depth, pipe length, air velocity, and thermal conductivity for PVC and HDPE pipes). This table serves as a key platform for visualizing the findings of RSM.

THE RESULTS OF SINGLE-FACTOR

An analysis of Figures 7a-d reveals several key factors influencing outlet temperature in (EATHE) system. Pipe depth exhibits a negative correlation with outlet temperature (Figure 7a). Deeper pipes (5 m) lead to significantly lower outlet temperatures (301.562 K) compared to shallower installations (2 m, 305.159 K). Notably, the rate of decrease is not uniform, with a steeper decline observed beyond 3.5 m depth. Similarly, pipe length (Figure 7b) demonstrates a negative correlation, with longer pipes (20 m) achieving lower outlet tempera-

tures (303.4791 K) compared to shorter lengths (10 m, 305.8593 K). This indicates more efficient heat transfer with increased pipe length due to extended air-soil contact.

Table 5. Simulation Results of EATHE System for Various Factor Combinations

Run order	Pipe depth (m)	Pipe length (m)	Air velocity (m/s)	Pipe thermal conductivity (w/m·K)	Outlet Temperature (K)
1	2	10	3	0.16	306.369
2	2	10	3	0.461	305.74
3	2	10	6	0.16	307.282
4	2	10	6	0.461	306.449
5	2	15	4.5	0.3105	305.156
6	2	20	3	0.16	304.582
7	2	20	3	0.461	304.164
8	2	20	6	0.16	305.414
9	2	20	6	0.461	304.621
10	3.5	10	4.5	0.3105	305.686
11	3.5	15	3	0.3105	303.798
12	3.5	15	4.5	0.16	304.899
13	3.5	15	4.5	0.3105	304.448
14	3.5	15	4.5	0.3105	304.448
15	3.5	15	4.5	0.461	304.016
16	3.5	15	6	0.3105	304.633
17	3.5	20	4.5	0.3105	303.557
18	5	10	3	0.16	303.665
19	5	10	3	0.461	302.576
20	5	10	6	0.16	305.25
21	5	10	6	0.461	303.804
22	5	15	4.5	0.3105	301.562
23	5	20	3	0.16	300.567
24	5	20	3	0.461	299.842
25	5	20	6	0.16	302.01
26	5	20	6	0.461	300.642

Air velocity (Figure 7c) shows a positive correlation with outlet temperature, with a modest increase observed from 303.77 K (3 m/s) to 304.75 K (6 m/s). However, the rate of rise diminishes at higher velocities, suggesting a trend of diminishing returns. Finally, pipe thermal conductivity (Figure 7d) exhibits a negative correlation with outlet temperature. Higher conductivity (0.416 W/m·K) results in lower outlet temperatures (304.0506 K) compared to lower conductivity (0.16 W/m·K, 304.9599 K). This indicates more efficient heat transfer with higher conductivity, leading to improved cooling performance.
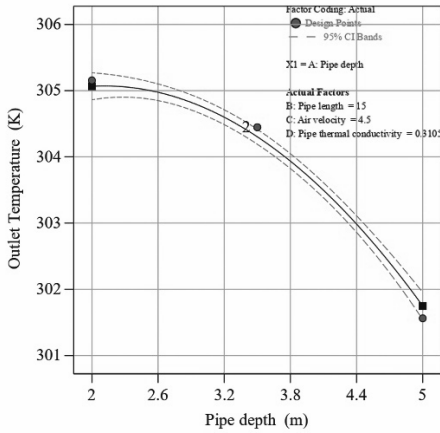
Figure 7a. Impact of Pipe Depth on Outlet Temperature.
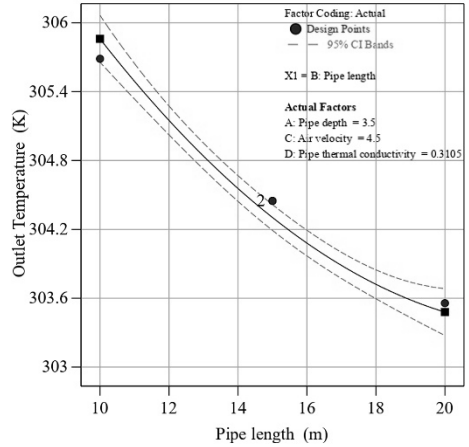
Figure 7b. Impact of Pipe Length on Outlet Temperature.
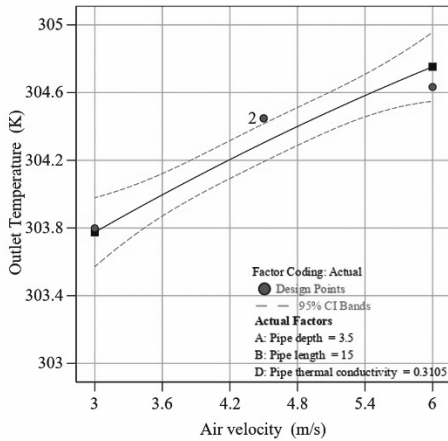
Figure 7c. Impact of Air Velocity on Outlet Temperature.
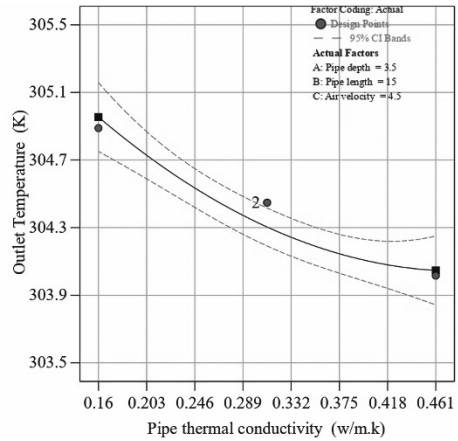
Figure 7d. Impact of Pipe Thermal Conductivity on Outlet Temperature.

OPTIMIZATION BY RSM

This study employed regression analysis to develop a predictive model for the temperature inside the (EATHE) system utilizing data generated by the numerical model. The coded factors obtained from RSM served as input variables for the model, resulting in a first-order polynomial equation, Equation [15].

$$
\begin{aligned}
Y = {} & 303.3 - 1.66X_1 - 1.19X_2 + 0.489X_3 - 0.4541X_4 \\
& \dots - 0.3234X_1X_2 + 0.1341X_1X_3 - 0.122X_1X_4 - 0.0564X_2X_3 + 0.0433X_2X_4 - 0.0987X_3X_4 \\
& \dots - 0.8965X_1^2 + 0.3660X_2^2 - 0.04X_3^2 + 0.197X_4^2
\end{aligned} \tag{15}
$$

The (ANOVA) results (Table 6) revealed a highly significant model (F-value = 379.22, p-value < 1.122e-12), indicating that the model explains a substantial portion of the varia-

tion in outlet temperature. All main effects (X_1-Pipe depth, X_2-Pipe length, X_3-Air velocity, X_4-Pipe thermal conductivity) and several interaction terms (X_1X_2, X_1X_3, X_1X_4, X_3X_4) along with some quadratic terms (X_1^2, X_2^2, X_4^2) were statistically significant (p-value < 0.05). This suggests that the influence of one factor on outlet temperature can be dependent on the level of another factor (interaction) and the relationships between factors and temperature might not be entirely linear. Terms X_2X_3 and X_2X_4 with p-values exceeding 0.1000 were considered non-significant. The high values of Predicted R^2 (0.9905) and Adjusted R^2 (0.9953) indicate a good model fit with the data, and the small difference between them suggests the absence of over fitting due to insignificant terms. Furthermore, the Adeq Precision value (77.587) being much larger than 4 demonstrates a high signal-to-noise ratio, implying the model's reliability for navigating the design space and making predictions.

Table 6. ANOVA for RSM model

Source	SS	df	MS	F-value	P-value
Model	87.928	14	6.280	379.219	1.12e-12
X_1	49.531	1	49.531	2990.647	9.42e-15
X_2	25.494	1	25.494	1539.340	3.57e-13
X_3	4.304	1	4.304	259.882	5.32e-09
X_4	3.711	1	3.711	224.121	1.16e-08
X_1X_2	1.673	1	1.673	101.062	7.01e-07
X_1X_3	0.287	1	0.287	17.362	0.0015
X_1X_4	0.238	1	0.238	14.423	0.0029
X_2X_3	0.05	1	0.050	3.077	0.1071
X_2X_4	0.03	1	0.03	1.812	0.2053
X_3X_4	0.155	1	0.155	9.408	0.0107
X_1^2	2.058	1	2.058	124.284	2.46e-07
X_2^2	0.343	1	0.343	20.710	0.00082
X_3^2	0.0041	1	0.0041	0.2477	0.6284
X_4^2	0.0993	1	0.0993	5.9995	0.0322
Residual	0.1821	11	0.0165		
Lack of Fit	0.1821	10	0.0182		
Pure Error	0	1	0		
Total SS	88.11103	25			
R^2 =0.9979; R^2_{Adj}=0.9953; R^2_{Pre}=0.9905. Adeq. Precision=77.587					

Response surface plots, including contour and surface representations, are crucial in determining optimal response values and operational conditions (38). Figures 8 and 9 present contour and surface plots of the interaction between pipe length and depth, air velocity, and pipe depth. These plots illustrate that reducing air velocity to 3 m/s or lower, employing a pipe depth of 4 m, and extending pipe length all lead to temperatures below 301 K. This outcome can be attributed to the longer residence time of slower-moving air within the heat exchange system. This extended exposure facilitates increased heat exchange with the surrounding soil, resulting in a temperature reduction. Additionally, greater pipe depth provides access to subsurface layers with more stable and cooler temperatures compared to the

surface due to the earth's insulating properties. Consequently, deeper pipe depths allow for harnessing cooler temperatures. To optimize the cooling performance of (EATHE) system, maintaining air velocities below 3 m/s and using pipe depths of 4 meters or more is recommended. These adjustments ensure consistent cooling by minimizing turbulence-related temperature fluctuations and capitalizing on the subsurface cooling potential.
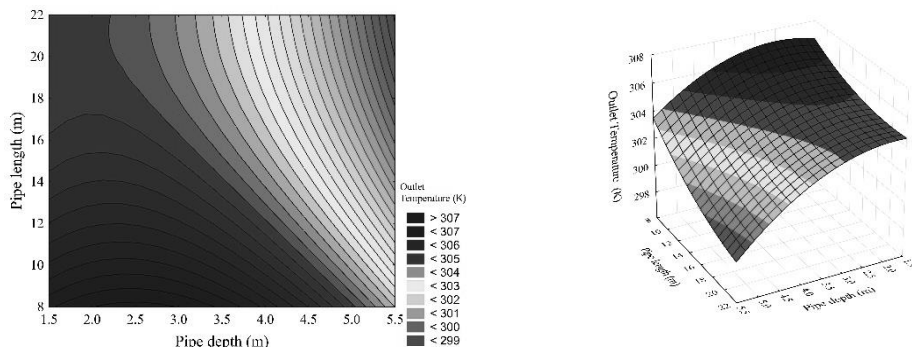
Figure 8. Interaction of Pipe Depth and Pipe Length: Contour and Surface Plots.
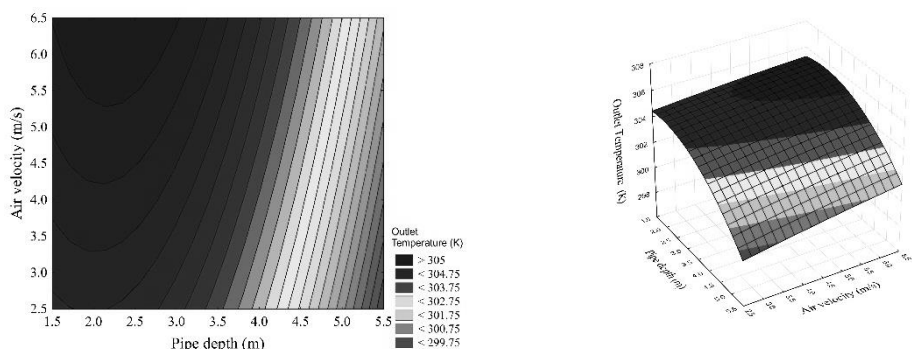
Figure 9. Interaction of Pipe Depth and Air Velocity: Contour and Surface Plots.
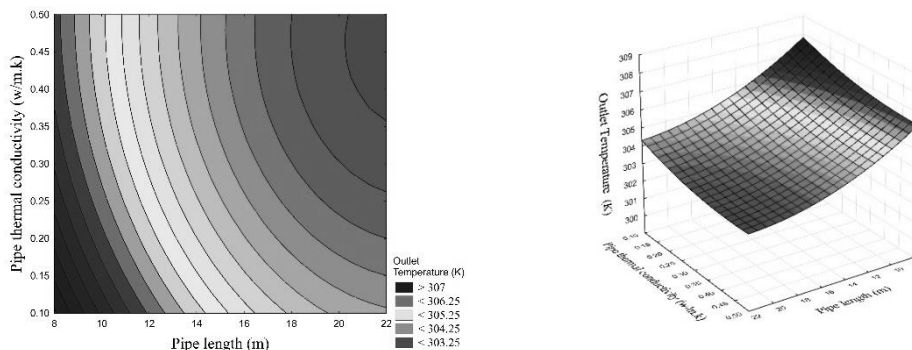
Figure 10. Correlation between Pipe Length and Pipe Thermal Conductivity: Contour and Surface Plots.

Figure 10 demonstrates the correlation between pipe thermal conductivity and pipe length, highlighting their impact on temperature outcomes. Increasing pipe thermal conduc-

tivity and length decreases temperatures from 306 K to 301.75 K. This phenomenon occurs because higher thermal conductivity enhances heat transfer in high-density polyethylene (HDPE) pipes, while the opposite effect is observed in polyvinyl chloride (PVC) pipes. The conductivity of 0.461 W/m·K for HDPE facilitates temperatures below 303.5 K with a 15-meter pipe length. However, achieving the same temperature with lower conductivity in PVC requires a 19-meter length. This material-dependent difference necessitates adjusting pipe lengths to achieve desired temperatures. Therefore, it is recommended to use HDPE pipes with higher conductivity and extend lengths to 18 meters or more for optimal cooling.

PERCENTAGE CONTRIBUTION OF EACH PARAMETER

The contributions calculated using Equation [13] and visualized in Figure 11 shed light on the relative influence of each parameter on the response variable's variability. The results reveal that "pipe depth" (X_1) exerts the most significant influence, accounting for 56.21 % of the variability. This is followed by "pipe length" (X_2) with a contribution of 28.29 %. Both "air velocity (X_3) and "pipe thermal conductivity" (X_4) contribute considerably less, at 4.88 % and 4.21 %, respectively. These percentage contributions offer valuable insights into the hierarchy of factors impacting the system's performance.
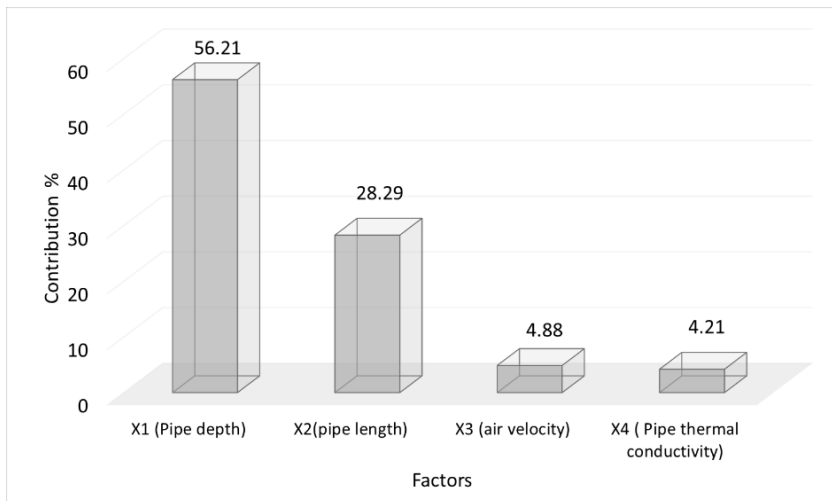
Figure 11. Relative Influence of Parameters on Response Variability: Insights from Percentage Contributions.

CONCLUSIONS

In conclusion, this research leveraged Ansys Fluent and a comprehensive factorial design approach to enhance the thermal efficiency of (EATHE) in Algeria's Timimoun region. Twenty-six simulations and subsequent ANOVA analysis yielded the following key findings:

- Deeper pipe depths, facilitating greater heat dissipation, lead to lower temperatures. Elongated pipes exhibit an inverse relationship between length and temperature due

to amplified heat dissipation effects. Conversely, increased air velocities result in higher temperatures, negatively impacting overall cooling efficiency.

- Significant differences in pipe thermal conductivity highlight the distinct characteristics of materials. Notably, higher thermal conductivity in HDPE pipes leads to cooler temperatures compared to PVC pipes.
- The ANOVA analysis underscores the statistically significant influence of factors such as pipe depth, pipe length, air velocity, and pipe thermal conductivity on thermal efficiency outcomes.
- Response surface and contour plots reveal valuable insights into optimal operational configurations. These visualizations highlight the importance of maintaining air velocities below 3 m/s, longer pipes (18 to 20m) and employing pipe depths exceeding 4 meters for enhanced cooling effectiveness.
- The correlation between pipe thermal conductivity and pipe length highlights HDPE's superior heat transfer capabilities.
- Percentage contribution analysis identifies "pipe depth" (X_1) as the most influential factor, accounting for 56.21 % of the variability, followed by "pipe length" (X_2) with a significant 28.29 %. Meanwhile, "air velocity" (X_3) and "pipe thermal conductivity" (X_4) play more minor roles, contributing 4.88% and 4.23%, respectively.
- While prioritizing thermal efficiency, this study did not consider economic factors like material costs (HDPE vs. PVC) or construction. A life cycle cost analysis for future research is recommended to assess the economic viability of EATHE systems with different materials and techniques. Additionally, exploring EATHE integration with renewables or storage holds promise for developing more sustainable and cost-effective cooling solutions for Timimoun's climate.

Table 7. Nomenclature

EAHE	Earth-to-Air Heat Exchanger
RES	Renewable Energy Sources
CO_2	Carbon Dioxide
CCD	Central Composite Design
ANOVA	Analysis of Variance
RSM	Response Surface Methodology
FFD	Full factorial design
CFD	Computational Fluid Dynamics
TRNSYS	Transient System Simulation Tool
DoE	Design of Experiments
PVC	Polyvinyl Chloride
SIMPLE	Semi-Implicit Method for Pressure-Linked Equations
LSCB	least squares cell-based
HDPE	High-Density Polyethylene
X_1	Pipe Depth
X_2	Pipe Length
X_3	Air Velocity
X_4	Pipe Thermal Conductivity

REFERENCES

1. Singh, R.; Sawhney, R.; Lazarus, I.; Kishore, V. Recent advancements in earth air tunnel heat exchanger (EATHE) system for indoor thermal comfort application: A review. *Renewable and Sustainable Energy Reviews*, **2018**, *82,* 2162-2185. https://doi.org/10.1016/j.rser.2017.08.058

2. Abergel, T.; Dean, B.; Dulac, J. Towards a zero-emission, efficient, and resilient buildings and construction sector: Global Status Report 2017. *UN Environment and International Energy Agency: Paris, France*, **2017**, *22,*

3. Nejat, P.; Jomehzadeh, F.; Taheri, M.M.; Gohari, M.; Majid, M.Z.A. A global review of energy consumption, CO2 emissions and policy in the residential sector (with an overview of the top ten CO2 emitting countries). *Renewable and sustainable energy reviews*, **2015**, *43,* 843-862. https://doi.org/10.1016/j.rser.2014.11.066

4. Soares, N.; Bastos, J.; Pereira, L.D.; Soares, A. Amaral, A.; Asadi, E.; Rodrigues, E.; Lamas, F.;Monteiro, H.; Lopes, M. A review on current advances in the energy and environmental performance of buildings towards a more sustainable built environment. *Renewable and Sustainable Energy Reviews*, **2017**, *77,* 845-860. https://doi.org/10.1016/j.rser.2017.04.027

5. Lund, H. Renewable energy strategies for sustainable development. *Energy*, **2007**, *32,* 912-919. https://doi.org/10.1016/j.energy.2006.10.017

6. Omer, A.M. Ground-source heat pumps systems and applications. *Renewable and sustainable energy reviews*, **2008**, *12,* 344-371. https://doi.org/10.1016/j.rser.2006.10.003

7. Kaushal, M. Performance analysis of clean energy using geothermal earth to air heat exchanger (GEAHE) in Lower Himalayan Region–Case study scenario. *Energy and Buildings*, **2021**, *248,* 111166. https://doi.org/10.1016/j.enbuild.2021.111166

8. Bisoniya, T.S. Design of earth–air heat exchanger system. *Geothermal Energy*, **2015**, *3,* 1-10. https://doi.org/10.1186/s40517-015-0036-2

9. Benhammou, M.; Draoui, B. Parametric study on thermal performance of earth-to-air heat exchanger used for cooling of buildings. *Renewable and Sustainable Energy Reviews*, **2015**, *44,* 348-355. https://doi.org/10.1016/j.rser.2014.12.030

10. Papakostas, K.; Tsamitros, A.; Martinopoulos, G. Validation of modified one-dimensional models simulating the thermal behavior of earth-to-air heat exchangers - Comparative analysis of modelling and experimental results. *Geothermics*, **2019**, *82,* 1-6. https://doi.org/10.1016/j.geothermics.2019.05.013

11. Su, H.; Liu, X.-B.; Ji, L.; Mu, J.-Y. A numerical model of a deeply buried air–earth–tunnel heat exchanger. *Energy and Buildings*, 2012, *48,* 233-239. https://doi.org/10.1016/j.enbuild.2012.01.029

12. Niu, F.; Yu, Y.; Yu, D.; Li, H. Heat and mass transfer performance analysis and cooling capacity prediction of earth to air heat exchanger. *Applied Energy*, **2015,** *137,* 211-221. https://doi.org/10.1016/j.apenergy.2014.10.008

13. Li, Q.; Su, H.; Lyu, Y.; Wei, S. Annual thermal performance analysis and optimization of earth-air heat exchanger by using a new 1D-2D hybrid numerical model. *Journal of Building Engineering*, **2023**, *71,* 106526. https://doi.org/10.1016/j.jobe.2023.106526

14. Xamán, J.; Hernández-López, I.; Alvarado-Juárez, R.; Hernández-Pérez, I.; Álvarez, G.; Chávez, Y. Pseudo transient numerical study of an earth-to-air heat exchanger for different climates of México. *Energy and Buildings*, **2015**, *99,* 273-283. https://doi.org/10.1016/j.enbuild.2015.04.041

15. Sawsan, M.; Ali, A.; Ayhem, D.; Wissam, Z. Optimization of bakers yeast production on grape juice using response surface methodology. *Acta Periodica Technologica*, **2021**, 89-110. https://doi.org/10.2298/APT2152089S

16. Weissman, S.A.; Anderson, N.G. Design of experiments (DoE) and process optimization. A review of recent publications. *Organic Process Research & Development*, **2015**, *19,* 1605-1633. https://doi.org/10.1021/op500169m

17. Sanusi, M.S.; Sunmonu, M.O.; Alasi, S.O. Influence of extrusion conditions on functional and textural properties of brown rice-watermelon seeds extruded snacks. *Acta Periodica Technologica*, **2023**, 81-91. https://doi.org/10.2298/APT2354081S

18. Budapanahalli, S.H.; Mallur, S.;Patil, A.Y.; Kumar, R. Optimization study on wear behaviour of aluminium 7075 hybrid composite containing silicon carbide and aluminium oxide using Taguchi method. *Acta Periodica Technologica*, **2023**, 129-136. https://doi.org/10.2298/APT2354129B

19. Amine Khorchef, M.; Serier, M.; Benariba, A. Optimizing Earth-Air Heat Exchangers for Sustainable Summer Cooling and Winter Heating. *Acta Mechanica Slovaca*, **2023,** *27,* 42-50. https://doi.org/10.21496/ams.2023.039

20. Ali, S.; Muhammad, N.; Amin, A.; Sohaib, M.; Basit, A.; Ahmad, T. Parametric optimization of earth to air heat exchanger using response surface method. *Sustainability*, **2019**, *11,* 3186. https://doi.org/10.3390/su11113186

21. Wang, X.; Bjerg, B.S.; Zhang, G. Design-oriented modelling on cooling performance of the earth-air heat exchanger for livestock housing. *Computers and electronics in agriculture*, **2018**, *152,* 51-58. https://doi.org/10.1016/j.compag.2018.07.006

22. Agrawal, K.K.; Bhardwaj, M.; Misra, R.; Das Agrawal, G.; Bansal, V. Optimization of operating parameters of earth air tunnel heat exchanger for space cooling: Taguchi method approach. *Geothermal Energy*, **2018**, *6,* 1-17. https://doi.org/10.1186/s40517-018-0097-0

23. Lin, Y.; Feng, H.; Yang, W.; Hao, X.; Tian, L.; Yuan, X. Thermal performance optimization of a semi-nested building coupled with an earth-to-air heat exchanger using iterative Taguchi method. *Renewable Energy*, **2022**, *195,* 1275-1290. https://doi.org/10.1016/j.renene.2022.06.116

24. Misra, R.; Bansal, V.; Agrawal, G.D.; Mathur, J.; Aseri, T.K. CFD analysis based parametric study of derating factor for Earth Air Tunnel Heat Exchanger. *Applied Energy*, **2013**, *103,* 266-277. https://doi.org/10.1016/j.apenergy.2012.09.041

25. Lebbihiat, N.; Atia, A.; Arıcı, M.; Meneceur, N.; Hadjadj, A.; Chetioui, Y. Thermal performance analysis of helical ground-air heat exchanger under hot climate: In situ measurement and numerical simulation. *Energy*, **2022**, *254,* 124429. https://doi.org/10.1016/j.energy.2022.124429

26. Entezari, S.; Taheri, A.; Khatibi, M.; Niazmand, H. Acceleration of melting process of phase change material using an innovative triplex-tube helical-coil storage unit: Three-dimensional numerical study. *Journal of Energy Storage*, **2021**, *39,* 102603. https://doi.org/10.1016/j.est.2021.102603

27. Entezari, S.; Shakiba, A.; Niazmand, H. Numerical investigation of the effects of cannula geometry on hydraulic blood flow to prevent the risk of thrombosis. *Computers in Biology and Medicine*, **2021**, *134,* 104484. https://doi.org/10.1016/j.compbiomed.2021.104484

28. Yang, D.; Guo, Y.; Zhang, J. Evaluation of the thermal performance of an earth-to-air heat exchanger (EAHE) in a harmonic thermal environment. *Energy Conversion and Management*, **2016**, *109,* 184-194. https://doi.org/10.1016/j.enconman.2015.11.050

29. Serageldin, A.A.; Abdelrahman, A.K.; Ookawara, S. Earth-Air Heat Exchanger thermal performance in Egyptian conditions: Experimental results, mathematical model, and Computational Fluid Dynamics simulation. *Energy Conversion and management*, **2016**, *122,* 25-38. https://doi.org/10.1016/j.enconman.2016.05.053

30. Misra, R.; Bansal, V.; Agrawal, G.D.; Mathur, J.; Aseri, T. Transient analysis based determination of derating factor for earth air tunnel heat exchanger in summer. *Energy and buildings*, **2013**, *58,* 103-110. https://doi.org/10.1016/j.enbuild.2012.11.001

31. Bhattacharya, S. *Central composite design for response surface methodology and its application in pharmacy*, in: *Response surface methodology in engineering science*, Kayaroganam P., Ed. IntechOpen, 2021. DOI: 10.5772/intechopen.95835

32. Montgomery, D.C. *Design and analysis of experiments*, John Wiley & Sons, 2017.

33. Granato, D.; de Araújo Calado, V.M. The use and importance of design of experiments (DOE) in process modelling in food science and technology. *Mathematical and statistical methods in food science and technology*, **2014,** *1,* 1-18.

34. Asfaram, A.; Ghaedi, M.; Agarwal, S.; Tyagi, I.; Gupta, V.K. Removal of basic dye Auramine-O by ZnS: Cu nanoparticles loaded on activated carbon: optimization of parameters using response surface methodology with central composite design. *RSC advances*, **2015,** *5,* 18438-18450. https://doi.org/10.1039/C4RA15637D

35. Myers, R.H.; Montgomery, D.C.; Anderson-Cook, C.M. *Response surface methodology: process and product optimization using designed experiments*, John Wiley & Sons,2016.

36. Srinivasan, A.;Viraraghavan, T. Oil removal from water by fungal biomass: a factorial design analysis. *Journal of Hazardous Materials*, **2010,** *175,* 695-702. https://doi.org/10.1016/j.jhazmat. 2009.10.065

37. Hacini, K.; Benatiallah, A.; Harrouz, A.; Belatrache, D. Efficiency assessment of an earth-air heat exchanger system for passive cooling in three different regions: The Algerian case. *FME Transactions*, **2021,** *49,* 1035-1046. https://doi.org/10.5937/fme2104035H

38. Boubakri, A.; Helali, N.; Tlili, M.; Amor, M.B. Fluoride removal from diluted solutions by Donnan dialysis using full factorial design. *Korean Journal of Chemical Engineering*, **2014,** *31,* 461-466. https://doi.org/10.1007/s11814-013-0263-9.

EVALUATION OF YAM (*Dioscorea rotundata*) CHIPS PRE-TREATMENT CONDITIONS (SALTING, SULPHITING, AND BLANCHING) COMBINED WITH DEHYDROFROZEN STORAGE FOR FRIES PRODUCTION

Kazeem Osuolale JIMOH, Simeon Olayiwola ADEDOKUN,
Oludolapo Akinyemi OSUNRINADE* ORCID

Department of Food Science and Technology, The Oke-Ogun Polytechnic Saki, Oyo State, Nigeria.

Yam is a highly perishable commodity lacking commercial utilization, like potato for French fries production. Frozen yam chips could be a panacea for its increased utilization as fries and export commodity for Nigeria. Hence, Yam (Dioscorea rotundata) Chips pre-treatment conditions (Salting, sulphiting, blanching) combined with dehydrofrozen storage for fries production was studied. Yam chips were pre-treated (Salting, sulphiting, and blanching), dehydrated (60 °C for 10 min), and stored for five months at frozen temperature. Standard methods were used to determine the proximate composition, textural and sensory properties of yam fry samples. Yam fries proximate composition ranged as 5.19-11.33% (moisture), 14-36.92% (Fat), 0.74-2.34% (Protein), 0.67-2.01% (Crude fibre), 0.97-1.06% (ash), and 51.7-75.93% (carbohydrate). The range of the textural properties of the yam fries were hardness (27.38-442.13 N), energy to peak (0.07-0.87 N·m), gumminess (8.55-271.98 N), chewiness (3.57-238.48 N), springiness (0.23-0.91 mm), stringiness (0.52-3.67 mm) and cohesion (0.1-0.75). Salted and blanched fried yam chips showed lesser variation in textural properties throughout storage. Sensory scores for appearance, aroma, taste, palatability, texture, and overall acceptability of the yam fries decreased as the storage duration of the yam chips increased, except for yam fries pre-treated by blanching and salting. The blanched and salted dehydrofrozen yam chips were acceptable by panelists until the fourth month of storage. High-quality and acceptable yam fries could be produced by combining salting and blanching of yam chips before dehydrofrozen storage. The commercial success of this product will reduce the huge post-harvest losses of yams and provide income to the farmers.

Keywords: Yam fries, dehydrofrozen, salting, blanching, sulphiting.

INTRODUCTION

Yam is commonly used as a food crop in many parts of the world and is often consumed as boiled, roasted, fried, mashed, or processed into flour, which is used to make bread, cakes, and other baked products. Yam belongs to the genus *Dioscorea* (Family *Dioscoreaceae), a* widely consumed staple food in Nigeria (Tamiru et al., 2017). Yams are Nigeria's fifth most harvested crops, following after cassava, maize, guinea corn, and beans/cowpeas (Nanbol & Namo, 2019). Yams are nutritious vegetables containing both macro- and micronutrients. Yam contains soluble and insoluble fiber, which can help reduce the risk of colon cancer and other digestive disorders (Bede & Zaixiang, 2021).

However, due to its high moisture content, large size, and high respiration rates, yam is highly perishable (Ferraro et al., 2016). Post-harvest losses of yam have been reported to range from 10-50% (Rees et al., 2012). The post-harvest losses stemmed from the fact that much of the yam cultivated is consumed fresh, and not much has been done to extend the

shelf life by value addition or in new product development. Yam tubers are usually stored under ambient tropical conditions, and changes in wholesomeness occur under such conditions. Diseases and pests' infestations during storage also lead to spoilage (Kiaya, 2014; Oluwole et al., 2016). The effect of these storage methods on yam's composition, appearance, and physical properties created more need for further research into its utilization, pre-treatment, and storage.

Chemical and biological changes occur in yam during processing which affects some of the quality attributes of the final product (Oyinloye & Yoon, 2020; Xiao et al., 2017); hence pre-treatments are employed to minimize some of these undesirable changes. Pre-treatments include dipping the processed yams into food-grade preservatives such as sulphites and their derivatives, citric acid, and sodium chloride (Agyei-Amponsah et al., 2014; Bobo-García et al., 2020; Hamdan et al., 2022). Some foods are blanched by hot water or steam (Moscetti et al., 2019). Dehydrofreezing is also a pre-treatment operation that involves dehydration to an appropriate moisture level before freezing (Hajji et al., 2019; Hissham et al., 2023). The prior dehydration leads to a reduction in ice crystal formation in the cell during freezing; therefore, post-thawing quality of products, such as colour, texture, flavour, and nutrients are preserved (Ando et al., 2011). Previous research (Li et al., 2019; Setyawan et al., 2021; Suriya et al., 2016) reported that dehydrofreezing is effective in producing high-quality yam flour with good sensory attributes and nutritional composition.

Yam fries can be made from different yams and prepared by boiling, baking, or frying (Ampofo et al., 2021). Yam fries are a popular food in Western Africa, especially in Nigeria. They are known by many names, such as Isu Dindin or Dundun. In recent years French fries have become popular in fast food restaurants in many tropical and developing countries where yams are also produced in large quantities. Potatoes, used for French fries production, are not locally available in many of these countries, thus making them expensive (Asogwa et al., 2017; Graham-Acquaah et al., 2015). Using yam as a substitute for potato in French fries' production will not only make the fries more affordable. Still, it will also help reduce post-harvest losses and enhance its distribution network.

Yam is produced in large quantities in Nigeria and is a highly perishable commodity, and it has not been processed to any significant extent commercially like potatoes (Glover-Amengor et al., 2013). Although Quansah et al. (2010) and Adedeji et al. (2022) reported the processing of yam tubers into frozen yam chips that can be used like frozen potato chips in baked or fried products, nonetheless the storability of the frozen chips was not considered. To utilize the full potential of yam (*Dioscorea* spp.), given their contributory role in food security as a staple crop to a large number of the world's population (Nanbol & Namo, 2019; Obidiegwu et al., 2020), the knowledge of its frozen storage will help to promote its utilization in the production of fries and as an export commodity, thus contributing to the attainment of United Nations (UN) sustainable development goals (SDGs 1, 2 and 3), especially in the developing countries.

In Nigeria, yam exportation could not be feasible without adding value. Developed nations are already used to consuming potatoes processed into frozen French fries (Wang et al., 2023; Wijesinha-Bettoni & Mouillé, 2019). This is often obtained from supermarkets and other retailers' houses. This is possible because they have a standardized processing procedure which is lacking in Nigeria. Thus, yam does not have the desired level of patronage that can significantly minimize post-harvest losses. The Nigerian economy could be improved if studies and manufacturing processes were standardized for frozen yam chips. The present study evaluated yam (*Dioscorea rotundata*) chips' pre-treatment conditions (salting, sulphiting, and blanching) combined with dehydrofrozen storage for fries production.

MATERIALS AND METHODS

MATERIALS

Fresh Yam tuber of *D. rotundata* cv. was purchased from the local market in Saki, Oyo state Nigeria. Ziploc bag, sodium metabisulphite, sodium Chloride, and vegetable oil (Kings®) were obtained for yam chips processing.

EQUIPMENT

Yam slicer (Chipper), solar powered Haier Thermocool freezer (HTF-2191HA/IW), Bosch Food dehydrator (BS 6605, China), 9 L steamer (Tosco 20116, ST11, China) were used for processing and storage of yam chips.

PROCESSING OF YAM CHIPS

Yam tubers were processed into frozen yam chips, like frozen potato chips in baked or fried products. Rapid yam peeling was done manually with a knife and chipped using yam chippers into a 1 cm x 1 cm chip surface. Afterward, the chips were washed with clean water before applying the pre-determined pre-treatments as shown in the experimental design (Table 1), before storage at frozen temperature (-20 °C) for five months.

Table 1. Experimental design for Yam pre-treatment

	Sample code	Treatment
1	SOG	Salting only
2	SUP	Sulphiting only
3	BLG	Blanching Only
4	SBA	Salting and blanching
5	SPG	Sulphiting and blanching
6	SUT	Untreated

Samples were salted only by soaking the chipped yam (100 g) in 100 ml water containing 2% NaCl. Sulphiting was done by submerging 100 g of chipped yam in 100 ml of water containing 1% sodium metabisulphite. Blanching was done using the steamer (Tosco 20116, ST11, China) operated at 80 °C for 3 min. Other samples involve the combination of salting, sulphiting, and blanching operations. After the yam sample pre-treatment, residual moisture on the yam surface was removed by a food dehydrator (Bosch 6605, China) operated at 60 °C for 10 min before frozen storage. The procedure for the preparation of yam chips is presented in Figure 1.

STORAGE CONDITIONS OF YAM CHIPS

The pre-treated and dehydrated yam chip samples were packaged individually in Ziploc packaging films and stored in the solar-powered Haier Thermocool freezer at freezing conditions.

Yam (Fully matured)
↓
Washing
↓
Sorting (Removal of defective and small tuber)
↓
Peeling
↓
Trimming
↓
Cutting (Cutting into strips by strip cutter)
↓
Sorting of strips
↓
Blanching/Salting/ Sulphiting
↓
Removal of excess moisture
↓
Packaging
↓
Storage in frozen condition (temperature -20°C)
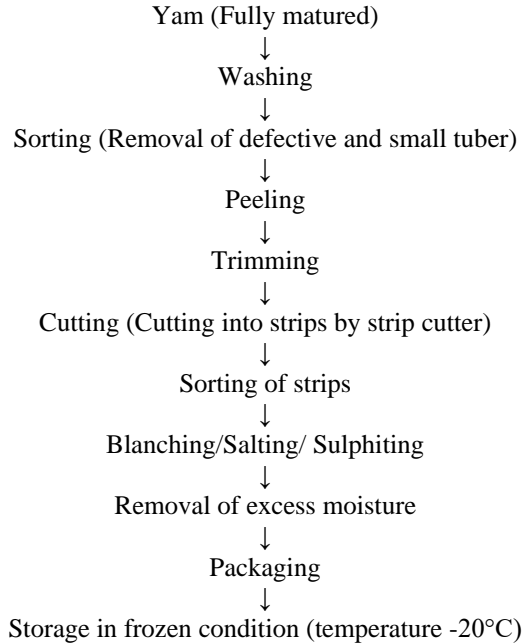
Figure 1. Flow chart for processing of yam chips

FRYING OF YAM CHIPS

Frozen yam chips were fried from stored samples using a deep fryer to manufacture yam chips fry for further analysis and sensory evaluation. The process is shown in Figure 2.

Taking out yam chips from storage
↓
Thawing to room temperature
↓
Deep Frying
↓
Yam chips fry
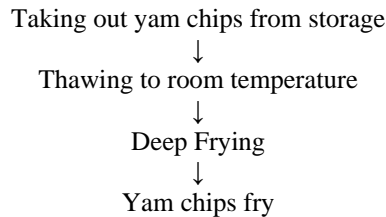
Figure 2. Flow chart for frying of yam chips

PROXIMATE COMPOSITION OF YAM CHIPS

The moisture, crude fiber, ash, and protein content of fried yam chips were determined in triplicate by the analysis methods of the Association of Official Analytical Chemists (AOAC, 2005). Briefly, the Soxhlet extraction of 5 g of yam chips samples determined the fat content. The Kjeldhal method, which involves the digestion of 5 g fried yam chips, and the distillation and titration, determined the protein content. A Muffle furnace operated at 550 °C was used to determine the ash content of 2 g of fried yam chips, while a forced draught oven operated at 105 °C determined the moisture content of the fried yam chips.

The crude fiber content was determined by boiling 2 g of fried yam chips with H_2SO_4 under reflux, followed by NaOH, before ashing. The fried yam chips' carbohydrate content and energy value were determined by difference and Atwater factor (Crude protein = 3.82, Crude fat= 8.37, and Carbohydrate= 4.16), respectively.

TEXTURE PROFILE ANALYSIS (TPA)

The fried yam chips texture profile analysis was done by the Testometric materials testing machines (0500-10080, Lancashire, England) using a winTest™ analysis approach. The machine is operated with 0.5 N preload, 50% deflection, 100 mm probe diameter, and 60 mm/min preload speed. The parameters determined were hardness (N), springiness, Adhesiveness (N·s), cohesiveness, Chewiness (N), gumminess (N), Energy to peak (N·m), and stringiness (mm).

SENSORY ANALYSIS

Thirty semi-trained panelists did the sensory evaluation of the fried yam chips to determine differences in the appearance, aroma, taste, palatability, and texture of yam fries from the different treatments. The average panelist's score on appearance, aroma, taste, palatability and texture of yam fries determined the overall acceptability. Panelists were provided with (coded) samples on paper plates and were instructed to score them on a 9-point hedonic scale.

STATISTICAL ANALYSIS

The data reported from the study were averages of triplicate observation. The results were analyzed using SPSS version 21.0, and the mean and standard error of the mean (SEM) of the triplicate analysis were calculated. The analysis of variance (ANOVA) was performed to determine significant differences between the mean (p<005). Correlation analysis was used to establish the model treatments for the optimum quality of yam chips and French fries.

RESULTS AND DISCUSSION

PROXIMATE COMPOSITION OF FRIED YAM CHIPS

The result of the proximate composition of the fresh and fried yam chips is presented in Table 2. The moisture and fat content of the raw and fried yam chips were significantly different at p<0.05. Specifically, the moisture content of the fresh yam chips (61.21%) was significantly higher than that of the fried yam chips (5.19-11.33%), whereas the fat content of the fresh yam chips (0.41%) was significantly (p<0.05) lower than that of the fried samples (14-36.92%) irrespective of the duration of storage. The values obtained for moisture and fat content agree with the study by Ojokoh & Gabriel (2010), which reported that the moisture content of fresh yam chips was significantly higher than that of fried yam chips, while the fat content of fresh yam chips was significantly lower than that of fried samples. Another study by Sobukola et al. (2008) found that the moisture content of fried yam chips decreased with increased frying time. The frying process is responsible for the changes in moisture and oil content in yam chips. During frying, moisture is displaced with

oil in the yam chips. Frying is both a cooking and a dehydration process that involves the transfer of heat and moisture. Heat is transferred from the hot oil to the yams during frying, providing enough energy to vaporize the moisture from the chips, while oil is absorbed simultaneously (Dodoo et al., 2022).

Table 2. Proximate composition of Fresh yam and Yam fries

		Moisture	Fat	Protein	Crude fibre	Ash	Carbohydrate	Energy
Raw yam	RYY	61.21[a]	0.41[i]	1.46[bc]	0.67[p]	0.97[efg]	33.82[m]	149.70[j]
0 Month	SOG	8.245[c]	18.44[gh]	1.44[bc]	1.4[h]	0.98[defg]	75.93[a]	421.88[i]
	SUP	11.33[b]	20.5[fg]	0.86[de]	1.11[l]	0.97[efg]	65.23[def]	446.22[g]
	BLG	7.32[cd]	14[i]	0.85[de]	1.06[m]	0.99[cdef]	75.78[a]	435.66[gh]
	SBA	10.46[b]	18.75[gh]	1.7[b]	0.96[o]	1.01[bcd]	67.11[cde]	442.63[g]
	SPG	11.76[b]	16.805[h]	0.8[de]	1.3[i]	1.00[cde]	68.33[bcd]	427.98[hi]
	SUT	6.62[cde]	19[gh]	0.74[e]	1.02[mn]	0.96[fg]	71.66[b]	459.96[f]
2½ Month	SOG2	8.26[c]	27.19[de]	2.37[a]	1.32[i]	0.955[g]	59.92[ghi]	485.86[de]
	SUP2	6.3[cde]	25.71[e]	1.61[bc]	1.01[n]	1.03[abc]	64.35[ef]	488.98[d]
	BLG2	6.94[cde]	25.71[e]	1.45[bc]	1.47[g]	1.05[ab]	63.40[fg]	484.46[de]
	SBA2	5.31[e]	21.58[f]	1.125[cde]	1.16[k]	1.06[a]	69.77[bc]	475.17[e]
	SPG2	7.44[cd]	30.73[c]	1.21[bcde]	1.26[j]	1.02[bc]	58.35[ij]	504.51[c]
	SUT2	15.68[a]	25.27[e]	1.51[bc]	1.26[j]	1.01[bcd]	55.27[ik]	447.20[g]
5th Month	SOG3	7.32[cd]	28.34[cd]	2.34[a]	1.90[c]	1[cdef]	59.1[hi]	491.99[d]
	SUP3	6.35[cde]	36.92[a]	2.4[a]	1.64[f]	1[cdef]	51.7[l]	533.24[a]
	BLG3	6.45[cde]	34.2[b]	1.76[b]	1.96[b]	0.97[fg]	54.68[kl]	520.35[b]
	SBA3	5.19[e]	28.75[cd]	1.41[bc]	1.74[d]	1[cdef]	61.91[fgh]	503.58[c]
	SPG3	7[cde]	25.89[e]	1.51[bc]	2.01[a]	1[cdef]	62.6[fgh]	482.84[de]
	SUT3	5.68[de]	30.05[c]	1.31[bcd]	1.70[e]	0.98[defg]	60.28[ghi]	507.27[c]

Results as mean. Values in the row with the same letter as superscript are not significantly different from each other (p ≤ 0.05). SOG-salted yam chips; SUP - Sulphited yam chips; BLG-Blanched yam chips; SBA-salted and blanched yam chips; SPG-sulphited and blanched yam chips; SUT-untreated yam chips.

Fried yam chips pre-treated by salting only, blanching only, and non-treatment of yam chips showed no significant difference in their moisture content throughout the five months of frozen storage. However, the moisture content of yam chips samples sulphited, salted before blanched, and sulphited before blanched decreased during storage, although this decrease was not significant (p<0.05) for 2 ½ and 5 months of yam chips storage. The decrease in moisture content of fried yam chips could be linked to drip losses during thawing. There was variation in drip loss of dehydrofrozen yam chips due to different pre-treatment conditions and duration of storage. This variation could be due to differences in the chips' mechanical behavior due to differing pre-treatment conditions and storage duration. Liu et al. (2021) demonstrated variation in the mechanical behaviour of fruit and vegetables due to differences in pre-drying conditions.

The fat content of fried yam chips increased as the duration of storage increases. The increase in fat content could have been caused by possible cellular damage of the yam chips during storage, thus making the yam chips absorb more fat due to losses in moisture. All samples except the salted and blanched yam chips had a significant (p<0.05) increase in the protein content of the fried yam chips as the duration of yam chips storage increased. However, the increase was not significant for fried samples from salted yam chips for 2 ½ and 5 months of yam chips storage. Frying increased the crude fibre composition of the fried yam chips, and the percentage of crude fibre was highest at five months of storage for all samples. An increase in crude fibre due to frying could be attributed to the loss of moisture due to evaporation during the frying process (Vora & Srinivasan, 2015) and possible cellular damage (Chen & Tengku, 2020).

For all treatments explored in this study, the ash content of the fried yam chips was not significantly different (p<0.05) for the 5-month frozen storage. The ash content was highest for the salted and blanched yam chips sample at 2 ½ months of storage. The carbohydrate content obtained by difference showed that the highest carbohydrate content for each treatment [SOG (75.93), SUP (65.23%), BLG (75.78), SPG (68.33) and SUT (71.66)] was obtained from fried yam chips produced before storage. However, the Salted and blanched (SBA) yam chips had its highest carbohydrate content of 69.77% at 2 ½ months of storage. As the storage duration increased, the carbohydrate content of the fried yam chips of salted, sulphited, and blanched samples decreased. The decrease in carbohydrate content during storage could be linked to drip losses that occurs during thawing. Irrespective of the treatment method used, the energy content was highest for fried yam chips produced at five months of fried yam chips storage. Generally, as the storage duration increased, the energy value of the fried yam chips increased significantly (p<0.05) for each treatment. This could be due to the higher fat content of fried yam chips caused by an increase in the absorption of frying oil (Damto & Chala, 2019), occasioned by cellular damage that occurred via freezing.

TEXTURAL PROPERTIES OF FRIED YAM CHIPS

Textural properties, a quality index for consumer acceptability of fried chips and fries, were investigated in this work. The effect of yam chip treatment and storage on the textural properties of fried yam chips is presented in Figure 3. The range of the textural properties of the yam fries were hardness (27.38-442.13 N), energy to peak (0.07-0.87 N·m), gumminess (8.55-271.98 N), chewiness (3.57-238.48 N), springiness (0.23-0.91 mm), stringiness (0.52-3.67 mm) and cohesion (0.1-0.75). The hardness (The peak force required to cut through yam chips) for fried yam chips from blanched, salted before blanching, and salted yam chips decreased as the storage duration increased. In comparison, the stored sulphited (SUP and SPG) and untreated yam chips samples had an initial decrease for the first two months of storage and a sudden increase in hardness, which later decreased during subsequent storage.

The energy to peak did not reflect a regular pattern of change in the fried yam chips. The cohesiveness (the degree to which the fried yam chips are compressed between the teeth before they break) of fried yam chips from salted and sulphited (SPG and SUP) yam chips decreased as the storage duration increased. In contrast, that of untreated yam chips increased with the duration of storage. However, blanched only and salted before blanching samples did not show a defined pattern of variation in their cohesiveness during storage. Generally, blanched yam chips did not show a regular pattern of change in their gumminess, chewiness, energy to peak, springiness, stringiness, and chewiness during storage.

Salted and blanched fried yam chips showed lesser variation in their textural properties throughout storage than others. This indicates reduced structural cell damage when the pretreatment of salting or blanching is adopted before dehydrofreezing. The fried yam chips from sulphited and blanched yam chips showed lesser variation in their hardness and springiness. In contrast, sulphited-only yam chips showed reduced variation in their chewiness and gumminess during storage. Reduced structural damage for blanched yam chips in this study corroborated previous reports that blanching significantly enhanced the textural properties of plant tissue after frying (Tiwari et al., 2018). Blanching causes starch gelatinization and thus reduces oil absorption of yam during frying, consequently improving its textural property. Also, Tiwari et al. (2022) reported that the increased firmness of plant tissue by blanching is attributable to the loss of non-fibre components and an increase in dry matter content.
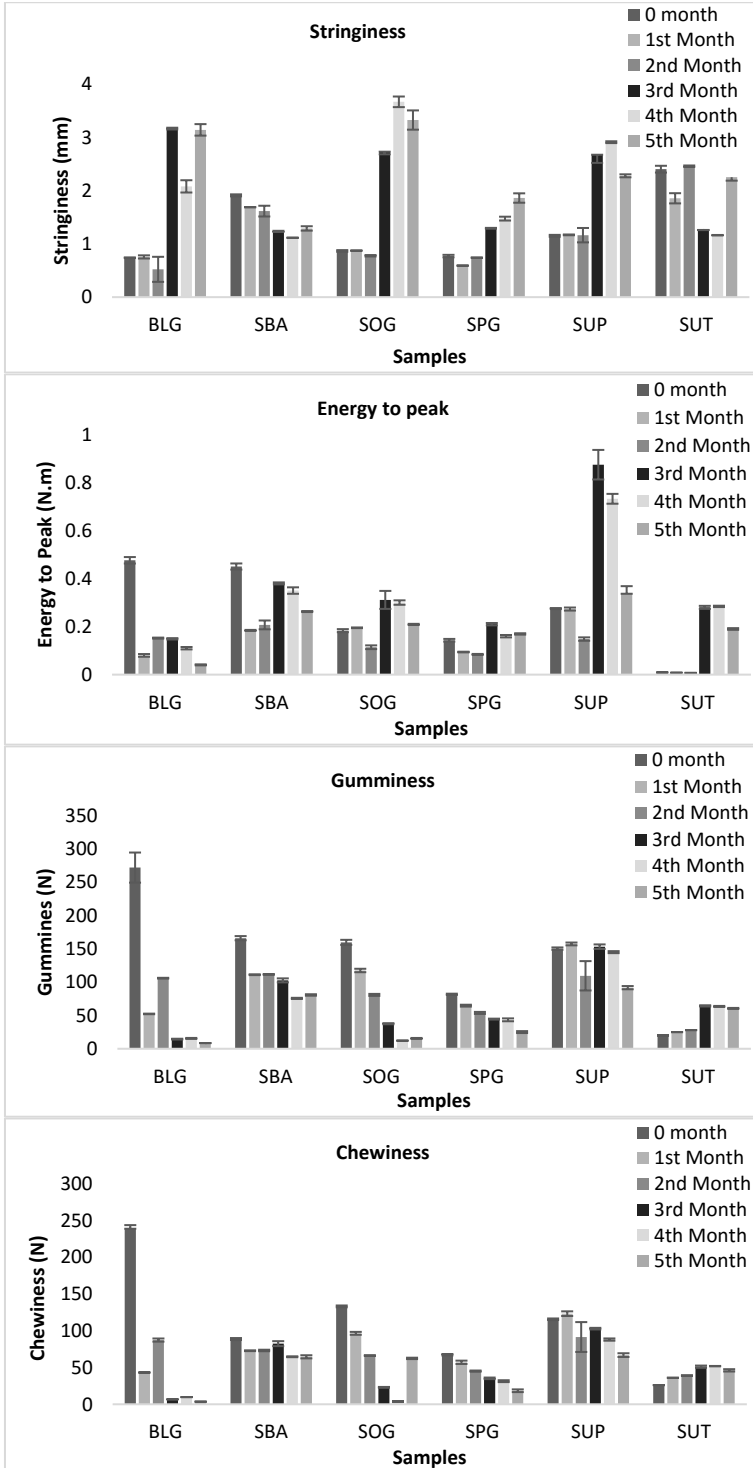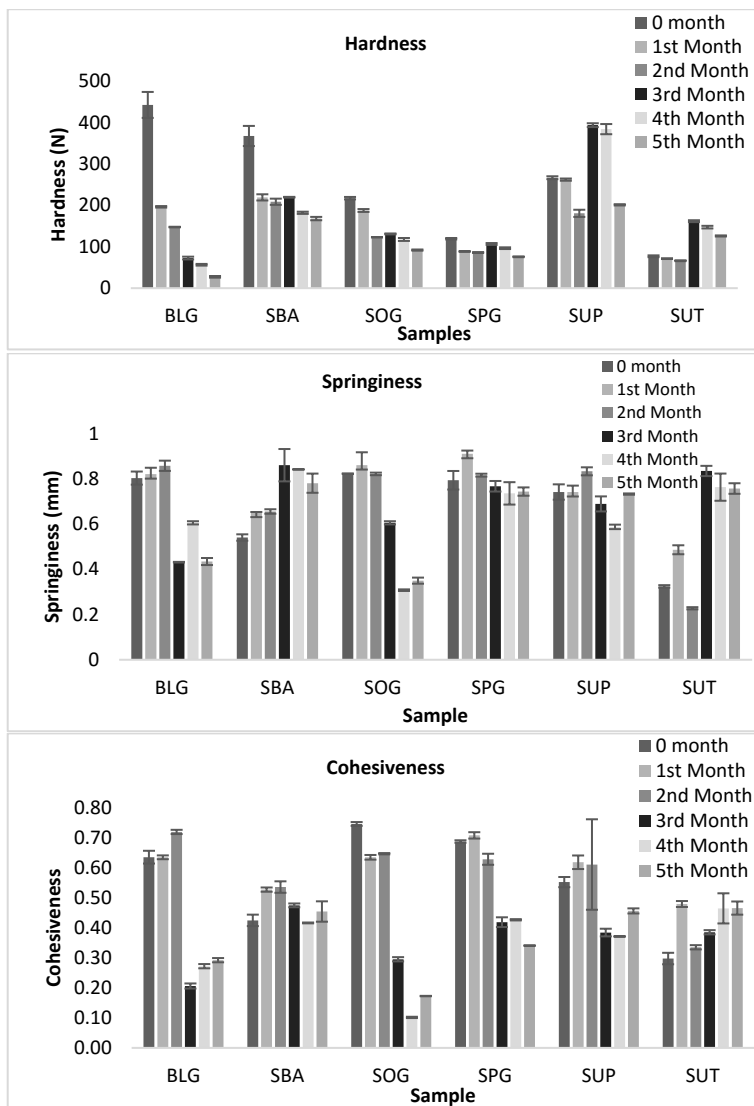
Figure 3. Textural Properties of Yam Fries

SENSORY PROPERTIES OF FRIED YAM CHIPS

The sensory ranking of fried yam chips produced from stored yam chips for five months is depicted in Figure 4. The result showed that aside from samples BLG and SOG, the sensory scores for appearance, aroma, taste, palatability, texture, and overall acceptability of the fried yam decreased as the storage duration of the yam chips increased. The panellist adjudged that fried yam chips stored up to 2 months without yam chips pre-treatment were acceptable, whereas samples BLG and SOG were still sensorially ranked acceptable until the 4th month of storage. Generally, for all fried yam chips from stored yam chips, the sensory panellist for the first two months of storage was not significantly different from fried

yam chips from fresh yam before storage. Considering the aforementioned pre-treated dehydrofrozen yam chips studied in this work did not show a significant variation in all the sensory parameters studied. At the same time, the blanched and salted dehydrofrozen yam chips were acceptable by panellists until the fourth month of storage. Also, the work of (Oluwole et al., 2016) reported that the heat treatment given to the raw yam chips by blanching positively influenced the sensory attributes of the resulting Deep-fried yam chips. However, the salting could have acted as a natural preservative and flavourant, impeding the yam chips storage to remain acceptable for the consumers (Sen, 2021).
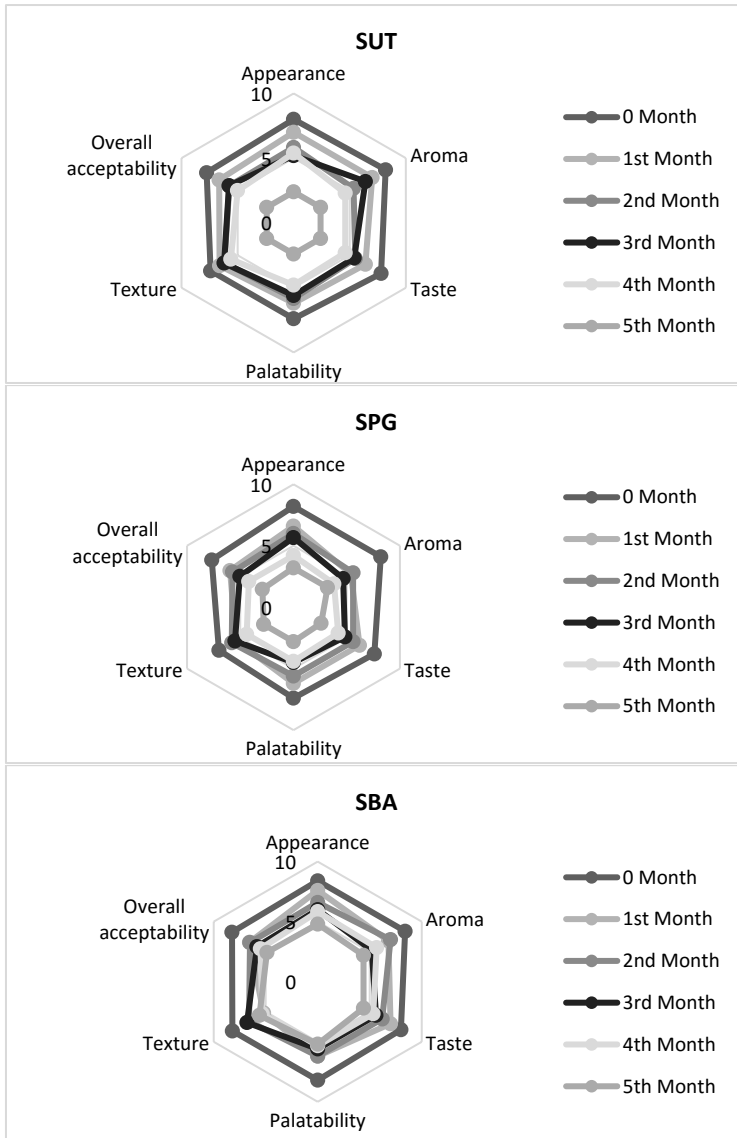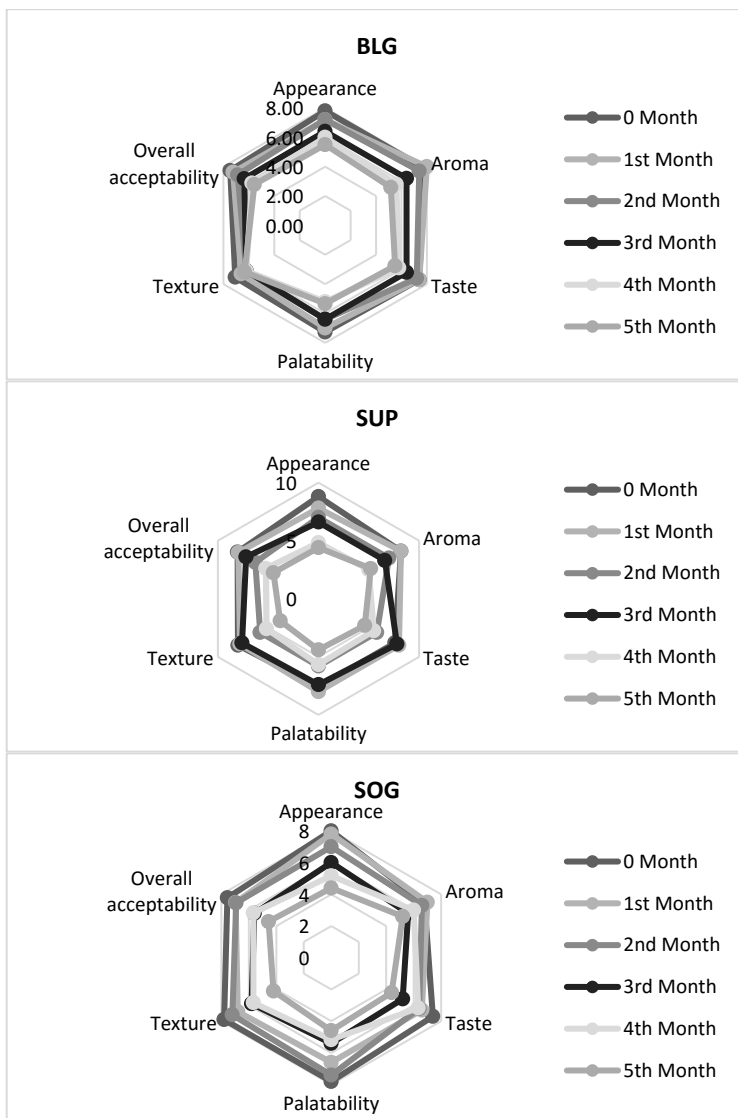
Figure 4. Radar chart for sensory acceptability of yam fries

PRINCIPAL COMPONENT ANALYSIS

Principal component analysis has been reported to be a significant chemometric tool for obtaining information from primary data (Granato et al., 2018). Yam fries' quality parameters of proximate composition, textural and sensory properties were analyzed by principal component analysis. As presented in Table 3, the first four principal components accounted for 83.13% of the total variation. The quality of yam fries was significantly explained by the first principal component, which accounted for the highest percentage of variation (43.6%). The factor loadings indicated that the first principal component was dominated by the yam fries sample produced before the storage of yam chips.

Concerning the biplot (Figure 5), the yam fries sample produced from pre-treated yam chips lies on the positive side of the first principal component and clusters with moisture and all sensory and textural properties except stringiness, thus indicating their positive correlation. At the same time, samples of yam fries produced from frozen-stored yam chips lie on the negative side of the first principal component and form a cluster with fat, protein, crude fibre, ash, carbohydrate, energy, and stringiness, thus their correlation.

The correlation result (Table 4-6) at a 5% significance level indicated that stringiness positively correlated with all sensory parameters except aroma and palatability. Also, cohesiveness positively correlated with all sensory parameters except aroma. In contrast, only the protein content of yam fries positively correlated with taste and overall acceptability. The moisture content of the yam fries positively correlated with stringiness, chewiness, hardness, and cohesiveness. Meanwhile, yam fries' fat, protein, and ash content positively correlated with springiness, energy-to-peak, and gumminess, respectively.

Table 3. Eigenvalues of First Four Principal Components

PC	Eigenvalue	% variance	Cumulative percentage (%)
1	8.72036	43.602	43.602
2	4.495	22.475	66.077
3	2.19405	10.97	77.047
4	1.2169	6.0845	83.1315

Figure 5. Biplot of the proximate, sensory and textural Properties of Yam fries
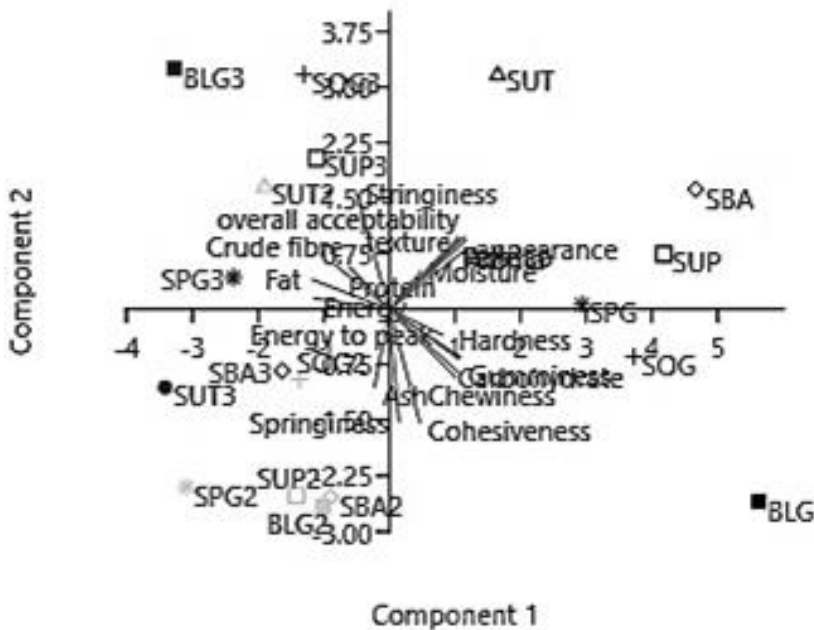
Table 4. Pearson's correlation between proximate composition and textural properties of the yam fries

	Stringi-ness	Energy to peak	Gum-miness	Chewiness	Hardness	Springiness	Cohesiveness
Moisture	**0.89**[b]	0.64	0.73	**0.89**[b]	**0.91**[b]	0.16	**0.95**[b]
Fat	0.08	0.27	0.00	0.01	0.02	**0.83**[b]	0.16
Protein	0.13	**0.88**[b]	0.29	0.30	0.41	0.67	0.26
Crude fibre	0.05	0.50	0.04	0.05	0.02	0.80	0.07
Ash	0.33	0.70	**0.81**[b]	0.76	0.63	0.47	0.32
Carbohydrate	0.05	0.24	0.00	0.01	0.02	0.35	0.08
Energy	0.13	0.51	0.01	0.03	0.06	0.87	0.18

b - Significant correlation at 5% level

Table 5. Pearson's correlation between Textural properties and sensory parameters of the yam fries

	Appearance	Aroma	Taste	Palatability	Texture	Overall acceptability
Stringiness	**0.94**[b]	0.80	**0.88**[b]	0.66	**0.86**[b]	**0.91**[b]
Energy to peak	0.10	0.12	0.09	0.06	0.04	0.25
Gumminess	0.08	0.09	0.18	0.15	0.15	0.21
Chewiness	0.14	0.17	0.15	0.12	0.16	0.32
Hardness	0.05	0.06	0.06	0.04	0.04	0.13
Springiness	0.45	0.33	0.54	0.39	0.55	0.43
Cohesiveness	**0.87**[b]	0.74	**0.96**[b]	**0.80**[b]	**0.85**[b]	**0.87**[b]

b - Significant correlation at 5% level

Table 6. Pearson's correlation between proximate composition and sensory parameters of the yam fries

	Appearance	Aroma	Taste	Palatability	Texture	Overall acceptability
Moisture	0.14	0.18	0.28	0.19	0.22	0.11
Fat	0.01	0.01	0.06	0.04	0.12	0.04
Protein	0.10	0.32	**0.85**[b]	0.62	0.68	**0.92**[b]
Crude fibre	0.22	0.14	0.22	0.26	0.45	0.23
Ash	0.14	0.09	0.07	0.16	0.13	0.13
Carbohydrate	0.03	0.05	0.14	0.09	0.21	0.13
Energy	0.00	0.01	0.05	0.02	0.06	0.02

b - Significant correlation at 5% level

CONCLUSION

The effect of salting, blanching, and sulphiting on the quality of fried yams from yam chips dehydrated and frozen for five months showed a significant variation in the proximate composition, textural properties and sensory acceptability of yam fries. Yam chips pretreated by salting only, blanching only, and non-treatment showed no significant difference in their moisture content throughout the five months of yam chips frozen storage. However, the moisture content of yam chips samples sulphited, salted before blanched, and sulphited before blanched decreased during storage compared with others. Salted and blanched fried yam chips showed lesser variation in their textural properties throughout storage. The blanched and salted dehydrofrozen yam chips were acceptable by panelists until the 4th month of storage. Therefore, high-quality and acceptable yam fries could be produced by blanching or salting yam chips before dehydrofreezing.

REFERENCES

1. Adedeji, O.; Samuel, J.; Ayoola, B. Chemical composition, physical and sensory properties of dehydrofrozen yam chips as influenced by pre-drying conditions. *Carpathian Journal of Food Science & Technology*, **2022**, *14*(3), 86-93.
2. Agyei-Amponsah, J.; Owureku-Asare, M.; Agbemavor, W. S. K.; Armah, J.; Okyere, A.; Baidoo, E.; Dowuona, S.; Tortoe, C. Quality characteristics of pre-treated yam chips produced from irradiated yams. *British Journal of Applied Science & Technology*, **2014**, *4*(36), 5045–5057.
3. Ampofo, D.; Agbenorhevi, J. K.; Firempong, C. K.; Adu-Kwarteng, E. Glycemic index of different varieties of yam as influenced by boiling, frying and roasting. *Food Science & Nutrition*, **2021**, *9*(2), 1106–1111.
4. AOAC. *Official method of Analysis.* (18th ed.). Association of Officiating Analytical Chemists, Washington DC, 2005.
5. Asogwa, I. S.; Okoye, J. I.; Oni, K. Promotion of indigenous food preservation and processing knowledge and the challenge of food security in Africa. *Journal of Food Security*, **2017**, *5*(3), 75–87.
6. Bede, D.; Zaixiang, L. Recent developments in resistant starch as a functional food. *Starch‑Stärke*, **2021**, *73*(3–4), 2000139.
7. Bobo-García, G.; Arroqui, C.; Merino, G.; Vírseda, P. Antibrowning compounds for minimally processed potatoes: A review. *Food Reviews International*, **2020**, *36*(5), 529–546.
8. Chen, S. Y.; Tengku, R. T. M. Effect of cooking methods on nutritional composition and antioxidant properties of lotus (*Nelumbo nucifera*) rhizome. *Food Research*, **2020**, *4*(4), 1207–1216.
9. Damto, T.; Chala, G. Effect of blanching and frying time on the sensory quality of fried sweet potato chips. *Food and Nutrition Science-An International Journal*, **2019**, *3*, 1-17.
10. Dodoo, D.; Adjei, F.; Tulashie, S. K.; Adukpoh, K. E.; Agbolegbe, R. K.; Gawou, K.; Manu, G. P. Quality evaluation of different repeatedly heated vegetable oils for deep-frying of yam fries. *Measurement: Food*, **2022**, *7*, 100035.
11. Ferraro, V.; Piccirillo, C.; Tomlins, K.; Pintado, M. E. Cassava (Manihot esculenta Crantz) and yam (Dioscorea spp.) crops and their derived foodstuffs: Safety, security and nutritional value. *Critical Reviews in Food Science and Nutrition*, **2016**, *56*(16), 2714–2727.
12. Glover-Amengor, M.; Quansah, J.; Peget, F. M. Performance and acceptability of legume-fortified yam flours. *Food Science and Quality Management*, **2013**, *17*, 14-19.

13. Graham-Acquaah, S.; Ayernor, G. S.; Bediako-Amoa, B.; Saalia, F. S.; Afoakwa, E. O.; Abbey, L. Effect of Blanching and Frying on Textural Profile and Appearance of Yam (D ioscorea rotundata) French Fries. *Journal of Food Processing and Preservation*, **2015**, *39*(1), 19–29.

14. Granato, D.; Putnik, P.; Kovačević, D. B.; Santos, J. S.; Calado, V.; Rocha, R. S.; Cruz, A. G. D.; Jarvis, B.; Rodionova, O. Y.; Pomerantsev, A. Trends in chemometrics: Food authentication, microbiology, and effects of processing. *Comprehensive Reviews in Food Science and Food Safety*, **2018**, *17*(3), 663–677.

15. Hajji, W.; Gliguem, H.; Bellagha, S.; Allaf, K. Impact of initial moisture content levels, freezing rate and instant controlled pressure drop treatment (DIC) on dehydrofreezing process and quality attributes of quince fruits. *Drying Technology*, **2019**, *37*(8), 1028–1043.

16. Hamdan, N.; Lee, C. H.; Wong, S. L.; Fauzi, C. E. N. C. A.; Zamri, N. M. A.; Lee, T. H. Prevention of enzymatic browning by natural extracts and genome-editing: A review on recent progress. *Molecules*, **2022**, *27*(3), 1101.

17. Hissham, M. H.; Kamarudin, K. H.; Isa, M. I. N.; Md Salim, N. S. Characterization of freeze-dried ginger slices with carboxymethyl cellulose as potential coating material prior to osmotic dehydration. *Food Research*, **2023**, *7*(3), 48–54.

18. Kiaya, V. Post-harvest losses and strategies to reduce them. *Technical Paper on Post-harvest Losses, Action Contre La Faim (ACF)*, **2014**, *25*, 1–25. https://www.actioncontrelafaim.org/wp-content/uploads/2018/01/technical_paper_phl.pdf

19. Li, L.; Zhang, M.; Bhandari, B. Influence of drying methods on some physicochemical, functional and pasting properties of Chinese yam flour. *LWT*, **2019**, *111*, 182–189.

20. Liu, C.; Xue, Y.; Guo, J.; Ren, H.; Jiang, S.; Li, D.; Song, J.; Zhang, Z. Citric acid and sucrose pre-treatment improves the crispness of puffed peach chips by regulating cell structure and mechanical properties. *LWT*, **2021**, *142*, 111036.

21. Moscetti, R.; Raponi, F.; Monarca, D.; Bedini, G.; Ferri, S.; Massantini, R. Effects of hot-water and steam blanching of sliced potato on polyphenol oxidase activity. *International Journal of Food Science & Technology*, **2019**, *54*(2), 403–411.

22. Nanbol, K. K.; Namo, O. The contribution of root and tuber crops to food security: A review. *J. Agric. Sci. Technol. B*, **2019**, *9*, 221–233.

23. Obidiegwu, J. E.; Lyons, J. B.; Chilaka, C. A. The Dioscorea Genus (Yam) - An appraisal of nutritional and therapeutic potentials. *Foods*, **2020**, *9*(9), 1304.

24. Ojokoh, A. O.; Gabriel, R. A. O. A comparative study on the storage of yam chips (gbodo) and yam flour (elubo). *African Journal of Biotechnology*, **2010**, *9*(21), 3175–3177.

25. Oluwole, O.; Odediran, O.; Alagbe, G.; Eboagwu, I.; Jegede, A.; Ogundeji, K.; Olokoshe, A.; Asieba, G.; Onyibe, J. Polyphenol oxidase activity and inhibition in white yam (Dioscorea rotundata. Var. Laasirin) chips as African fries for human consumption. *Journal of Food Science and Engineering*, **2016**, *6*(1), 43.

26. Oyinloye, T. M.; Yoon, W. B. Effect of freeze-drying on quality and grinding process of food produce: A review. *Processes*, **2020**, *8*(3), 354.

27. Quansah, J. K.; Saalia, F. K.; Abbey, L. D.; Annor, G. A. Performance of yam as an alternative to frozen potato French fries. *Nature and Science*, **2010**, *8*(12), 70–78.

28. Rees, D.; Westby, A.; Tomlins, K.; Van Oirschot, Q.; Cheema, M. U.; Cornelius, E.; Amjad, M. *Tropical root crops*. In: Rees, D., Farrell, G., Orchard, J., Eds.; Crop Post-harvest: Science and Technology, Perishables. Wiley-Blackwell, Chichester, UK, 2012; pp. 392-413.

29. Sen, M. *Food chemistry: Role of additives, preservatives, and adulteration*. In Sen, M. Ed.; Food Chemistry: The Role of Additives, Preservatives and Adulteration, Scrivener Publishing LLC, 2022; pp. 1–42. https://doi.org/10.1002/9781119792130.ch1

30. Setyawan, N.; Maninang, J. S.; Suzuki, S.; Fujii, Y. Variation in the physical and functional properties of Yam (Dioscorea spp.) Flour produced by different processing techniques. *Foods*, **2021**, *10*(6), 1341.

31. Sobukola, O. P.; Awonorin, S. O.; Sanni, L. O.; Bamiro, F. O. Deep-fat frying of yam slices: Optimization of processing conditions using response surface methodology. *Journal of Food Processing and Preservation*, **2008**, *32*(3), 343–360.

32. Suriya, M.; Baranwal, G.; Bashir, M.; Reddy, C. K.; Haripriya, S. Influence of blanching and drying methods on molecular structure and functional properties of elephant foot yam (Amorphophallus paeoniifolius) flour. *LWT-Food Science and Technology*, **2016**, *68*, 235–243.

33. Tamiru, M.; Natsume, S.; Takagi, H.; White, B.; Yaegashi, H.; Shimizu, M.; Yoshida, K.; Uemura, A.; Oikawa, K.; Abe, A. Genome sequencing of the staple food crop white Guinea yam enables the development of a molecular marker for sex determination. *BMC Biology*, **2017**, *15*, 1-20.

34. Tiwari, P.; Joshi, A.; Varghese, E.; Thakur, M. Process standardization and storability of calcium fortified potato chips through vacuum impregnation. *Journal of Food Science and Technology*, **2018**, *55*, 3221–3231.

35. Tiwari, P.; Thakur, M.; Joshi, A.; Raigond, P.; Arora, B. Development of Iron fortified potato fries through Vacuum assisted processing strategies. *Journal of Food Science and Technology*, **2022**, *59*(12), 4644–4652.

36. Vora, J. D.; Srinivasan, P. Biochemical, organoleptic and anti-microbial assessment of lotus stem (Nelumbo nucifera). *International Journal of Food and Nutritional Sciences*, **2015**, *4*(3), 63.

37. Wang, Z.; Liu, H.; Zeng, F.; Yang, Y.; Xu, D.; Zhao, Y.-C.; Liu, X.; Kaur, L.; Liu, G.; Singh, J. Potato processing industry in China: Current scenario, future trends and global impact. *Potato Research*, **2023**, *66*(2), 543–562.

38. Wijesinha-Bettoni, R.; Mouillé, B. The contribution of potatoes to global food security, nutrition and healthy diets. *American Journal of Potato Research*, **2019**, *96*, 139–149.

39. Xiao, H.-W.; Pan, Z.; Deng, L.-Z.; El-Mashad, H. M.; Yang, X.-H.; Mujumdar, A. S.; Gao, Z.-J.; Zhang, Q. Recent developments and trends in thermal blanching – A comprehensive review. *Information Processing in Agriculture*, **2017**, *4*(2), 101–127.

EXPLORING HIGH-YIELD OILSEEDS: A STUDY OF RAPESEED AND CAMELINA VARIETIES AS VALUABLE SOURCES OF OIL AND PROTEIN

Nada GRAHOVAC[1], , Milica ALEKSIĆ[2] , Zorica STOJANOVIĆ[2] , Željko MILOVAC[1] ,
Slavko VASIN[1] , Vladimir MIKLIČ[1] , Ana MARJANOVIĆ JEROMELA[1]*

[1] Institute of Field and Vegetable Crops, Maksima Gorkog 30, Novi Sad, Serbia.
[2] Faculty of Technology Novi Sad, University of Novi Sad, Bulevar Cara Lazara 1, Novi Sad, Serbia.

Oilseeds such as camelina and rapeseed are cultivated primarily for their high-quality oil. The oil derived from both crops is characterized by a high content of unsaturated fatty acids, tocopherols, phenols, and vitamin E. The camelina and rapeseed oils are applied in various branches of industry including food, pharmaceutical, chemical, and for obtaining biofuels. These oilseeds synthesize a significant amount of protein. These oilseeds play a major role in addressing the growing issue of protein deficit in the diets of people worldwide because of their high protein content. Efforts in breeding are essential to develop genotypes with high yield and protein content, while also maintaining high oil content and ensuring adaptability to climatic changes. During 2022/2023, various genotypes of rapeseed and camelina were grown in the experimental fields of the Institute of Field and Vegetable Crops Novi Sad in order to select varieties with ideal attributes. Among these, genotype NS Svetlana exhibited the highest oil content of 44.85 %, whereas genotype NS Dunav demonstrated the highest protein content of 24%. While camelina generally presented lower oil content compared to rapeseed, Genotype III stood out with a maximum oil content of 37.82%. Camelina also displayed significantly higher protein content than rapeseed. Protein content in camelina reached 26.59% in the case of Genotype I.

Keywords: agricultural sustainability, breeding, camelina, high-yield verities, oilseeds, rapeseed, sustainable protein.

INTRODUCTION

The exponential growth of the global population has intensified the search for sustainable solutions to meet the growing demand for protein, ensure cleaner energy sources, and reduce environmental degradation. As a result, there has been intensive research on plants with high oil and protein content, such as rapeseed and camelina, in recent decades.

Rapeseed (*Brassica napus*) and camelina (*Camelina sativa*) belong to the Brassicaceae family (1). In recent decades, there has been a renewed interest in cultivating and improving the quality of these oil crops due to the diverse uses of their oil and protein. This renewed interest is driven by the escalating demand for alternative protein sources in the food industry and the pivotal role of their oil in diverse industrial applications, including biodiesel and biofuel production (1, 2, 3).

Rapeseed currently stands as the world's third ranked cultivated oilseed crop. The first rapeseed variety of the Institute of Field and Vegetable Crops was registered in 1997 under the name "Banaćanka". Thriving in regions with a moderate climate and under optimal agroecological conditions, along with precisely formulated fertilizer and effective pest and disease control, rapeseed consistently yields remarkably high outputs (1-6). The ongoing five-year grain yield for this oilseed in Serbia currently stands at 3 tons per hectare and

---

continues to grow (6). Renewed interest in the cultivation of camelina emerged in the twentieth century. The first registered spring camelina varieties in Serbia, were NS Slatka and NS Zlatka (2). Compared to rapeseed, camelina exhibited lower soil quality requirements, a shorter growing period (85-100 days), cold hardiness, lower moisture needs, and superior resistance to diseases and pests (2, 7, 8, 9, 10). Rapeseed seeds typically contain between 40% and 48% of oil, with protein content spanning from 18% to 25% (3). In comparison to rapeseed, camelina has lower oil content (~36%), but higher protein content, ranging from 24% to 35% (1, 3, 11, 12, 13). Camelina oil is distinguished by its higher proportion of polyunsaturated fatty acids, approximately 60% (16), compared to rapeseed, which contains 30% to 40% polyunsaturated fatty acids (14). The predominant unsaturated fatty acid in camelina oil is α-linolenic (~35%), followed by linolenic fatty acid (~20%) while rapeseed oil contains a high content of oleic fatty acid (~60%) followed by linolenic (~30%) and α-linolenic (~10%) (8, 11, 16-20). Due to their fatty acid composition and other beneficial components (tocopherols, polyphenol and carotenoids), rapeseed and camelina oil are high-quality edible oils and have positive effects on consumers health (11, 17, 19, 20). The oil derived from rapeseed and camelina finds diverse applications in human nutrition, the food industry, and the pharmaceutical sector. Additionally, rapeseed and camelina oil serve as technical oils in the production of biodiesel and bio-jet fuel (8, 15).

After oil extraction, the rapeseed and camelina cake retain up to 40% of the protein and are most commonly used as animal feed (1, 2). While some plant proteins may contain lower levels of amino acids such as methionine and cysteine, rapeseed and camelina proteins contain sufficient quantities of these amino acids. However, the quantity of lysine in these proteins is limited (2, 11, 15, 22, 23). Because of good digestibility and nutritional properties, rapeseed and camelina protein isolates can find applications in various food industries (15, 18, 24).

The breeding of camelina and rapeseed aims to improve the existing genotypes to increase the seed oil and protein content with a sustainable yield. In addition to increasing seed oil and protein content, breeding is carried out to obtain genotypes of camelina and rapeseed with reduced antinutrient content (erucic acid and glucosinolates) (25-27). This study investigates oil and protein levels in rapeseed and camelina seeds across different genotypes to identify those with desirable content. Future breeding endeavours for rapeseed and camelina strive to develop high-yielding varieties with elevated oil and protein levels, potentially benefiting diverse industries.

EXPERIMENTAL

MATERIALS

Fifteen genotypes of rapeseed and four genotypes of camelina (experimental lines) were cultivated on the fields of the Institute of Field and Vegetable Crops in Novi Sad at the site of Rimski Šančevi (latitude 45°20' N and longitude 19°51' E) at an altitude of 84 m and chernozem soil with the application of optimal agrotechnics for the plant species, during the 2022/2023 season. Seven winter rapeseed hybrids (NS Ras, NS Vid, NS Pek, NS Vir, NS Div, NS Marin, NS Dunav) and eight winter varieties (NS Zlatna, NS Jasna, NS Anna, NS Ilia, NS Zorica, NS Kata, NS Jelena, NS Svetlana) were investigated. All tested camelina genotypes were experimental lines (which are not yet registered, and after registration they will get a commercial name) from the breeding program of the Institute of Field and Vege-

table Crops. Rapeseed genotypes were planted with a spacing of 6 x 15 m, while camelina genotypes were planted with a spacing of 8 x 1.25 m, each replicated three times. Rapeseed was sown in winter, while camelina was sown in spring. The 2022/2023 season experienced a warm but extremely humid spring. Seed samples were collected from each genotype for assessment of seed quality traits, including oil and protein content, with three replicates.

METHODS

Chemical analyses

The Maran analyzer, utilizing the NMR (Nuclear Magnetic Resonance) method developed by Granlund and Zimmerman (1975) (28), was employed to determine the oil content, expressed as a percentage of the seed. The total seed protein content was assessed through the standard Dumas procedure. These analyses were conducted in the chemical laboratory of the Institute of Field and Vegetable Crops, specifically in the Oil Crops Department, located in Novi Sad, Serbia.

Statistical analyses

Data were processed using PCA (Principle Component Analysis) analysis using the computer program PAST 4.09.32.

RESULTS AND DISCUSSION

The results of the analysis on the content of oil and protein in seeds of rapeseed genotypes are shown in Table 1. PCA analysis was used to better understand the relationship between protein and oil content in the genotypes of camelina and rapeseed.

The average oil content across all genotypes was 43.35%. ranging from 41.22% to 44.85%. These values are consistent with literary data stating that the oil content falls within the range of 41.5% to 46.9% (1-4. 13). Genotype NS Svetlana (44.85%) and NS Jelena (44.83%) exhibited the highest seed oil content. while NS Zorica (41.22%) and NS Ilia (41.49%) had the lowest. Similarly. the average seed protein content was 22.72%. varying from 21.49% to 24.00% aligning with the literature stating that the seed protein content ranges from 18% to 25 % (1-4, 13). The highest seed protein content is in the genotypes NS Marin (23.86%) and NS Zorica (23.80%), and the lowest in the NS Pek (21.49%) and NS Svetlana (21.51%) genotypes. Various studies have explored how genotype and growing conditions influence these parameters. It has been observed that the seed oil and protein content are negatively correlated (29-33). Pritchard et al. (31) concluded that rapeseed cultivation conditions significantly affect the content of these components. High temperatures during flowering (over 16 °C) and insufficient moisture during seed filling tend to reduce the oil content. Rapeseed cultivated in humid and colder regions has the potential to produce seeds richer in oil (~41.4%). but poorer in protein (~20.1%) (31). In the 2006/2007 season, various rapeseed genotypes were grown at the same site of the Institute of Field and Vegetable Crops Novi Sad, under wet and colder spring conditions. Rapeseed exhibited an average protein content of 17.25% and an average oil content of 45.69% (7), while genotypes grown during the 2022/2023 season had an average seed oil content of 43.35% and an average seed protein content of 22.72%.

Table 1. Oil and protein content in the seed of 15 rapeseed genotypes grown in 2022/2023 season at fields of Institute of Field and Vegetable Crops Novi Sad

Rapeseed genotypes	Oil (%)	Protein (%)	Oil + Protein (%)
NS Ras	42.93	23.46	66.39
NS Vid	44.31	22.31	66.62
NS Pek	43.97	21.49	65.46
NS Vir	44.00	22.64	66.64
NS Div	43.88	22.50	66.38
NS Marin	42.97	23.86	66.83
NS Dunav	42.57	24.00	66.57
NS Zlatna	43.92	23.06	66.98
NS Jasna	43.73	21.92	65.65
NS Anna	42.18	23.37	65.55
NS Ilia	41.49	22.91	64.40
NS Zorica	41.22	23.80	65.02
NS Kata	43.45	22.15	65.60
NS Jelena	44.83	21.85	66.68
NS Svetlana	44.85	21.51	66.36
Average	43.35	22.72	66.07

In Figure 1. rapeseed genotypes are grouped into four clusters based on their seed oil and protein content. In the first group are the genotypes NS Gold, NS Vir, NS Vid, NS Div, and NS Jelena. These genotypes exhibited high seed oil content ranging from 43.88% to 44.83% and low seed protein content ranging from 21.85% to 22.64%. The second group consists of the genotypes NS Kata, NS Jasna, and NS Pek, which had a lower seed protein content in the range from 21.49% to 22.15 %. The second group is characterized by a high seed oil content in the range of 43.45% to 43.97% but is lower compared to genotypes in the first group. The third group consists of genotypes NS Martin, NS Dunav, and NS Ras, and they are characterized by high seed protein content ranging from 23.46% to 24% and low seed oil content compared to the groups 1 and 2, ranging from 42.57% to 42.97 %. The fourth group consists of the genotypes NS Anna, NS Zorica, and NS Ilia, and this is the group with the lowest seed oil content ranging from 41.22% to 42.97%. The seed protein content is lower compared to genotypes in the third group, but higher compared to geno-types in first and second and ranges from 22.91% to 23.80%. Notably, NS Svetlana stands out with the highest seed oil content (44.85%) and lowest seed protein content (21.51%), while NS Zlatna exhibits equally high levels of oil (43.92%) and protein (23.06%). Compa-red with previous studies, the seed oil content of rapeseed genotypes ranged from 43.11% to 49.26% in 2006/2007 (14), and from 40.97% to 43.07% in 2008/2009 (32, 33), seed pro-tein content ranged from 15.84% to 18.79% in 2006/2007, and from 20.27% to 22.73% in 2008/2009. Consistent with our findings, previous studies also observed a negative correla-tion between seed oil and protein content across different genotypes. High seed oil content is followed by low seed protein content (genotypes NS Zlatna (2022/20223), NS-L-102 (2006/2007) (32, 33), and Kata (2007/2008) (14)) and high seed protein content is followed by low seed oil content (genotypes NS Marin (2022/2023), NS-L-129 (2006/2007) (32, 33) and N-H-3 (2007/2008) (14)). The majority of genotypes have average seed oil and protein content.
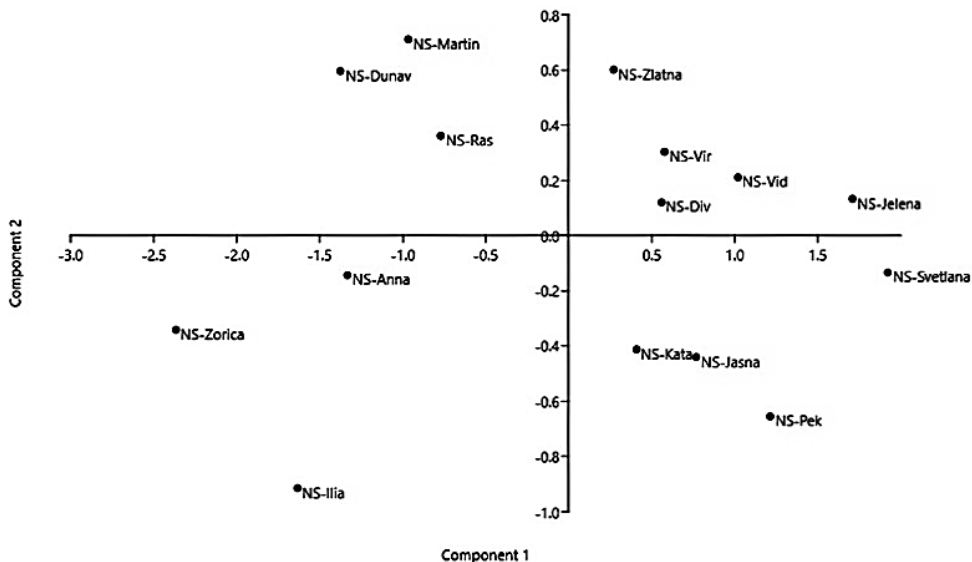
Figure 1. Principle Component Analysis for oil and protein content in rapeseed genotypes

Table 2. represents the seed oil and protein content in four camelina genotypes. The oil content ranged from 36.76% to 37.82%. while the protein content ranged from 24.54% to 26.59%. These values align closely with the literary data (2, 11, 16, 17).

Table 2. Oil and protein content in different camelina genotypes grown in 2022/2023 season at fields of Institute of Field and Vegetable Crops Novi Sad

Camelina genotype	Oil (%)	Protein (%)	Oil + Protein (%)
I	37.26	26.59	63.85
II	36.76	25.98	62.74
III	37.82	24.54	62.36
IV	37.62	25.20	62.82
Average	**37.36**	**25.57**	**62.93**

For instance, camelina grown in Canada typically exhibits a seed oil content ranging from 35% to 43%, while in China and Romania it ranges from 26% to 35% and from 28% to 40%, respectively (2, 11, 17). Similarly, varieties grown in Serbia in the period from 2004 to 2015 displayed a seed oil content ranging from 28.42% to 38.63%. consistent with our data (19). Contrary to this, camelina grown in America tended to have higher content of seed protein, ranging from 29% to 34% in comparison to varieties grown in Serbia (16). Varieties grown in Serbia during 2018 showed a slightly higher seed protein content, ranging from 27.07% to 27.95% (11). Based on research findings. it was determined that camelina behaves similarly to rapeseed, with seed oil content being negatively affected by high temperatures and dry conditions during flowering and grain-filling period, leading to higher seed protein content (16, 34). Studies on the environmental impact on the seed oil

content of camelina have shown that strains planted in Canada and America exhibited seed oil content of 40% to 43%, where as those grown in Greece and Spain range from 34% to 40% (10). Colder and wetter springs favour higher seed oil content compared to warmer and drier springs in the Mediterranean (10). Similar observations were made by Jiang in his research. In a location with an average temperature of about 22 °C during the flowering period, the seed oil content reached an average value of 40% and the seed protein content ranged from 27% to 28% (36). In contrast, the location with an average temperature of about 26 °C during the flowering showed an average seed oil content of 37%. and seed protein content ranging from 28.5% to 29% (36).
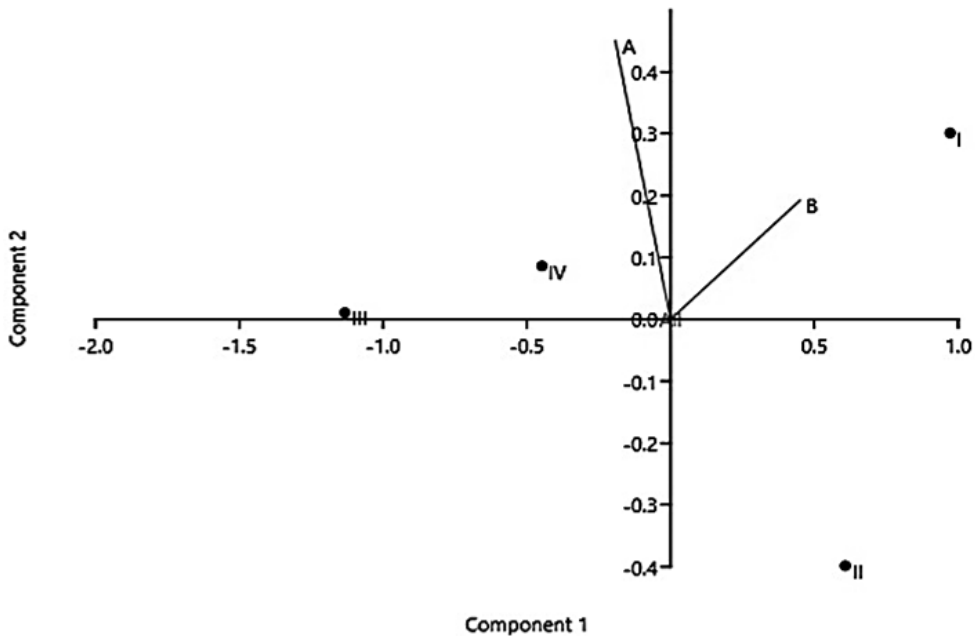
Figure 2. Principle component analysis (PCA) for content of seed oil and protein in different genotypes of camelina oil seed

From Figure 2. it is evident that Genotype III and Genotype IV are grouped together, characterized by higher oil content compared to Genotypes I and II. Specifically. Genotype III exhibits the highest oil content at 37.82%. followed closely by Genotype IV at 37.62% as shown in Table 2. However, these genotypes also display lower seed protein content. On the other hand. Genotype II has the lowest seed oil content while Genotype I has the highest seed protein content at 25.98% and 26.59%. respectively. The observed seed oil and protein content of the four analysed camelina genotypes aligns well with existing data. with an average seed oil content of approximately 36.57% and seed protein content of around 26.39% (9). Previous studies have also shown a negative correlation between seed oil and protein content. indicating that genotypes with the higher oil content tend to have lower protein content (10, 11, 35, 36).

CONCLUSION

The genotypes of rapeseed cultivated during the 2022/2023 season exhibited oil content consistent with literature data so far. Based on their seed oil and protein content, they can be classified into four distinct groups. The first group (NS Vir, NS Div, NS Vid, and NS Jelena) is characterized by high seed oil content and low seed protein content. Similarly, the second group (NS Kata, NS Jasna, and NS Pek) displays high seed oil content, but slightly lower than first group, with low seed protein content. The third group (NS Marin, NS Dunav, and NS Ras) and the fourth group (NS Anna, NS Zorica, and NS Ilia) exhibit low seed oil content but high seed protein content. The highest oil content in the genotype is often accompanied by low protein content, as is the case with genotypes NS Svetlana and NS Jelena... The genotype NS Zlatna demonstrated the most favourable oil to protein ratio. The oil content is 43.92%, and the protein content is 23.06%. Camelina genotypes generally display lower oil content compared to rapeseed. However, they compensate with higher protein content reaching a maximum of 26.59 % in Genotype I and 37.82% oil content in Genotypes III and IV. Camelina, renowned for its high protein yet low oil content, shows resilience to drought, poor soil, and diseases. There's a critical need to intensify breeding endeavours to enhance oil content in Camelina genotypes. Similarly, rapeseed breeding should emphasize varieties with high oil and protein content, underlining the significance of genotype selection and environmental factors for optimal crop traits.

REFERENCES

1. Crnobarac, J.; Marinković, R.; Marjanović-Jeromela, A.; Marinković, B.; Dušanić, N. Unapre-đivanje tehnologije proizvodnje uljane repice. *Traktori i pogonske mašine.* **2002**, (7), 34-42.
2. Veljković, V.; Marjanović-Jeromela, A.; Kostić, M.; Rajković, D.; Stamenković, O. *Lanik – Mogućnost u proizvodnji ulja i biogoriva;* Univerzitet u Nišu, Tehnološki fakultet u Leskovcu, Srpska akademija nauka i umetnosti - Ogranak SANU u Nišu, 2022; pp 9-12; 59-68; 101-123.
3. Marinković, R.; Marjanović-Jeromela, A.; Mitrović, P. Privredni značaj. osobine i tehnologija proizvodnje uljane repice, *Biljni lekar,* **2007**, *35* (4), 377-393.
4. Mitrović, P; Milovac, Ž.; Marinković, R. Aktuelni problemi u zaštiti ozime uljane repice (*Brassica napus* var. *Napus L)*, *Zaštita bilja*, **2009**, *60*, 127-144.
5. Miklič, V.; Ovuka, J.; Marjanović-Jeromela, A; Terzić, S.; Jocić, S.; Cvejić, S.; Miladinović, D.; Hladni, N.; Radić, V.; Ostojić, B.; Jocković, M.; Dušanić, N.; Dorđević, V.; Miladinović, J.; Belešević-Tubić, S.; Balalić I. Oplemenjivanje i semenarstvo uljanih biljnih vrsta u Srbiji, *Selekcija i semenarstvo*, **2018**, *24*, 1-9.
6. Marjanović-Jeromela, A.; Milovac, Ž.; Mitrovac, P.; Rajković, D.; Vasin, S.; Uljana repica, lanik i šafranika - odgovori na izazove, promenu klime i zahteve proizvođača; *57*. Savetovanje agronoma i poljoprivrednika Srbije i 3. Savetovanje agronoma Republike Srbije i Republike Srpske, Zlatibor, 30.01-03.02.2023, Zbornik referata*, 74-84.
7. Marjanović-Jeromela, A.; Mikić, A.; Marinković, R.; Mihailović, V.; Miladinović, D. Prinos semena i proteina uljane repice (*Brassica napus* L. Var. *Napus*), *Zbornik radova Instituta za ratarstvo i povrtarstvo, ***2007***, 44*(1), 237-241.
8. Berti, M.; Wilckens, R.; Fisher, S.; Solis, A.; Johnson, B.; Seeding data influence on camelina seed yield components and oil content in Chile, *Industrial Crops and Products, ***2011***, 34*, 1358-1365.
9. Mladenov, V.; Marjanović-Jeromela, A.; Cvejić, S.; Banjac, B.; Vollmann, J.; Jocić, S.; Miladinović, D.; Preliminarna karakterizacija lanika (*Camelina sativa L.),* za potrebe oplemenjivanja u Srbiji, *Selekcija i semenarstvo*, **2016**, *23*(1), 57-67.

10. Walia, K. M.; Zanetti, F.; Gesch, W.R.; Krzyzaniak, M.; Eynck, C.; Puttick, D.; Alexopoulou, E.; Royo-Esnal, A.; Stolarski, J.M.; Isbell, T.; Monti, A. Winter camelina seed quality in different growing environments across Northern America and Europe, *Industrial Crops and Products*, **2021**, *169*, 1-10.

11. Ilić, P.; Rakita, S.; Spasevski, N.; Đuragić, O.; Marjanović-Jeromela, A.; Cvejić, S.; Zanetti, F. Nutritive value of serbian camelina genotypes as an alternative feed ingredient, *Food and Feed Research*, **2022**, *49*, 209-221.

12. Shen, J.; Liu, Y.; Wang, X.; Bai, J.; Lin, L.; Luo, F.; Zhong, H. A Comprehensive Review of Health-Benefiting Components in Rapeseed oil, *Nutrients*, **2023**, *15*, 1-14.

13. Marinković, R.; Marjanović-Jeromela, A.; Mitrović, P. Osobenost i proizvodnje ozime uljane repice (*Brassica napus L*), *Zbornik radova Instituta za ratarstvo i povrtarstvo,* **2009,** *46*, 33-43.

14. Marjanović- Jeromela, A.; Marinković, R.; Miladinović, D.; Miladinović, F.; Jestrović, Z.; Stojšin, V.; Miklič, V. Uticaj spoljašnje sredine na prinos uljane repice (*Brassica napus L.*), *Ratarstvo i povrtarstvo*, **2010**, *47*, 173-178.

15. Li, N.; Qi, G.; Sun, S. X.; Wang, D.; Bean, S.; Blackwell, D. Isolation and Characterization of Protein Fractions Isolated from Camelina meal, *Agricultura and Food Sciences Transactions of the ASABE*, **2014**, *57*, 168-178.

16. Obour, K. A.; Obeng, E.; Mohammed, A. Y.; Ciampitty, A. I.; Durret, P. T.; Aznar-Moreno, A. J.; Chen, C.; Camelina Seed Yield and Fatty Acids as Influenced by Genotype and Environment; *Agronomy Journal*, **2017**, *109*(3), 947-956.

17. Domil, G.; Pirvulescu, L; Popescu, I.; The study of camelina oi characteristics, *Research Journal of Agricultural Science,* **2015**, *47*, 55-58.

18. Grady, K.; Nleya, T. Camelina Production, *Extension Extra,* **2010**, *369*, 1-4.

19. Mladenov, V.; Marjanović-Jeromela, A.; Cvejić, S.; Banjac, B.; Vollmann, J.; Jocić, S.; Miladinović, D.; Preliminarna karakterizacija lanika (*Camelina sativa L.)* za potrebe oplemenjivanja u Srbiji, *Selekcija i semenarstvo*, **2016**, *23*(1), 57-67.

20. Mondor, M.; Hernandez Alvarez, J. A. Camelina sativa composition, attributes and applications: A review, *European Journal of Lipid Science and Technology*, **2022**, *124*(3), 1-49.

21. Wanasundara, P.D. J.; McIntosh, C. T.; Perera, P. S.; Withana-Gamage, S. T.; Mitra, P. Canola/rapeseed protein-functionality and nutrition, *Oilseeds and fats Crops and Lipids*, **2016**, *23*, 1-15.

22. Perera, S.; McIntosh, T.; Coutu, C.; Tyler, R.; Hegedus, D.; Wanasundara J. Profiling and characterization of *Camelina sativa* (L.) Crantz meal proteins, *Journal of American oil chemist's society*, **2022**, *99*, 873-889.

23. Von Der Haar, D.; Muller, K.; Bader Mittermaier, S.; Eisner, P. Rapeseed-tremendous potential for added value generation, *Oilseeds and fats Crops and Lipids*, **2014**, *21*, 1-8.

24. Chmielewska, A.; Kozlowska, M.; Racwal, D.; Wnukowski, P.; Amarowicz, R.; Nebesny, E.; Rosicka Kaczmarek, J.; Canola/rapeseed protein-nutritional value, functionality and food application: a review, *Critical Reviews in Food Science and Nutrition,* **2020**, *61*(77), 1-21.

25. Wittkop, B.; Snowdon, R.J.; Friedt, W.; Status and perspectives of breeding for enhanced yield and quality of oilseed crops for Europe, *Euphytica*, **2009**, *170*, 131-140.

26. Abbadi, A.; Leckband, G. Rapeseed breeding for oil content, quality and sustainability, *Eur. J. Lipid Sci. Technol.*, **2011,** 113; 1198-1206.

27. Peltonen-Sainio, P.; Jauhiaanen, L.; Hyovela, M.; Nissila, E. Trade-off between oil and protein in rapeseed at high latitudes: Means to consolidate protein crop status? *Field Crops Research*, **2011**, *121*, 248-255.

28. Granlund. M.; Zimmerman, D.C. Effect of drying conditions on oil content of sunflower (*Helianthus annuus* L.) seeds as determined by wide-line nuclear magnetic resonance (NMR), *N. D. Acad. Sci. Proc*. **1975**, *27*, 128-132.

29. Si, P.; Mailer, R.; Galwey, N.; Turner, D.; Influence of genotype and environment on oil and protein concentration of canola (*Brassica napus* L.) grown across southern Australia, *Australian Journal of Agricultural Research*, **2003**, *54*, 397-407.

30. Kowalska, G.; Kowalski, R.; Hawlena, J.; Rowinski, R. Seeds of oilseed rape as an alternative source of protein and minerals, *Journal of Elementology*, **2019**, *25*, 513-522.

31. Pritchard, F.M.; Eagles, H.A.; Norton, M.R.; Salisbury, A. P.; Nicolas, M.; Environmental effects on seed composition of Victorian canola, *Australian Journal of Experimental Agriculture,* **2000**, *40*, 679-685.

32. Marjanović-Jeromela, A.; Marinković, R.; Mitrović, P.; Miklič, V. Proizvodna vrednost novih genotipova ozime uljane repice (Brassica napus L), *Zbornik radova Instituta za ratarstvo i povrtarstvo,* **2008**, *45*, 103-110

33. Marjanović Jeromela, A.; Atlagić, J.; Marinković, R.; Terzić, S.; Lečić, N.; Mogućnost korišćenja uljanih kultura iz Novosadske kolekcije, *Bilten za hmelj, sirak i lekovito bilje,* **2007**, *39*(80), 47-52.

34. Righini, D.; Zanetti, F.; Martinez-Force, E.; Mandrioli, M.; Gallina Toschi, T.; Monti, A. Shifting sowing of camelina from spring to autumn enhances the oil quality for bio-based applications in response to temperature and seed carbon stock, *Industrial Crops and Products*, **2019**, 137, 66-73.

35. Jiang, Y.; Caldwell, D. C.; Falk, C. K.; Camelina seed quality in response to applied nitrogen genotype and environment, *Can. J. Plant. Sci.*, **2014**, *94*, 971-980.

36. Kirkhus, B.; Lundan, R.A.; Haugen, J.E.; Vogt, G.; Borge, A. G. I.; Henriksen, I. F. B.; Effects of Environmental Factors on Edible Oil Quality of Organically Grown *Camelina sativa*, *Journal of Agricultural and Food Chemistry*, **2013**, *61*, 3179-3185.

PHYTOCHEMICAL ANALYSIS AND BIOLOGICAL ACTIVITIES OF *Matthiola livida* DC. EXTRACTS FROM OUED-SOUF REGION: INSIGHTS INTO ANTIOXIDANT AND ANTI-INFLAMMATORY POTENTIAL

Atef CHOUIKH[1,2] , *Anis BEN ALI*[1,2]* , *Aida BOUSBIA BRAHIM*[1,2]
Aicha BEKKOUCHE[2], *Salima SEGHAIER*[2]

[1] Laboratory of Biology, Environment and Health. El Oued University, PO Box 789, 39000 Algeria.
[2] Biology department, Faculty of Life and Natural Science, El Oued University, PO Box 789, 39000 Algeria.

This study aimed to assess the characteristics of Saharan plants by analyzing the chemical composition and evaluating the antioxidant and anti-inflammatory properties of raw extracts from Matthiola livida DC., collected from the Oued-Souf region. The primary metabolites analysis revealed carbohydrates as the dominant components, with a concentration of 35.70 ± 0.03 mg/g dry weight. Using the maceration technique, three unrefined extracts (methanolic, ethanolic, and aqueous) were produced, with the aqueous extract yielding the highest output at 14.61%. Total polyphenol content varied from 170.82 to 102.42 mg of GA/g dry extract, and the ethanol extract had the highest flavonoid content at 97.03 ± 4.14 mg of QE/g dry extract. The DPPH• test showed the methanolic extract as the most potent antioxidant, with an IC$_{50}$ of 153.56 µg/ml. The ethanolic extract offered the most protection to human erythrocytes, resulting in only 16.93% hemolysis at a concentration of 1 mg/ml. It also showed the strongest anti-inflammatory effects in vitro, with a protein denaturation inhibition equivalent to 11.29±1.10 mg of diclofenac sodium per milligram of dry extract. Additionally, IR spectroscopy identified several functional groups, including hydroxyl (O-H), carbonyl (C=O), and various carbon-hydrogen bonds (C-H, C=C, C-H). Future research should explore the clinical applicability of these findings to enhance the therapeutic potential of Matthiola livida extracts.

Keywords: *Matthiola livida* DC., Crude extracts, Total Polyphenols, Flavonoids, Antioxidant activity, Anti-inflammatory activity.

INTRODUCTION

The Algerian Sahara, a vast and diverse ecosystem, is home to an impressive array of plant species, with approximately 500 identified, out of which 162 are endemic to this arid region (1). Among these botanical treasures, *Matthiola livida* DC. stands out as a plant of particular interest due to its centuries-old tradition of traditional pharmacopoeia. The rich biodiversity of the Algerian Sahara has fuelled extensive exploitation of spontaneous plants by humans for various medicinal purposes, prompting researchers to delve into the pharmacological activities and chemical composition of these plant metabolites (2).

In this context, the study of plant chemistry remains highly relevant, as the plant kingdom serves as a prolific source of bioactive molecules with diverse applications in the food industry, cosmetology, and pharmacy (3). *M. livida*, a species found in Saudi Arabia, Palestine, and North Africa (4), including a narrow geographical stretch from Egypt to Morocco (5), has drawn attention for its remarkable therapeutic properties.

This paper focuses on *M. livida*, offering a comprehensive exploration of its botanical description, traditional uses, and previous studies conducted to unravel its phytochemical composition and pharmacological potential. The botanical profile of *M. livida* reveals a

* Corresponding author: Anis Ben Ali, e-mail: benali-anis@univ-eloued.dz

plant covered in stellate, glandular, and dendroid hairs, with narrow leaves and small, livid or purple flowers. The plant's aromatic odour after sunset contributes to its unique characteristics, and it thrives in sandy soils, stony wadis, and plains, particularly in protected closed areas (4).

Traditional uses of *M. livida* among nomads in Western Sahara involve employing its seeds as a warming agent in culinary practices, such as adding them to couscous sauces or soups (6). Additionally, nomads have historically utilized the plant for pastoral purposes. Previous studies on related species, such as *M. longipetala* (subspecies livida), have identified flavonoid compounds and cytotoxic activities against human tumour cell lines (7, 8). Notably, the oral administration of extracts from *M. livida* has demonstrated hypoglycaemic effects in both healthy and diabetic rat models (9).

This introduction sets the stage for an in-depth exploration of *M. livida*, emphasizing its and the existing body of knowledge on its phytochemical composition and pharmacological activities. The subsequent sections will delve into these aspects, contributing to our understanding of the potential therapeutic applications of this intriguing plant in the Algerian Sahara.

The novelty of this study lies in its systematic examination of *M. livida*'s specific bioactive components and their mechanisms of action, providing a foundation for future therapeutic applications and validating its traditional uses in the Algerian Sahara. The subsequent sections will delve deeper into these aspects, enhancing our understanding of this intriguing plant's potential therapeutic benefits.

MATERIALS AND METHODS

PLANT MATERIAL

The plant utilized in this experimental study is *M. livida*, a member of the Brassicaceae family. The harvest occurred on April 25, 2019 in the Hassi Khalifa locality within the El Oued province, located at coordinates 33°33'44" North and 6°59'25" East. The plant's identification was conducted by Prof. Chouikh Atef. The drying process was conducted under controlled conditions, at ambient temperature, shielded from both light and humidity. Once the aerial part of the plant was dried, it was pulverized to obtain the plant powder. Subsequently, the powder was stored in glass bottles in a location shielded from light and heat until it was ready for use.

ESTIMATED NUTRITIONAL VALUE

The methodology employed by Chouikh et al. (10) was adopted in this study. 1 gram of plant material was combined with 5 ml of trichloroacetic acid (TCA), followed by mixing on a magnetic shaking device for 5 minutes. Afterwards, the mixture was subjected to centrifugal separation at a speed of 3000 revolutions per minute for a duration of 10 minutes. The supernatant obtained was used to quantify carbohydrates, while deposit 1 was subjected to an additional 2 ml of ether/chloroform (V/V) and underwent a second centrifugal separation at 3000 rpm for 10 minutes. The second supernatant was collected to determine the lipid content, while the second deposit was treated with 2.5 ml of a 0.1 M solution of sodium hydroxide (NaOH) to determine the protein content.

Carbohydrate estimation

Carbohydrate estimation followed the procedure outlined by DuBois et al. (11). In this method, a combination of phenol (5%) and concentrated sulphurous acid was utilized, and the absorbance was measured at a wavelength of $\lambda = 490$ nm. Glucose served as the standard for calibration, and the outcomes were expressed in milligrams of carbohydrates per gram of plant material.

Protein estimation

Protein estimation was conducted following the procedure referenced in Lowry et al. (12). The method involved the use of Folin-Ciocalteau reagent (v/v), 0.1 M NaOH, 0.5 % $CuSO_4$, and 0.1 % $KNaC_4H_4O_6 \cdot 4H_2O$. Bovine Serum Albumin (BSA) served as the standard, and the absorbance was measured at 750 nm using a UV spectrophotometer. The results were quantified in milligrams of proteins per gram of plant material.

Lipid estimation

Lipid estimation was carried out following the procedure outlined in reference (13) with certain adjustments. The method involved the use of Sulphophosphovanillinic reagent and concentrated sulphurous acid, and the reaction tubes were subjected to a water bath at 100 °C. Absorbance readings were taken at a wavelength of $\lambda = 530$ nm, using Soy as the standard. The outcomes were expressed in milligrams of lipids per gram of plant material.

PREPARATION OF THE CRUDE EXTRACTS

The crude extracts were prepared by soaking ten grams of dried plant material in 150 ml of methanol (99 %), ethanol (96 %), or distilled water at room temperature, without exposure to light, for a period of 24 hours. After filtration, the solvent was evaporated under reduced pressure using a rotary evaporator maintained at 50 °C. This process yielded the methanol, ethanol, and aqueous crude extracts (14).

FOURIER-TRANSFORM INFRARED (FTIR) CHARACTERIZATION

The extracts underwent Fourier-Transform Infrared (FTIR) spectroscopy analysis using a Shimadzu-00463 spectrophotometer. The FTIR analysis was conducted with a resolution of 4 cm^{-1}, incorporating 64 coadded scans. The examined spectral range extended from 4000 to 650 cm^{-1}.

DETERMINATION OF THE TOTAL POLYPHENOLS CONTENT (TPC)

The quantification of overall phenolic concentrations in the raw extracts was performed using the Folin-Ciocalteu's phenol reagent method (15) with certain alterations. More precisely, a volume of 0.2 ml of the extract was combined with 1 ml of Folin-Ciocalteu reagent (10 %), and then 0.8 ml of sodium carbonate solution (7.5 %) was added. After vigorously agitating the test tubes, they were left undisturbed for a duration of 30 minutes, and the optical density was quantified at a wavelength of 765 nm using a UV spectrophotometer. The total phenolic content was quantified as milligrams of gallic acid equivalents per gram of dry extract (mg of GA/g Ex).

DETERMINATION OF TOTAL FLAVONOIDS CONTENT (TFC)

According to the approach used by Kherraz et al. (16), 1 ml of the extract was combined with 1 ml of a 2 % $AlCl_3$ solution. After vigorously agitating the test tubes, they were left undisturbed for 60 minutes at ambient temperature. The absorbance was determined at a wavelength of 430 nm, followed by the quantification of the flavonoid content in the extract. The results were expressed as milligrams of quercetin equivalent per gram of extract (mg of QE/g of dry extract).

EVALUATION OF ANTIOXIDANT ACTIVITY

DPPH$^\bullet$ free radical scavenging

The evaluation of the extracts' ability to scavenge DPPH$^\bullet$ was conducted using the methodology described by Chemsa et al. (17). To summarize, 1 ml of each extract at different concentrations was mixed with 1 ml of DPPH solution (10^{-4} mol) in methanol. Following a 15-minute incubation period at ambient temperature, the absorbance was quantified at a wavelength of 517 nm. The inhibition activity was determined by applying the following formula:

$$Inhibition\ (\%) = [(Absorbance_{Control} - Absorbance_{Sample})/Absorbance_{Sample}] \times 100$$

The IC_{50}, representing the concentration at which 50% of the free radicals were suppressed by the extract, was determined through linear regression analysis on the concentration-inhibition percentage relationship. A lower IC_{50} value indicates a higher antioxidant capacity (18). This method provides a reliable assessment of the extracts' ability to neutralize DPPH radicals, offering valuable insights into their antioxidant capabilities.

Hemolysis test

This assay is employed to assess the ability of plant extracts in safeguarding erythrocyte blood cells from membrane damage or disruption caused by oxidative stress and free radicals. The evaluation is based on quantifying the proportion of erythrocytes that have undergone dissolution (19).

Following the procedure outlined in reference (20), 40 µl of human erythrocytes were mixed with 2 ml of the plant extract and incubated for 5 minutes at 37 °C. Afterwards, 40 µl of hydrogen peroxide (30×10^{-3} M), 40 µl of ferric chloride (80×10^{-3} M), and 40 µl of ascorbic acid solution (50×10^{-3} M) were added in sequence. Following a 1-hour incubation at a temperature of 37 °C, the mixture was subjected to centrifugation at a velocity of 700 rpm for a duration of 10 minutes. The supernatant's absorbance was quantified at a wavelength of 540 nm. The haemolysis percentage was calculated using the following formula:

$$Haemolysis\ \% = (Absorbance_{Control}/Absorbance_{Sample}) \times 100$$

ANTI-INFLAMMATORY ACTIVITY

Albumin denaturation test

The albumin denaturation model was selected to assess the in vitro anti-inflammatory properties of crude extracts from *M. livida*. As per the methodology outlined by Elias &

Rao and Padmanabhan & Jangle, with certain alterations (20). 1 ml of the extract at various concentrations was combined with 1 ml of bovine serum albumin (5%). Following a 15-minute incubation period at 27 °C, the tubes are then subjected to further incubation in a water bath at a temperature of 70 °C for a duration of 10 minutes. The absorbance of the samples was measured at 660 nm after they had cooled to room temperature. Diclofenac sodium serves as a benchmark. The results are quantified in terms of milligrams of diclofenac sodium per milligram of dry extract.

STATISTICAL ANALYSIS

The results obtained are expressed as mean ± standard deviation. The IC_{50} values are calculated from the curve: % inhibition = f (concentrations). Using Excel software (version 2010) to perform the analysis of variance of the means with the one-way ANOVA test. This test gives us the degree of significance *p* where we say that the difference ($p < 0.05$, $p < 0.01$ and $p < 0.001$).

The correlation analysis also utilized the Pearson Correlation Coefficient Test to ascertain the correlation coefficients and the direction of correlation that integrates the variables under investigation.

RESULTS AND DISCUSSION

ESTIMATED NUTRITIONAL VALUE OF *M. LIVIDA*

The findings depicted in Figure 1 indicate that *M. livida* exhibits high levels of carbohydrates and lipids, while its protein content is notably low.
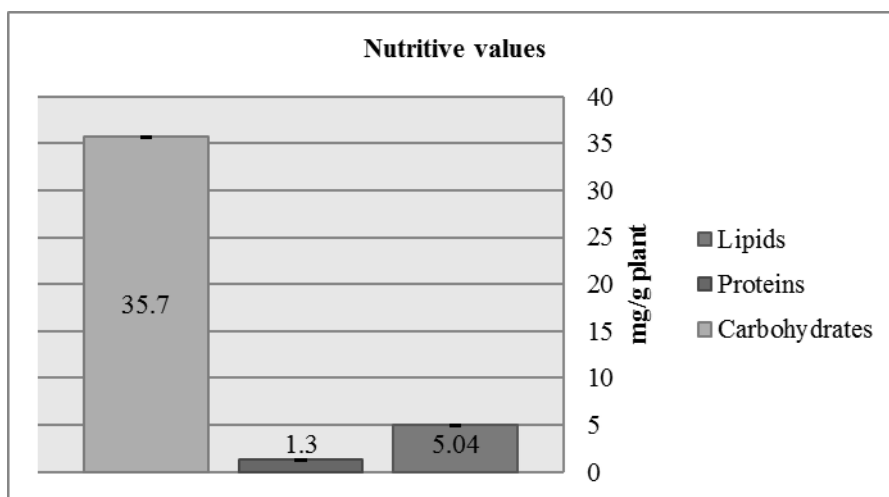
Figure 1. Nutritive values of *M. livida* plant.

The findings indicate that the plant *M. livida* possesses a substantial amount of carbohydrates that can be attributed to the physiological state associated with the plant's developmental stage during the fruiting period (21) knowing that they are primary metabolites

therefore, they are used as precursors of other secondary metabolites, as a source of energy (22).

Also, a low quantity for lipids and very low for proteins, this reduction perhaps because the plant's physiology is influenced by various environmental stresses. Over time, water stress leads to oxidative stress, resulting in the production of free radicals. This continuous and heightened oxidative stress disrupts the balance between antioxidants and oxidants. The latter cause the oxidation of lipids, particularly membrane lipids, which leads to the loss of their quantity, damage proteins and inhibition of the Enzymatic activity (23), water stress leads to a reduction in the efficiency of plant photosynthesis (23).

EXTRACTS YIELD

The aqueous extract obtained from the aerial parts of *M. livida* demonstrated a content of 14.61±0.24 %. In terms of the alcoholic extracts, ethanol production was notably high at 9.04±0.43 %, with methanol content being comparatively lower at 6.51±0.26 % (Table 1).

Table 1. Yields of some extracts from *M. livida*.

Extract type	Yields (%)
Aqueous extract	14.61±0.24[***]
Ethanolic extract	9.04±0.43[***]
Methanolic extract	6.51±0.26[***]

The results obtained are expressed as mean ± standard deviation. ***: Significantly different at $p < 0.001$.

Variations in extraction yields may be related to the diffusion of solvents in the plant powder in the maceration step and probably to the nature and polarity of the solvents used for extraction (24, 25). Also, the particle size and chemical composition of compounds in the plant (26). Structural diversity is responsible for the great variability of physicochemical properties influencing extraction (27). In general, other factors can influence the extraction efficiency alongside the extraction method, including: pH, temperature, extraction time (28).

Many studies have proven that adding a percentage of water to organic solvents especially methanol and ethanol can increase the yield, since this method represents the best and most used system to extract metabolic compounds in the plant because the Mixing works to increase the polarity of the solution and the attraction of polarized compounds (29).

FOURIER-TRANSFORM INFRARED (FTIR) CHARACTERIZATION

FTIR analysis is used to identify chemical bonds in organic molecules. They make it possible to determine these chemical functions. The following IR spectra show the bonds that can be found in our raw extracts. From Figure 2, the obtained spectra showed the presence of different functional groups characteristic of three crude extracts. The results are in (Table 2).
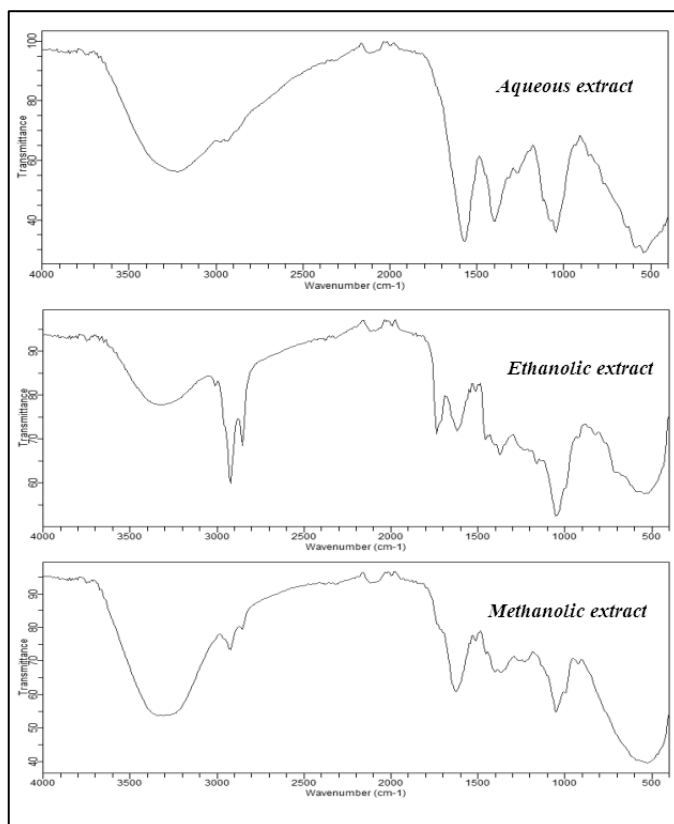
Figure 2. FTIR of crude extracts of *M. livida*.

Table 2. Interpretation of FTIR of crude extracts of *M. livida*.

Bond	Function or Family	Wavenumber (cm^{-1})	Intensity	Most Abundant In
O-H	Alcohol	3350	Strong, broad	three extracts
C-H	Aliphatic	2850-3000	Strong	Ethanolic
C=O	Carbonyl	1650-1730	Strong	Methanolic, ethanolic
C=C	Aliphatic	1400-1600	Medium	Aqueous
C-O	Alcohol	1050	Strong	Ethanolic, Aqueous
C-H	Aromatic	690-710	Strong	Methanolic, Aqueous

Crude extracts may exhibit antioxidant activity as a result of the presence of substances that contain hydroxyl groups (O-H). Flavonoids have a structure that is well-suited for sca-venging free radicals in this particular situation. This is because they have multiple hyd-roxyl groups that can act as hydrogen donors (30). In general, there is a positive correlation between the antioxidant activity and the structure of polyphenols, which is characterized by a high number of hydroxyl groups that help stabilize free radicals (31, 32). According to Mburu et al. (33), the C=C group is mainly presented by flavonoids, can C-O indicates the presence of glycosides which is in C-O-C glycosidic form. C=O is a carbonyl function that

generally characterizes aldehydes and ketones (34), C-H with a wave number of 2850-3000 cm^{-1} (35) and belongs to the benzoic cycle which forms the fundamental structural element of flavonoids and the aromatic C-H bond of wavenumber 659-710 cm^{-1} can return to the aromatic ring substituents (36).

ESTIMATION OF TOTAL POLYPHENOLS AND FLAVONOIDS

In Figure 3, a substantial and comparable concentration of polyphenols is observed in ethanol, followed by methanol, and to a lesser degree, aqueous extracts. The ANOVA test and subsequent statistical analysis (AV1) indicate that the variance among the raw extracts is not statistically significant ($p > 0.05$). The most favourable flavonoid values are evident in the methanol and ethanol extracts. The ANOVA test (AV1) for flavonoid contents reveals a highly significant difference depending on the crude extracts ($p < 0.001$).
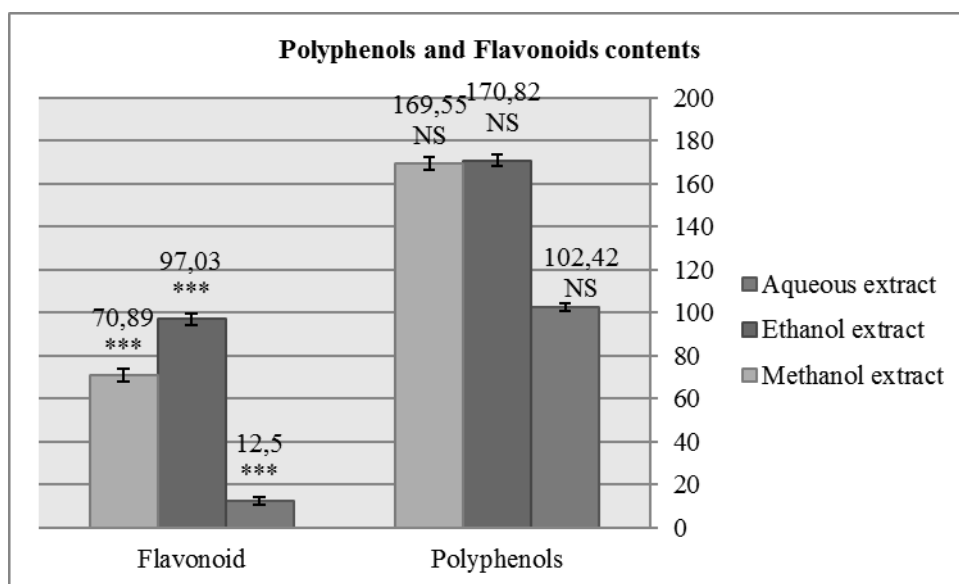
Figure 3. Polyphenols (mg GAE/g Extract) and Flavonoids content (mg QE/g Extract) in *M. Livida* crude extracts.
***: Significantly different at p < 0.001. NS: Not Significant (p > 0.05).

According to Hafedh et al. (37) the content of total polyphenols of ethanolic extract of *Oudneya Africana* leaves (species of the same family) is equal to 661.66 ± 0.08 mg E AG/g extract, this result is a higher value than that found in our study, in the same study concerning the dosage of flavonoids in the ethanolic extract is equal to 296.28 ± 1.49 mg E Q/g extract. Also, this result is very high compared to our results.

From Nabti and Belhatta (38) the polyphenol content of *M. livida* is higher than that of the methanolic extract of *Oudneya africana*, with a value of 137.16 ± 3.55 µg E AG/mg extract. However, the polyphenol content of *M. livida* is lower than that of the aqueous extract of *Oudneya africana*, with a value of 108.6 ± 7.01 µg E AG/mg extract. Furthermore, the methanolic extract of *Oudneya africana* was found to contain a flavonoid content of 21.96±

1.02 µg E Q /mg extract. The obtained result is lower in comparison to our own findings. Specifically, the aqueous extract of *Oudneya africana* is equivalent to 15.62 ± 0.78 µg E Q /mg extract. Conversely, this outcome is higher when compared to our own results. The variation in levels can be attributed to various factors, including the species, climatic conditions, and environmental conditions (39). The factors considered include the duration of time, the specific area where the crops were gathered (40), the specific components that were examined, the method used for extracting the components, and the specific conditions under which the extraction took place (41).

The presented results indicate that there are measurable variations in the levels of total polyphenols and flavonoids among the different extracts. The variation in contents can be attributed to the fact that phenolic compounds differ in concentration depending on their chemical structures and exhibit distinct behaviours in different extracts (42). Various factors, including extrinsic (geographic and climatic) and intrinsic (genetic) factors, can affect the composition of phenolic compounds. However, the level of plant maturation and the duration of storage have a significant impact on the content of phenolic compounds (43).

Several studies have examined the impact of different solvents, including methanol, ethanol, acetone, and ethyl acetate, on the extraction of phenolic compounds (44, 45). The selection of solvent plays a crucial role in determining the levels of total polyphenols and flavonoids.

The results indicate that the choice of extraction solvent affects the extraction of phenolic compounds from *M. livida*. The solubility of total polyphenols is influenced by the polarity of the solvent, the degree of polymerization resulting from an increase in hydroxyl groups, as well as interactions with other components and the formation of insoluble complexes (26, 46). In addition, Zeghad et al. (47) found that the polarity of the solvent used for extracting polyphenols from plants has an impact on the total polyphenol content. Water, ethanol, and methanol are commonly recommended solvents for extracting polyphenols due to their polarity. Consequently, these solvents were chosen for the extraction process in this study. According to Onofre et al. (48), ethanol is the most effective solvent for extraction. Furthermore, Abarca-Vargas et al. (49) have demonstrated that methanol is the optimal solvent for extracting polyphenols, a finding that aligns with our own results.

On the other hand the purity of the extract, if the solvent is likely to extract non-phenolic compounds such as sugars, proteins and pigments, due to these compounds are generally combined with other substances which can influence during the evaluation of total polyphenols and flavonoids (50). In addition, the quantification method can also influence the estimation of the content of total phenols (24). The Folin-Ciocalteu test determines the presence of reducing molecules. The reagent used in this test is highly sensitive to the reduction of hydroxyl groups, including those found in phenolic compounds, sugars, and proteins. As a result, this assay is not selective specifically for polyphenols (51, 52).

EVALUATION OF ANTIOXIDANT ACTIVITY

DPPH$^\bullet$ free-radical scavenging test

The outcomes presented in Figure 4 indicate IC_{50} values of 153.56 µg/ml, 351.84 µg/ml, and 658.20 µg/ml for methanol, aqueous, and ethanol extracts, respectively. In comparison, the registered value with Ascorbic acid as the standard is 14.65 µg/ml. The statistical analysis using the ANOVA test (AV1) for IC_{50} demonstrates that the variation among the raw extracts is not statistically significant ($p > 0.05$).
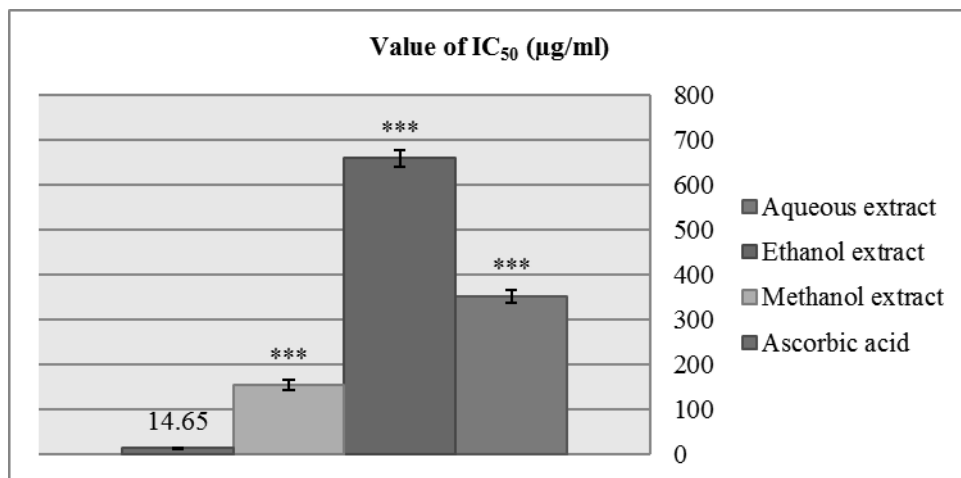
Figure 4. Value of IC$_{50}$ (µg/ml) of DPPH free radical scavenging test of extracts of
M. livida and Ascorbic Acid.
*** Significantly different at $p < 0.001$.

Comparing the results obtained with previous studies, the study by Nabti and Belhattab (38) found that the aerial part of *Oudneya africana* showed significant antioxidant activity with an IC$_{50}$ value=12.05 µg/ml for methanolic extract. This result is higher in antioxidant power compared to our result. Also according to Maroua et al. (53) found that the IC$_{50}$ of aqueous extract of *Oudneya africana* equals 45.41µg/ml, this lower value indicating a higher antioxidant activity compared to our result.

The results suggest that *M. livida* possesses compounds that can effectively eliminate free radicals. The antioxidant activity of these extracts is likely due to the presence of polyphenols, as numerous studies have demonstrated that phenolic compounds are primarily responsible for the antioxidant effect (20).

Phenolic compounds, especially flavonoids, are acknowledged for their potential as antioxidant substances. They have the ability to capture radical species and reactive forms of oxygen (12). This anti-radical capacity is attributed to their ability to reduce DPPH$^{•}$, a stable radical that can accept hydrogen from an antioxidant and form Reduced DPPH$^{•}$ (54). The variation in antioxidant activity among extracts may be attributed to the composition and concentration of phenolic compounds present in the extracts. Previous studies have demonstrated a correlation between the chemical structure of phenolic compounds and their ability to scavenge free radicals (51). Khelef et al. (55) further reported that the antioxidant potential of extracts is influenced by both the concentration and structure of polyphenols.

Haemolysis test

In the haemolysis test, the haemolysis percentage (Figure 5) varied among *M. livida* extracts. The ethanolic extract showed a percentage close to that of ascorbic acid, with values of 16.93% and 16.32%, respectively. Following were the methanolic extract with a value of 35.55% and the aqueous extract with a value of 44.09%. The statistical analysis using the ANOVA test (AV1) for haemolysis percentages indicates a significant difference depending on the crude extracts ($p < 0.05$).
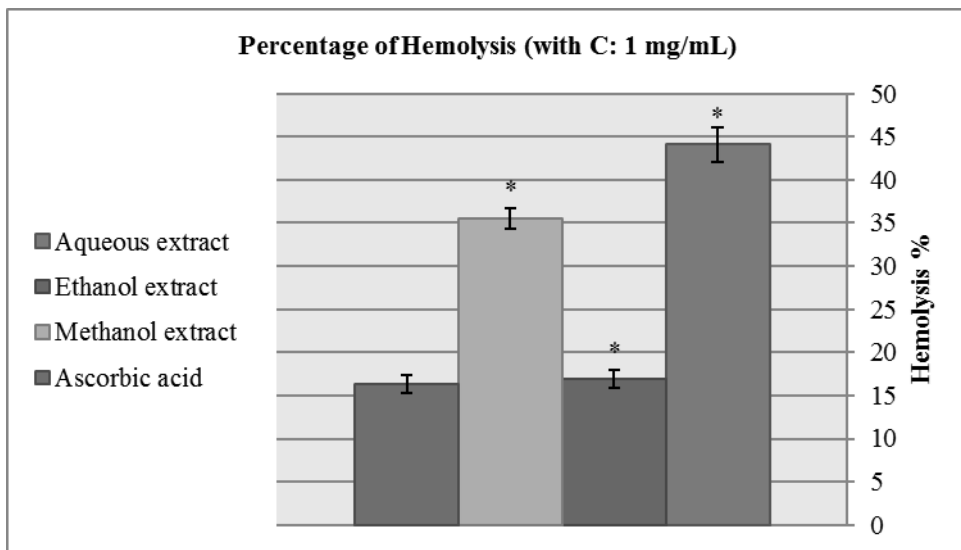
Figure 5. Percentage of haemolysis (with C: 1 mg/ml) of crude extracts of *M. livida* and
Ascorbic Acid.
* Significantly different at $p < 0.05$.

Erythrocytes are an ideal cellular model for investigating the interactions between oxidants and antioxidants due to their accessibility, simplicity, high concentration of polyunsaturated fatty acids on the membrane, and their involvement in oxygen transport through haemoglobin molecules. Consequently, erythrocytes are a primary target for free radicals (56, 57). Free radicals cause the oxidation of erythrocyte membranes, therefore causing an alteration influencing their membrane functions, these imbalances are at the origin of haemolyses and the release of erythrocyte contents into the extracellular environment (58).

Hydrogen peroxide (H_2O_2) causes the breakdown of haems when in contact with haemoglobin with the release of Fe^{2+} ions (59), H_2O_2 stimulates the production of the hydroxyl radical ($OH^•$) in the presence of Fe^{2+} thanks to the Fenton reaction. $OH^•$ is extremely reactive and will very quickly oxidize neighbouring molecules, sometimes forming other free radicals, it is the origin of enormous biological damage by lipid peroxidation (60). The process of radical oxidation of polyunsaturated fatty acids in plasma membranes results in the modification of their functionality, including changes in permeability, fluidity, and the loss of activity in enzymes and receptors. These factors collectively contribute to the destabilization of the erythrocyte membrane, leading to haemolysis and the subsequent release of haemoglobin (61).

The variation in activity could be attributed to the solubility of the compounds in the reaction media. The antihaemolytic activity of plant extracts might be attributed to bioactive compounds, such as phenolic compounds. Multiple studies have shown that phenolic compounds have the ability to shield erythrocytes from oxidative stress(62). Polyphenolic compounds work by transferring electrons to hydrogen peroxide, effectively converting it into a water molecule (63). It may also be due to the interaction of flavonoids with cell membranes which are the sites of lipid peroxidation, flavonoids inactivate and stabilize free radicals thanks to their highly reactive hydroxyl group (64).

ANTI-INFLAMMATORY ACTIVITY

Albumin denaturation test

The outcomes of protein denaturation (Figure 6) reveal that ethanol extracts exhibited superior values compared to methanol and aqueous extracts. The statistical analysis using the ANOVA test (AV1) for the inhibition of BSA denaturation indicates a highly significant difference depending on the crude extracts ($p < 0.001$).
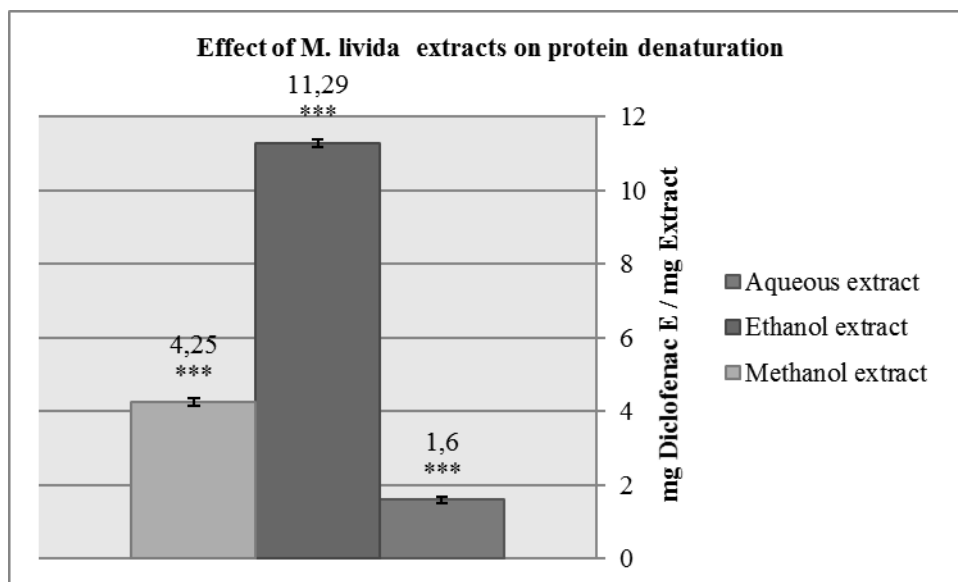
Figure 6. Effect of *M. livida* extracts on protein denaturation.
*** Significantly different at $p < 0.001$.

Protein denaturation refers to the disruption of the three-dimensional structure of proteins due to the influence of physical or chemical agents. These agents can include strong acids or bases, concentrated inorganic salts, changes in pH, organic solvents, and heat. Denaturation often leads to the loss of the protein's biological function. Denatured proteins contribute to the occurrence of the inflammatory response (65). The denaturation process involves the modification of electrostatic, hydrogen, hydrophobic, and disulphide bonds that are responsible for maintaining the three-dimensional structure of proteins (66). BSA is susceptible to temperature increases, resulting in a reduction in its solubility (67).

The presence of excessive polyphenols can be attributed to the activity that prevents BSA denaturation (68). As a result of interactions between specific components and two sites rich in proteins such as albumin, which are abundant in Tyrosine, Threonine, and Lysine. Additionally, it includes a signal from the therapeutic molecules that can stimulate the receptor abundant in tyrosine motifs, such as Threonine, which controls the biological aspects of signal transmission for overall biological function (69, 70).

STATISTICAL STUDY

Correlation analysis test (Pearson Linear Correlation Coefficient Test) was used to determine the correlation coefficient (R^2) and the direction of the correlation relationship between the variables studied; the results shown in (Table 3).

Table 3. Correlation coefficient (R^2) between the different variables studied.

Variable	Yields	Total polyphenols	Flavonoids	DPPH	Haemolysis	Anti-inflammatory
Yields	1	-0.95	-0.81	-0.54	0.50	-0.46
Total polyphenols		1	0.96	0.25	-0.75	0.72
Flavonoids			1	-0.04	-0.91	0.89
DPPH				1	0.45	-0.49
Haemolysis					1	-0.99
Anti-inflammatory						1

According to the results obtained, we observe the presence of a strong inverse correlation between the yields and the contents of total polyphenols (R^2=-0.95) also, a medium correlation between the yields and the contents of flavonoids (R^2=-0.81), DPPH (R^2=-0.54), haemolysis (R^2=0.50) and anti-inflammatory activity (R^2=-0.46).

The results showed a strong positive correlation between the total polyphenol contents and the flavonoid contents of the crude extracts (R^2 =0.96), this is explained by the flavonoids representing a group of total polyphenols therefore, this positive correlation is caused by the relationship of the whole with the part where the higher the quantity of the whole, the more the quantity of the part is increased.

Within the same table, a tenuous correlation is observed between the DPPH trapping capacity and the total polyphenol contents (R^2 = 0.25), while no correlation is found with the flavonoid contents (R^2 = -0.04). This discrepancy can be attributed to the fact that the relationship is not solely quantitative, but also qualitative. The antioxidant activity of polyphenols, particularly flavonoids, is largely determined by their chemical structure and overall quality (71).

Furthermore, it is important to mention that there is a negative relationship between haemolysis and the levels of total polyphenols and flavonoids (R^2=-0.75; R^2=-0.91, respectively). This can be attributed to the significant contribution of total polyphenols, particularly flavonoids, which exhibit a strong correlation and have a protective effect against haemolysis and oxidation of haematites (60). Hence, any augmentation in the concentration of polyphenols and flavonoids is counterbalanced by a reduction in red blood cell haemolysis, and vice versa.

The relationship between DPPH and haemolysis shows a moderate positive correlation (R^2=0.45), while there is a moderate inverse correlation between DPPH and anti-inflammatory activity (R^2=-0.49). Conversely, there exists a significant negative correlation between haemolysis and anti-inflammatory activity, with a correlation coefficient (R^2) of -0.99.

Conversely, we observe a direct relationship between the anti-inflammatory activity and the levels of total polyphenols and flavonoids (R^2 = 0.72; R^2 = 0.89 respectively). This indicates that the anti-inflammatory effects of the raw extracts are attributed to their concentrations of total polyphenols and flavonoids, which possess inhibitory properties against protein denaturation (66).

CONCLUSION

This study provides insight into the phytochemical composition and biological characteristics of extracts from *Matthiola livida* DC. obtained from the Oued-Souf region. The analysis uncovered a substantial presence of carbohydrates in the plant material, with variations observed in the overall levels of polyphenols and flavonoids among the extracts. The methanolic extract showed exceptional antioxidant activity in removing DPPH radicals, whereas the ethanolic extract displayed the strongest defence against erythrocyte haemolysis. Furthermore, the ethanol extract exhibited encouraging anti-inflammatory properties by effectively preventing protein denaturation. The results emphasize the potential therapeutic benefits of *M. livida* extracts in treating conditions associated with oxidative stress and inflammation. Additional investigation is necessary to better understand how they work and to fully exploit their therapeutic benefits in clinical settings.

STATEMENTS AND DECLARATIONS

Authorship contribution statement:
1. Atef CHOUIKH: Investigation, Methodology and Supervision.
2. Anis BEN ALI: Investigation and Writing.
3. Aida BOUSBIA BRAHIM: Supervision assistant and proofreading.
4. Aicha BEKKOUCHE: Investigation.
5. Salima SEGHAIER: Investigation.

REFERENCES

1. Fellous, A. La station d'élevage de la gazelle dorcas (gazelle dorcas) dans le sudouest algérien. IIème séminaire antilopes sahelo saharienne, 2003.
2. Amrani, S. The Holocene Flora and Vegetation of Ti-n Hanakaten (Tassili n'Ajjer, Algerian Sahara). In *Plants and People in the African Past: Progress in African Archaeobotany*; Mercuri, A.M., D'Andrea, C.A., Fornaciari, R., Höhn, A., Eds.; Springer, **2018**, 123-145. https://doi.org/10.1007/978-3-319-89839-1_8
3. Salehi, B.; Sharifi-Rad, J.; Seca, A.M.; Pinto, D.C.; Michalak, I.; Trincone, A.; Mishra, A.P.; Nigam, M.; Zam, W.; Martins, N. Current trends on seaweeds: Looking at chemical composition, phytopharmacology, and cosmetic applications. *Molecules,* **2019**, *24*(22), 4182. https://doi.org/10.3390/molecules24224182
4. Khalik, K.A.; Van der Maesen, L. Seed morphology of some tribes of Brassicaceae (implications for taxonomy and species identification for the flora of Egypt). Blumea: Biodiversity, *Evolution and Biogeography of Plants,***2002**, *47*(2), 363-383.
5. Hammami, S.; Ciavatta, M.; Ben Jannet, H.; Cimino, G.; Mighria, Z. Three phenolic and a sterol glycosides identified for the first time in *Matthiola longipetala* growing in Tunisia. *Croatica chemica acta,* **2006**, *79*(2), 215-218.
6. Maire, R. Flore de l'Afrique du Nord, volume VI, Paul Lechevalier, Paris, France, 1959.
7. Marzouk, M.M.; Kawashty, S.A.; Ibrahim, L.F.; Saleh, N.A.; Al-Nowaihi, A-SM. Two new kaempferol glycosides from *Matthiola longipetala* (subsp. *livida*) (Delile) Maire and carcinogenic evaluation of its extract. *Natural Product Communications,* **2008**, *3*(8), 1325-1328. https://doi.org/10.1177/1934578X0800300817.

8. Hammami, S.; Bergaoui, A.; Ayed, A.; Mighri, Z. Phytochemicals from *Mattiola longipetala* (Ssp LIVIDA) growing in tunisia. *Journal of the Algerian Chemical Society/Journal de Société Algérienne de Chimie,* **2009**, *19*(2).

9. Bnouham, M.; Ziyyat, A.; Mekhfi, H.; Tahri, A.; Legssyer, A. Medicinal plants with potential antidiabetic activity-A review of ten years of herbal medicine research (1990-2000). *Dubai Diabetes and Endocrinology Journal,* **2006**, *14*(1), 1-25. https://doi.org/10.1159/000497588

10. Chouikh, A.; Chemsa, A.E.; Aounallah, C.; Aounallah, I.; Fatma, A. Phytochemical study, nutritive value, antioxidant and anti-inflammatory activities of phenolic extracts from desert plant *Calligonum comosum* L'Hér. *Algerian journal of biosceinces,* **2020**, *1*(02), 68-75. http://dx.doi.org/10.5281/zenodo.4395515

11. DuBois, M.; Gilles, K.A.; Hamilton, J.K.; Rebers, P.; Smith, F. Colorimetric method for determination of sugars and related substances. *Analytical chemistry,* **1956**, *28*(3), 350-356. https://doi.org/10.1021/ac60111a017

12. Classics Lowry, O.; Rosebrough, N.; Farr, A.; Randall, R. Protein measurement with the Folin phenol reagent. *J biol Chem,* **1951**, *193*(1), 265-275. https://doi.org/10.1016/S0021-9258(19)52451-6

13. Goldsworthy, G.; Mordue, W.; Guthkelch, J. Studies on insect adipokinetic hormones. *General and Comparative Endocrinology,* **1972**, *18*(3), 545-551. https://doi.org/10.1016/0016-6480(72)90034-2

14. Chouikh, A.; Alia, F. Phytochemical properties, antibacterial and anti-free radical activities of the phenolic extracts of (Forssk) Webb. & Berthel. collected from Algeria Desert. *Ovidius University Annals of Chemistry,* **2021**, *32*(1), 33-39. https://doi.org/10.2478/auoc-2021-0005

15. Chouikh, A.; Rebiai, A. The influence of extraction method on the composition and analgesic activity of phenolic extracts. *Ovidius University Annals of Chemistry,* **2020**, *31*(1), 33-37. https://doi.org/10.2478/auoc-2020-0007

16. Kherraz, K.; Chouikh, A.; Chefrour, A.; Ghemam Amara, D. Estimation of total phenolic and fla-vonoids content and anti-free radical scavenger, antibacterial and antifungal activities of extract of *Matricaria pubescens* (DESF.) SCH. BIP. Collected from south easte of Algeria. *Analele Uni-versitatii din Oradea, Fascicula Biologie,* **2019**, *26*(1).

17. Chemsa, A.E.; Derdouri, S.; Labbi, Z.; Acila, S.; Amara, D.G.; Chouikh, A.; Kherraz, K.; Allali, A.; Zellagui, A. Total phenolic and total flavonoid contents of different solvent extracts of *Bassia muricata* (L.) Asch. and evaluation of antibacterial and antioxidant activities. *J Chem Pharm Res,* **2016**, *8*(4), 1317-1321.

18. Chouia, A.; Chouikh, A.; Alia, F.; Adjal, E.H.; Chefrour, A.; Ait Kaki, Y. Antibacterial activity and DPPH˙ radical scavenging of differents metabolites extracted from two plants: essential oil from (*Matricaria recutita* L.) and flavonoids from flowers and leaves of (*Hibiscus rosa-sinensis* L.). *Analele Universităţii din Oradea, Fascicula Biologie,* **2018**, *25*(1), 26-32.

19. Dolci, A.; Panteghini, M. Harmonization of automated hemolysis index assessment and use: Is it possible?. *Clinica Chimica Acta,* **2014**, *432*, 38-43. https://doi.org/10.1016/j.cca.2013.10.012

20. Ben Ali, A.; Chouikh, A.; Haddad, L. *Cyperus rotundus* tubers resin from Algeria: a promising source of natural antioxidants, anti-inflammatory, and photoprotective compounds. *Ovidius Uni-versity Annals of Chemistry,* **2023**, *34*(2), 132-139. https://doi.org/10.2478/auoc-2023-0017

21. Mebirouk-Boudechiche, L.; Cherif, M.; Boudechiche, L.; Sammar, F. Teneurs en composés pri-maires et secondaires des feuilles d'arbustes fourragers de la région humide d'Algérie. *Revue Méd Vét,* **2014**, *165*(11-12), 344-352.

22. Drew, S.W.; Demain, A.L. Effect of primary metabolites on secondary metabolism. *Annual Review of Microbiology,* **1977**, *31*(1), 343-356.

23. Blokhina, O.; Virolainen, E.; Fagerstedt, K.V. Antioxidants, oxidative damage and oxygen depri-vation stress. *a review. Annals of botany,* **2003**, *91*(2), 179-194. https://doi.org/10.1093/aob/mcf118

24. Lee, K.W.; Kim, Y.J.; Lee, H.J.; Lee, C.Y. Cocoa has more phenolic phytochemicals and a higher antioxidant capacity than teas and red wine. *Journal of agricultural and food chemistry,* **2003**, *51*(25), 7292-7295. https://doi.org/10.1021/jf0344385

25. Barroso, M.R.; Barros, L.; Dueñas, M.; Carvalho, A.M.; Santos-Buelga, C.; Fernandes, I.P.; Barreiro, M.F.; Ferreira, I.C. Exploring the antioxidant potential of *Helichrysum stoechas* (L.) Moench phenolic compounds for cosmetic applications: Chemical characterization, microencapsulation and incorporation into a moisturizer. *Industrial crops and products,* **2014**, *53*, 330-336. https://doi.org/10.1016/j.indcrop.2014.01.004

26. Naczk, M.; Shahidi, F. Phenolics in cereals, fruits and vegetables: Occurrence, extraction and analysis. *Journal of pharmaceutical and biomedical analysis,* **2006**, *41*(5), 1523-1542. https://doi.org/10.1016/j.jpba.2006.04.002

27. Mahmoudi, S.; Khali, M.; Mahmoudi, N. Etude de l'extraction des composés phénoliques de différentes parties de la fleur d'artichaut (*Cynara scolymus* L.). *Nature & Technology,* **2013**, (9), 35.

28. Do, Q.D.; Angkawijaya, A.E.; Tran-Nguyen, P.L.; Huynh, L.H.; Soetaredjo, F.E.; Ismadji, S.; Ju Y.H. Effect of extraction solvent on total phenol content, total flavonoid content, and antioxidant activity of *Limnophila aromatica*. *Journal of food and drug analysis,* **2014**, *22*(3), 296-302. https://doi.org/10.1016/j.jfda.2013.11.001

29. Sultana, B.; Anwar, F.; Ashraf, M. Effect of extraction solvent/technique on the antioxidant activity of selected medicinal plant extracts. *Molecules,* **2009**, *14*(6), 2167-2180. https://doi.org/10.3390/molecules14062167

30. Shazia, U.; Arshad, H.; Farooqui, A. Determination of infochemicals, phytochemical screening and evaluation of antioxidant potential of *Digera muricata*. *Der Pharmacia Lettre,* **2013**, *5*(2), 3-4.

31. Adedapo, A.A.; Jimoh, F.O.; Afolayan, A.J.; Masika, P.J. Antioxidant activities and phenolic contents of the methanol extracts of the stems of *Acokanthera oppositifolia* and *Adenia gummifera*. *BMC Complementary and Alternative Medicine,* **2008**, *8*, 1-7. https://doi.org/10.1186/1472-6882-8-54

32. Popovici, C.; Saykova, I.; Tylkowski, B. Evaluation de l'activité antioxydant des composés phénoliques par la réactivité avec le radical libre DPPH. *Revue de génie industriel,* **2009**, *4*(8).

33. Mburu, C.; Kareru, P.; Kipyegon, C.; Madivoli, E.; Maina, E.; Kairigo, P.; Kimani, P.; Marikah, D. Phytochemical screening of crude extracts of *Bridelia micrantha*. *European Journal of Medicinal Plants,* **2016**, *16*(1), 1-7. https://doi.org/10.9734/EJMP/2016/26649

34. Belboukhari, N.; Merzoug, Z.; Cheriti, A.; Sekkoum, K.; Yakoubi, M. Etude de la caractérisation et lacomposition qualitative des huiles essentielles de six plantes médicinales par spectroscopie IR. *PhytoChem & BioSub J.* **2013**, *7*(1), 14-17.

35. Butnaru, E.; Pamfil, D.; Stoleru, E.; Brebu, M. Characterization of bark, needles and cones from silver fir (Abies alba mill.) towards valorization of biomass forestry residues. *Biomass and Bioenergy,* **2022**, *159*,106413. https://doi.org/10.1016/j.biombioe.2022.106413

36. Easmin, S.; Sarker, M.Z.I.; Ghafoor, K.; Ferdosh, S.; Jaffri, J.; Ali, M.E.; Mirhosseini, H.; Al-Juhaimi, F.Y.; Perumal, V.; Khatib, A. Rapid investigation of α-glucosidase inhibitory activity of Phaleria macrocarpa extracts using FTIR-ATR based fingerprinting. *journal of food and drug analysis,* **2017**, *25*(2), 306-315. https://doi.org/10.1016/j.jfda.2016.09.007

37. Hajlaoui, H.; Arraouadi, S.; Mighri, H.; Chaaibia, M.; Gharsallah, N.; Ros, G.; Nieto, G.; Kadri A. Phytochemical constituents and antioxidant activity of *Oudneya africana* L. leaves extracts: Evaluation effects on fatty acids and proteins oxidation of beef burger during refrigerated storage. *Antioxidants,* **2019**, *8*(10), 442. https://doi.org/10.3390/antiox8100442

38. Nabti, L.Z.; Belhattab, R. In vitro antioxidant activity of *Oudneya africana* R. Br. aerial parts. *IBSPR,* **2016**, *4*, 58-64. http://dx.doi.org/10.15739/ibspr.16.008i

39. Fahmi, F.; Tahrouch, S.; Hatimi, A. Geoclimatic influences on flavonoids contents of the leaves of the argan tree Influences géoclimatiques sur la composition en flavonoides des feuilles de l'arganier *Argania spinosa*. *J Mater Environ Sci.* **2013**, *4*(6), 881-886.

40. Miliauskas, G.; Venskutonis, P.; Van Beek, T. Screening of radical scavenging activity of some medicinal and aromatic plant extracts. *Food chemistry,* **2004**, *85*(2), 231-237. https://doi.org/10.1016/j.foodchem.2003.05.007

41. Oumar, Y.S.; Nathalie, G.K.; Karamoko, O.; Alexis, B.G.; Adama, C. In vitro antioxidant activity of extracts of the root *Cochlospermum planchonii* Hook. f. ex. Planch (Cochlospermaceae). *Journal of Pharmacognosy and Phytochemistry,* **2014**, *3*(4), 164-170.

42. Hayouni, E.A.; Abedrabba, M.; Bouix, M.; Hamdi, M. The effects of solvents and extraction method on the phenolic contents and biological activities in vitro of Tunisian *Quercus coccifera* L. and *Juniperus phoenicea* L. fruit extracts. *Food chemistry,* **2007**, *105*(3), 1126-1134. https://doi.org/10.1016/j.foodchem.2007.02.010

43. Cheurfa, M.; Allem, R. Evaluation of antioxidant activity of different extracts of *Aloysia triphylla* leaves (L'Herit.) from Algeria in vitro. *Phytothérapie,* **2016**, *14*, 181-187. https://doi.org/10.1007/s10298-015-0969-4

44. Dai, J.; Mumper, R.J. Plant phenolics: extraction, analysis and their antioxidant and anticancer properties. *Molecules,* **2010**, *15*(10), 7313-7352. https://doi.org/10.3390/molecules15107313

45. Alia, F.; Chouikh, A.; Djahra, A.B. Comparative study of some physicochemical and biological properties of effect host species variation on the relationship Saharan parasitic plant *Cistanche violaceae* (Desf.) Beck. *Notulae Scientia Biologicae,* **2021**, *13*(4). https://doi.org/10.15835/nsb13411054

46. Falleh, H.; Ksouri, R.; Chaieb, K.; Karray-Bouraoui, N.; Trabelsi, N.; Boulaaba, M.; Abdelly, C. Phenolic composition of *Cynara cardunculus* L. organs, and their biological activities. *Comptes rendus biologies,* **2008**, *331*(5), 372-379. https://doi.org/10.1016/j.crvi.2008.02.008

47. Zeghad, N.; Ahmed, E.; Belkhiri, A.; Vander Heyden, Y.; Demeyer, K. Antioxidant activity of *Vitis vinifera*, *Punica granatum*, *Citrus aurantium* and *Opuntia ficus* indica fruits cultivated in Algeria. *Heliyon,* **2019**, *5*(4), 1-19. https://doi.org/10.1016/j.heliyon.2019.e015

48. Onofre, S.B.; Abatti, D.; Tessaro, A.A.; Tessaro, A.B. Total phenolic, flavonoid content and antioxidant activity of *Vitex megapotamica* (Spreng.) Moldenke. *Ciência e Natura,* **2016**, *38*(3), 1197-1204. https://doi.org/10.5902/2179460X21363

49. Abarca-Vargas, R.; Pena Malacara, C.F.; Petricevich, V.L. Characterization of chemical compounds with antioxidant and cytotoxic activities in bougainvillea x buttiana holttum and standl (Var. rose) extracts. *Antioxidants,* **2016**, *5*(4), 45. https://doi.org/10.3390/antiox5040045

50. Djeridane, A.; Yousfi, M.; Nadjemi, B.; Vidal, N.; Lesgards, J.; Stocker, P. Screening of some Algerian medicinal plants for the phenolic compounds and their antioxidant activity. *European Food Research and Technology,* **2007**, *224*, 801-809. https://doi.org/10.1007/s00217-006-0361-6

51. Gómez-Caravaca, A.; Gómez-Romero, M.; Arráez-Román, D.; Segura-Carretero, A.; Fernández-Gutiérrez, A,. Advances in the analysis of phenolic compounds in products derived from bees. *Journal of pharmaceutical and biomedical analysis,* **2006**, *41*(4), 1220-1234. https://doi.org/10.1016/j.jpba.2006.03.002

52. Fukushima, Y.; Ohie, T.; Yonekawa, Y.; Yonemoto, K.; Aizawa, H.; Mori, Y.; Watanabe, M.; Takeuchi, M.; Hasegawa, M.; Taguchi, C. Coffee and green tea as a large source of antioxidant polyphenols in the Japanese population. *Journal of agricultural and food chemistry,* **2009**, *57*(4), 1253-1259. https://doi.org/10.1021/jf802418j

53. Maroua, Z.; Iman, S.; Zineb, M.; Samir, D. Evaluation of in-vitro Antioxidant and Anti-diabetic activities of leave aqueous extracts of *Oudneya Africana*. *World Journal of Pharmaceutical Sciences,* **2018**, 48-53.

54. Abdelmadjide, S.; Mounir, A.; Atef, C.; Nadia, Z.; Néji, B. Phytochemical study, antioxidant and antimicrobial activities of flavonoids and diethyl ether extracts from leaves and seeds of medicinal plant of Algerian flora: *Retama monosperma* (L.) Boiss. *Ponte International Scientific Researches Journal,* **2020**, *76*(4), 42-52. https://doi.org/10.21506/j.ponte.2020.4.4

55. Khelef ,Y.; Chouikh, A.; Rebiai, A.; Neffar, S.; Chefrour, A.; Adjal, E.H.; Alia, F. Biochemical, quantitative and qualitative phenolic compounds, anti-free radical's activities of *Calligonum comosum* collected from different sites in the Algerian Desert. *Biharean Biologist,* **2019**, *13*(2), 71-76.

56. Baccarin, T.; Mitjans, M.; Lemos-Senna, E.; Vinardell, M.P. Protection against oxidative damage in human erythrocytes and preliminary photosafety assessment of *Punica granatum* seed oil nano-emulsions entrapping polyphenol-rich ethyl acetate fraction. *Toxicology in Vitro,* **2015**, *30*(1), 421-428. https://doi.org/10.1016/j.tiv.2015.09.020

57. Abirami, A.; Nagarani, G.; Siddhuraju, P. In vitro antioxidant, anti-diabetic, cholinesterase and tyrosinase inhibitory potential of fresh juice from *Citrus hystrix* and *C. maxima* fruits. *Food Science and Human Wellness,* **2014**, *3*(1), 16-25. https://doi.org/10.1016/j.fshw.2014.02.001

58. Lippi, G.; Luca Salvagno, G.; Montagnana, M.; Brocco, G.; Cesare Guidi, G. Influence of hemolysis on routine clinical chemistry testing. *Clinical Chemistry and Laboratory Medicine (CCLM),* **2006**, *44*(3), 311-316. https://doi.org/10.1515/CCLM.2006.054

59. Okoko, T.; Ere, D. Reduction of hydrogen peroxide–induced erythrocyte damage by *Carica papaya* leaf extract. *Asian Pacific journal of tropical biomedicine,* **2012**, *2*(6), 449-453. https://doi.org/10.1016/S2221-1691(12)60074-4

60. Chouikh, A.; Alia, F.; Neffar, S.; Rebiai, A.; Adjal, E.H.; Chefrour, A. Evaluation of phenolic contents (quantitative and qualitative) and antioxidant activities in different physiological phases of *Genista saharae* COSS. & DUR. growing in the sahara of Algeria. *Analele Universitatii din Oradea, Fascicula Biologie,* **2018**, *25*(2).

61. Chakraborty, D.; Shah, B. Antimicrobial, antioxidative and antihemolytic activity of *Piper betel* leaf extracts. *International Journal of Pharmacy and Pharmaceutical Sciences,* **2011**, *3*(3), 192-199.

62. Valente, M.J.; Baltazar, A.F.; Henrique, R.; Estevinho, L.; Carvalho, M. Biological activities of Portuguese propolis: protection against free radical-induced erythrocyte damage and inhibition of human renal cancer cell growth in vitro. *Food and Chemical Toxicology,* **2011**, *49*(1), 86-92. https://doi.org/10.1016/j.fct.2010.10.001

63. Afsar, T.; Razak, S.; Khan, M.R.; Mawash, S.; Almajwal, A.; Shabir, M.; Haq, I.U. Evaluation of antioxidant, anti-hemolytic and anticancer activity of various solvent extracts of *Acacia hydaspica* R. Parker aerial parts. *BMC complementary and alternative medicine,* **2016**, *16*(1), 1-16. https://doi.org/10.1186/s12906-016-1240-8

64. Chaudhuri, S.; Banerjee, A.; Basu, K.; Sengupta, B.; Sengupta, P.K. Interaction of flavonoids with red blood cell membrane lipids and proteins: antioxidant and antihemolytic effects. *International journal of biological macromolecules,* **2007**, *41*(1), 42-48. https://doi.org/10.1016/j.ijbiomac.2006.12.003

65. Mizushima, Y.; Kobayashi, M. Interaction of anti-inflammatory drugs with serum proteins, especially with some biologically active proteins. *Journal of Pharmacy and Pharmacology,* **1968**, *20*(3), 169-173. https://doi.org/10.1111/j.2042-7158.1968.tb09718.x

66. Boizot, N.; Charpentier, J.P. Méthode rapide d'évaluation du contenu en composés phénoliques des organes d'un arbre forestier. *Amélioration, Génétique et Physiologie Forestières, Laboratoire d'Analyses Biochimiques,* **2006**, 79-82.

67. Borzova VA, Markossian KA, Chebotareva NA, Kleymenov SY, Poliansky NB, Muranov KO, Stein-Margolina, V.A.; Shubin, V,V.; Markov, D.I.; Kurganov, B.I. Kinetics of thermal denaturation and aggregation of bovine serum albumin. *PloS one,* **2016**, *11*(4), 1-29. https://doi.org/10.1371/journal.pone.0153495

68. Owoyele, B.V.; Negedu, M.N.; Olaniran, S.O.; Onasanwo, S.A.; Oguntoye, S.O.; Sanya, J.O.; Oyeleke, S.A. Ibidapo AJ, Soladoye AO: Analgesic and anti-inflammatory effects of aqueous extract of *Zea mays* husk in male Wistar rats. *Journal of medicinal food,* **2010**, *13*(2), 343-347. https://doi.org/10.1089/jmf.2008.0311

69. Duganath, N.; Kumar, S.; Kumanan, R.; Jayaveera, K. Evaluation of anti-denaturation property and anti-oxidant activity of traditionally used medicinal plants. *International Journal of Pharma and Bio Sciences,* **2010**, *1*(2),1-7.

70. Heendeniya, S.; Ratnasooriya, W.; Pathirana, R. In vitro investigation of anti-inflammatory activity and evaluation of phytochemical profile of *Syzygium caryophyllatum*. *Journal of Pharmacognosy and Phytochemistry,* **2018**, *7*(1), 1759-1763.

Adida, H, Benariba, N.; Bechiri, A.; Chekroun, E.; Djaziri, R. Étude phytochimique et évaluation du pouvoir antiradicalaire des extraits de *Pituranthos scoparius*. *Phytothérapie*, **2016**, *14*(4), 207-212. https://doi.org/10.1007/s10298-015-0932-4

NUTRITIONAL VALUE, ANTI-NUTRIENT AND AMINO ACID PROFILE OF RAW AND PROCESSED WILD AERIAL YAM (*Dioscorea bulbifera*) MEAL

M. D. UDO[1]* , B. A. UGBE[1], G. D. EYOH[1] , E. M. UDO[3], U. E. EKPO[2]

[1] Department of Animal Science, Akwa Ibom State University, Uyo, Nigeria
[2] Training/Educational Department, Vika Farms Limited, Mbak Etoi, Uyo, Akwa Ibom State, Nigeria
[3] McIntire Secondary Commercial School Utu Abak, Akwa Ibom State, Nigeria

The study evaluated the effect of different processing methods (boiling, toasting and soaking) on the nutrient and of wild aerial yam (Dioscorea bulbifera). One kilogram of raw wild Dioscorea bulbifera (RWDB) was boiled for 30 minutes at 100 °C, another one kg was soaked for 24 hours. Toasting of another one kg of Dioscorea bulbifera tubers were carried out for 30 minutes. The raw and processed tubers were dried, milled and chemically analysed for proximate compositions, phytochemical components, minerals and amino acid content. Mean dry matter, crude protein, lipid, fibre, ash and carbohydrate contents of boiled wild Dioscorea bulbifera meal were 10.86%, 89.14%, 11.63%, 32.28%, 4.10%, 3.61% and 66.53% respectively. There were significant differences (p<0.05) in all parameters for all the processing methods. RWDB meals was a good source of Calcium (0.27%), Phosphorus (0.38%), Magnesium (0.29%), Potassium (0.75%), Sodium (0.25%), Iron (56.78%), Copper (9.91%), Zinc (52.87%), Manganese (17.51%) and Cobalt (0.52%). Increase in contents of macro and micro minerals were observed during toasting and these were significantly (p<0.05) superior to raw and other processing methods. Values obtained for soaked WDB meal were significantly lower (p<0.05) in all the phytochemical substances (tannin 0.0012, oxalate 1940, flavonoid 0.002) determined, while boiled WDB meal had the least HCN. Boiling process improved the amino acid profile of WDB meal, and there were significant differences (p<0.05) in all its parameters. Boiling compared to other methods appeared to be the best in terms of nutrient content, anti-nutritional factors and amino acid profile, therefore stands as the preferred method for preparing WDB as a livestock feed ingredient

Keywords: *Dioscorea bulbifera*, processing, proximate, amino acid and fibre fractions.

INTRODUCTION

Plant based nutrients play important roles in human/livestock nutrition, especially in developing countries where escalating cost of conventional feedstuffs (maize, soya bean, groundnut, etc.) have become a constant threat to livestock production. This has led to constant search for unconventional feedstuffs for use as both functional feed ingredients and nutritional supplements (1). To solve these challenges; interests have been in search for relatively low cost, available and nutritionally viable feedstuffs to enhance livestock production.

One of such alternative feedstuff is wild aerial yam (*Dioscorea bulbifera).* Wild *Dioscorea bulbifera* (WDB) occur as aggressive weed in farmlands and forest. The plant possesses brownish bulbils with irregular shape, dotted and rough surface (2). Unlike the cultivated edible varieties, WDB variety is not readily consumed by man (3). Hence the bulbils are found littering in farmland and wasting away in the uncultivated lands. Wild aerial yam (*Dioscorea bulbifera*) locally referred to as Ukad ekpo in Efik is a member of the *Diosco-*

---

reaceae family which is consumed among rural dwellers in parts of Eastern, Western and Southern Nigeria (4). This specie of yam is well known for its aerial bulbils which are rich in nutrients and have many traditional therapeutic and pharmaceutical uses (5-7). Raju and Rao (8) reported that *Dioscorea bulbifera* is rich in diosgenin, a steroid saponin which possesses antherapeutic properties against several ailments including arthritis, gastrointestinal disorders, high cholesterol and inflammation. However, other properties of wild aerial yam such as functional and antioxidant properties are still gaining importance. Thus, the present work was carried out to study the various chemical components (crude protein, crude fibre, ether extract, and nitrogen free extract), minerals, phytochemical and amino acids of wild aerial yam.

MATERIALS AND METHODS

EXPERIMENTAL LOCATION

WDB tubers were harvested from fallow lands in Obio Akpa, Oruk Anam, Akwa Ibom State, Nigeria. Obio Akpa is located between latitude 5°17'N and 5°27'N and between longitude 7°27'N and 7°58'E with an annual rainfall ranging between 3500 – 5000mm and an average monthly temperature of 25 °C and a relative humidity of 60-90% (9).

PROCESSING OF EXPERIMENTAL MATERIALS

One kilogram for each treatment was prepared. Tubers were introduced into the boiling water at 100 °C. Boiling continued for 30 minutes before the tubers were decanted. Second sample was soaked in 20 litres of water for 24 hours at temperature of 22 °C-23 °C. The soaked water was decanted and samples were drained out. Third sample were sliced and toasted in a frying pan for 30 minutes. At the end of the processing, raw, boiled, soaked and toasted samples of aerial yam were peeled, chopped into pieces, sundried and milled to obtain raw and processed wild *Dioscorea bulbifera* meal (WDBM). Triplicate samples, each of raw and processed WDBM were taken for laboratory analysis.

ANALYTICAL PROCEDURE

Proximate compositions of WDBM samples were assayed using Association of AOAC procedure (10). The samples were also analyzed for gross energy according to the method of McDonald et al. (11). Calcium, sodium and potassium were determined by flame photometry using Jenway Digital Flame photometer (PEPT model). Zinc, copper, cobalt, iron, magnesium and manganese were determined using Atomic Absorption Spectrophotometry (Buck 211 VGP) (10). Total phosphorus was determined using Vanadomolybdate colorimeter and method described in work of Raun *et al.* (12). Quantitative assay of tannin, oxalate, flavonoid and hydrogen cyanide (HCN) in raw and processed WDBM were done according to the methods of AOAC and Arntfield et al. (10, 13). Amino acid profiles of raw and processed WDBM were carried out using Thin Layer Chromatography (TLC) and Modified Colorimeter or spectrophotometric techniques (10). Fibre fractions in raw and processed WDBMs were analyzed according to the method of (14).

Data were obtained in duplicates and subjected to Analysis of Variance (ANOVA) using GENSTAT version 12.10. Duncan Multiple Range Test (15) was used to separate significant differences among treatment means.

RESULTS AND DISCUSSION

The effect of processing methods on proximate composition of WDBMs are presented in Table 1.

Table 1. Composition of raw and differently processed wild *Dioscorea bulbifera* meals (WDBM)

Parameters	Control (Raw)	Boiled	Toasted	Soaked	SEM
Dry Matter (DM)%	88.77[a]	89.14[a]	89.46[a]	88.56[b]	0.16
Crude Protein (CP)%	7.84[c]	11.63[a]	9.74[b]	7.24[b]	0.65
Crude Fibre (CF)%	9.23[b]	4.10[d]	13.57[a]	8.94[c]	1.27
Ether extract	2.64[b]	3.28[a]	2.41[d]	2.55[c]	0.13
Ash%	4.27[a]	3.61[c]	3.99[b]	3.93[b]	0.08
Nitrogen free Extract (NFE)%	64.79[c]	66.53[a]	59.75[d]	65.91[b]	1.14
Gross Energy (GE) (Kcal/g)	2.89[c]	3.12[a]	2.91[b]	2.80[d]	0.04

Means within the same row with different superscripts (a-d) are significantly ($p<0.05$) different.

The crude protein (CP) content in this study differed ($p<0.05$) significantly among the processed WDBMs. Crude protein content of the boiled DBM (11.63%) was significantly ($p<0.05$) higher than CP of other samples. Indicating that boiled DBM can be used as a supplemental source of protein in livestock diet (5). The crude protein values of 7.24 – 11.63% obtained in this study were higher when compared with values reported by Godfrey *et al.* (17) and Nwachukwu and Okoroafor (18), 8.64% and 6.40%, respectively. The variation in crude protein values may be due to species diversity, stage of harvesting and differences in soil nutrients. The results showed that ether extract (EE) content of WDB tuber meals ranged between 2.41% and 3.28% across the treatment groups. The values reported in the present study did not agree with the levels of 5.70%, 1.60% and 0.51-0.97% obtained by Nwachukwu and Okoroafor (18), Godfrey *et al.* (17), and Olatoye and Arueya, (21) .The EE of boiled WDBM was higher ($p<0.05$) when compared with the EE content of raw, toasted and soaked samples, likely due to cells burst and membrane lipids liberation during boiling. The result indicated that boiled DBM may supplement energy needs from lipids.

The crude fibre range for raw and processed WDBMs was 4.10% - 13.57% and was higher than 1.28% and 2.30% reported by Nwachukwu and Okoroafor (18), and Godfrey *et al.* (17) respectively. The composition of the crude fibre for toasted sample was significantly superior ($p<0.05$) to the fibre content of other treatment methods. Fibre has nutritional and health benefits to both human and ruminant animals (22). The reported ash values for this study did not agree with the values of 2.34% and 3.35% reported previously (18, 19).

Geographical locations, stage of maturity and soil type may have caused the variations observed (23). The nitrogen free extract (NFE) of boiled DBM (66.53%) differed ($p<0.05$) significantly from toasted (59.75%) and soaked (65.91%) which were significantly ($p<0.05$)

higher than raw (64.79%). These values, however, are different from those of the same plant that were reported in (18, 17) at 73.55% and 77.51%, respectively. Raw, boiled, toasted and soaked WDBMs, gross energy values agree with some alternative energy sources such as *Caladium bicolor* meal with gross energy values ranging from 2.83-2.85kcal/g (20). Boiling leads to an increase in gross energy due to the destruction of the toxic substances in the yam (24), through leaching and denaturing of those substances.

The results of both macro and micro minerals of raw and processed WDBMs are presented in Table 2. Significant differences ($p<0.05$) were observed between raw and processed WDBMs. Processing enhanced reduction in mineral content of the samples. Boiled WDBM had the highest reducing effect followed by soaked and toasted samples. Lower values of minerals obtained for boiled and soaked WDBMs may be due to leaching of minerals into the water and the removal of WDB tuber peels before toasting (20).

Table 2. Mineral constituent of raw and differently processed wild *Dioscorea bulbifera* meal (WDBM)

Minerals	Raw	Boiled	Toasted	Soaked	SEM
Macro Minerals (%)					
Calcium	0.27[a]	0.09[d]	0.25[b]	0.22[c]	0.03
Phosphorus	0.38[a]	0.21[d]	0.35[b]	0.32[c]	0.02
Magnessium	0.29[a]	0.10[d]	0.27[b]	0.24[c]	0.03
Potassium	0.75[a]	0.13[d]	0.72[b]	0.68[c]	0.10
Sodium	0.25[a]	0.05[d]	0.23[b]	0.22[c]	0.03
Micro Minerals (mg/kg)					
Iron	56.78[a]	67.47[d]	155.81[b]	153.81[c]	14.41
Copper	9.71[a]	3.06[d]	9.25[b]	8.92[c]	1.03
Zinc	52.87[a]	13.20[d]	48.92[b]	42.63[c]	5.88
Manganese	17.51[a]	7.87[d]	17.07[b]	16.95[c]	1.52
Cobalt	0.52[a]	0.14[d]	0.46[b]	0.35[c]	0.06

Means within the same row with different superscripts (a,b,c,d) are significantly ($p<0.05$) different.

Values obtained for macro minerals (Ca, P, M, K and Na) indicated that toasted WDBM had significantly ($p<0.05$) higher values among the processed meals. The values obtained in this study indicate that toasted WDBM recorded higher values for Fe, Cu, Zn, Mn and Co. This implies that using toasted WDBM as ingredient in animal diet could potentially enhance blood formation, promote zinc for wound healing, improved appetite and growth, provide copper as a component of cytochrome oxidase which is important in oxidative phosphorylation (20, 25).

Table 3. Phytochemical components of raw and differently processed wild *Dioscorea bulbifera* meals (WDBM)

Parameters	Raw	Boiled	Toasted	Soaked	SEM
Tannin (%)	0.0030[a]	0.0021[b]	0.0016[c]	0.0012[c]	0.0002
Oxalate (%)	0.2260[a]	0.2140[b]	0.2100[b]	0.1940[c]	0.0040
Flavonoid (%)	0.0031[a]	0.0016[c]	0.0025[b]	0.0020[c]	0.0002
Hydrogen Cyanide (mg/kg)	3.4400[a]	1.3500[d]	3.2800[b]	2.9700[c]	0.3100

Means within the same row with different superscripts (a-d) are significantly (P<0.05) different.

Table 3 revealed the results of phytochemical components of both raw and processed WDBMs. All the parameters measured differed significantly (p<0.05) between the raw and processed WDBMs. There was a general reduction in the content of the assayed components: tannin, oxalate, flavonoid and hydrogen cyanide (HCN)) as a result of processing WDB tubers. However, this reduction varies in degree with different processing techniques. It has been reported that some anti-nutrients are heat liable and soluble in water, therefore will be reduced to a great extent by the application of these processing methods (27, 28). This may mean better digestibility of available nutrients if processed WDBMs are fed to animals. Values of tannin, oxalate and flavonoid in wild *Dioscorea bulbifera* meals fell below the range of 2-4% for tannin (19), <2% for oxalate (29) and less than 60mg/kg BW for flavonoid (30) allowed in the diets of ruminant animals. However, hydrogen cyanide (HCN) values were within the range of the lethal dose (2.0-4.0mg/kg body weight) recommended as not detrimental to ruminant animals with exception to boiled WDBM that has the least value. Recharla *et al.* (25) reported that ruminant animals are susceptible to cyanide toxicity than non-ruminants since hydrolytic reactions takes place in the rumen.

The values of amino acid profile of raw and differently processed WDBMs are presented in Table 4. The amino acid values differed (p<0.05) significantly between the treatment means. WDBMs (raw, boiled, soaked and toasted) could be used as an alternative protein ingredient for animal; however, boiled WDBM was significantly higher in values, particularly in methionine and lysine compared to other processing methods, thus could be more preferred method to process wild aerial yam. The results of the present study indicate that samples of WDBMs are rich in both essential and non-essential amino acids.

Table 4. Amino acid profile of raw and differently processed wild *Dioscorea bulbifera* meals (WDBM)

Parameters (%)	Raw	Boiled	Toasted	Soaked	SEM
Alanine	2.44[c]	3.08[a]	2.96[b]	2.33[d]	0.12
Arginine	3.55[c]	4.78[a]	4.03[b]	3.49[c]	0.20
Aspartic Acid	5.08[c]	6.60[a]	6.10[b]	5.01[d]	0.26
Cysteine	1.22[c]	1.68	1.55[b]	1.16[c]	0.08
Glutamic Acid	3.83[c]	4.11[a]	3.95[b]	3.67[d]	0.06
Glycine	2.94[b]	3.14[a]	2.87[c]	2.83[c]	0.05
Histidine	3.08[c]	4.19[a]	3.93[b]	2.97[d]	0.20
Isoleucine	1.77[c]	2.08[a]	1.88[b]	1.65[d]	0.06
Leucine	5.35[c]	6.52[a]	5.84[b]	5.16[d]	0.19
Lysine	1.21[c]	2.32[a]	2.17[b]	1.12[d]	0.21
Methionine	0.87[c]	1.10[a]	1.00[b]	0.78[d]	0.05
Phenylalanine	3.74[c]	5.81[a]	4.94[b]	3.65[d]	0.34
Proline	2.26[c]	3.33[a]	2.95[b]	2.20[d]	0.18
Threonine	1.76[c]	2.87[a]	2.78[b]	1.71[c]	0.21
Tryptophan	0.71[b]	0.82[a]	0.74[b]	0.63[c]	0.03
Tyrosine	3.05[c]	4.14[a]	3.85[b]	2.92[d]	0.20
Ornithine	0.22[c]	0.32[a]	0.26[b]	0.17[d]	0.02
Cystine	0.27[b]	0.57[a]	0.50[a]	0.22[b]	0.06
Serine	1.23[c]	2.55[a]	2.30[b]	1.16[d]	0.23
Valine	2.11[c]	3.24[a]	3.05[b]	1.99[d]	0.21

Means within the same row with different superscript (a- d) are significantly (P<0.05) different.

CONCLUSION

Wild *Dioscorea bulbifera* tubers investigated contained high amount of carbohydrates, lipid, protein and minerals, therefore carries an important nutritional value. The values obtained for proximate composition and gross energy, increased considerably after boiling and toasting. WDBMs (raw, boiled, soaked and toasted) could be used as alternative protein ingredient for animal. However, boiled WDBM had a significantly higher value, particularly in methionine and lysine compared to other processing methods, thus could be more preferred processing method. Processing, particularly boiling, rendered WDB tuber a veritable feed ingredient in animal diet due to its high nutritional value, low phytochemical composition and high energy content.

REFERENCES

1. Oosting, S.; Van, D. L. J.; Verdegem, M.; De vries, M.; Bonillacedrez, C.; Kabir, K. Farm animal production in tropical circular food systems. *Food security*, **2022**, *14*(1), 273-292.
2. Ogunjobi, A. A.; Adebayo-Tayo, B. C.; Ogunshe, A.A. Microbiological, proximate analysis and sensory evaluation of processed Irish potato fermented in brine solution. *African J. Biothnol.* **2005**, *14*, 1409-1412.
3. Ogunjobi, J. K.; Balogun, O. M. Isolation, modification and characterization of cellulose from wild *Dioscorea bulbifera. Scienctific Reports*, **2021**, *11,* 1025. https://doi.org/10.1038/s41598-020-78533-6
4. Nwachukwu, C. W.; Njoku, C. C.; Anusionwu, D. C. Anti-Nutrient composition of Aduh (*Dioscorea bulbifera*) and its performance as what substitute in bread production. *International Journal of Innovation Food Nutrition and Sustainable Agriculture,* **2020**, *8*(3), 36-42.
5. Princewill-Ogbonna, I.; Ezembaukwu, N. Effect of various processing methods on the pasting and functional properties of yam (*Dioscorea rotundala*) flour. *British Journal of Applied Sciences and Technology,* **2015**, *9*(5), 517-526.
6. Adetunji; I. L.; Rahman, A. Physical properties, proximate composition and antioxidant activities of aerial yam (*Dioscorea bulbifera*) bulbils grown in Nigeria. *APTEFF,* **2019**, *50,* 143-151.
7. Yamada, T.; Hoshino, M.; Hayakawa, T.; Ohhara, H.; Yamada, H.; Nakazawa, T.; Uchida, A.; Hasegawa, C.; Murasaki, G.; Miyaji. M.; Hirata, A.; Takeuchi, T. Dietary diosgenin attenuates subacute intestinal inflammation associated with indomethacin in rats. *American Journal of Physiology*, **2009**, *273*, 355-364.
8. Raju, J.; Rao, C. V. Diosgenin a steroid saponin constituent of yams and fenugreek: Emerging evidence for application in medicine. In *Bioactive compounds in Phytomedicine*, Rasooli, I., Ed.; Tech Publishers, Rijeka, Croatia. 2012, pp 125-132.
9. Wikipedia: The free encyclopedia, Akwa Ibom State, https://en.wikipedia.org/wiki/Akwa-Ibom
10. AOAC: Association of Official Analytical Chemists Official Methods of Analysis (18[th]ed). Gaithersburg: AOAC. 2005, Press, USA.
11. McDonald, P.; Edwards, R.A.; Greenhalgh, J.F.D.; Morgan, C.A.; Sinclair, L.A.; Wilkinson, R.G. Animal Nutrition. Seventh Edition, Prentice Hall, Pearson, Hoboken 2010, New Jersey, USA.
12. Raun, W.R.; Olson, R.A.; Sander, D.H.; Westerman, R.L. Alternative procedure for total phosphorous determination in plant tissue. *Communications in soil science and Plant Analysis*, **1987**, *18*(5), 543-557.
13. Arntfield, S. D.; Ismond, M. A. H.; Murray, E. D. The fate of anti-nutritional factors during the preparation of faba bean protein isolates using a micellization technique, *Canadian Institute of Food Science and Technology Journal*, **1985**, *18*(2), 137-143.
14. Van Soest, P.J. Nutrirional ecology of ruminant (2[nd]edn), Cornell University Press Ithaca, New York. 1994, pp 476.
15. Duncan, D. B. New Multiple Range-Test. *Biometrics,* **1955**, *11*, 1-42.

16. Tenyang, N.; Ponka, R.; Tiencheu, B.; Tonfack, D.F.; Azemeera, T.; Karuna, M.S.L.; Prasad, R.B.N.; Womeni, H.M. Effects of boiling and roasting on proximate composition, lipid oxidation, fatty acid profile and mineral content of two sesame varieties commercialized and consumed in far-north region of Cameroon. *Food Chemistry*, **2021**, *221*, 1308-1316.

17. Godfrey, E. O.; Ibrahim, I. E.; Obuye, F. Proximate Composition Levels of some essential mineral elements and anti-nutritional components of some yam species found in Minna, Niger State. Biology, *Medicine and Natural product chemistry*, **2023**, *12*(1), 9-16.

18. Nwachukwu, C. N.; Okoroafor, C. N. Nutrient and phytochemical composition of Aduh (*Dioscorea bulbifera*) an indigineous crop. *Journal of Agriculture and Food Sciences,* **2019**, *17*(1), 54-64.

19. Njidda, A.A. Chemical composition fibre fractions and anti-nutritional substances of semi-arid browse forages of North-Eastern Nigeria. *Nigerian Journal of Basic and Applied Sciences,* **2010**, *18*(2), 181-188.

20. Udo, M. D.; Eyoh, G. D.; Jimmy, C. P.; Ekpo, U. E. Nutrient Composition, mineral and anti-nutrient components of processed wild cocoyam (*Caladium bicolor,* (Ait) vent). *Current Agricultural Research Journal*. 2020, *8*(2): 137-145.

21. Olatoye, K. K.; Arueya, G. L. Nutrient and phytochemical composition of flour made from selected cultivars of aerial yam (*Dioscorea bulbifera*) in Nigeria. *Journal of Food Composition and Analysis,* **2019**, *79*, 23-27.

22. Amadi, J. A.; Ihemeje, A.; Afam-anene, O. C. Nutrient and phytochemical composition of jackfruit (*Artocarpus heterophyllus*) pulp, seeds and leaves. *International Journal of Innovative Food Nutrition and Sustainable Agriculture*, **2018**, *6*(3), 27-32.

23. McClements, D.J. Analysis of Food Products.Analysis of ash and minerals. Lecture Note, Food Science 58l, Department of Food Science, University of Massachusetts, Amherst, MA. 01003, 2023, USA. https://people.umass.edu/~mcclemen/581Ash&Minerals.html.

24. Mbah, B. O.; Eme, P. E.; Ogbusu, O. F. Effect of cooking methods (boiling and roasting) on nutrients and anti-nutrients content of *MoringaOleifera* seeds. *Pakistan Journal of Nutrition,* **2012**, *11*(3), 211-215.

25. Recharla, N.; Balasubramanian, B.; Song, M.; Pulinundla, P.; Kim, S.H.; Jeong, J.Y.; Park, S. Dietary turmeric (*Curcuma longa L*) supplementation improves growth performance, short chain fatty acid production, and modulates bacterial composition of weaned piglets. *Journal of Animal Science and Technology,* **2021**, *63*(3), 575-578.

26. Pugh, D.G. Nutritional requirements of Goats. MSD. Veterinary Manual. htpps://www.msdvetmanual.com/management-and-nutrition/nutrition-goats/nutritional-requirements of goats. Accessed August 21, 2023.

27. Saulawa, L.A.; Yara due, A.I.; Shuaibu, L. Effect of different processing methods on proximate mineral and anti-nutritional factors content of Baobad (*Adansoniadigitata*) seeds. *Pakistan Journal of Nutrition*, **2014**, *13*(6), 314-318.

28. Yilkal, T. Important anti-nutritional substances and inherent toxicants of feed. *Food Science and Quality Management*, **2015**, *36*, 1-8.

29. Akpan, I.E.; Eyoh, G.D.; Udo, M.D.; Ekpo, U.E. Growth performance and economics of production of West African Dwarf Bucks fed different forms of *Coelocaryon preussi* seed meal. *AKSU Journal of Agriculture and Food Sciences*, **2022**, *6*(2): 122-132.

30. Zhang, L.; Yang, Z.; Chen, F.; Su, P.; Chen, D.; Pan, W.; Fang, Y.; Dong, C.; Zheng, X.; Du, Z. Composition and bioactivity assessment of essential oils of *Curcuma longa L.* collected in China. *Industrial crops and products*, **2017**, *109*, 60-73.

CHROMIUM NANOSTRUCTURED COATINGS FORMED BY THE PVD METHOD

Ravshan SAYDAKHMEDOV[1], Gulirano SAIDAKHMEDOVA[2]*

[1]Tashkent State Transport University, Mirabad district, Temiryulchilar street 1, Tashkent, Uzbekistan.
[2]Turin Polytechnic University in Tashkent, Olmazar district, Kichik Halka street 17, Tashkent, Uzbekistan.

Practical interest in materials with high physicomechanical properties has increased in nanomaterials and, in particular, nanocoating. First of all, it is the protection of metals from corrosion, the increase in wear resistance of parts and tools, and reflective properties. Environmentally friendly technologies are used in the vacuum sputtering process of producing chromium-based coatings. Consider the technological capabilities of a magnetron-sputtering vacuum system. It was proposed to pre-treat the surface of the substrate with argon ions before applying the chrome plating. For this purpose, a designed ion source and a magnetron sputtering device for the chromium cathode are located in the chamber. Chromium-based nanostructured coatings formed by magnetron sputtering with preliminary treatment of the surface with an ion source are investigated. During the measurements, the thickness, adhesion strength, and corrosion resistance of chromium coatings were determined. The strong corrosion resistance of samples with chromium-based coatings was demonstrated by their chemical resistance in nitric and hydrofluoric acid solutions. The novelty of this work was the effect of the thickness of the chromium-based nanostructured coating on the corrosion resistance. With an increase in coating thickness, the corrosion resistance of chromium coatings changes several times. For coatings less than 1 micron thick, the number of corrosion points (pores in the coating) was 5–10 times larger than for coatings 2.3–2.5 microns thick. The size and surface appearance of nanoparticles in the chromium coating structure were examined using electron microscopy. It was revealed that, depending on the formation modes, the coatings consist of crystallites with sizes ranging from 45 nm to 200 nm.

Keywords: Magnetron sputtering, Vacuum chamber, Adhesive strength, Physicochemical properties, Technological regimes, electron microscopy.

INTRODUCTION

The interest in the study of materials with a nanocrystalline structure has increased compared to a few decades ago, since a decrease in the size of crystals below a certain threshold value leads to a significant change in their physicochemical properties. The most noticeable change in the properties of nanomaterials is achieved in the range of crystallite sizes up to 100 nm. The technology for producing thin coatings of this thickness can be attributed to nanotechnology. Thin films and coatings can be obtained by PVD and CVD. Thus, well-known coatings of titanium carbide and nitride are obtained by ion-plasma deposition, which leads to the formation of a nanocrystalline structure (1-7).

Steels, as wrought alloys, are the most important technological materials widely used in industry. Coatings based on chromium and chromium nitrides are used in industry as hard, thin layers to protect parts. They have excellent wear resistance, sufficient strength, good adhesion to the base, high corrosion resistance, and heat resistance up to 600 °C (8-12).

Currently, the industry widely uses chromium plating on steels and alloys, which are characterized by high chemical and mechanical resistance, but they are formed using an environmentally harmful chemical technology that requires expensive treatment facilities. In galvanic chromium plating, toxic hexavalent chromium is used, and significant tensile stresses are also formed, which lead to the appearance of a network of cracks in the coating after deposition (13-20).

Vacuum coating technologies do not have these drawbacks. Therefore, in some cases, it is advisable to use vacuum methods for the deposition of chromium coatings by ion-plasma (magnetron) sputtering. Due to the low temperature of deposition of coatings by magnetron sputtering, they can be formed on tools and non-metallic materials, in particular on reflective surfaces, as decorative coatings on various parts of cars.

DESCRIPTION OF THEORETICAL STUDIES

Currently, aluminum alloys are used in the automotive industry to produce reflective and decorative coatings. Coatings based on aluminum do not always meet the requirements for their reflective and corrosive parameters. And coatings based on chromium or Al-Cr composites can be successfully used as reflective coatings. Chromium nitride-based coatings are hard coatings that can be successfully applied as wear-resistant coatings to protect the wear surfaces of parts and tools. The study of chromium vacuum coatings is of interest both for science and for practical applications.

The physical and mechanical properties of coatings based on chromium depend on the structure, phase, and chemical composition. Therefore, in order to achieve the required properties, it is necessary to know which phases are formed during the production of coatings by the PVD method.

Gilewicz et al. (22) studied the multilayer coatings based on chromium nitride and chromium carbonitride. Multilayer alternating layers of coatings based on CrN/CrCN, formed by PVD (CAD-cathode-arc deposition). The multilayer coating consists of a seven-layer module. The thickness of each layer is approximately 400 nm, differing in the different arrangement of the CrN and CrCN layers in modulus. It has been experimentally established that the durability of multilayer coatings based on chromium nitride and chromium carbonitride is higher than that of CrN and CrCN coatings taken separately. A chromium sublayer 0.1 µm thick was used as a sublayer. The adhesion of the coatings was determined by scratching and Rockwell methods. By changing the ratio of layer thicknesses, you can adjust the adhesion of the coating to the base and wear resistance.

The properties of chromium coatings obtained by the PVD (Physical Vapor Deposition) method were studied by Perillo (23). CrN coatings are obtained on titanium substrate using advanced physical vapor deposition (PVD). The composition, microstructure and residual stresses of the coating were determined by scanning electron microscopy (SEM), X-ray diffraction (XRD) and X-ray photoelectron spectroscopy (XPS).

In the chromium-nitrogen system, the existence of Cr_2N (11.87% N) and CrN (21.22% N) compounds was established, and the existence of CrN_2 nitride (35.01% N) is assumed. Cr_2N (β-phase) has a hexagonal structure of the CdI_2 type with parameters a=0.4806÷0.4760 nm and c=0.4479-0.4438 nm (10). CrN nitride (δ-phase) has a cubic NaCl-type lattice with parameters a=0.4148 nm.

The melting point of chromium significantly decreases when it absorbs nitrogen, and the hardness increases sharply. At the same time, the microhardness of chromium nitride CrN is -1083±93 kgf/mm^2, and that of Cr_2N is -1571 kgf/mm^2 (21).

Chromium nitride CrN is a very chemically stable compound. It is completely resistant to the action of water both in the cold and when heated, does not dissolve in alkalis, is not reduced by hydrogen, and with great difficulty lends itself to the action of acids, including aqua regia. Cr2N nitride is less resistant to acids than CrN nitride.

Gilewicz et al. (22) studied multilayer coatings based on chromium nitride and carbonitride. Multilayer alternating layers based on CrN/CrCN were formed by the PVD (CAD-cathode arc deposition) method. It has been experimentally established that the wear resistance of multilayer coatings based on chromium nitride and chromium carbonitride is higher than that of individual CrN and CrCN coatings. As a sublayer, a 0.1 μm-thick chromium sublayer was used.

The composition, microstructure, and residual stresses, as well as the properties of chromium coatings obtained by the PVD (Physical Vapor Deposition) method, were studied by Perillo (23) and Lippitz (24). CrN coatings are produced on a titanium substrate by advanced physical vapor deposition (PVD).

In these works, coatings obtained by vacuum arc deposition were mainly studied, which is not always acceptable for nonmetallic materials due to the high deposition temperature. For the formation of coatings on non-metallic materials with low heat resistance, it is advisable to use magnetron sputtering.

Based on the foregoing, it is necessary to note the relevance of studying the technology of forming coatings based on chromium by the method of magnetron sputtering.

The purpose of this study is to study the structure, composition, and properties of chromium-based coatings formed by magnetron sputtering, as well as the effect of magnetron sputtering modes on the thickness and structure of coatings.

EXPERIMENTAL

Chromium-based coatings were deposited by magnetron sputtering with preliminary surface treatment by an ion source.

We used carbon steel AISI 1020 in the form of sheets (plates) with a thickness of 1.5–2.0 mm. Plates up to 50x60 mm in size on one (front) side were previously subjected to mechanical grinding and polishing using silicon carbide powders and ACM diamond paste. R6M5 tool steel was also used for processing.

The final surface roughness, according to measurements of the average deviations of the surface profile (Ra), was about 0.16-0.20 μm. The measurements were carried out using a standard MII-4U micro interferometer. Immediately prior to coating deposition, the plates were cleaned with organic solvents in an ultrasonic bath and dried in a centrifuge. The interoperative time did not exceed 20 minutes.

The formation of chromium coatings in the modernized working chamber of the UVN-75R installation included the following treatments (operations in one vacuum cycle):
- ion-plasma treatment (cleaning) of the steel surface immediately before coating application using an ion source with a cold cathode;
- magnetron deposition of chromium coatings on moving samples, including those with a negative voltage applied to them.

After the "starting" degree of vacuum of the order of 10^{-3} Pa was reached in the working chamber, the rotation of the equipment with steel samples was turned on, and pure technical argon was injected to a level of $2 \cdot 10^{-1}$ Pa using a VIT-3 vacuum gauge. The upgraded ion source with a cold cathode type II-4-0.15 was turned on, and the electromagnet current was

set to 1.5–2.0 A. The voltage on the annular anode was up to 4 kV, and the discharge current was about 100 mA. In this case, the equipment with samples fell into the zone of influence of the ion flow (beam-plasma flow) for the selected processing time. The developed ion source with a permanent magnet was also used.

Then the power supply of the magnetron sputtering source was switched on, and the power supply of the ion source was switched off. Thus, within 20–60 seconds, there was a simultaneous deposition of coatings as well as ion treatment of the steel surface. Coating was carried out in the following modes: voltage at the cathode of the magnetron sputtering source: 500–550 V; discharge current up to 3.2 A. When a negative voltage was applied to the equipment with samples, the ion current appeared only at voltages of minus 20–30 V, increased to voltages of the order of -100 V, and then changed slightly. The current density on the samples did not exceed 1 mA/cm^2.

In a vacuum working chamber with standard means of pumping and measuring vacuum, a device for ionic surface treatment and a device for magnetron sputtering of the cathode are located on the flanges. Also, a rotary mechanism is installed in the chamber, which allows you to change the position of the workpiece in the technological cycle. These devices can simultaneously or sequentially process the surface of a rotating fixture with samples. In this case, an adjustable negative voltage can be supplied to the equipment. The ion source includes an annular anode in the discharge chamber, at the exit of which there is an annular gap (diaphragm), into which the plasma flow is extracted. A permanent magnet and a magnetic circuit provide a magnetic field in the gap.

Ion (beam-plasma) surface treatment of steels was carried out in the modes presented in Table 1.

Table 1. Modes of ionic surface treatment

Technological modes	Quantities and units
Working gas pressure (argon)	2 10^{-1} Pa
Discharge voltage	4.5 kV
Ion source discharge current	80-100mA
Current density on the treated surface	up to 1 mA/cm^2
Sample surface treatment time	3 minutes

Ion-plasma deposition of chromium coatings was carried out in the following technological modes (table 2).

Table 2 - Modes of vacuum deposition of chromium

Technological modes	Quantities and units
Distance from the cathode to the surface of the samples	120-130 mm
Working gas pressure (argon)	2 10^{-1} Pa
Sputtering cathode voltage	minus 550 V
Spray discharge current	2.0-2.5 A
Chromium coating deposition time	5-20 minutes

The temperature of the samples during the deposition of coatings did not exceed 150 °C.

The thickness of the formed vacuum coatings was measured with a micro interferometer on individual control samples of polished silicon along a step formed by lithography and etching of the chromium coating in hydrochloric acid. The thickness of the coatings almost linearly depended on the deposition time, other things being equal, and amounted to 0.3–3.0 μm in the deposition time range of 2–20 minutes.

For comparative studies of the adhesive strength of coatings, the method of normal separation of steel rods was used. The test sample with the coating was firmly fixed to the cassette. 7 steel rods were vertically lowered onto the surface of the coating, having an area of about 1 mm2 in the final section. A special adhesive of the VIAM type was applied to the platform, which, after heat treatment, had a tensile strength of about 100 MPa (1000 kg/cm^2).

The cassette was installed in a specially designed tensile machine, which made it possible to tear off the rods in turn with a smoothly increasing force up to 200 n (20 kgf). The pull-off force was recorded according to the readings of an electronic dynamometer. Then, under an MBS-type microscope, the tear-off area of the coating under study was determined, and the adhesive strength was evaluated as the ratio of the tear-off force to the area. At high adhesive strength, separation, as a rule, occurred along the glue.

To determine the durability of the steel-coating structure under certain corrosive conditions, accelerated tests were carried out in artificially created environments. To do this, the test samples from the reverse side and from the ends were covered with a paint sprayer with a layer (50–60 μm) of chemically resistant varnish HV-784 (a solution of chlorinated polyvinyl chloride resin in a mixture of organic solvents with the addition of a plasticizer). After drying at 50–60 °C for 2 hours, they were additionally covered with adhesive tape. The front side with the coating remained free. The samples were fixed on a fluoroplastic tool and placed in a container with acid solutions (for example, a 5% HNO_3 solution) for a fixed time (from 1 to 144 hours).

Corrosion resistance was evaluated on the basis of a study of corrosion lesions in the visual determination (calculation) of the area of destruction (corrosion centers). To do this, a transparent photographic film with a thin grid with bright-field cells (5x5 mm) was superimposed on the surface under study. Using an MBS-10 microscope at a minimum magnification, the area of corrosion damage in the form of dots and spots or continuous corrosion covering the entire metal surface in each cell was estimated.

There are three varieties of the transmission electron microscopy method for determining the size of small particles: direct, semi-direct, and indirect.

To study by the direct method, it is necessary to prepare a thin film transparent or translucent for electrons. Typically, foils are obtained by thinning massive samples. And in the case where it is necessary to study a thin coating with a thickness of several microns, it is necessary to separate it from the substrate.

The indirect method is associated with the study not of the material itself but of thin replicas obtained from the surface of the sample. In methodological terms, it is the simplest, since the production of foils is a complex and rather lengthy process. Making replicas is much easier.

Information on the structure and size of chromium nanoparticle agglomerates was obtained using PEM-100 transmission electron microscopy. To study the surface, two-stage Pt/C replicas were obtained (25-27). First, an impression was made by pressing the sample against a polystyrene-coated glass plate in a special mould at 80 °C for 2 hours. The sample was then removed from the surface of the polystyrene. Platinum and carbon were sputtered

onto the primary print at an angle of 30–40 °C in a VUP-4 vacuum unit, after which the prints were placed on grids with a substrate film and polystyrene was dissolved in xylene.

An object examined in an electron microscope is in some cases placed directly on a grid or diaphragm, but most often the object is placed on a substrate film previously placed on the grid. Support films have the same meaning as glass slides in light microscopy. Just as glass slides should not noticeably absorb light rays, substrate films should not absorb electrons and scatter them as weakly as possible. Therefore, substrate films must be prepared from a substance with a low atomic number and have a small thickness. Typically, the film thickness should not exceed 10-15 nm.

The essence of the method lies in the fact that a thin film is removed from the object, reproducing the relief of its surface, which is studied under an electron microscope. In some cases, the object examined in an electron microscope is placed directly on a grid or diaphragm, but most often the object is placed on a substrate film previously placed on the grid. Substrate films should be prepared from a substance with a low atomic number and a small thickness. Typically, the film thickness should not exceed 10–15 nm.

Films are made of collodion, formvar, polystyrene, and quartz. The most widely used are collodion films. Collodion films are most often prepared directly on the water surface. A drop of a 1% solution of collodion in amyl acetate is placed on the purified surface of distilled water in a vessel 90 mm in diameter and 60 mm deep. The drop spreads over the surface of the water over a large area, almost reaching the walls of the vessel. Several grids are placed on the surface of the film in parallel rows. The distance between adjacent grids should be 5–6 mm. Gently press down on each mesh with some clean object so that the collodion film adheres to the mesh.

RESULTS AND DISCUSSION

The thickness of the coatings and the uniformity of their distribution over the surface of the substrate are of great importance, which ensures the properties of the products. According to the measurements, the maximum thickness of the chromium coating was about 2.4 μm at a deposition time of 20 minutes. Studies have shown that the thickness of the chromium coatings is proportional to the deposition time in the range of 2–20 minutes.

An important characteristic of the coating is the fulfilment of its functional purpose - not to exfoliate from the surface of the product but to have high mechanical stability. This indicator is determined by the adhesion of the coating and the hardness of the material. Studies have shown that the experimentally determined adhesive strength exceeds 70–80 MPa (700 kg/cm^2). In this case, the wear resistance of the tools increases at least twice.

The problem of corrosion observed in coating materials is usually the result of the penetration of aggressive reagents through coating defects and their contact with the substrate. Coating, especially multi-layer, improves the corrosion resistance of the material. Coatings based on Cr with a dense structure and fine crystals make them less permeable to aggressive media. An increase in the corrosion resistance of chromium coatings in a solution of nitric and hydrofluoric acids was determined.

For coatings with a thickness of less than 1 μm, the number of corrosion points (pores in the coating) was 5–10 times greater than for coatings with a thickness of 2.3–2.5 μm. As the experiment shows, with a change in the thickness of the chromium-based nanostructured coating, the corrosion resistance changes several times. This suggests the existence of through channels or their absence with increasing coating thickness.

Another important feature of nanostructured chromium coating is the structural components that have a significant impact on the corrosion resistance of the "coating-substrate" system.

Figure 1 shows a photo of the steel surface at the coated interface after exposure to an acid environment. One can see traces of continuous etching and individual pits of etching up to 200 µm in diameter.
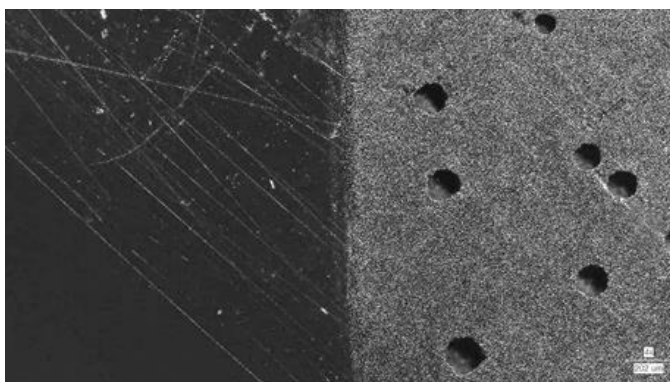
Figure 1. Steel surface after exposure to acids

Studies have shown that with increasing time, the area affected by corrosion increases. For uncoated steels, 100% damage occurs after 3–4 hours. For steel coated with a thickness of 1.2 microns, after 24 hours, the area of corrosion damage does not exceed 5%; after 144 hours, it reaches 15-20%.

Comparative studies were carried out on the wear resistance of tools coated with chromium with a thickness of about 0.8–1.0 µm (taps M4, M6, and M8). Studies of several batches of products showed an increase in their wear resistance by 2–3 times compared to conventional ones. The tools were used for the processing of copper strips at JSC Electro shield. The wear resistance of taps was determined by the number of processed products. Figure 2 shows photographs of original taps and taps with chrome coatings.

Figure 2. Taps M6 without processing and with chromium coating

It should be noted that, in addition to the increase in wear resistance, tools are less sensitive to storage conditions and the effects of aggressive environments in production conditions.

Electron microscopy was used to study the structure of chromium coatings. In Figure 3 shown the images (replicas) of chromium coating. A special computer program was used to quantify the volume content of nanoparticles in the coatings. The volumetric number of nanoparticles depending on the modes of the sputtering process is shown in Figures 4 and 5.

a   b

15000^x,   1sm =660 nm

c   d
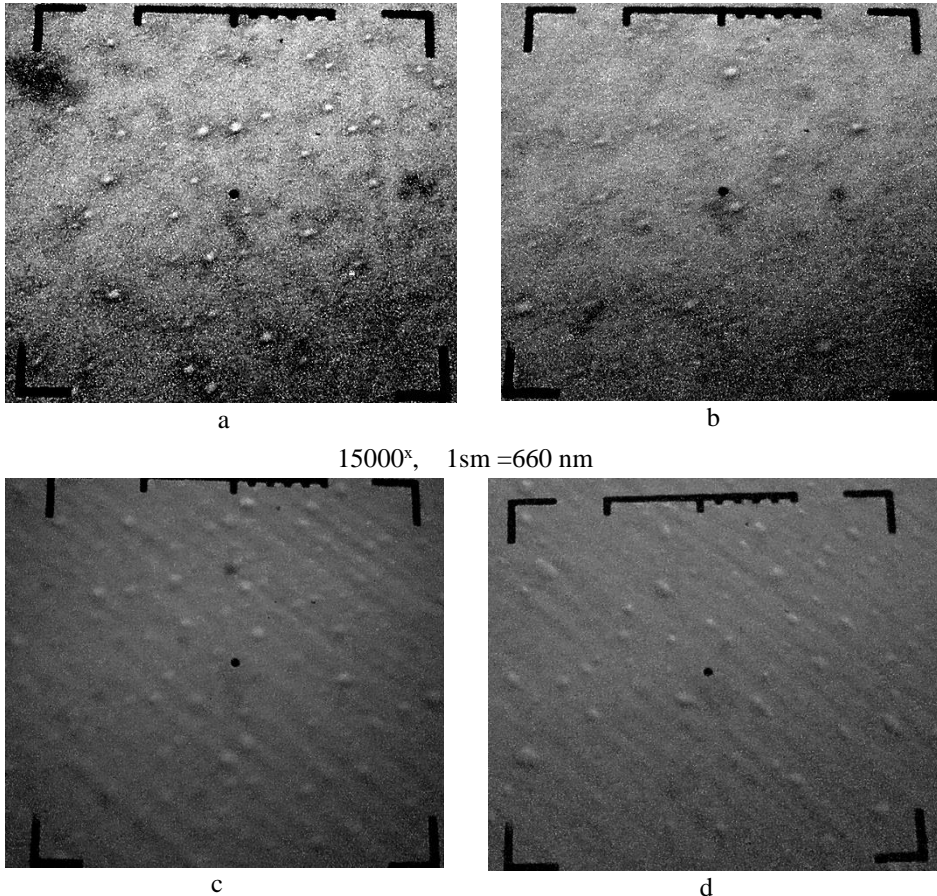
Figure 3. Electron microscopic images of chromium coatings

It has been determined that during the formation of nanostructures from Cr with the maximum amount of chromium-containing phase obtained at pressure ($P=3\cdot10^{-2}$ Pa), spherical nanostructures are formed with chromium nanoparticles ranging in size from 45 nm to 130 nm (Figure 4), and for the sample obtained at pressure ($P=3\cdot10^{-3}$ Pa), larger chromium nanoparticles (66–200 nm) are observed (Figure 5).
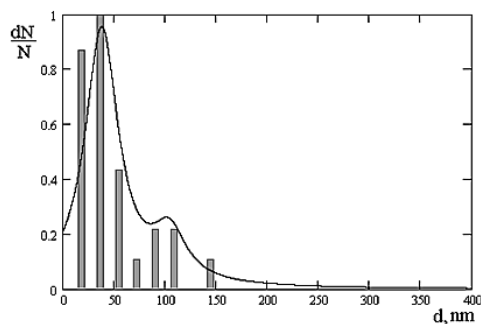
Figure 4. Number of nanoparticles: 97% - 45nm, the largest amount nanoparticles with sizes of 50-100 nm.
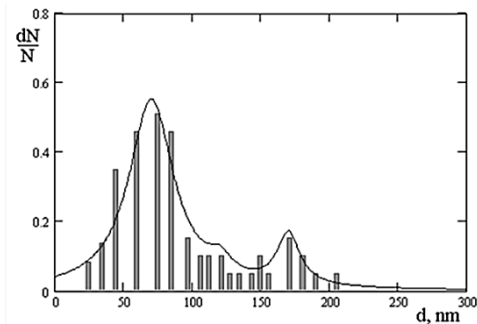
Figure 5. Number of nanoparticles: 55% 70 nm; 15% 120 nm; 30% 170 nm.

CONCLUSIONS

In a combined vacuum setup with an ion source and a magnetron sputtering device, nanostructured chromium coatings with high adhesive strength can be formed. It was found that by varying the technological modes of the deposition process, it is possible to control the size and volumetric number of nanostructures in chromium coatings. For example, at a pressure in a vacuum chamber of $3 \cdot 10^{-2}$ Pa, the dimensions of structures range from 50 to 100 nm, and at a pressure of $3 \cdot 10^{-3}$ Pa, the volume content of nanoparticles is distributed as follows: particles with a size of 70 nm are present in the coatings in an amount of 55%, with a size of 120 nm = 15%, and with a size of 170 nm = 30%. It has been established that with an increase in thickness, the corrosion resistance of the coating-base systems changes several times. With an increase in the coating thickness from 1.0 μm to 2.3–2.5 μm, the corrosion resistance increases by 5–10 times.

REFERENCES

1. Liu, L.; Li, T.; Ruan, Q. Enhanced mechanical properties of CrN coatings by plasma immersion ion implantation and deposition. *Ceramics International*, **2022**, *49*(1–2), 1842- 1848.
2. Garg, R.; Anjum, A. *Sustainable Approach to Protective Nanocoatings*; IGI Global, 2024; p. 443.
3. Kumar, A.; Jaiswal, J.; Tsuchiya, K.; Mulik, R. Modern Coating Processes and Technologies. In *Coating Materials. Computational Aspects, Applications and Challenges*; Verma, A., Seti, K. S., Ogata, S., Eds.; Springer Nature Singapore Pte Ltd. 2023; p. 421.
4. Yang, Z.; Zhang, N.; Li, H.; Chen, B., Yang, B. Comparison to Micro Wear Mechanism of PVD Chromium Coatings and Electroplated Hard Chromium. *Materials*, 2023, 16(7), 2695.
5. Avelar-Batista, J.C.; Spain, E. Effect of coating thickness and deposition methods on the stripping rate of Cr–N coatings. *Surface & Coatings Technology*, **2005**, *200*(5-6), 1842-1848.
6. Vasin, V. A.; Krit, B. L., Somov, B. L.; Sorokin, V. A., Frantskevich, V. P. Epel'fel'd, A. V. Development of the modern vacuum coating technologies. *Surface Engineering and Applied Electrochemistry*, **2016**, *52*(4), 392-397.
7. Heinze, S.; Krulle, T. Influence of the deposition process and substrate on microstructure, phase composition, and residual stress state on as-deposited Cr-Al-C coatings. *Materials & Design*, 2022, 225, 111535.

8. Volkov, O.; Subbotina, V., Subbotin, O.; Vasilchenko, A.; Shyogoleva, M. Methods of structural surface engineering in solving problems of multifactorial improvement of materials performance. *Solid State Phenomena*, **2023**, 350, 3-12.

9. Ferreira, A.A.; Silva, F. J. G.; Pinto, A. M. G.; Sousa, V. F. C. Characterization of Thin Chromium Coatings Produced by PVD Sputtering for Optical Applications. *Coatings*, **2021**, 11(2), 215.

10. Richert M.; Mazurkiewicz, A.; Smolik, J. Chromium carbide coatings obtained by the hybrid PVD methods. *Journal of Achievements of Materials and Manufacturing Engineering*, **2010**, 43(1), 145-152.

11. Gusev, A.I.; Rempel, A.A. Nanokristallicheskie materialy (Nanocrystal materials). FIZMATLIT, 2001, p. 224. (in Russian)

12. Suzdalev, I.P. Nanotekhnologiya: fiziko-khimiya nanoklasterov, nanostruktur i nanomaterialov (Nanotechnology: physical-chemistry of nanoclusters, nanostructures and nanomaterials). Kom-Kniga, 2006, p. 592. (in Russian)

13. Saydahmedov, R., Kadirbekova, K. Study of the composition and properties of vacuum coatings based on titanium carbide, E3S Web Conf. International Scientific Conference "Construction Mechanics, Hydraulics and Water Resources Engineering" (CONMECHYDRO – 2021), **2021**, *264*, 05023. DOI https://doi.org/10.1051/e3sconf/202126405023.

14. Suh, C.M., Hwang, B.W.; Murakami, R.I. Behaviors of residual stress and high-temperature fatigue life in ceramic coatings produced by PVD. *Material Science Engineering*, **2003**, *343*, 1–7.

15. Lamastra, F.R.; Leonardi, F.; Montanari, R.; Casadei, F.; Valente, T.; Gusmano, G. X-ray residual stress analysis on CrN/Cr/CrN multilayer PVD coatings deposited on different steel substrates, *Surface and Coatings Technology*, **2006**, *200*, 6172-6175.

16. Saydakhmedov, R. Kh.; Kadyrbekova, K. K.; Kamardin, A. I. Nanostrukturnye pokrytiya i sovremennye metody obrabotki materialov [Nanostructured coatings and modern methods of material processing]. Tashkent: Fan, 2012, p. 200. (in Russian)

17. Saydakhmedov, R. Kh.; Kadyrbekova, K. K. O svoystvakh zashitnykh nanopokrytiy na osnove khroma (The properties of protective nanocoatings based on chromium). *Metallurgiya mashinostroeniya (Metallurgy of machine building)*, **2011**, *5*, 29-30. (in Russian)

18. Pankov, R. B., Nadtoka, V.N., Maslyanyy, N.V.; Deyneko, L.N. Svoystva Khromovykh vakuumno-dugovykh pokrytiy (Properties of chrome vacuum-arc coatings). *Visnik Dnipropetrovskogo universitetu. Seriya "Fizika, Radioelektronika"*, **2012**, *20*(2), 106-111. (in Ukrainian)

19. Arieta, F.G.; Gawne, D.T. The wettability and durability of chromium plating. *Surface and Coatings Technology*, **1995**, *73*(1), 105-110.

20. Kogan, Ya. D.; Kolachev, B. A.; Levinsky, Yu. V. Konstanty vzaimodeystviya metalallov s gazami: Spravoznoe izdaniye (Constants of interaction of metals with gases). A Reference Book, *Metallurgiya*, **1987**, p. 368. (in Russian)

21. Haig, J. R.; Lynch, J. F.; Rudnick, A.; Houlden, F. S.; Duckworth, W. H. Ogneupory dlya kosmosa. Spravochnik: per. s angl. Orlovksii, Ya. A., Moskva: Metallrugia, 1967. 266 p. (in Russian)

22. Gilewicz, A.; Warcholinski, B.; Myslinski, P.; Szymanski W. Anti-wear multilayer coatings based on chromium nitride for wood machining tools. *Wear*, **2010**, *270*(1), 32–38.

23. Perillo, P.M. Properties of CrN Coating Prepared by Physical Vapour Deposition. *American Journal of Materials Science and Application*, **2015**, *3*(2), 38-43.

24. Lippitz, A.; Hübert, Th. XPS investigations of chromium nitride thin films. *Surface and Coatings Technology*, **2005**, *200* (1-4), 250-253.

25. Tekhnika elektronnoy mikroskopii [Electron microscopy technique]. Pod redaktsiey D. Key, M.: Mir,. 1965. (in Russian)

26. Jayme, G.; Hunger, G. Eine elektronenoptische Studie über das Verhalten der Zellulosemikrofibrillen bei der Trocknung; Ausbildung von Ringnetzstrukturen und Fibrillensträngen [Electron microscopic strdy on cellulose microfibril content during drying; formation or ring net structures & fibril cords]. *Mikroskopie*. **1958**, *13*(1-2), 24-38. (In German)

27. Daure, J.; Carrington, M.; Shipway, P. A comparison of the galling wear behaviour of PVD Cr and electroplated hard Cr thin films. Surface and Coatings Technology, **2018**, *350*, 40-47.

RANKING-BASED SELECTION OF NON-LINEAR QUANTITATIVE STRUCTURE-PROPERTY RELATIONSHIP MODELS FOR PREDICTION OF BIOCONCENTRATION FACTOR OF TRIAZINE DERIVATIVES AS PESTICIDE CANDIDATES

Strahinja KOVAČEVIĆ [ID], *Milica KARADŽIĆ BANJAC** [ID],
Sanja PODUNAVAC-KUZMANOVIĆ [ID], *Lidija JEVRIĆ* [ID]

Faculty of Technology Novi Sad, University of Novi Sad, Bulevar Cara Lazara 1, Novi Sad, Serbia.

The estimation of ecotoxicity and bioaccumulation of compounds as pesticide candidates is an important step in the estimation of their potential practical use. The present study is aimed to form several non-linear regression models based on artificial neural networks (ANN) for prediction of bioconcentration factor of a series of 6-chloro-1,3,5-triazine derivatives and to their ranking and selection based on sum of ranking differences (SRD) approach. The obtained networks represent quantitative structure-property relationship (QSPR) models. The input variables were selected based on hierarchical forward selection procedure and those are the following molecular descriptors: ATSm5 (autocorrelation descriptor mass descriptor weighted by scaled atomic mass), minHBa (minimum E-states for (strong) hydrogen bond acceptors), sumI (sum of the intrinsic state values) and DELS2 (sum of all atoms intrinsic state differences, measure of total charge transfer in the molecule). The total number of the established QSPR models was twelve and all models were validated and confirmed to be of high statistical quality and significant predictive ability. In order to rank and select the most suitable networks, the SRD approach was applied based on row average as the reference ranking.

Keywords: Bioaccumulation, Chemometrics, Ecotoxicity, Triazines, QSPR.

INTRODUCTION

Design and development of novel pesticides is a quite complex task. It starts with an analysis of the characteristics of the existing pesticide compounds in order to gain knowledge of which characteristics should be modified and improved (1, 2). Also, the screening of natural compounds regarding their pesticide activity is desirable as well (3). The main problem with the application of pesticides is their potential toxicity, bioaccumulation and degradation to more toxic products and pest resistance (1, 4). Initial step of pesticide design includes the screening of prepared derivatives of a compound whose pesticide activity has already been confirmed. The prepared derivatives are further subjected to quantitative structure-activity relationship (QSAR) analysis, including the molecular docking approach (5). Based on the QSAR, the pesticide activity of the compounds structurally similar to the synthesized ones can be predicted and those compounds that are predicted to be the most promising ones can be synthesized and subjected to animal testing to estimate their toxicity. Usually, after the first screening around 90% of the synthesized compounds are discarded due to significant toxicity and unsatisfactory efficiency (1). The effects of pesticides on non-target organisms are also one of the main tasks in contemporary pesticide research.

Together with QSAR approach, quantitative structure-property relationship (QSPR) modeling is one of inevitable chemometric approaches in prediction of pesticide candidates'

properties (1, 6, 7). The QSPR modeling is aimed to predict certain physicochemical properties of the compounds, including their melting point, boiling point, vapor pressure, bioaccumulation, lipophilicity, solubility, etc. (8-10). The QSPR approach is based on mathematical modeling of structure-property relationships by using various regression methods, such as univariate linear regression, multiple linear regression, principal component regression, polynomial regression, regression based on artificial neural networks, etc. (11-13).

Artificial neural networks (ANNs) are an artificial intelligence tool that has been successfully used in modern QSPR/QSAR analysis for decades (14). In chemometric analysis, ANNs can be used as classification and regression tool. Regression based on ANNs provides non-linear ANN models that can predict a molecular feature with high accuracy (15), however strict validation procedures are needed to confirm the statistical quality of the models as well as absence of overtraining of the networks and overfitting of the data.

The main focus of the present study is the modeling of bioconcentration factor (BCF) of a series of 6-chloro-1,3,5-triazine derivatives by using ANN regression method and ranking and selection of the established networks. Bioconcentration factor is a factor that numerically represents the absorption of a contaminant by the organism from surrounding environment (16). It is a very important factor in the estimation of chemical bioaccumulation and biomonitoring of hazardous chemicals (16). BCF can be experimentally determined or predicted by the corresponding software that uses a large data base of experimentally determined BCF of known compounds. After the ANN modeling of BCF of the analyzed set of *s*-triazine derivatives, the obtained ANNs were subjected to sum of ranking differences (SRD) analysis in order to rank and select the networks most suitable for prediction of BCF of the studied series of compounds.

MATERIAL AND METHODS

DATA SET: THE ANALYZED COMPOUNDS AND MOLECULAR DESCRIPTORS

There is a significant number of triazine derivatives that are used as herbicides (1). The group of 6-chloro-4,6-alkylated diamino-*s*-triazines is the first group of derivatives to be developed and it is of great practical importance in agriculture and crop protection (1). Propazine is the representative compound from this group of pesticides. Also, some 2,6-dichloro-6-alkylated amino-*s*-triazines are typical contact herbicides, however due to their instability and skin-irritating ability, they have not found widespread practical applications (1). In the present study, the set of the analyzed *s*-triazine derivatives has twenty-one compounds including 6-chloro-N^2,N^4-, 6-dichloro-*N*- and 6-chloro-N^2,N^4-bis(1-methylcycloalkyl)- derivatives. The compounds were synthesized at the Faculty of Technology and Metallurgy, University of Belgrade, based on the procedures described earlier (17, 18). The IUPAC names of the studied compounds are given in Table 1.

Based on two-dimensional molecular structures, the set of physicochemical and topology descriptors was calculated. Firstly, the BCF was calculated by using VegaNIC software (19) based on the incorporated QSAR model for fish BCF implementing the radial basis function neural network (BCF model – CAESAR, version 2.1.13). The molecular descriptors were calculated by PaDEL-Descriptor program (20).

Table 1. The IUPAC names of the analyzed compounds

Compound	IUPAC name
1	6-chloro-N^2,N^4-dipropyl-1,3,5-triazine-2,4-diamine
2	6-chloro-N^2,N^4-bis(propan-2-yl)-1,3,5-triazine-2,4-diamine (propazine)
3	N^2,N^4-bis(butan-2-yl)-6-chloro-1,3,5-triazine-2,4-diamine
4	6-chloro-N^2,N^4-bis(2-methylpropyl)-1,3,5-triazine-2,4-diamine
5	6-chloro-N^2,N^4-dicyclopentyl-1,3,5-triazine-2,4-diamine
6	6-chloro-N^2,N^4-dicyclohexyl-1,3,5-triazine-2,4-diamine
7	6-chloro-N^2,N^4-dicycloheptyl-1,3,5-triazine-2,4-diamine
8	6-chloro-N^2,N^4-dicyclooctyl-1,3,5-triazine-2,4-diamine
9	6-chloro-N^2,N^4-bis(1-phenylethyl)-1,3,5-triazine-2,4-diamine
10	6-chloro-N^2,N^4-bis(1-(*p*-tolyl)ethyl)-1,3,5-triazine-2,4-diamine
11	6-chloro-N^2,N^4-bis(1-(4-chlorophenyl)ethyl)-1,3,5-triazine-2,4-diamine
12	N^2,N^4-bis(1-(4-bromophenyl)ethyl)-6-chloro-1,3,5-triazine-2,4-diamine
13	6-chloro-N^2,N^4-dicyclohexyl-N^2,N^4-dimethyl-1,3,5-triazine-2,4-diamine
14	6-chloro-N^2,N^4-dicyclohexyl-N^2-phenyl-1,3,5-triazine-2,4-diamine
15	6-chloro-N^2,N^4-dicyclohexyl-N^2,N^4-diphenyl-1,3,5-triazine-2,4-diamine
16	6-chloro-N^2,N^4-bis(1-methylcyclopentyl)-1,3,5-triazine-2,4-diamine
17	6-chloro-N^2,N^4-bis(1-methylcyclohexyl)-1,3,5-triazine-2,4-diamine
18	6-chloro-N^2,N^4-bis(1-methylcycloheptyl)-1,3,5-triazine-2,4-diamine
19	4,6-dichloro-*N*-(1-methylcyclopentyl)-1,3,5-triazine-2-amine
20	4,6-dichloro-*N*-(1-methylcyclohexyl)-1,3,5-triazine-2-amine
21	4,6-dichloro-*N*-(1-methylcycloheptyl)-1,3,5-triazine-2-amine

Descriptors that were used as input variables for the ANN were selected from the pool of 55 calculated descriptors by using hierarchical forward selection procedure in NCSS 2023 program (21). The total number of selected input variables was 4, including ATSm5 (autocorrelation descriptor weighted by scaled atomic mass), minHBa (minimum E-states for strong hydrogen bond acceptors), sumI (sum of the intrinsic state values I) and DELS2 (sum of all atoms intrinsic state differences, the measure of total charge transfer in the molecule). Their values, including the logarithm of BCF, are given in Table 2. It also can be seen in Table 2 how the compounds were split into training, test and validation sets. Therefore, test and validation set contain 3 randomly selected compounds each, whilst the training set contains 15 compounds.

Table 2. The values of input (logBCFcaesar) and output variables (ATSm5, minHBa, sumI, DELS2) used in the QSPR modeling

Compound	Set	logBCFcaesar	ATSm5	minHBa	sumI	DELS2
1	Train	0.88	25.07	0.66	30.35	12.12
2	Train	1.08	27.74	0.65	31.01	11.94
3	Train	1.40	29.74	0.65	34.01	13.62
4	Train	1.13	27.07	0.65	34.01	13.51
5	Train	1.85	31.74	0.68	35.01	14.70
6	Test	2.02	34.07	0.67	38.01	15.35

Table 2. Continuation

Compound	Set	logBCFcaesar	ATSm5	minHBa	sumI	DELS2
7	Train	2.07	36.40	0.67	41.01	16.01
8	Validation	1.93	44.40	0.67	44.01	16.51
9	Train	1.97	42.40	0.57	50.35	15.17
10	Train	1.90	44.40	0.57	53.68	16.86
11	Train	2.59	48.30	0.58	52.37	21.65
12	Validation	1.75	55.71	0.59	51.81	17.97
13	Train	2.06	42.07	0.68	41.01	14.31
14	Train	1.96	51.90	0.63	49.18	17.06
15	Train	1.58	69.73	0.59	60.35	18.80
16	Train	2.06	36.40	0.66	38.85	16.59
17	Train	2.08	40.73	0.65	41.85	17.34
18	Test	2.00	45.07	0.65	44.85	18.09
19	Train	1.38	34.84	0.72	28.44	13.55
20	Validation	1.56	37.01	0.72	29.94	13.96
21	Test	1.71	39.17	0.72	31.44	14.36

NON-LINEAR QSPR MODELING: ARTIFICIAL NEURAL NETWORKS

The non-linear QSPR modeling was performed by using ANN method with Broyden–Fletcher–Goldfarb–Shanno (BFGS) learning algorithm. The networks were trained with feedforward multilayer perceptron (MLP) and radial basis function (RBF) in Statistica 12.0 software (22). Prior the networks' training, the number of minimum hidden units was set at 2, whilst the maximum was 10. The total number of the trained networks was 200 among which 12 networks were selected based on their statistical and predictive performance. The global sensitivity analysis (GSA) was used to estimate the influence of each input variable on networks' performance (23). The GSA coefficient presents how the output of the ANNs changes by variations in the parameters that affect the ANN. The GSA higher than 1 means the greater change in the ANNs performance. If the GSA is less than 1, the variable should be omitted from the modeling (14). The validity of the ANNs was estimated based on: correlation coefficient (R), correlation coefficients of training set (R_{train}), correlation coefficients of test set (R_{test}), correlation coefficients of validation set (R_{valid}), root mean square error of training set ($RMSE_{train}$), root mean square error of test set ($RMSE_{test}$), root mean square error of validation set ($RMSE_{valid}$). The predictive ability of the ANNs was checked by the residual's analysis and comparison of observed and predicted logBCFcaesar values.

SUM OF RANKING DIFFERENCES APPROACH

The sum of ranking differences is a non-parametric robust method (24) that was applied to rank and compare the established QSPR models. It is based on calculation of absolute differences of ranks between the established reference ranking and the values predicted by each ANN-QSPR model. In the present study, row average was used as a reference ranking since it is most likely that the ranking will be achieved by the average values (25). The ranking procedure was validated by comparison of ranks by random numbers (CRRN) and

7-fold cross-validation (26). The SRD methodology is explained in details in the literature (24-26).

RESULTS AND DISCUSSION

ANN-QSPR MODELS

The ANN modeling resulted in high quality ANNs whose statistical parameters are presented in Table 3. There are twelve selected ANNs with a number of hidden neurons going from 5 to 10. There are different hidden and output activation functions used in the ANNs modeling, including exponential (Exp), logistic (Log), hyperbolic tangent function (Tanh), sine and identity functions. As it can be seen from the data in Table 3, there are different numbers of training cycles after which a network is obtained (the numbers in brackets given in the names of each network). The inputs and outputs are highly correlated ($R_{train} > 0.94$) by all the networks. Also, there is a good concurrence between the data from the training and validation sets ($R_{test} > 0.90$, $R_{valid} > 0.99$). All the networks are described by quite acceptable root mean square errors for the data from the training, test and validation sets.

The training set was used for the training of the networks so the inputs could precisely predict the output, whilst the test set was used to estimate the generalization error. The purpose of the validation set was to detect the most suitable network configuration and parameters of the training procedure by comparing validation set error and training set error during training (27). The input and output data were not normalized prior to the training of the networks since the training with the normalized data did not result in any network with acceptable statistical characteristics.

VALIDATION OF THE ANN-QSPR MODELS AND APPLICABILITY DOMAIN

One of the aspects of validation of the established QSPR models is comparison of experimental or target data and the data predicted by the models. This approach, besides the validation based on evaluation of calculated statistical parameters, provides more specific view on predictive ability of the QSPR models since it compares the actual amplitude of the differences between target and predicted data, as well as randomness of their distribution. This is particularly important in determination of error predictability, which should be minimized.

The comparison of the target data and the data predicted by twelve ANN-QSPR models is presented in Figure 1a. It can be seen that significant amount of the data is concentrated around $y = x$ line. For some models certain deviations of the points from the $y = x$ line are observable. The regression analysis of the target and predicted data showed that all the equations have the intercept equal to zero, whilst the slope is very close to one. The model MLP 4-5-1 (76) is described by the relationship between target and predicted data which is closest to the ideal case: $y = 0.9999\,x$. The strong relationship between target and predicted data implies that the networks are well trained and have a good predictive ability.

The residual amplitude, presented as the absolute difference between the target and predicted data and their distribution around $y = 0$ axis is presented in Figure 1b. The absolute value of the residuals is less than 0.32 which can be considered satisfactory. The highest positive absolute error in the predicted logBCFcaesar parameter is noticeable in the MLP 4-10-1 (18) model (+0.32), whilst the highest negative error is observable in the MLP 4-6-1 (28) model (-0.28). The average value of positive and negative residuals is ±0.16.

Table 3. Statistical parameters of the trained ANNs

ANN identity	R_{train}	R_{test}	R_{valid}	$RMSE_{train}$	$RMSE_{test}$	$RMSE_{valid}$	Training algorithm	Hidden activation	Output activation
MLP 4-10-1 (18)	0.9618	0.9068	0.9988	0.0093	0.0042	0.0044	BFGS 18	Exp	Log
MLP 4-9-1 (17)	0.9764	0.9675	0.9983	0.0050	0.0025	0.0037	BFGS 17	Tanh	Exp
MLP 4-9-1 (64)	0.9982	0.9961	0.9993	0.0004	0.0036	0.0049	BFGS 64	Tanh	Log
MLP 4-9-1 (65)	0.9962	0.9143	0.9987	0.0009	0.0066	0.0023	BFGS 65	Exp	Tanh
MLP 4-7-1 (33)	0.9951	0.9960	1.0000	0.0012	0.0002	0.0067	BFGS 33	Tanh	Exp
MLP 4-8-1 (96)	0.9950	0.9325	0.9998	0.0010	0.0044	0.0050	BFGS 96	Exp	Sine
MLP 4-6-1 (46)	0.9933	0.9005	0.9998	0.0014	0.0043	0.0034	BFGS 46	Tanh	Identity
MLP 4-8-1 (13)	0.9773	0.9999	0.9989	0.0055	0.0003	0.0016	BFGS 13	Tanh	Exp
MLP 4-6-1 (28)	0.9467	0.9124	1.0000	0.0109	0.0062	0.0063	BFGS 28	Exp	Sine
MLP 4-7-1 (31)	0.9932	0.9827	0.9994	0.0017	0.0015	0.0022	BFGS 31	Tanh	Log
MLP 4-10-1 (65)	0.9945	0.8821	0.9995	0.0013	0.0060	0.0091	BFGS 65	Exp	Log
MLP 4-5-1 (76)	0.9941	0.9643	0.9998	0.0012	0.0016	0.0002	BFGS 76	Tanh	Tanh

The applicability domain of the established ANN-QSPR models is defined based on the ranges of the input and output data: logBCFcaesar (0.88-2.59), ATSm5 (25.07-69.73), minHBa (0.57-0.72) and DELS2 (11.94-21.65). In order to predict logBCFcaesar parameter for a novel compound, the values of its input parameters (molecular descriptors) should fall into the defined ranges so the prediction output can be considered reliable.
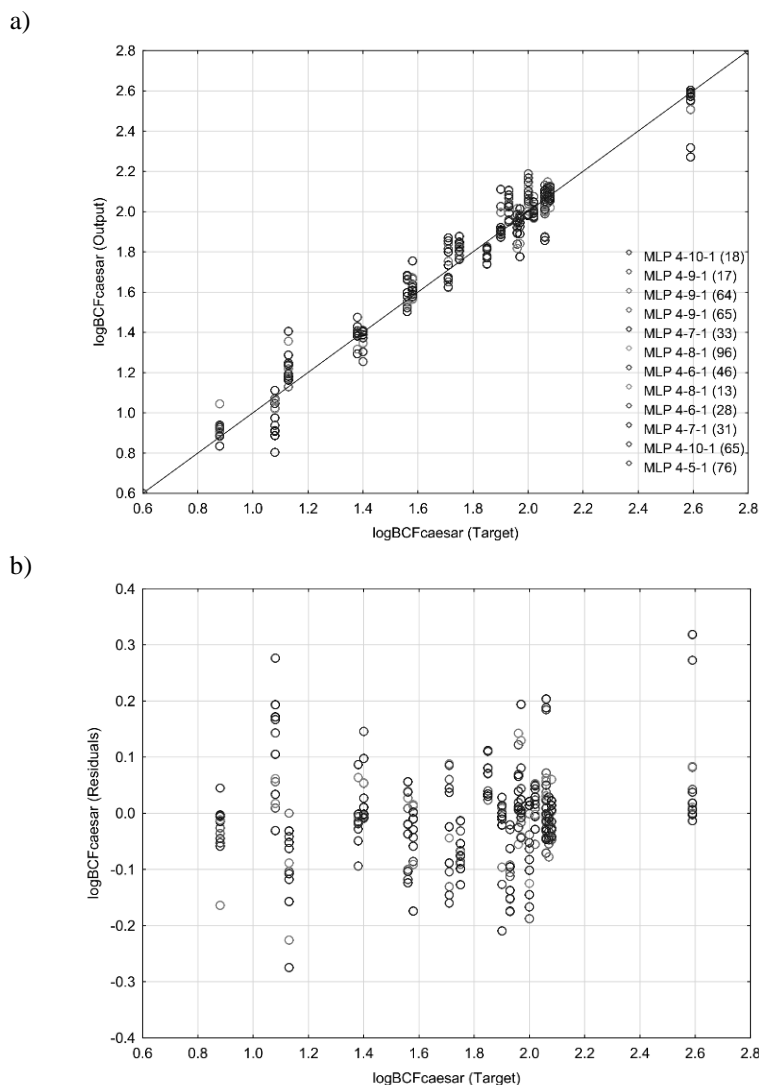
a)

b)

Figure 1. The relationships between target logBCFcaesar data and logBCFcaesar data predicted by the established ANN-QSPR models (a) and distribution of the residuals presented *versus* target logBCFcaesar data for the established ANN-QSPR models (b).

The results of conducted GSA analysis are presented in Table 4. It can be noticed that the GSA coefficients of all input parameters are significantly higher than 1, meaning that all the parameters have significant influence on the network's performance and prediction out-

put. Based on average GSA values, it can be seen that the sumI descriptor has the highest significance, followed by DELS2, ATSm5 and minHBa descriptors. The order of significance of descriptors in individual models deviates from the order of average values. For example, minHBa descriptor has the highest significance in the MLP 4-5-1 (76) model (GSA = 179.92), whilst in the model MLP 4-10-1 (65) its significance is barely above the limit (GSA = 1.16).

Table 4. The GSA coefficients of the input variables of the ANN-QSPR models

ANN identity	sumI	DELS2	ATSm5	minHBa
MLP 4-10-1 (18)	9.01	4.98	4.22	2.46
MLP 4-9-1 (17)	8.90	8.20	10.83	2.94
MLP 4-9-1 (64)	79.14	14.54	29.55	4.84
MLP 4-9-1 (65)	83.32	70.88	35.01	51.80
MLP 4-7-1 (33)	27.88	18.93	28.55	10.72
MLP 4-8-1 (96)	45.10	12.64	46.90	12.50
MLP 4-6-1 (46)	68.75	7.25	29.76	4.34
MLP 4-8-1 (13)	27.98	10.41	12.90	3.20
MLP 4-6-1 (28)	15.08	4.64	4.68	5.57
MLP 4-7-1 (31)	25.70	32.43	28.16	4.13
MLP 4-10-1 (65)	20.58	11.07	16.98	1.16
MLP 4-5-1 (76)	142.08	156.84	85.21	179.92
Average	46.13	29.40	27.73	23.63

SRD ANALYSIS OF THE ANN-QSPR MODELS

The selection of "the best" QSPR model for prediction of certain features is not an easy task. Besides the simple comparison of the statistical parameters, sometimes it is necessary to have another point of view in the model's selection. The SRD procedure provides better distinctive and pattern recognition ability; it can clearly divide the QSPR models into good and bad ones and reveal certain similarities to experimental or target data (28).

The results of the SRD procedure are presented in Figure 2. Here it can be noticed that all the networks are placed quite close to the reference ranking (left side of the graph), but the network closest to the reference is MLP 4-9-1 (65). The network that is furthest from the reference is MLP 4-6-1 (28) and it can be considered "the worst". The networks that have the same ranking as the target values are MLP 4-6-1 (46) and MLP 4-7-1 (31).

The target values are included in the ranking analysis for checking purposes. The analysis indicates that the models MLP 4-10-1 (18), MLP 4-8-1 (13) and MLP 4-6-1 (28) are not better than target values, so their application should be avoided.
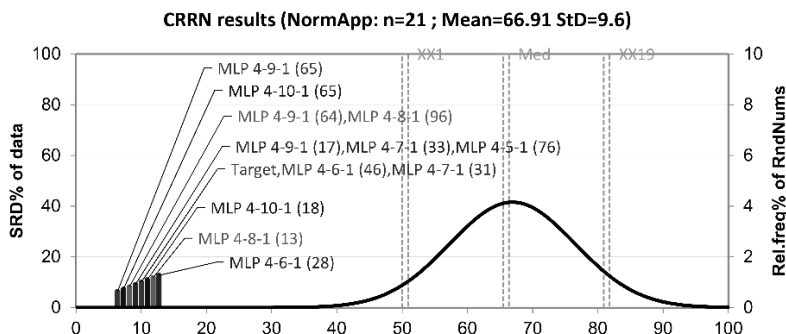
CRRN results (NormApp: n=21 ; Mean=66.91 StD=9.6)

Figure 2. The ranking of 12 ANN-QSPR models by SRD together with target logBCFcaesar values with row average as a reference ranking. The statistical characteristics of Gaussian fit are the following: first icosaile (5%), XX1 = 112; first quartile, Q1 = 132; median, Med = 146; last quartile, Q3 = 160; last icosaile (95%), XX19 = 180.

The data in Table 5 indicate that all the established ANN-QSPR models are depicted by negligible probability of having random character. The model MLP 4-9-1 (65) has the lowest probability, whilst the model MLP 4-6-1 (28) has the highest but minor probability. The SRD procedure was validated by 7-fold cross-validation approach which confirmed the validity of the conducted SRD analysis as well as the order of the analyzed networks.

Table 5. The values of *p%*–intervals and the ranking of the ANNs (first icosaile – XX1, first quartile – Q1, median – Med, last quartile – Q3, last icosaile – XX19)

Ranking results		*p%*	
Name	SRD	x < SRD < y	
MLP 4-9-1 (65)	14	1.09E-08	2.02E-08
MLP 4-10-1 (65)	16	2.02E-08	3.67E-08
MLP 4-9-1 (64)	18	3.67E-08	6.58E-08
MLP 4-8-1 (96)	18	3.67E-08	6.58E-08
MLP 4-9-1 (17)	20	6.58E-08	1.17E-07
MLP 4-7-1 (33)	20	6.58E-08	1.17E-07
MLP 4-5-1 (76)	20	6.58E-08	1.17E-07
Target	22	1.17E-07	2.04E-07
MLP 4-6-1 (46)	22	1.17E-07	2.04E-07
MLP 4-7-1 (31)	22	1.17E-07	2.04E-07
MLP 4-10-1 (18)	24	2.04E-07	3.64E-07
MLP 4-8-1 (13)	26	3.64E-07	6.44E-07
MLP 4-6-1 (28)	28	6.44E-07	1.13E-06
XX1	112	4.35	5.31
Q1	132	22.27	25.19
Med	146	49.80	53.57
Q3	160	74.46	77.55
XX19	180	94.61	95.53

CONCLUSION

The results described in the present study show that the obtained ANN-QSPR models are suitable for prediction of bioconcentration factor (logBCFcaesar) based on *in silico* molecular descriptors of a series of *s*-triazine compounds as pesticide candidates. The models were formed based on autocorrelation descriptor weighted by scaled atomic mass (ATSm5), minimum E-states for strong hydrogen bond acceptors (minHBa), sum of the intrinsic state values I (sumI) and sum of all atoms intrinsic state differences, the measure of total charge transfer in the molecule (DELS2). All models have high predictive power which was confirmed by the applied validation procedures. The SRD procedure was used in order to rank and select the most suitable models. The results of the SRD indicate that most of the models are suitable for applications, whilst the application of the models MLP 4-10-1 (18), MLP 4-8-1 (13) and MLP 4-6-1 (28) is questionable.

Acknowledgment

REFERENCES

1. Matolcsy, G.; Nádasy, M.; Andriska, V. *Pesticide Chemistry*; Akadémia Kiadó: Budapest, 1988; pp 15.
2. Daoui, O.; Mazoir, N.; Bakhouch, M.; Salah, M.; Benharref, A.; Gonzalez-Coloma, A.; Elkhattabi, S.; Yazidi, M. E.; Chtita, S. 3D-QSAR, ADME-Tox, and molecular docking of semisynthetic triterpene derivatives as antibacterial and insecticide agents. *Struct Chem*. **2022**, *33*, 1063-1084.
3. Gramatica, P.; Papa, E.; Francesca, B. Ranking and classification of non-ionic organic pesticides for environmental distribution: a qsar approach. *Int. J. Environ. Anal. Chem.* **2004**, *84*, 65-74.
4. Sule, R. O.; Condon, L.; Gomes, A. V. A Common Feature of Pesticides: Oxidative Stress-The Role of Oxidative Stress in Pesticide-Induced Toxicity. *Oxid Med Cell Longev* **2022**, *2022*: 5563759.
5. Salaković, B.; Kovačević, S.; Karadžić Banjac, M.; Podunavac-Kuzmanović, S.; Jevrić, L.; Pajčin, I.; Grahovac, J. New Perspective on Comparative Chemometric and Molecular Modeling of Antifungal Activity and Herbicidal Potential of Alkyl and Cycloalkyl s-Triazine Derivatives. *Processes* **2023**, *11*, 358.
6. Milošević, N.; Janjić, N.; Milić, N.; Milanović, M.; Popović, J.; Antonović, D. Pharmacokinetics and Toxicity Predictors of New s-Triazines, herbicide Candidates, in Correlation with Chromatographic Retention Constants. *J. Agric. Food Chem*. **2014**, *62*, 8579-8585.
7. Tukur, S.; Shallangwa, G. A.; Ibrahim, A. Theoretical QSAR modelling and molecular docking studies of some 4-hydroxyphenylpyruvate dioxygenase (HPPD) enzyme inhibitors potentially used as herbicides. *Heliyon* **2019**, *19*, e02859.
8. Nisterenko, W.; Kułaga, D.; Woziński, M.; Singh, Y. R.; Judzińska, B.; Jagiello, K.; Greber, K. E.; Sawicki, W.; Ciura, K. Evaluation of Physicochemical Properties of Ipsapirone Derivatives Based on Chromatographic and Chemometric Approaches. *Molecules* **2024**, *29*, 1862.
9. Khairullina, V.; Martynova, Y.; Safarova, I.; Sharipova, G.; Gerchikov, A.; Limantseva, R.; Savchenko, R. QSPR Modeling and Experimental Determination of the Antioxidant Activity of Some

Polycyclic Compounds in the Radical-Chain Oxidation Reaction of Organic Substrates. *Molecules* **2022**, *27*, 6511.

10. Diem-Tran, P. T.; Ho, T. T.; Tuan, N. V.; Bao, L. Q.; Phuong, H. T.; Chau, T. T. G.; Minh, H. T. B.; Nguyen, C. T.; Smanova, Z.; Casanola-Martin, G. M.; Rasulev, B.; Pham-The, H.; Cuong, L. C. V. Stability Constant and Potentiometric Sensitivity of Heavy Metal-Organic Fluorescent Compound Complexes: QSPR Models for Prediction and Design of Novel Coumarin-like Ligands. *Toxics* **2023**, *11*, 595.

11. Joudaki, D.; Shafiei, F. QSPR Models to Predict Thermodynamic Properties of Cycloalkanes Using Molecular Descriptors and GA-MLR Method. *Curr Comput Aided Drug Des* **2020**, *16*, 6-16.

12. Wang, Y.; Chen, X. QSPR model for Caco-2 cell permeability prediction using a combination of HQPSO and dual-RBF neural network. *RSC Adv.* **2020**, *10*, 42938-42952.

13. Liu, F.; Cao, C.; Cheng, B. A Quantitative Structure-Property Relationship (QSPR) Study of aliphatic alcohols by the method of dividing the molecular structure into substructure. *Int J Mol Sci* **2011**, *12*, 2448-2462.

14. Kovačević, S. Z.; Podunavac-Kuzmanović, S. O.; Jevrić, L. R.; Djurendić, E. A.; Ajduković, J. J. Non-linear assessment of anticancer activity of 17-picolyl and 17-picolinylidene androstane derivatives-chemometric guidelines for further syntheses. *Eur J Pharm Sci* **2014**, *62*, 258-266.

15. Gupta, R.; Srivastava, D.; Sahu, M.; Tiwari, S.; Ambasta, R. K.; Kumar, P. Artificial intelligence to deep learning: machine intelligence approach for drug discovery. *Mol Divers* **2021**, *25*, 1315-1360.

16. Wang, W.-X. Chapter 4 - Bioaccumulation and Biomonitoring. In Marine Ecotoxicology; Blasco, J., Chapman, P. M., Campana, O., Hampel, M., Eds.; Academic Press, 2016; pp 99-119.

17. Bončić-Caričić, G.A.; Tadić, Ž.D.; Jeremić, D.S. Electron impact mass spectrometry of some 2,4,6-substituted s-triazines. Effect of the ring size. *Int. J. Mass Spectrom. Ion Phys.* **1983**, *47*, 451-454.

18. Antonović, D.; Bončić-Caričić, G.A. Gas chromatographic retention indices for *N*-substituted amino s-triazines on DB-1 and DB-5 capillary columns. *J. Serb. Chem. Soc.* **1994**, *59* (12), 993-996.

19. VegaNIC application, Laboratory of Environmental Chemistry and Toxicology of Mario Negri Institute of Pharmacological Research, http://vega-qsar.eu.

20. Yap, C.W. PaDEL-descriptor: An open source software to calculate molecular descriptors and fingerprints. *J. Comput. Chem.* **2011**, *32* (7), 1466-1474.

21. NCSS 2023 Statistical Software (2023). NCSS, LLC. Kaysville, Utah, USA, ncss.com/software/ncss.

22. TIBCO Software Inc. (2020). Data Science Workbench, version 14. http://tibco.com.

23. Shojaeefard, M. H.; Akbari, M.; Tahani, M.; Farhani, F. Sensitivity analysis of the artificial neuran network outputs in friction stir lap joining of aluminium to brass. *Adv. Mater. Sci. Eng.* **2013**, *2013*, 1-7.

24. Héberger, K. Sum of ranking differences compares methods or models fairly. *TRAC-Trends Anal. Chem.* **2010**, *29*, 101-109.

25. Héberger, K.; Kollár-Hunek, K. Sum of ranking differences for method discrimination and its validation: comparison of ranks with random numbers. *J. Chemometr.* **2011**, *25*, 151-158.

26. Kollár-Hunek, K.; Héberger, K. Method and model comparison by sum of ranking differences in cases of repeated observations (ties). *Chemom. Intell. Lab. Syst.* **2013**, *127*, 139-146.

27. Priddy, K. L.; Keller, P. E. *Artificial Neural Networks – An Introduction*; SPIE: USA, **2005**; pp 44-47.

28. Vračko, M.; Minovski, N.; Héberger, K. Ranking of QSAR Models to Predict Minimal Inhibitory Concentrations Toward Mycobacterium tuberculosis for a Set of Fluoroquinolones. *Acta Chim Slov.* **2010**, *57*, 586-590.

DESIGN & DEVELOPMENT OF CRACK FILLING MATERIAL FOR COMPOSITE BEAMS USING MWCNTS AND CARBON FIBERS AS REINFORCEMENT AT NANO AND MICRO LEVEL

Sandhya R. JALGAR* [iD], *A.M. HUNASHYAL* [iD], *Megharaj V. CHANNALLI,*
Sai Sohan BAGNAL, Sagar S. RATHOD, Yashraj A. PATIL, Sudeep K. POOJARI

School of Civil Engineering, KLE Technological University, Vidyanagar, Hubballi 580031, Karnataka, India.

Structural engineers, in particular, face the ongoing challenge of ensuring the durability and safety of critical infrastructure components, such as composite beams in bridges and buildings. With aging infrastructure and increasing demands for sustainability and longevity, innovative solutions are essential. The safety and longevity of structures, such as composite beams in buildings and bridges, are paramount concerns. As our infrastructure ages and environmental sustainability becomes increasingly important, innovation in materials and methods is crucial. In this context, we explore a transformative solution the development of advanced crack-filling materials. These materials hold the promise of revolutionizing civil engineering by addressing structural challenges and ex-tending the lifespan of critical infrastructure components. This exploration will delve into the significance of infrastructure, the challenges faced by structural engineers, and the potential impact of advanced crack-filling materials on the field. In this paper we are highlighting the development of a crack filling material for the composite section using Multi Walled Carbon Nanotubes (MWCNTs) and Carbon fibers (CFs). The use of these two nano materials will subsequently be able to reduce the cracks and heal the composite section wherever necessary. The flexural strength of the beams is significantly increased 15% by the addition of MWCNTs and 67% by the addition of MWCNTs and CFs. The cracked MWCNTs beam coated with MWCNTs, epoxy, CFs gained strength and failed at 1100 N. This is because the coating helped to distribute the load across the crack and prevented the crack from propagating further. The cracked carbon fibers beams coated with MWCNTs, Epoxy and CFs gained strength and failed at 1760 N. This is because the MWCNTs + CFs helped to bridge the crack and transfer the load across the crack. Cement mortar with MWCNTs + CFs after coating increased by 400% This suggests that the coating is effective at restoring the strength of the cracked beams.

Keywords: Durability, Composite beams, Crack-filling, Sustainability, Infrastructure.

INTRODUCTION

The drying process is usually responsible for volume changes in concrete. However, early drying shrinkage poses an issue as well, since it happens without any moisture transfer to the atmosphere. Autogenous shrinkage is the word used to describe this volume decrease, which is associated with chemistry and internal structure alterations (1, 2). Since autogenous shrinkage causes cracking, it should be managed (3). Although the phenomena of autogenous shrinkage have long been known about, only recently has its practical significance in concrete technology come to light. When silica fume or other natural admixtures are applied to high-strength concrete with a low water-binder ratio, there is a noticeable drop in the paste specimen's internal relative humidity value during sealed hydration (4). The autogenous shrinkage that causes internal tensile strains as a result of constraint from the aggregates is intimately linked to this autogenous shift in relative humidity. In order to

address the previously described issue, researchers began experimenting with macro- and microfibers as a micro-level reinforcing method in cementitious composites (5, 6). Cementitious composites, however, exhibit defects at the nanoscale where fiber reinforcing is ineffective (7). The outstanding mechanical, electrical, and thermal properties of carbon nanotubes (CNTs), as well as their capacity to stop cracks from growing at the nanoscale, make them particularly interesting (8, 9). The unique strength and stiffness of the nanotubes are attributed to the carbon-carbon-carbon bond. Carbon nanotubes are supposed to be the toughest and hardest nanomaterials found to date in terms of elastic modulus and tensile strength (10, 11). To make an effective cement composite with CNTs, the criteria needed is well-dispersed CNTs within the cement paste matrix and the bond between nanotubes and the cement paste (12). It is very difficult to disperse the CNTs in Cement paste due to the reason that it has a strong surface attraction and high aspect ratio (13). Insufficient dispersion leads to development of defect sites, which encourages the creation of CNT packs and reduces the usefulness of CNTs (14). To improve the dispersion of CNTs in cement-based materials, researchers used chemical (using surfactant) and physical (using ultrasonication) approaches (15). Nevertheless, problems with the connectivity of carbon nanomaterials inside the cement matrix can arise when a surfactant is used as a dispersant (16). Cement paste and CNTs surfaces must adhere firmly to one another in order to facilitate crack bridging, which can offer significant mechanical reinforcement (17). To get around problems with nanofiber dispersion and bonding inside the cement matrix, Sanchez and Ince (18) use extremely fine silica fume particle sizes, ranging from 100 to 500 nm. The practice of ultra-sonication can be eliminated since silica fume particles have the ability to instinctively isolate the grouped MWCNTs within the cement paste matrix. Functionalized carbon nanotubes were employed by Cwirzen (19) to reduce autogenic shrinkage. In his first test, the amount of CNTs (1.4 wt.%) decreased by about 50%. Comparing experimental data from Konsta-Gdotous et al. (20) to the plain cement paste, a decrease in autogenic shrinkage was detected with an increase in the number of long MWCNTs. The flexural strength of specimens reinforced with 0.048 wt.% percent MWCNTs was 30-40% greater than that of specimens reinforced with ordinary paste. The cement paste specimen doped with MWCNTs (0.045 wt.%), which were distributed by sonication before mixing with matrix, produced a 50% greater compressive strength, according to Cwirzen et al. (21). According to Collins et al. (22), the compressive strength of cement paste was completely impacted by the use of polycarboxylate additive in unification with ultrasonication. In cement paste specimens, Shah et al. (20, 23) examined the effects of different doses of CNTs, varying between 0.02 wt.% and 0.1 wt.% by weight of cement, less CNTs lead to enhancement in the mechanical properties of nanocomposites. Researchers have also looked into how CNTs affect paste and concrete sensing capabilities as well as resilience to frost (24). The first piezo-resistive composites of cement with MWCNTs were made by Li et al. (25) using functionalized CNTs, and the resistivity was assessed under uniaxial compression. A piezo-resistive sensor of SWCNT (Single Walled Carbon Nanotubes) with cement was created by Saafi (26) to detect mutilation in concrete constructions. The present study experimentally investigates the development of a crack filling material for the composite section using MWCNTs and CFs. The use of these two nano materials will subsequently be able to reduce the cracks and heal the composite section wherever necessary. The mechanical properties for Plain Cement to Coated beam under single point load is evaluated. Scanning electron microscopy (SEM) analysis is also done to study the microstructure of the composite beams.

MATERIALS AND METHODOLOGY

MATERIALS

Cement: Ordinary Portland Cement (OPC) confirming to IS 8112-1989 has been used, it is used for all types of building.

Carbon fibers: They are five to ten micro meters in diameter and are made up of carbon atoms as shown in Figure 1. Chopped CFs shows high aspect ratio and high ductility. It has electrical conductivity and good mechanical properties. The CFs will be long in length, they are chopped and made into fine particles as shown in the figure, so that it would be helpful to mix in the cement mixture.
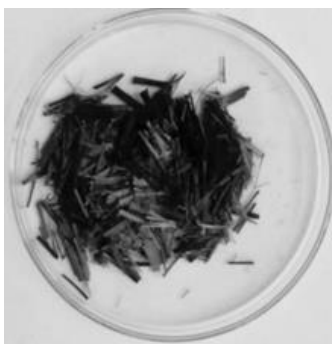

Figure 1. Carbon fibers

Table 1. Stipulations of CFs

Sl No.	Distinctive Property	Implications
01	Sourced from	Arrow Tex, India
02	Diameter	8μm
03	Length	10mm
04	Weight	200g/m^2
05	Density	1.8 g/cc
06	Tensile strength	3500 N/mm^2
07	Tensile Modulus	285 x 10^3 N/mm^2
08	Poisson ratio	0.25

MWCNTs: Nano filler which is used in this project is MWCNTs (Figure 2), which is multifunctional element and has electrical properties and mechanical properties. This is a nano filler in which good properties are present and also helps to get the good results while testing (Table 2).
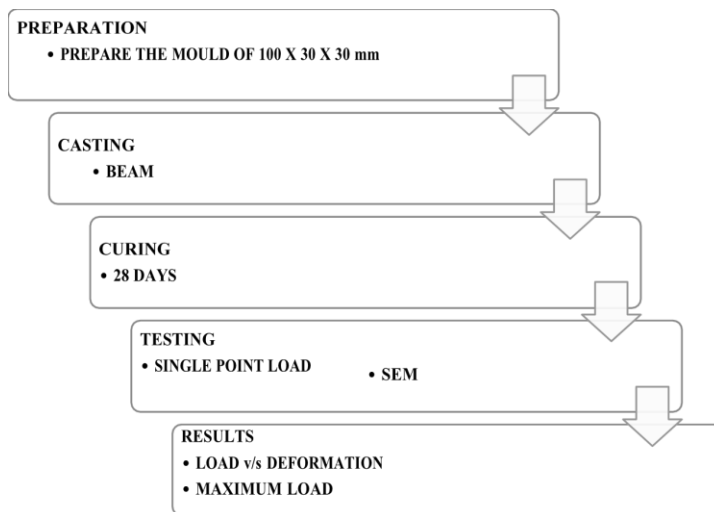
Figure 2. MWCNTs

Table 2. Stipulations of MWCNTs

Sl no	Material	Multi walled Carbon Nanotubes (MWCNTs)
01	Manufacturing Process	Chemical Vapor Deposition (CVD)
02	Diameter	10-30 nm
03	Length	1-2 microns
04	Purity	>95% (MWCNTs)
05	Amorphous carbon	< 3%
06	Residue (Calcination in air)	<2%
07	Average interlayer distance	0.34 nm
08	Special surface area	> 350 m^2/g
09	Bulk density	0.05-0.17 g/cm^3
10	Real density	1-2 g/cm^3
11	Charging	2180 (capacity: mA h/g)
12	Discharging	534 (capacity: mA h/g)
13	Volume Resistivity	0.1-0.15 ohm·cm (measured at pressure in powder)

Epoxy resin primarily acts as an excellent adhesive or bonding agent. Epoxy resin can enhance the performance and durability of beams, it is typically used in combination with traditional structural materials like concrete, steel, or wood. Epoxy resin typically exhibit minimum shrinkage during curing which helps to maintain tight and secure bond.

This research involves casting of M20 grade column with dimensions of 150 x 150 x 300 mm. The column will be wrapped with twill weave carbon fiber sheets of 200bGSM Bonded using Epoxy resin and Hardener. Additionally, a damper of 150 x150 x 10 mm is composed of M25 grade concrete added with 3% of 1mm chopped carbon fiber will be embedded within the column at the C.G. of failure point to enhance its structural integrity and performance.

Specimens to be cured for 28 days and Conducting Compression test using a Universal Testing Machine to determine the ultimate load-carrying capacity of the column and individual dampers. Impact test to know the energy absorption in concrete.

PREPARATION
• PREPARE THE MOULD OF 100 X 30 X 30 mm

CASTING
• BEAM

CURING
• 28 DAYS

TESTING
• SINGLE POINT LOAD   • SEM

RESULTS
• LOAD v/s DEFORMATION
• MAXIMUM LOAD

Scheme 1. Experimental procedure

MIX DESIGN

Table 3 represents the Mix design for casting of the cement composite beams. It indicates the volume of cement, sand and nanomaterials used for the experimental research.

Table 3. Mix Design of Beams

Item	Specification	Units
No. Of Beams	33	
Size of Beam	100 x 30 x 30	mm
Volume of 1 Beam	90000	mm^3
Volume of 33 Beam	2970000	mm^3
	297 x 10^{-5}	m^3
Dry Volume	1.54	m^3
Grade of Beam Cement Mortar	M25	
Mix Proportion	1: 1	
Water/Cement Ratio	0.5	
Volume of Cement for 1 m^3	1109	kgs
Volume of Sand for 1 m^3	1232	kgs
Volume of Water	4.30	liters
Cement for 1 beam	100	gm
Sand for 1 beam	111	gm
MWCNTs (0.3% weight of cement)	0.3	gm
Carbon Fiber (1% volume of beam)	1.8	gm
Cement for 33 beams	3300	gm
Sand for 33 beams	3663	gm
MWCNTs (mixing + coating)	10	gm
Carbon Fiber (mixing + coating)	20	gm
Epoxy gel (For Coating)	200	gm

Figure 3 indicates the steps followed in casting of beams which include weighing and mixing of materials, ultrasonication for proper mixing of nano materials and the casting the samples in the mold and curing them (Figure 4).
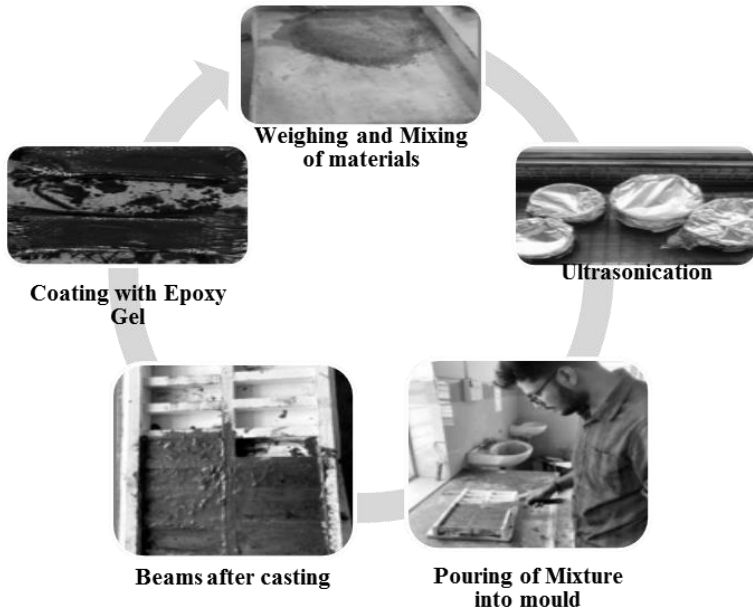

Figure 3. Method of casting beams

Figure 4. Casted beams after curing

RESULTS AND DISCUSSIONS

FLEXURAL STRENGTH TEST

The flexural strength of the beams is significantly increased by the addition of MWCNTs and CFs. The cracked beams coated with MWCNTs, epoxy, and CFs also have a higher flexural strength than the cracked plain beams. This suggests that the coating is effective at restoring the strength of the cracked beams.

CONTROLLED BEAM SAMPLE

The graph in Figure 5 illustrates the interplay between applied force and displacement for an unaltered cement beam. Serving as a crucial benchmark, the ultimate flexural strength for this plain cement beam stands at 1200N. This value establishes a baseline for subsequent comparisons of flexural strength among mixed and coated beams.
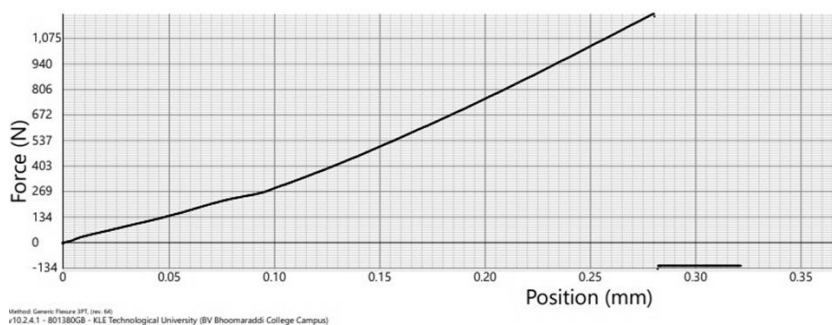

Figure 5. Force/Displacement Graph of Controlled (without nanomaterials) beam samples

The graph in Figure 6 under consideration illustrates the relationship between applied force and displacement for a cement beam treated with a graphene oxide coating. Of particular significance is the observation that the flexural strength of the sample, once it reaches the point of cracking, registers at 350N. This indicates a noticeable decline in flexural strength from an initial value of 1200N to the observed 350N after the sample undergoes cracking.
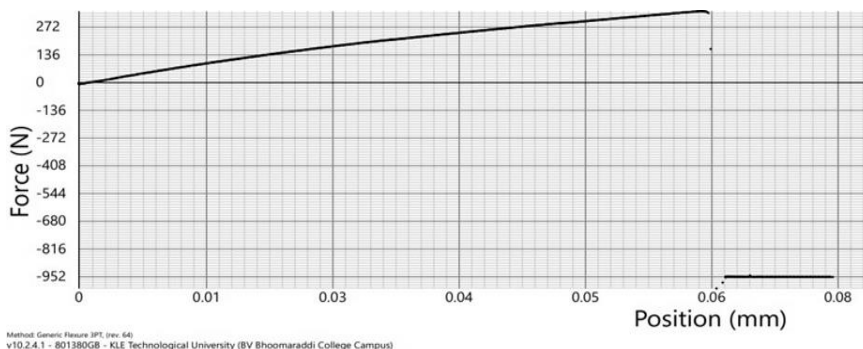

Figure 6. Force/Displacement Graph of Controlled Beam after Cracking

CEMENT MORTAR WITH MWCNTs MIXING

The graph in Figure 7 illustrates the correlation between applied force and displacement for a cement beam mixed with MWCNTs. Notably, the ultimate flexural strength, determined as 1350N, indicates a significant and substantial increase in flexural strength attributed to the incorporation of MWCNTs from 1200N of controlled beam.
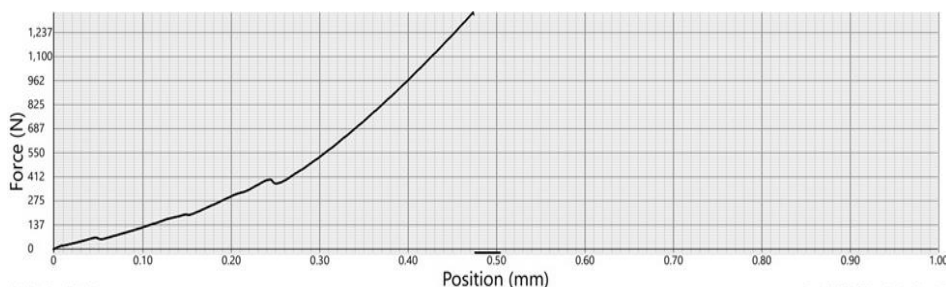

Figure 7. Force/Displacement Graph of Cement Mortar with MWCNTs mixing

MWCNTs COATING WITH EPOXY RESIN

The graph in Figure 8 illustrates the correlation between applied force and displacement for a MWCNTs coating with Epoxy Resin applied to beams. Notably, the ultimate flexural strength, measured at an impressive 1120N, is attributed to the self-healing ability of MWCNTs. This remarkable recovery in strength occurs after the beams have experienced cracking, showcasing the efficacy of MWCNTs in restoring structural integrity. In contrast, the flexural strength of plain beams post- cracking was only 350N. This stark difference underscores the substantial enhancement brought about by the MWCNTs coating
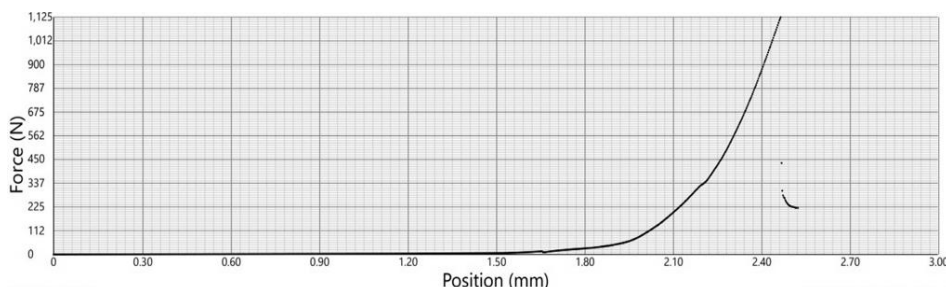

Figure 8. Force/Displacement Graph of MWCNTs coating with Epoxy resin

CEMENT MORTAR WITH MIXING MWCNTs AND CFs

The graph in Figure 9 illustrates the correlation between applied force and displacement for Cement Mortar enhanced with MWCNTs and CFs. Notably, the ultimate flexural strength achieved is 2000, surpassing the strength of plain beams, which stands at 1200. This substantial increase in flexural strength underscores the effectiveness of incorporating MWCNTs and CFs in the Cement Mortar mixture.
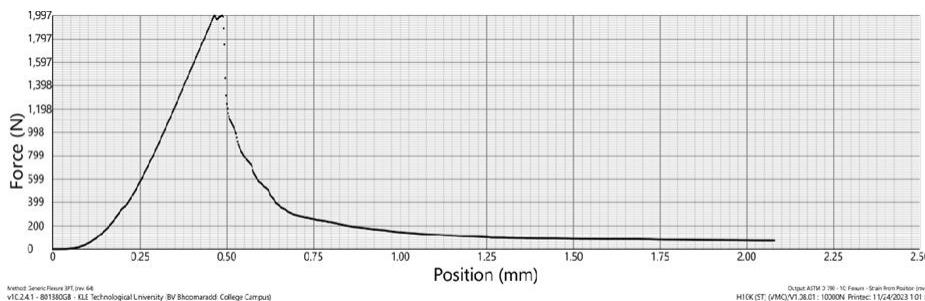
Figure 9. Force/Displacement Graph of Cement Mortar with mixing MWCNTs and CFs fiber

MWCNTs + CFs COATING WITH EPOXY RESIN

The graph in Figure 10 illustrates the correlation between applied force and displacement for a coating comprising MWCNTs and CFs, combined with Epoxy resin. Notably, the ultimate flexural strength, determined at 1750N, is achieved after the beams undergo cracking and subsequent healing. It's noteworthy that the ultimate flexural strength of a plain beam after cracking is 350N.
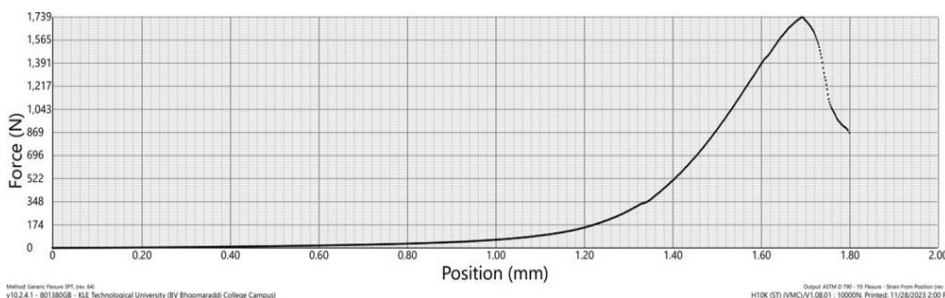

Figure 10. Force/Displacement Graph of Cement Mortar with MWCNTs + CFs coating with Epoxy resin

CFs and MWCNTs are renowned for having similar high stiffness and strength properties. They strengthen the structure when integrated into a material matrix, increasing its resistance to the spread of cracks. Because it more evenly distributes stresses throughout the material, this reinforcement aids in the prevention of cracks from occurring in the first place. Because of their special structure, MWCNTs potentially have self-healing capabilities. When fractures arise, the migration of carbon atoms inside the nanotubes can help the breaches close at the nanoscale. Over time, this self-healing mechanism aids in preserving the material's structural integrity.

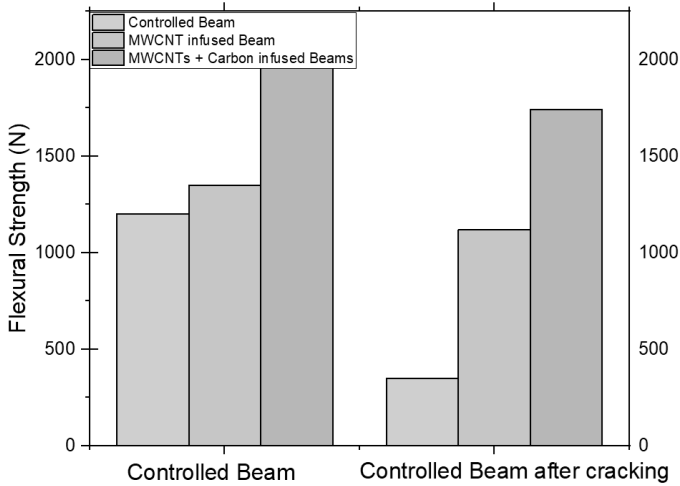The results of Flexural strength test are as shown in Figure 11.

Figure 11. Flexural strength

COMPRESSION STRENGTH TEST

The cubes were tested for Compressive strength in Concrete Compression Machine (specimen sizes were 100mm x 30 mm × 30 mm). At the age of 28 days, compressive tests were performed on an automatic pressure machine with a loading rate of 0.5 kN/s. The results of Compression test are as shown in Figure 12.

The mechanical characteristics of materials can be greatly improved by the addition of MWCNTs and carbon fibres. The material's resistance to fracture initiation and propagation is facilitated by enhancements in its tensile strength, flexural strength, and toughness, all of which work together.
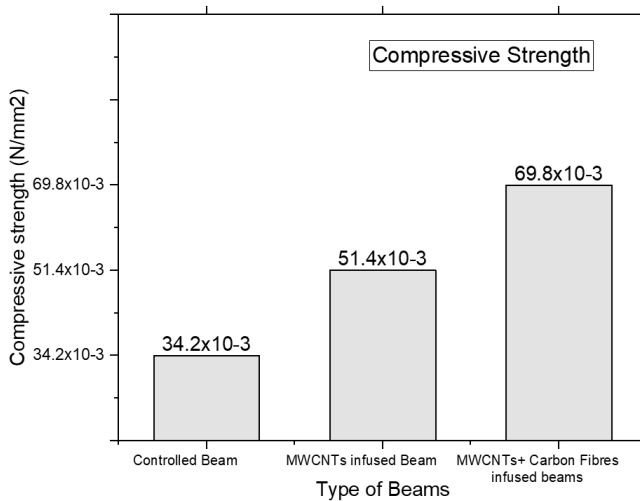

Figure 12. Compressive strength

SEM ANALYSIS

SEM analysis is a non-destructive analytical technique. When the sample material is subjected to electrons, x-rays that are distinctive of the elements present are released. The various inorganic elements contained in the sample are identified by the spectrum profile, which is produced when the energy emissions are converted into spectral peaks of differing intensities (i.e. lead, iron, copper, zinc etc.).

In the SEM analysis of a controlled cement beam as shown in Figure 13, the image reveals the presence of cracks. These cracks are notable features that can provide insights into the structural characteristics of the cement beam. SEM allows for a detailed examination of the surface, and the observed cracks may offer valuable information about the material's behavior under different conditions.
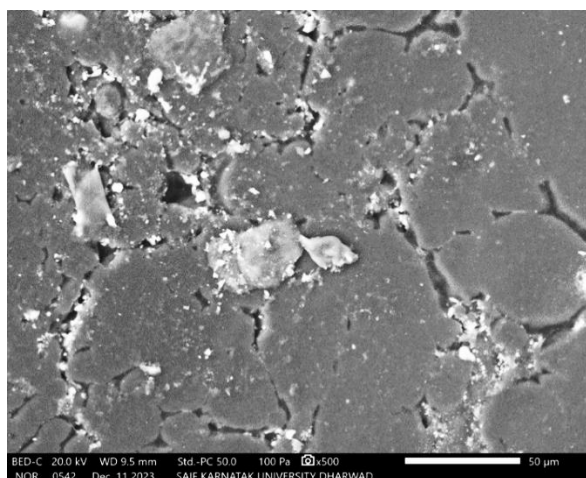

Figure 13. SEM analysis of Controlled beam

In the SEM analysis of a cement beam enhanced with MWCNTs and CFs, the image in Figure 14 reveals a noteworthy observation: there are fewer cracks compared to the plain controlled cement beam. This finding indicates an improvement in the structural integrity of the cement beam when reinforced with MWCNTs and CFs. The incorporation of these materials seems to contribute to minimizing the formation of cracks, suggesting enhanced strength and durability. This is a promising result as it implies that the modified cement beam may exhibit better performance and resilience under various conditions.

Within the material matrix, MWCNTs and CFs both serve as reinforcement. These reinforcing features serve to redistribute loads around the crack tip during crack propagation, which stops the crack from spreading farther. These materials can lessen the stress concentration at the crack tip, which slows or stops the crack from propagating, by dispersing mechanical loads efficiently.

The interfacial connection between the reinforcement and the matrix can be strengthened by adding MWCNTs and CFs to a matrix material. By reducing the amount of crack propagation and encouraging crack closure, stronger interfacial bonding contributes to the material's integrity.
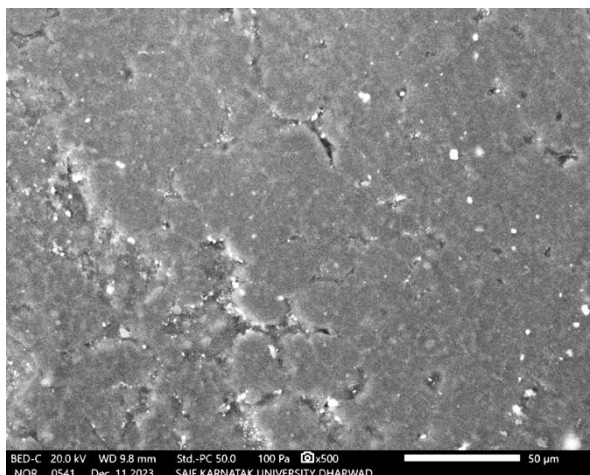
Figure 14. SEM analysis of MWCNTs + CFs

CONCLUSIONS

The flexural strength of the beams is significantly increased 15% by the addition of MWCNTs and 67% by the addition of MWCNTs and CFs.

- The cracked plain beam did not gain its original strength and failed early during the flexural test. This is because the crack in the beam weakened the beam and made it more susceptible to failure.
- The cracked MWCNTs beam coated with MWCNTs, epoxy, CFs gained strength and failed at 1100 N. This is because the coating helped to distribute the load across the crack and prevented the crack from propagating further.
- The cracked CFs beams coated with MWCNTs, Epoxy and CFs gained strength and failed at 1760 N. This is because the MWCNTs + CFs helped to bridge the crack and transfer the load across the crack.
- The cracked beams coated with MWCNTs, Epoxy and CFs also have a higher flexural strength than the cracked plain beams.
  - Cement mortar with MWCNTs after coating = Increased by 220%
  - Cement mortar with MWCNTs + CFs after coating = Increased by 400% This suggests that the coating is effective at restoring the strength of the cracked beams.

Strong covalent connections forming a tubular arrangement between carbon atoms give MWCNTs their distinctive structure. When a crack appears, the movement of carbon atoms inside the nanotubes can help the cracks close at the nanoscale. Through the reorganization of carbon bonds, this self-healing mechanism enables the material to regain its integrity.

In Conclusion, the addition and coating of MWCNTs and CFs to the beams is an effective way of restoring the strength of the beams at Nano & Micro Levels.

REFERENCES

1. Holt E. Contribution of mixture design to chemical and autogenous shrinkage of concrete at early ages. *Cem. Concr. Res.* **2005**, *35*, 464-472.

2. Justnes, H.; Sellevold, E.; Reyniers, B.; Loo, D.; Gemert, A.; Verboven, F. The influence of cement characteristics on chemical shrinkage. In: *Autogenous shrinkage of concret;* Ei-ichi Tazawa, Ed.; London: E& FN Spon, UK, 1998; p. 71–80.

3. Lura, P.; Jensen, O.M.; van Breugel, K. Autogenous shrinkage in high-performance cement paste: an evaluation of basic mechanisms. *Cem. Concr. Res.* **2003**, *33*, 223-232.

4. Jensen, M.; Hansen, P.F. Autogenous deformation and change of the relative humidity in silica fume-modified cement paste. *ACI. Mater. J.* **1996**, *93*, 539-543.

5. Altoubat, S.; Yazdanbakhsh, A.; Rieder, K-A. Shear behavior of macro-synthetic fiber-reinforced concrete beams without stirrups. *ACI. Mater. J.* **2009**, *106*, 381-389.

6. Fischer, G.; Li, V.C. Effect of fiber reinforcement on the response of structural members. *Eng. Fract. Mech.* **2007**, *74*, 258-272.

7. Konsta-Gdoutos, M. S.; Metaxa, Z. S.; Shah, S. P. Multi-scale mechanical and fracture characteristics and early-age strain capacity of high-performance carbon nanotube/cement nanocomposites. *Cem. Concr. Res.* **2010**, *32,* 110-115.

8. Coleman, J. N.; Khan, U.; Blau, W. J.; Gun'ko, Y.K. Small but strong: a review of the mechanical properties of carbon nanotube–polymer composites. *Carbon*, **2006**, *44*(9)*,* 1624-1652.

9. Marrs, B.; Andrews, R.; Pienkowski, D. Multiwall carbon nanotubes enhance the fatigue performance of physiologically maintained methyl methacrylate–styrene copolymer. *Carbon*, **2007**, *45*(2), 98-104.

10. Yue-Feng, Z.; Chan, Z.; Jing-Dong, W.; Lei, S.; Ji, L. Influence of electric field on dispersion of carbon nanotubes in liquids. *J. Disper. Sci. Technol.* **2006**, *27,* 371-375.

11. Yu, M-F.; Lourie, O.; Dyer, M.J.; Moloni, K.; Kelly, T.F.; Ruoff, R.S. Strength and breaking mechanism of multiwalled carbon nanotubes under tensile load. *Science*, **2000**, *287*, 637-640.

12. Yazdanbakhsh, A.; Grasley, Z.; Tyson, B.; Abu Al-Rub, R. Distribution of carbon nanofibers and nanotubes in cementitious composites. *J. Trans. Res. Board.* **2010**, *2142*(1), 89-95.

13. Xie, X-L.; Mai, Y-W.; Zhou, X-P. Dispersion and alignment of carbon nanotubes in polymer matrix: a review. *Mater. Sci. Eng. R. Rep.* **2005**, *49*, 89-112.

14. Odegard, G.; Gates, T.; Wise, K.; Park, C.; Siochi, E. Constitutive modelling of nanotube-reinforced polymer composites. *Compos. Sci. Technol.* **2003**, *63*, 1671-1687.

15. Luo, J.; Duan, Z.; Li, H. The influence of surfactants on the processing of multi-walled carbon nanotubes in reinforced cement matrix composites. *Phys. Status Solidi.* **2009**, *206*, 2783-2790.

16. Yu. X.; Kwon, E. A carbon nanotube/cement composite with piezoresistive properties. *Smart Mater. Struct.* **2009**, *18*, 055010 (5 pp).

17. Stynoski, P.; Mondal, P.; Marsh, C. Effects of silica additives on fracture properties of carbon nanotube and carbon fiber reinforced Portland cement mortar. *Cement Concrete Comp*. **2015**, *55,* 232-240.

18. Sanchez, F.; Ince, C. Microstructure and macroscopic properties of hybrid carbon nanofiber/silica fume cement composites. *Compos. Sci. Technol.* **2009**, *69*,1310–1318.

19. Cwirzen, A. Controlling physical properties of cementitious matrixes by nanomaterials. *Adv. Mater. Res.* **2010**, *123-125*, 639-642.

20. Konsta-Gdoutos, M. S.; Metaxa, Z. S.; Shah, S. P. Highly dispersed carbon nanotube reinforced cement-based materials. *Cem. Concr. Res.* **2010**, *40*, 1052–1059.

21. Cwirzen, A.; Habermehl-Cwirzen, K.; Penttala, V. Surface decoration of carbon nanotubes and mechanical properties of cement/carbon nanotube composites. *Adv. Cem. Res.* **2008**, *20*, 65-73.

22. Collins, F.; Lambert, J.; Duan, W. H. The influences of admixtures on the dispersion, workability, and strength of carbon nanotube–OPC paste mixtures. *Cement Concrete Comp.* **2012**, *34*, 201-207.

23. Shah, S.P.; Konsta-Gdoutos, M.; Metaxa, Z.; Mondal, P. Nanoscale modification of cementitious materials. In *Nanotechnology in construction 3;* Bittnar, Z., Bartos, P.J.M., Němeček, J., Šmilauer, V., Zeman, J. Eds.; Springer, Berlin, Heidelberg, 2009; p. 125-130.

24. Cwirzen, A.; Habermehl-Cwirzen, K. The effect of carbon nano-and microfibers on strength and residual cumulative strain of mortars subjected to freeze–thaw cycles. *J. Adv. Concr. Technol.* **2013**, *11*, 80-88.

25. Li, G.Y.; Wang, P. M.; Zhao, X. Pressure-sensitive properties and microstructure of carbon nanotube reinforced cement composites. *Cement Concrete Comp.* **2007**, *29*, 377-382.

26. Saafi, M. Wireless and embedded carbon nanotube networks for damage detection in concrete structures. *Nanotechnology*, **2009**, *20*(39), 395502 (7 pp).

27. Han, B.; Yu, X.; Kwon, E. A self-sensing carbon nanotube/cement composite for traffic monitoring. *Nanotechnology*, **2009**, *20*(44), 445501 (5 pp).

28. Kim, H.; Nam, I. W.; Lee, H-K. Enhanced effect of carbon nanotube on mechanical and electrical properties of cement composites by incorporation of silica fume. *Compos. Struct.* **2014**, *107*, 60-69.

IDENTIFICATION OF C8-C22 FATTY ACID ESTERS IN DOMESTIC FRUIT BRANDY SAMPLES

Tanja TRIFKOVIĆ[1] , *Marina KUBURIĆ[2], Biljana DAVIDOVIĆ-PLAVŠIĆ[1]* ,
Radoslav DEKIĆ[1] , *Biljana KUKAVICA[1]**

[1] University of Banja Luka, Faculty of Natural Sciences and Mathematics, Mladena Stojanovića 2,
78000 Banja Luka, Bosnia and Herzegovina
[2] Medical School Banja Luka, Cetinjska 1, 78000 Banja Luka, Bosnia and Herzegovina

The production and consumption of fruit brandy (rakija) in Bosnia and Herzegovina has a long tradition. The imperative of every brandy producer is to have a quality product that is appealing to the consumer. The aim of our work was to examine the content of C8-C22 fatty acid esters in three samples of domestic fruit brandy (labeled Sample I, II and III). Samples I and II were made from pear, while sample III was from plum. After liquid-liquid extraction, using the solvent system hexane and diethyl ether (1:1), analysis of fatty acid esters was performed using the GC/MS method (gas chromatography with a mass detector). In Sample I and Sample II, eleven C8-C22 fatty acids esters were detected, while in Sample III, eight esters were detected. In Sample I and Sample II, the following fatty acid esters have been identified: Ethyl benzoate, Ethyl octanoate, Ethyl nonanoate, Ethyl decanoate, Ethyl undecanoate, Ethyl dodecanoate, Ethyl tridecanoate, Ethyl tetradecanoate, Ethyl pentadecanoate, Ethyl hexadecanoate, Ethyl eicosanoate. In Sample III the following fatty acid esters have been identified: Ethyl hexanoate, Ethyl benzoate, Ethyl octanoate, Ethyl nonanoate, Ethyl decanoate, Ethyl undecanoate, Ethyl dodecanoate, Ethyl tridecanoate. In all three Samples Ethyl decanoate and Ethyl undecanoate had the highest percentage, which reached up to 11% of the total percentage of detected compounds. As our results show, the developed methodology is effective for the identification of C8-C22 fatty acid esters in fruit brandies, and its further development is needed to be a tool for the quality determination of fruit brandies.

Keywords: volatile compounds, GC/MS, liquid-liquid extraction, quality, taste.

INTRODUCTION

Fruit brandy (native name rakija) production is highly prevalent in the Western Balkans region due to the long tradition and culture of consuming this alcoholic beverage. This is a traditional alcoholic beverage, produced by distilling fermented fruits. To produce fruit brandy in Bosnia and Herzegovina, plums are the most used, followed by pears, while apples are used the least. The largest share of plums from the region of Bosnia and Herzegovina is used for the production of the fruit brandy (1). The long tradition of homemade production of this spirit is more and more transferred to the modern distilleries, either large-scale producers or small, family-owned distilleries.

What makes fruit brandy unique is its aroma and flavor. The sensory properties of alcoholic beverages (such as taste, aroma, color, texture) are influenced by a large number of compounds such as alcohols, volatile acids, volatile esters, terpenes, volatile aldehydes and acetals, with the most important being alcohols (isoamylol, 1-hexanol, 2-phenylethyl alcohol etc.), terpenes and esters. Although present in small quantities, their impact is significant (2,3). The properties are also influenced by the preparation and fermentation of fruits raw material, distillation technology and maturation (4). Also, the quality and local charac-

ter of fruit brandy can be influenced by the soil, climate and varieties of the fruit (5,6). The aroma and flavor of fruit brandy originate from compounds present in the fruit used for its production, as well as from compounds formed during the production process. There are four types of compounds that influence the aroma of brandy, and they are categorized based on the phase in which they are formed. Primary compounds are those present in the fruit used for brandy production. The secondary compounds are formed during the fermentation process, while tertiary compounds arise during the distillation process. Lastly, quaternary compounds develop during the maturation of brandy, often in wooden barrels, imparting a yellow color to the spirit. All these compounds together contribute to the final aroma and flavor of fruit brandy (7,8). The aromatic compounds defining the flavor and aroma of alcoholic beverages depend on the type of drink and their origin. Group of compounds that contribute significantly to the aroma and taste of brandy are esters. Esters are formed in the esterification process of alcohols with acids, during fermentation and aging. This can be influenced by many factors, such as the temperature, oxygen availability and yeast strains used for the fermentation (7). Determining the content of volatile compounds can be used as the method for qualifying alcoholic beverages according to the type, country and provenience region (9). Gas chromatography coupled with a suitable detector, such as FID (Flame Ionization Detector) or mass detector (MS), is commonly used to determine the qualitative and quantitative composition of aromatic compounds of alcoholic beverages (7).

As the number of distilleries increases, the quality of the fruit brandy is crucial for the sale. There is a need for an affordable, objective, and replicable method to evaluate the quality of fruit brandy produced by local distilleries. In this work we offer a simple methodology to analyze esters of C8-C22 fatty acids as one of the most important groups of volatile compounds present in these beverages that affect flavor and aroma. The extraction of C8-C22 fatty acid esters from fruit brandy samples was performed using the liquid-liquid extraction method. The qualitative composition of volatile aromatic compounds was determined using gas chromatography with a mass detector (GC/MS).

EXPERIMENTAL

The following chemicals were used for the extraction and analysis: Hexane, purchased by Lach-Ner; Diethyl Ether, purchased by Lach-Ner; Sodium Chloride, purchased by Lach-Ner.

Three types of fruit brandy were kindly donated for this work by the local producers from the municipality of Sanski Most and municipality of Novi Grad, Bosnia and Herzegovina. One producer donated a spirit made of pears (Sample I), while the other producer donated one spirit made of pears (Sample II) and another made of plums (Sample III). The fruit origin, geographical origin, and alcohol content in percentages of the samples can be found in Table 1.

Table 1. Characteristics of fruit brandy used in the experiment

Samples	Fruit origin	Geographical origin	Alcohol content, (%)
Sample I	pears	Lušci Palanka, Sanski Most	48
Sample II	pears	Mala Novska Rujiška, Novi Grad	45
Sample III	plums	Mala Novska Rujiška, Novi Grad	45

For each sample three replicas were analyzed to test the replicability of the method.

EXTRACTION OF THE VOLATILE COMPOUNDS

For the extraction of the volatile compounds present in the samples, liquid-liquid extraction was chosen, using two organic solvents (hexane and diethyl ether, 1:1 v/v). In the Erlenmeyer flask 15 mL of the solvent mixture was placed, together with 20 mL of sample, 10 mL of distilled water and 7.65 g of NaCl. The magnetic stir bar was placed in the flask and the opening was sealed with laboratory stretch film to minimize loss of volatile compounds during the extraction. The mixture was placed on the magnetic stirrer for 45 minutes at room temperature, while the speed was set to 750 rpm.

After extraction, the mixture was left for a couple of minutes for layers to separate, and the upper, organic layer was taken with the pipette and transferred to vials and analyzed by gas chromatography.

GC-MS ANALYSIS

GC conditions: HP-5 column (30 m × 0.25 mm i.d., 0.25 µm film thickness, Agilent Technologies 7890B). Helium gas was used as the carrier gas was used, at a flow rate of 1 mL/min. The temperature of the injector was 250 °C. The oven temperature was held at 40 °C for 2 min, and then increased to 80 °C at a rate of 5 °C/min, to 160 °C at a rate of 7 °C/min, to 200 °C at a rate of 9 °C/min, to 280 °C at a rate of 20 °C/min, and finally held at 280 °C for 10 min. Samples were injected in splitless mode with the injection volume of 1 µL.

MS conditions: The electron impact (EI) energy was 70 eV, and the ion source temperature was set at 230 °C. Scanning was performed from m/z 33 to 348.

For each sample, its mass spectrum was compared with that of the standard in the NIST05a Database (Agilent Technologies Inc.). The compound was identified when its matching rate was higher than 80%.

RESULTS AND DISCUSSION

By liquid-liquid extraction and GC-MS analysis methods, the qualitative composition of the examined samples was determined, identifying fatty acid esters that influence the aroma and taste of the spirit. The aromatic volatile compounds obtained through GC-MS analysis of the samples are presented in Table 2. In addition, representative GC-MS spectra of the samples are given in Figures 1-3.

Table 2 includes only compounds obtained in all three replicates, enhancing the method's reliability in analyzing brandy and identifying compounds that may influence its taste and aroma. In Sample I and Sample II, eleven C8-C22 fatty acids esters were detected, while in Sample III, eight esters were detected. Supplemental Table 1 presents values of esters retention times and percentage overlap with the database. In Sample I and Sample II, the following fatty acid esters have been identified: Ethyl benzoate, Ethyl octanoate, Ethyl nonanoate, Ethyl decanoate, Ethyl undecanoate, Ethyl dodecanoate, Ethyl tridecanoate, Ethyl tetradecanoate, Ethyl pentadecanoate, Ethyl hexadecanoate, Ethyl eicosanoate. In the Sample III following fatty acid esters were detected: Ethyl hexanoate, Ethyl benzoate, Ethyl octanoate, Ethyl nonanoate, Ethyl decanoate, Ethyl undecanoate, Ethyl dodecanoate, Ethyl tridecanoate.

Table 2. Identified esters in fruit brandy samples with GC/MS chromatography

Class	Chemical compound	Sample I	Sample II	Sample III	Aroma description according to: (8) (10) (11) (12) (13) (14) (15)
Ester	Ethyl hexanoate	-	-	+	Chamomile, flower, celery, fruit
	Ethyl benzoate	+	+	+	Fruity, fat
	Ethyl octanoate	+	+	+	Pineapple pear-like aroma
	Ethyl nonanoate	+	+	+	Grape
	Ethyl decanoate	+	+	+	Cognac, coconut
	Ethyl undecanoate	+	+	+	Coconut and fat flavor
	Ethyl dodecanoate	+	+	+	Characteristic fruity aroma
	Ethyl tridecanoate	+	+	+	Baked apple
	Ethyl tetradecanoate	+	+	-	Ether
	Ethyl eicosanoate	+	+	-	Fruity, waxy smell
	Ethyl hexadecanoate	+	+	-	Fatty, fruit, sweet, wax
	Ethyl pentadecanoate	+	+	-	Wax
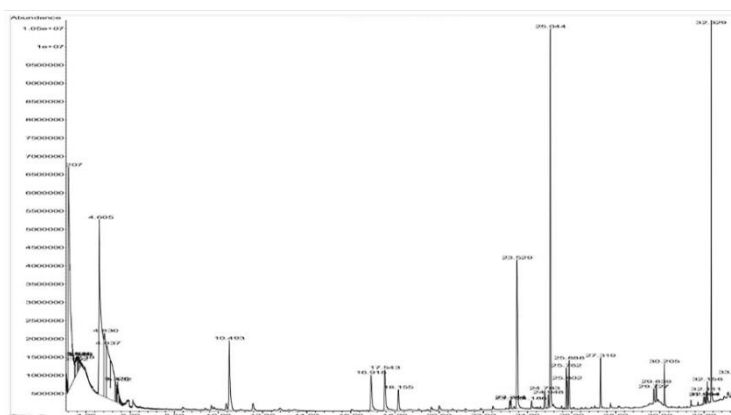
Figure 1. Representative GC/MS spectra of fruit brandy Sample I (fruit origin pears, geographical origin Lušci Palanka, Sanski Most, Bosnia and Herzegovina).
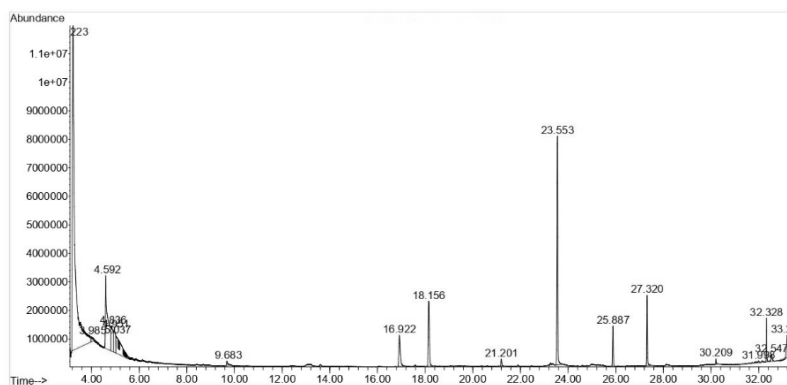
Figure 2. Representative GC/MS spectra of fruit brandy Sample II (fruit origin pears, geographical origin Mala Novska Rujiška, Novi Grad, Bosnia and Herzegovina).
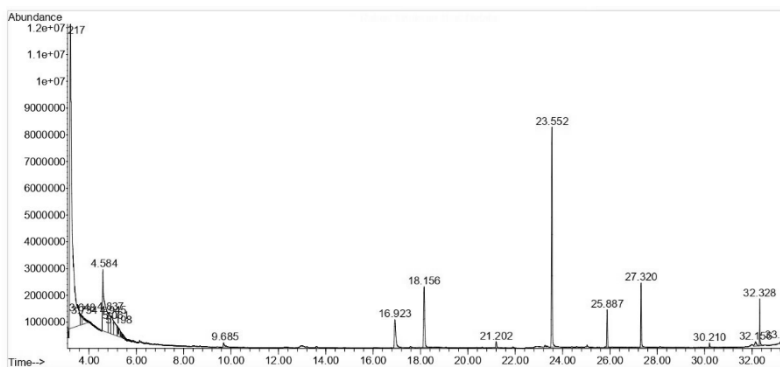
Figure 3. Representative GC/MS spectra of fruit brandy Sample III (fruit origin plum, geographical origin Mala Novska Rujiška, Novi Grad, Bosnia and Herzegovina).

The three most prevalent aromatic compounds, in terms of the area they cover, in Sample I are Ethyl decanoate (4,66%), Ethyl undecanoate (4,66%) and Ethyl benzoate (1,59%), in Sample II are Ethyl decanoate (10,58%), Ethyl undecanoate (10,58%) and Ethyl octanoate (4,16%) and in the Sample III are Ethyl decanoate (10,80%), Ethyl undecanoate (10,80%) and Ethyl octanoate (4,42%). As we can see, the most prevalent aromatic compounds in all three samples are Ethyl decanoate and Ethyl undecanoate, whose percentage reaches up to 11% in relation to the total percentage of detected compounds. The percentage of detected compounds is more similar between Samples II and III which is made from different types of fruit but originate from same geographical area (Mala Novska Rujiška, Novi Grad). It is possible that the type of aromatic compounds found in fruit brandy is also influenced by the geographical origin of the fruit from which the brandy is made. During GC-MS analysis of brandy, Coldea et al. (9) also have shown that detected fatty acid esters significantly depend on the type of brandy as well as the region of their origin.

The quality of a fruit brandy depends on its composition, which is responsible for its aroma and taste. To determine the composition of fatty acid esters in the samples, we used the GC-MS analysis method with appropriate analysis parameters described in Material and Methods. Esters contribute significantly to the aroma and taste of the brandy and they have a low organoleptic threshold (16). The floral and fruity aroma precisely originates from esters of fatty acids (17, 18) and it is considered that ethyl esters are beneficial for the spirit (7).

Tešević et al. (7) have shown that the most abundant esters in the analyzed samples of brandy were esters of fatty acids between C9 and C20. In our samples of fruit brandy, esters were also in the range of C8 and C22. However, the number of esters varies among the samples. In Samples I and II, eleven esters were detected, while in Sample III, eight esters were detected. The formation of esters is influenced by numerous factors such as the type of fruit, yeast, fermentation and distillation process (19).

Cvetković et al. (8) concluded that ethyl esters of C8, C10 and C12 acids positively affect the quality of fruit spirits, because of the fruity and floral flavor and odor. All these esters were identified by our methodology. Cvetković et al. (8) also found that ethyl hexanoate with the green apple and anise aroma, ethyl benzoate (floral and fruity), ethyl decanoate (fruity) and ethyl dodecanoate (floral and fruity) mostly contribute to the aroma of lo-

cal spirits. The authors found ethyl hexadecanoate only in the sample of grape spirit and concluded that this compound together with ethyl tetradecanoate influence the aroma/taste of this spirit. However, we found ethyl hexadecanoate in our Samples I and II (pear originated brandies). These results may indicate that the formation of ethyl hexadecanoate depends not only on the fruit of origin, but also on the fermentation process and yeast strains.

According to Stanzer et al. (20) ethyl esters of long chain fatty acids (e.g. ethyl dodecanoate, ethyl tetradecanoate, ethyl hexadecanoate) contribute to a positive aroma profile, when present in low concentrations, while otherwise they are responsible for candle wax and clear tones. In our study, we also detected long chain fatty acids (C14-C22) with the highest percentage detected in ethyl dodecanoate (2.96%) in the Sample III. The percentage of other esters of long chain fatty acids was below 2%.

For the flavor of distilled spirits special importance have the low-boiling ethyl esters like ethyl hexanoate, ethyl octanoate and acetates (21). In our work ethyl hexanoate was found only in the Sample III, while the ethyl octanoate was found in all three samples. The percentage of the area covered by ethyl hexanoate in Sample III was 0.56%, while the percentage of ethyl octanoate varies between samples, where the smallest percentage was in Sample I, 0.70% and in the Sample II and III was very similar, 4.16 and 4.42% respectively. Tešević et al. (7) have shown that these two compounds, ethyl hexanoate and ethyl decanoate, cover a large percentage of area. Similar to our results, ethyl decanoate has the largest percentage, up to 20% in one plum brandy sample, of all detected compounds. However, they found a small percentage of ethyl undecanoate, which is contrary to our results. Exactly, the different qualitative and quantitative composition of fruit brandy is what makes it unique in terms of taste and aroma, giving it its distinctive character, a "rakija fingerprint".

CONCLUSION

We can conclude that our methodology is effective in identifying fatty acid esters in different types of fruit brandies, that contribute to its flavor and aroma, and can influence the quality of a spirit. However, as not only the presence, but also the concentration of these compounds influences the flavor of the spirits, further development of the methodology to enhance quantitative analysis is necessary. Also, future research will go in the direction of developing methods for extraction and GC/MS detection of other classes of volatile brandy components that contribute to their quality.

Acknowledgement

REFERENCES

1. Ostojić, A.; Vasko, Z.; Cvetković, M.; Pašalić, B. Fruit self-sufficiency assessment in Bosnia and Herzegovina. *Western Balkan Journal of Agricultural Economics and Rural Development*, **2019**, *1*, 85-160

2. Wei, X.F.; Ma, X.L.; Cao, J.H.; Sun, X.Y.; Fang, Y.L. Aroma characteristics and volatile compounds of distilled Crystal grape spirits of different alcohol concentrations: Wine spirits in the Shangri-La region of China. *Food Sci. Technol.* **2018,** 38, 50-58.

3. Raičević, D.; Popović, T.; Jančić, D.; Šuković, D.; Pajović-Šćepanović, R. The impact of type of brandy on the volatile aroma compounds and sensory properties of grape brandy in Montenegro. *Molecules*, **2022**, *27*(9), 2974.

4. Kostik, V.; Memeti, S.; Bauer, B. Gas-chromatographic analysis of some volatile congeners in different types of strong alcoholic fruit spirits. *Journal of hygienic engineering and design*, **2013**, *4*, 98-102.

5. Popović, B.; Nikićević, N.; Gavrilović-Damnjanović, J.; Mitrović, O.; Srećković, M.; Ogašanović, D. The yield of plum brandy as influenced by different plum cultivars. *Voćarstvo*, **2008**, *42*(163/164), 111-118.

6. Satora, P.; Kostrz, M.; Sroka, P.; Tarko, T. Chemical profile of spirits obtained by spontaneous fermentation of different varieties of plum fruits.*European Food Research and Technology*, **2017**, *243*, 489-499.

7. Tešević, V.; Nikićević, N.; Jovanović, A.; Djoković, D.; Vujisić, L.; Vučković, I.; Bonić, M. Volatile components from old plum brandies. *Food technology and biotechnology*, **2005**, *43*(4), 367-372

8. Cvetković, D.; Stojilković, P.; Zvezdanović, J.; Stanojević, J.; Stanojević, L.; Karabegović, I. The identification of volatile aroma compounds from local fruit based spirits using a headspace solid-phase microextraction technique coupled with the gas chromatography-mass spectrometry. *Advanced Technologies*, **2020**, *9*(2), 19-28.

9. Coldea, T.E.; Socaciu, C.; Moldovan, Z.; Mudura, E. Minor volatile compounds in traditional homemade fruit brandies from Transylvania-Romania, as determined by GC-MS analysis. *Notulae botanicae horti agrobotanici cluj-napoca*, **2014**, *42*(2), 530-537.

10. https://www.flavornet.org/flavornet.html

11. https://www.medchemexpress.com/ethyl-icosanoate.html

12. Puškaš, V.S.; Miljić, U.D.; Vučurović, V.M.; Muzalevski, A.B. Aromatic compounds of brandies produced from three apricot varieties cultured in Serbia. *Journal on Processing and Energy in Agriculture*, **2017**, *21*(2), 101-103.

13. Matijašević, S.; Popović-Djordjević, J.; Ristić, R.; Ćirković, D.; Ćirković, B.; Popović, T. Volatile aroma compounds of brandy 'Lozovača′ produced from Muscat table grapevine cultivars (Vitis vinifera L.). *Molecules,* **2019**, *24*(13), 2485.

14. Lan, T.; Wang, J.; Yuan, Q.; Lei, Y.; Peng, W.; Zhang, M.; Ma, T. Evaluation of the color and aroma characteristics of commercially available Chinese kiwi wines via intelligent sensory technologies and gas chromatography-mass spectrometry. *Food Chemistry*, **2022**, *15*, 100427.

15. Weiss, T.; Barretto, R.; Chen, G.; Hong, S.; Li, Y.; Zheng, Y.; Wang, D. Blue, red and white maize as a sustainable resource for production of distilled spirit. *Journal of Agriculture and Food Research*, **2023**, *14*, 100770.

16. Ramsay, C.M.; Berry, D.R. Effect of temperature and pH on the formation of higher alcohols, fatty acids and esters in the malt whisky fermentation. *Food microbiology,* **1984**, *1*(2), 117-121.

17. Karagiannis, S.; Lanaridis, P. Insoluble grape material present in must affects the overall fermentation aroma of dry white wines made from three grape cultivars cultivated in Greece. *Journal of food science,* **2002**, *67*(1), 369-374.

18. Coldea, T.E.; Socaciu, C.; Mudura, E.; Socaci, S.A.; Ranga, F.; Pop, C.R.; Pasqualone, A. Volatile and phenolic profiles of traditional Romanian apple brandy after rapid ageing with different wood chips. *Food chemistry*, **2020**, *320*, 126643.

19. Spaho, N.; Gaši, F.; Leitner, E.; Blesić, M.; Akagić, A.; Žuljević, S.O.; Meland, M. Characterization of volatile compounds and flavor in spirits of old apple and pear cultivars from the Balkan region. *Foods*, **2021**, *10*(6), 1258.

20. Stanzer, D.; Hanousek, Č.K.; Blesić, M.; Smajić Murtić, M.; Mrvčić, J.; Spaho, N. Alcoholic fermentation as a source of congeners in fruit spirits. *Foods*. **2023**, *12*(10), 1951.

21. Christoph, N.; Bauer-Christoph, C. Flavour of spirit drinks: Raw materials, fermentation, distillation, and ageing. In *Flavours and fragrances: chemistry, bioprocessing and sustainability*. Berlin, Heidelberg: Springer Berlin Heidelberg. **2007**, pp 219-239.

EFFECT OF MECHANISMS OF DISCRETE-PULSE ENERGY INPUT ON THE PHYSICO-CHEMICAL INDICATORS OF OAK EXTRACTS

Oleksandr OBODOVYCH [ID]*, Vitalii SYDORENKO** [ID]*, Bogdan TSELEN* [ID]

Institute of Engineering Thermophysics of the National Academy of Sciences of Ukraine 2, Akademika Bulakhovskoho St., 03164 Kyiv, Ukraine

One of the most important stages in the creation of a number of spirits is aging. The aim of the work is to study the effect of discrete-pulse energy input on the physicochemical parameters of oak extracts. It was determined that it is most effective to process oak chips in a rotor-pulsation apparatus with a flow shear rate of $50 \cdot 10^3$ s-1 and a duration of 11 hours and an extractant strength of 60% by volume. An increase in the extraction temperature from 25 to 40 ℃ contributes to an increase in the optical density of solutions from 0.64 to 0.78 units, while energy consumption does not increase. It was determined that when the solid/liquid ratio decreases from 1:10 to 1:20, the content of tannins in the extract decreases almost twice. The dependence of the change in the average surface diameter of oak particles on the processing duration in the rotor-pulsation apparatus was determined at a flow shear rate of $50 \cdot 10^3$ s-1, a solid/liquid ratio of 1:10, a temperature of 40 ℃, and an ethanol concentration of 60% vol. The most intensive dispersion took place in the first two hours. The particle size decreased by more than 2000 µm. After 4 hours of processing, the reduction was 150 µm, and after 6 hours - 100 µm. Further processing from 6 to 12 hours led to a decrease in the size of the particles by 50 µm. The maximum concentration of tannins was 7.4 g/L with an average particle size of 400 µm, which corresponds to 10–12 hours of processing.

Keywords: alcoholic beverages, extraction, oak, rotor-pulsation apparatus, discrete-pulse energy input.

INTRODUCTION

One of the stages in the creation of a number of alcoholic beverages, namely, whisky, brandy, or cognac is aging (1). This stage is associated with the gradual extraction of compounds contained in the wood of oak barrels in which wine or water-alcohol mixtures are aged (2).

This stage also promotes the micro-oxidation reactions associated with the diffusion of oxygen through the wood pores. These reactions significantly affect the final sensory and aromatic properties of alcoholic beverages.

The use of wood barrels for wine aging involves long times (from 6 to 18 months in barrels) and high economic costs, so various techniques have been investigated to obtain similar products (3).

Some alternative ways to age alcoholic beverages are described below:

Wood fragments. The principle of the method is to use for alcoholic beverages production residual material from the manufacturing of oak barrels or old discarded barrels instead of whole barrels. *Advantages*. Low cost-wood is reused. Testing new botanical varieties with low investment. Increase very old barrels. Possibility of dosage variation. *Disadvantages*. De-standardization of formats, and lack of knowledge, regarding the sensory contribution. Need for combined use with micro-oxygenation (4,5).

Micro-oxygenation (MOX) is a technique that consists in introducing small and measured amounts of oxygen into wines with the objective of improving wine color, aroma, and texture. It involves the use of specialized equipment to regulate the oxygen doses applied. An important stipulation of micro-oxygenation is that the oxygen is introduced at a rate equal to or less than the oxygen uptake rate of the wine thus, avoiding the accumulation of dissolved oxygen (6). The basic equipment needed for MOX includes an oxygen supply, a dosing system and a micro-porous diffuser. *Advantages*. Simulates gas transfer in barrels. Possibility of using steel tanks for aging and not just wooden barrels. Combined use with wood fragment. *Disadvantages*. Specialized equipment required. When unregulated, it can oxidize the drink in excess, sensory compromise. *Main effects*. Presence of O_2 for yeast during fermentation. Reduction in addition of SO_2. Improved color. Reduced contamination. (7).

Pulsed electric field technology. Pulsed electric field (PEF) processing is a method that uses short bursts of high voltage electric. It is one of the most promising nonthermal novel processing technologies that is utilized to increase the extraction of various polyphenols from red and white grape varieties during winemaking and to improve color properties (8, 9, 10). *Advantages*. Decreased aging time. Use of grapes in pre-fermentation. The use in wines, in addition to accelerating esterification, also acts on contamination. *Disadvantages*. Specialized equipment required. It can give the product a metallic flavor. Reduction in energy activation of chemical reactions. *Main effects*. Reduction in addition of SO_2. Increased extraction of compounds from grapes (6).

High hydrostatic pressure. This technology consists in exposing the wine at room temperature to high hydrostatic pressure (up to 600 MPa). *Advantages*. Decreased aging time. Low cost equipment. No heating. *Disadvantages*. If time is prolonged, it can destroy aromatic compounds. *Main effects*. Reduction in energy activation of chemical reactions. Increased extraction of compounds from grapes (11, 12, 13).

Microwaves. The principle of microwave processing is the dissipation of electromagnetic waves in the irradiated medium. Microwaves are non-ionizing electromagnetic waves of frequency between 300 MHz and 300 GHz, even though, only a few frequencies are allowed for industrial, scientific, and medical uses (ISM frequencies), generally comprised between 0.915 and 2.45 GHz (14). *Advantages*. Decreased aging time. Microbiological control. *Disadvantages*. Specialized equipment is required. Hot spots. Difficult to scale up. High specific energy consumption. *Main effects*. Increased extraction of compounds from grapes. Induction of free radical formation. Reduced contamination (15).

Ozonization. It is known that ozone, which is a modification of oxygen, has a greater oxidizing capacity than oxygen. A broad review of research on the effect of ozone on bioactive compounds in grapes and wine is made in the paper (16). In particular, most of the published papers report an increase in antioxidant compounds (e.g., polyphenols) and stress-related volatiles, confirming the hypothesis that ozone could be used to improve berry and wine compositional and sensory quality.

The experience of the possibility of improving bioactive compounds and, consequently, the health-related properties of grapes and wine by using ozone was summarized. As a result of the research on the influence of ozonization of wood extracts on their physical and chemical and organoleptic indicators, it was determined that ozonization has a complex effect on extracts. The positive aspects of ozonization of extracts include an increase in the content of such volatile compounds as ethers and aldehydes, the degree of oxidation of tannins, and as the negative an increase in the content of methanol, the main components of the sow fraction, and the creation of traces of acetone (17). The research on the effect of

ultrasound on the extraction process in the technology of wine (18-22) and whiskey (23) production was more extensive.

In particular, the effect of ultrasonic treatment of extracts on physicochemical and organoleptic properties was studied (17). The dynamics of the dyes and tannins concentration during ultrasound treatment of extracts with a frequency of 22 and 44 kHz, an intensity of 0.5 W/cm^2 was investigated. Before ultrasonic treatment, pre-infusion was carried out for 16 hours at a temperature of 25 °C. Moreover, treatment of extracts with ultrasound was carried out for 10 hours, every 30 min., and duration of action of 5 min. The optical density of the extracts was measured every 60 min. within 10 hours.

It was showed that ultrasonic treatment intensifies the extraction of wood dyes. The duration of extraction was reduced when using ultrasound treatment to 10 hours compared to periodic infusion. The optical density of extracts at 7 hours of infusion with ultrasound reached a value of 0.38, which was observed in the process of infusion without processing at 25 °C for only 16 days.

A comparative analysis of some quality parameters of extracts obtained during the infusion of oak chips without ultrasound treatment for 18 days (control) and treated with ultrasound was also carried out (24). The amount of extracted carbohydrates increased by an average of 38% regardless of the frequency of ultrasound treatment. Additionally, the amount of total extracts increased depending on the frequency of ultrasound treatment: at a frequency of 22 kHz - by 8.5%, at 44 kHz - by 19% relative to the control. The tannins concentration in the extracts increased by 5.13% as a result of ultrasound treatment with a frequency of 22 and 44 kHz, respectively. The amount of gallic acid in the extracts did not depend on the frequency of ultrasound treatment. The increase in the amount of total extract and tannins when using ultrasound was probably due to the effects of heating and mixing in the liquid phase. Furthermore, the pyrogallic hydroxyl groups concentration decreased from 19.0 during extraction without the use of ultrasound to 14.2 and 13.6% during treatment with a frequency of 22 and 44 kHz, respectively.

A significant decrease in the content of aromatic aldehydes in the extracts was also found under ultrasonic exposure, which negatively affects the intensity of their aroma.

As noted in the literature, the use of ultrasound to intensify the extraction of target products from different types of raw materials is associated with the phenomenon of ultrasonic cavitation caused by the passage of ultrasonic waves in a liquid medium (25). The essence of this phenomenon is the formation and subsequent collapse of cavities or bubbles in a liquid medium, suddenly subjected to a pressure release. At the same time, local high-amplitude pressure pulses are emitted throughout the entire working volume, exerting a powerful dynamic effect on the surrounding medium. When initiating cavitation in the volume of the extractant with raw material particles, periodic formation and collapse of bubbles occur both in the volume of the extractant outside the particles and in the raw extract reagent, which is in the pores and cells inside the particles. As a result, molecular diffusion in the capillaries is replaced by convective diffusion, which accelerates the penetration of the solvent into the cellular structures of the raw material and the movement of target substances into the extractant, which ultimately contributes to the intensification of mass exchange. Due to the action of shock pulses at the stage of bubble collapse, destruction of cellular structures and transfer of useful substances into the extractant can occur due to their washing out (26). The applicability of ultrasonic cavitation and its implementation devices, however, for industrial applications is limited due to high specific energy costs, difficulty in equipment design and process scale-up, safety and regulatory issues (27). These disadvantages are absent in devices that generate hydrodynamic cavitation – the process of formation,

growth and collapse of cavitation bubbles in a liquid caused by the passage of liquid through sharply narrowing holes.

One of the methods for intensifying mass transfer processes in the liquid media, the phenomenon of hydrodynamic cavitation is corresponding to, is the method of discrete-pulse energy input (28-32).

Its principle is to concentrate the energy stationary introduced and arbitrarily distributed in the working volume in local discrete points of the system and then pulse it to achieve the necessary thermal physical effects. The application of the method involves the creation of a large number of working bodies or working elements evenly distributed in a dispersed media, which transform stationary thermal, mechanical, or other types of energy into energetically powerful pulses, discrete in time and space, which ensures the most efficient and economical use of energy (33).

This principle is implemented to varying degrees in developing innovative methods for intensifying extraction processes primarily in ultrasonic, microwave, pulsation, and electric discharge extraction, as well as in the use of rotor-pulsation and vibration devices. All these methods use the effects of cavitation, which is considered one of the powerful mechanisms of the discrete-pulse energy input principle.

The objective of our study was to investigate the impact of discrete-pulse energy input on the physicochemical parameters of oak extracts used for aging (maturation of alcohols).

EXPERIMENTAL

Oak chips with an average surface diameter of particles of 3000 μm and water-ethanol solution with a volume fraction of ethanol of 40, 50, 60, and 65% were used as the material for studies.

The extraction was carried out on an experimental setup with a rotor-pulsation apparatus. The rotor-pulsation unit of the rotor-pulsation apparatus consists of two rotors, a stator, and a centrifugal pump impeller (34).

The studies were carried out as follows. Through the receiving pipeline, the mixture of water-alcohol solution with oak waste is sent to the rotor-pulsation apparatus, where it is exposed to shock waves, interphase turbulence, microcavitation and vortices, which leads to intensive crushing of the particles of the substance, an increase in the surface area of phase contact. Thanks to this, the rate of mass transfer of extractive substances from the solid phase (oak) to the liquid phase (water-alcohol solution) increases. If it is necessary to carry out oxidation processes, the design of the rotor-pulsation apparatus provides for the supply of air to the receiving pipe, where the mixture of the extractant and the extracting substance circulates. For this purpose, the rotor-pulsation apparatus has an ejector equipped with a flowmeter and a vacuum gauge.

The efficiency of the rotor-pulsation apparatus is determined by the fact that the following processes are simultaneously carried out, namely, dispersion, mixing, heating, dissolution, and extraction. One of the main parameters of the rotor-pulsation apparatus operation is the shear flow rate inside the rotor-pulsation unit. It can be changed by changing the angular speed of the rotor`s rotation, the inner radius of the rotor, and the thickness of the gap between the stator and the rotor. During the experiments, the flow shear rate was $20 \cdot 10^3$, $30 \cdot 10^3$, and $50 \cdot 10^3$ s^{-1}.

The effect of the shear flow rate, temperature, processing duration, and the average surface diameter of the particles on the indicators of the extracts was determined. The change in optical density, the content of the total extract, and tannins were measured.

The effect of the volume fraction of ethanol in the water-ethanol solution, as well as the extraction temperature on the yield of target components from chopped wood was studied, based, first of all, on the requirement for the accumulation of a greater number of extractive components of wood, which correlates with the value of the optical density of the extracts.

The efficiency of the extraction of substances from oak shavings was judged by the dynamics of changes in the color of the extracts and by the amount of extract extracted from wood, which characterizes the intensity of accumulation of colored substances. The color of the extracts was determined by the photocalorimetric method. The optical density of the samples was measured at a wavelength of 440 nm.

The concentration of tannins was determined by the method based on the oxidation of the tannins of cognacs and cognac spirits with a solution of potassium permanganate in the presence of the indigo carmine indicator and their determination by the titrimetry (35).

The mass concentration of the total extract was measured by a gravimetric method based on drying at a temperature of 105±2° C to a constant mass of the residue obtained as a result of the evaporation of a certain volume of the product in an evaporating cup brought to a constant mass. The mass of the empty cup and the mass of the cup with dry residue was determined by weighing. The mass concentration of the total extract was calculated from the difference in the mass of the cups (36).

The granulometric composition was determined by the method of sieve analysis. The weight of the studied material was sifted through a set of sieves, and then the percentage of the residue on each of the sieves was determined relative to the weight of the initial weighing (37, 38).

RESULTS AND DISCUSSION

In the course of the experiments, the dynamics of changes in the optical density of the extracts depending on the duration of processing in the rotor-pulsation apparatus were studied at flow shear rates of $20 \cdot 10^3$, $30 \cdot 10^3$, and $50 \cdot 10^3$ s^{-1} at different concentrations of ethanol in the extractant (Figures 1-3). The temperature of the process in all cases was 25 ºC.

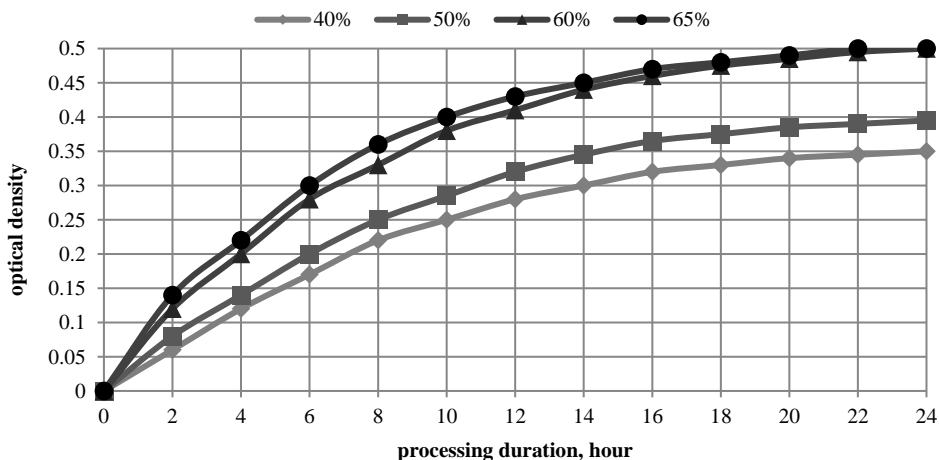**Figure 1.** Dependence of the optical density of the extracts on the duration of processing at a shear flow rate of $20 \cdot 10^3$ s^{-1} and the concentration of ethanol in the extractant

Figure 2. Dependence of the optical density of the extracts on the duration of processing at a shear flow rate of $30 \cdot 10^3$ s^{-1} and the concentration of ethanol in the extractant

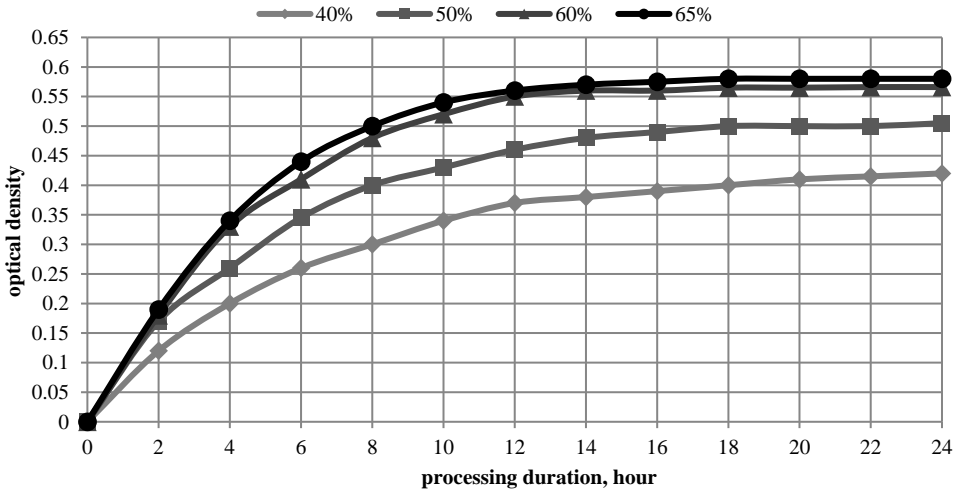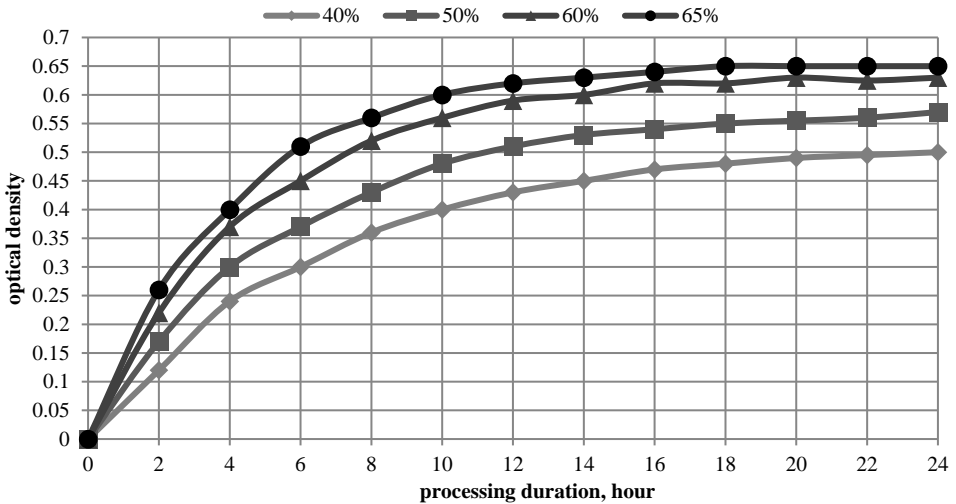**Figure 3.** Dependence of the optical density of the extracts on the duration of processing at a shear flow rate of $50 \cdot 10^3$ s^{-1} and the concentration of ethanol in the extractant

The value of the optical density of the extracts increases with the increasing strength of the extract ant and the processing duration. An increase in the flow shear rate from 20 to $50 \cdot 10^3$ s^{-1} has a positive effect on the optical density. Thus, the optical density value of 0.5 units was observed with a processing duration of 18 hours, an extractant strength of 60-65%, and a shear flow rate of $20 \cdot 10^3$ s^{-1}.

When the shear flow rate increased to $30 \cdot 10^3$ s^{-1}, the maximum value of the optical density was 0.57 units and it was reached in 16 hours of processing at extractant strength of 60-65% by volume.

Increasing the shear flow rate to $50 \cdot 10^3$ s^{-1} made it possible to increase the optical density to 0.64 in 11 hours of processing, and the strength of the extractant to 60-65% by volume. It is most effective to process oak raw materials in a rotor-pulsation apparatus with a shear flow rate of $50 \cdot 10^3$ s^{-1} for duration of 11 hours and extractant strength of 60% vol. Increasing the shear flow rate by more than $50 \cdot 10^3$ s^{-1} is impractical for technical and energy reasons.

It is well known that an increase in the extraction temperature contributes to an increase in the total extract in the solution. For this purpose, the dynamics of changes in the optical density of the extracts depending on the processing temperature and the volume fraction of ethanol in the extractant were determined. The processing duration of the mixture of extracted raw materials and the extractant was 11 hours at a flow shear rate of $50 \cdot 10^3$ s^{-1} (Figure 4).
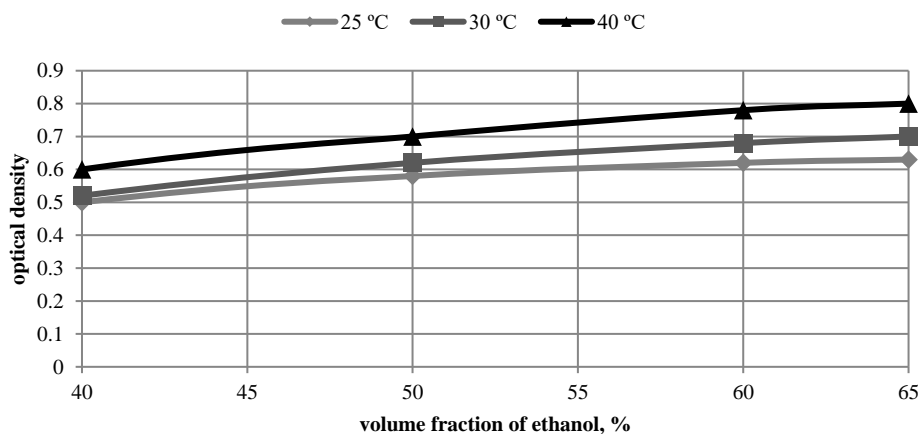

Figure 4. Dependence of the optical density of the extracts on the volume fraction of ethanol in the extractant at the processing temperature

Increasing the extraction temperature from 25 to 40 °C helps to increase the optical density of solutions from 0.64 to 0.78 units, while energy consumption does not increase. The solution is heated due to dissipation energy. A further increase in the extraction temperature leads to a decrease in the volume of the mixture and a loss of its strength. Continuation of studies on the extraction of oak chips was carried out at a temperature of 40 °C.

The solid/liquid ratio is of great importance during extraction. The results of studies on the effect of the solid/liquid ratio on the concentration of tannins in extracts are presented in Table 1. During the experiment, the solid/liquid ratio was 1:10, 1:15, 1:20. Processing of the mixture of the extracted substance and the extractant was carried out in a rotor-pulsation apparatus for 11 hours at a flow shear rate of $50 \cdot 10^3$ s^{-1}, a temperature of 40 °C and water-ethanol solution strength of 60% vol.

Table 1. Dependence of the concentration of tannins in the extracts on the solid/liquid ratio

solid/liquid ratio	1:10	1:15	1:20
Concentration of tannins, g/L	7.4	5.7	3.8

Intensification of extraction is associated with an increase in the specific surface of the particles and, accordingly, the contact area between the surface of the oak particles and water-ethanol solution.

Above in the work, it was indicated that several processes take place at the same time, including dispersion, during the processing of various media in the rotor-pulsation apparatus. The dependence of the average surface diameter of oak particles on the processing duration in the rotor-pulsation apparatus at a flow shear rate of $50 \cdot 10^3$ s^{-1}, solid/liquid ratio 1:10, temperature 40 ºC, ethanol concentration 60% vol is presented in Table 2.

Table 2. The dependence of the average surface size of oak particles and the concentration of tannins in extracts on the processing duration

Processing duration, hour	0	2	4	6	8	10	12	14
Average surface size of particles, µm	3000	900	750	650	500	450	400	400
Concentration of tannins, g/L	0	2.9	3.8	4.6	6.0	7.2	7.4	7.4

The initial average surface diameter of the particles was 3000 µm. After 12 hours of processing in a rotor-pulsation apparatus, it decreased to 400 µm. Further processing practically did not reduce the size. The most intensive dispersion took place in the first two hours. The particle size decreased by more than 2000 µm. After 4 hours of processing, the reduction was 150 µm, after 6 hours - 100 µm. Further processing from 6 to 12 hours led to a decrease in the size of the particles by 50 µm.

Table 2 shows the dependence of the concentration of tannins in the extracts on the average surface size of the particles. The maximum concentration was 7.4 g/L with an average particle surface size of 400 mm, which corresponds to 11-12 hours of processing in the rotor-pulsation apparatus under the above-mentioned conditions. As in the case of the average surface diameter of the particles, the concentration of tannins changes more intensively in the first two hours. It increases almost 3 times, while afterwards decreases. After 10-12 hours of processing, the tannins concentration practically does not change. The obtained experimental data confirm the results of the studies presented in Figure 3.

According to the process duration of processing a mixture of oak waste with an average particle diameter of 3000 µm and a water-alcohol solution with the strength of 60% vol. in the rotor-pulsation apparatus, it is possible to judge a decrease in the average particle size and an increase in the concentration of tannins. Increasing the dispersion of oak waste affects not only the change in the concentration of tannins in the extracts but also the yield of the total extract. Table 3 shows the change in the total extract concentration from the average diameter of the particles.

Table 3. Dependance of the total extracts concentration from the average diameter of the particles

Average surface size of particles, µm	3000	900	750	650	500	450	400
Total extract, g/L	0.1	4.9	8.8	11.2	14.7	15.1	15.2

With a decrease in the average diameter of the particles, an increase in the concentration of the total extract is observed. The concentration increases most intensively when the particle size decreases from 3000 to 900 μm. Additionally, in the particle diameter range of 500-400 μm, the concentration of the specified components changes very little.

CONCLUSION

The paper examines the method of extracting substances from oak chips by the method of discrete-pulse energy input in a rotor-pulsation apparatus in order to intensify the process of artificial aging of alcoholic beverages. As a result of the work, it was established that due to the complex physical effects of impact on the media, extraction occurs much faster compared to conventional methods of extraction. The dependence of the optical density of the extractant, as an indicator of the efficiency of extracting substances from oak shavings, on the intensity of processing of the mixture of water-alcohol solution and oak shavings and the strength of the water-alcohol solution was determined. The dependence of the concentration of tannins total extract on the dispersion of raw material particles during processing is also determined.

REFERENCES

1. Tarko, T.; Krankowski, F.; Duda-Chodak, A. The Impact of Compounds Extracted from Wood on the Quality of Alcoholic Beverages. *Molecules*. **2023**, 28(2), 620. https://doi.org/10.3390/molecules28020620

2. Eliseev, M.N.; Gribkova, I.N.; Kosareva, O.A.; Alexeyeva, O.M. Effect of organic compounds on cognac sensory profile. *Foods and Raw Materials*. **2021**, 9(2), 244–253. https://doi.org/10.21603/2308-4057-2021-2-244-253

3. Carpena, M.; Pereira, A.G.; Prieto, M.A.; Simal-Gandara, J. Wine Aging Technology: Fundamental Role of Wood Barrels. *Foods*. **2020**, 9(9), 1160. https://doi.org/10.3390/foods9091160

4. Jordão, A.M.; Correia, A.C.; DelCampo, R.; González SanJosé, M.L. Antioxidant capacity, scavenger activity, and ellagitannins content from commercial oak pieces used in winemaking. *European Food Research and Technology*. **2021**, 235, 817-825. https://doi.org/10.1007/s00217-012-1803-y

5. Rodríguez Madrera, R.; Suárez Valles, B.; Diñeiro García, Y.; del Valle Argüelles, P.; Picinelli Lobo, A. Alternative Woods for Aging Distillates-An Insight into Their Phenolic Profiles and Antioxidant Activities. *Food Science and Biotechnology*. **2010**, 19, 1129-1134. https://doi.org/10.1007/s10068-010-0161-4

6. Krüger, R.T.; Alberti, A.; Nogueira, A. Current Technologies to Accelerate the Aging Process of Alcoholic Beverages: A Review. *Beverages*. **2022**, 8, 65. https://doi.org/10.3390/beverages8040065

7. Gómez-Plaza, E.; Cano-López, M. A review on micro-oxygenation of red wines: Claims, benefits and the underlying chemistry. *Food Chemistry*. **2011**, 125, 1131–1140. https://doi.org/10.1016/j.foodchem.2010.10.034

8. Akdemir Evrendilek, G. Pulsed Electric Field Processing of Red Wine: Effect on Wine Quality and Microbial Inactivation. *Beverages*. **2022**, 8(4), 78. https://doi.org/10.3390/beverages8040078

9. Yang, N.; Huang, K.; Lyu, C.; Wang, J. Pulsed electric field technology in the manufacturing processes of wine, beer, and rice wine: A review. *Food Control*. **2016**, 61, 28-38. https://doi.org/10.1016/j.foodcont.2015.09.022

10. Clodoveo, M. L.; Dipalmo, T.; Rizzello, C. G.; Corbo, F.; Crupi, P. Emerging technology to develop novel red winemaking practices: An overview. *Innovative Food Science & Emerging Technologies*. **2016**, 38, 41-56. https://doi.org/10.1016/j.ifset.2016.08.020

11. Santos, M. C.; Nunes, C.; Jourdes, M.; Teissedre, P. L.; Rodrigues, A.; Amado, O.; Saraiva, J.A.; Coimbra, M. A. Evaluation of the potential of high pressure technology as an enological practice for red wines. *Innovative Food Science & Emerging Technologies*. **2016**, 33, 76-83. https://doi.org/10.1016/j.ifset.2015.11.018

12. Santos, M.C., Nunes, C., Ferreira, A.S., Jourdes, M., Teissedre, P.L., Rodrigues, A., Amado, O., Saraiva, J.A., Coimbra, M.A. Comparison of high pressure treatment with conventional red wine aging processes: Impact on phenolic composition. *Food Research International*. **2019**, 116, 223-231. https://doi.org/10.1016/j.foodres.2018.08.018

13. Lukić, K.; Ćurko, N.; Tomašević, M.; Kovačević Ganić, K. Phenolic and Aroma Changes of Red and White Wines during Aging Induced by High Hydrostatic Pressure. *Foods*. **2020**, 9(8), 1034. https://doi.org/10.3390/foods9081034

14. Meda V.; Orsat V.; Raghavan V. Microwave heating and the dielectric properties of foods In The Microwave Processing of Foods (Second Edition); Regier M., Knoerzer K. and Schubert H, Eds. Woodhead Publishing, 2017 ; pp. 23-43. https://doi.org/10.1016/B978-0-08-100528-6.00002-4

15. Chemat, F.; Rombaut, N.; Meullemiestre, A.; Turk, M.; Perino, S.; Fabiano-Tixier, A.S.; Abert-Vian, M. Review of Green Food Processing techniques. Preservation, transformation, and extraction. *Innovative Food Science & Emerging Technologies*. **2017**, 41, 357–377. https://doi.org/10.1016/j.ifset.2017.04.016

16. Modesti, M.; Macaluso, M.; Taglieri, I.; Bellincontro, A.; Sanmartin, C. Ozone and Bioactive Compounds in Grapes and Wine. *Foods*. **2021**, 10(12), 2934. https://doi.org/10.3390/foods10122934

17. Novikova, I.V.; Vostrikov, S.V. Research of ultrasonic processing and ozonization influence on the physical, chemical and organoleptic parameters of wood extracts. *Storage and Processing of Farm Products*. **2007**, 2, 44-48. https://elibrary.ru/item.asp?id=15570172

18. Delgado-González, M.J.; Sánchez-Guillén, M.M.; García-Moreno, M.V., Rodríguez-Dodero, M.C.; García-Barroso, C.; Guillén-Sánchez, D.A. Study of a laboratory-scaled new method for the accelerated continuous ageing of wine spirits by applying ultrasound energy. *Ultrasonics Sonochemistry*. **2017**, 36, 226–235. https://doi.org/10.1016/j.ultsonch.2016.11.031

19. Del Fresno, J.M.; Loira, I.; Morata, A.; González, C.; Suárez-Lepe, J.A.; Cuerda, R. Application of ultrasound to improve lees ageing processes in red wines. *Food Chemistry*. **2018**, 261, 157–163. https://doi.org/10.1016/j.foodchem.2018.04.041

20. Zhang, Q.A.; Wang, T.T. Effect of ultrasound irradiation on the evolution of color properties and major phenolic compounds in wine during storage. *Food Chemistry*. **2017**, 234, 372–380. https://doi.org/10.1016/j.foodchem.2018.04.041

21. Shyr, J. J.; Yang, S.H. Acceleration of the Aging Process in Coffee Liqueur by Ultrasonic Wave Treatment. *J. Food Process*. **2016**, 40, 502–508. https://doi.org/10.1111/jfpp.12629

22. Zheng, X.; Zhang, M.; Fang, Z.; Liu, Y. Effects of low frequency ultrasonic treatment on the maturation of steeped greengage wine. *Food Chemistry*. **2014**, 162, 264–269. https://doi.org/10.1016/j.foodchem.2014.04.071

23. Rogerson, L. E. High intensity ultrasound assisted extraction of oak compounds for accelerated aging of wines and whiskies. Master's Thesis, University of Tennessee, May 2016. https://trace.tennessee.edu/utk_gradthes/3804

24. Novikova, I.V. Theoretical and practical aspects of the intensive technology of alcoholic beverages from grain raw materials using wood extracts: monography; Direct-Media: Moskow-Berlin, 2014. https://biblioclub.ru/index.php?page=book&id=257356

25. Panda, D.; Manickam, S. Cavitation Technology - The Future of Greener Extraction Method: A Review on the Extraction of Natural Products and Process Intensification Mechanism and Perspectives. *Applied Sciences*. **2019**, 9, 766. https://doi.org/10.3390/app9040766

26. Tselen, B. Ya.; Gozhenko, L. P.; Radchenko, N. L.; Ivanitsky G. K. Use of cavitation effects in extraction processes. *Scientific Works*. **2020**, 84(1), 92–97. https://doi.org/10.15673/swonaft.v84i1.1876

27. Hoo, DY; Low, ZL; Low, DYS; Tang, SY; Manickam, S; Tan, KW; Ban, ZH. Ultrasonic cavitation: An effective cleaner and greener intensification technology in the extraction and surface modification of nanocellulose. *Ultrasonics Sonochemistry*. **2022**, 90, 106176.

https://doi.org/10.1016/j.ultsonch.2022.106176

28. Dolinsky A. A. (ed). Micro- and nano-level processes in DPIE technologies; Akadeperiodica: Kyev, 2015. http://ittf.kiev.ua/wp-content/uploads/2019/08/dolinskij-2-tekst.pdf

29. Droździel, P.; Vitenko, T.; Voroshchuk, V.; Narizhnyy, S.; Snizhko, O. Discrete-Impulse Energy Supply in Milk and Dairy Product Processing. *Materials*. **2021**, 14, 4181. https://doi.org/10.3390/ma14154181

30. Dubovkina, I.O. Change of physical and chemical parameters of the liquid binary systems by alternating impulses of pressure. *Ukrainian Food Journal*. **2017**, 6(1), 142-153. https://doi.org/10.24263/2304-974X-2017-6-1-16

31. Obodovych, O.M.; Tselen, B.Ya; Sydorenko, V.V.; Ivanytsky, G.K.; Radchenko, N.L. Application of the method of discrete-pulse energy input for water degassing in municipal and industrial boilers. *Acta Periodica Technologica*. **2022**, 53, 123-130. https://doi.org/10.2298/APT2253123O

32. Yushchenko, N.; Grabova, T.; Kuzmyk, U.; Pasichnyi, V. Determination of technological parameters for producing sumac extract for further use in dairy pastes technology. *Scientific Works of National University of Food Technologies*. **2017**, 23(5), 242–247. https://doi.org/10.24263/2225-2924-2017-23-5-1-30

33. Avdieieva, L.Yu. Implementation of the Principle of Discrete-Pulse Energy Input to the Creation of Nanotechnologies for Food Industry. *Science and Innovation*. **2016**, 12(4), 11-15. https://doi.org/10.15407/scine12.04.011

34. Dolinskiy A.A.; Obodovich A.N.; and Sydorenko V.V. Intensification of aeration and mass transfer in wastewater treatment by discrete-pulse energy input (DPEI). *Thermophysics and Aeromechanics*. **2018**, 24(4), 623–630 https://doi.org/10.1134/S0869864318040145

35. Rajković, M.B.; Sredović, I.D. The determination of titratable acidity and total tannins in red wine. *Journal of Agricultural Sciences Belgrade*. **2009**, 54(3), 223-246 https://doi.org/10.2298/JAS0903223R

36. Peschanskaya,V.A.; Osipova ,V. P.; Tochilina, R.P.; Trofimchenko, V.A. A new method for assessing the quality of brandy products. Innovative research and development for scientific support of production and storage of environmentally friendly agricultural and food products. *FGBNU VNIITTI*. 2017, 522-525.
http://www.vniitti.ru/conf/conf2017/article/PeschanskayaV.A._OsipovaV.P._statya.pdf

37. Bitra, V.S.P.; Womac, A.R.; Yang, Y.T.; Miu, P.I.; Igathinathane, C.; Nehru, C.; Sokhansanj, S. Characterization of wheat straw particle size distributions as affected by knife mill operating factors. *Biomass & Bioenergy*. **2011**, 35, 3674-3686. https://doi.org/10.1016/j.biombioe.2011.05.026

38. Wills, B. A.; Finch, J. A. Particle Size Analysis. Wills' Mineral Processing Technology; Elsevier Science & Technology Books, 2016; pp. 91–107. https://doi.org/10.1016/b978-0-08-097053-0.00004-2

PHYSICOCHEMICAL CHARACTERIZATION OF A POMEGRANATE PEEL-BASED NEW ADSORBENT GENERATION USED IN BISPHENOL A ELIMINATION

Rihab BOUSSAID[1] , Goussem MIMANNE[1,2] , Hayat MOKDAD[1,3] , Karim BENHABIB[2] , Mohammed BEZZINA[4] *

[1]Laboratory of Materials & Catalysis, Faculty of Exact Sciences, Djillali Liabes University, BP 89, Sidi Bel Abbes, Algeria
[2]Eco-Process, Optimization and Decision Support. Jules Verne University of Picardie (EPROAD, UR 4669), France
[3]Department of Sciences and Technology, Faculty of Sciences. Saad Dahlab University of Blida 1, Soumaa Route 09000, Algeria
[4]Laboratory for functional analysis of chemical processes. University of Blida 1, 09000. Algeria

Bisphenol A (BPA) is one of the chemical compounds used in the industry. The ongoing accumulation of this organic compound has a significant and harmful impact on the environment and human health. This study has several objectives, including the reduction of waste rates, the development of a less inexpensive adsorbent material than commercial activated carbon, and the purification of polluted water. The choice of waste used is based on its abundance and availability. To this end, pomegranate peel was selected as a precursor for the preparation of activated carbon using H_3PO_4 at different temperatures was carried out. The characterization of the best adsorbent by SEM, TGA/DTA, XRF, FTIR, and XRD depicted that AC500 has a heterogeneous surface with a higher carbon percent (93%), the disappearance of several organic functions, giving way to C-C bonds, and an amorphous structure. The rates of moisture and ash are 2.69% and 3.9%, respectively. The values of the iodine and methylene blue numbers are 842.45 $mg\cdot g^{-1}$, and 476.23 $mg\cdot g^{-1}$, respectively, indicating the microporous and mesoporous structure of AC_{500}, which confirms the SEM results. The acidic character of AC_{500} has been proven by PZC (5.1), zetametry, and Boehm titration. This new structure imparts it with an adsorption capacity exceeding 91% for the removal of BPA. The obtained results suggest that pomegranate peel holds promising potential as a sustainable resource, offering a hopeful perspective for environmental pollution remediation.

Keywords: Bisphenol A, agri-food waste, pomegranate peel, adsorption.

INTRODUCTION

The issue of the phenolic endocrine disruptor raised worries among people because the contaminants have been often detected in the different water sources recently. There are various sources that allow Bisphenol A (BPA) into the environment. Low quantities of BPA are allowed to be thrown in the atmosphere and surface water by the industry and elaboration firms because a food contamination would take place if the objects that contain BPA or BPA monomer are found in the environment (air, water and soil). Therefore, humans shall be affected through the oral track due to the consumption of the foods conserved in packages that contain polymerized BPA. The molecules of the monomer or non-monomer BPA may move to the foods matrices or the drinking water through plastic (bottles, conserves, cans, baby bottles…) (1). New discoveries showed that the Bisphenol A represents the estrogenic activity at a low dose of 0.23 pg/ml of the culture milieu. Moreover, many

tests in vitro and in vivo confirmed that the Bisphenol A increases the infertility, affects the genital tracts, and causes the breast cancer (2).

Therefore, it is important to develop an efficient technology to eliminate the Bisphenol A of the hydric milieu. Many methods of degradation and/ or removal Bisphenol A from wastewater have been researched, including the biological treatment (3), photocatalysis (4), electrochemical processes (5), piezocatalysis (6), and adsorption (7).Various adsorbents have been used for removing Bisphenol A from wastewater, such as zeolites, polymers, chitosan, clays and activated carbons (8).

The adsorption on the activated carbon is generally considered as one of the most efficient methods to control the organic contaminants in water. Many studies found out the efficiency of the activated carbon in adsorption the Bisphenol A. Bautista-Toledo (9) considers that the Bisphenol A adsorption depends mainly on the nature of the surface of the activated carbon and the chemical properties of the solution.

The choice of pollutant was made based on its toxicity, knowing that it is used in the manufacture of plastic utensils (bottle, box, feeding bottle...). The transfer of Bisphenol A to containers has been proven. Even at low doses, the BPA is considered as a major endocrine disruptor, it is carcinogenic, and exposure to BPA can cause hypertension, diabetes type 2, cardiovascular diseases, and blood disorders. To the best of our knowledge, pomegranate peel has not been used for the removal of BPA. This agri-food is rich in carbon (63%), its physical and/or chemical modification gave an adsorbent as effective as commercial activated carbon in the removal of BPA.

Thus, our work aims at valorizing the agri-food waste through activating it to get a performing activated carbon to eliminate the endocrine disruptor "Bisphenol A". The prepared activated carbon is considered a new generation adsorbent that is inexpensive and as efficient as commercial activated carbon.

EXPERIMENTAL

PRE-TREATMENT OF THE RAW MATERIAL

A very important collection of the pomegranate peel has been carried out. The preparation of the barks takes three physical steps:
a) Washing has been made through contacting waste with distilled water to eliminate the residues.
b) Drying the waste was carried out with the solar energy and in furnace between 40 °C and 50 °C in order to prevent the eventual alteration of the physiochemical properties of the materials.
c) The grinding has been conducted to get homogenous powder needed for the laboratory studies. The process gave little grains of less than 2 mm.

Preparation of the activated carbon

The dry pomegranate peel has been impregnated during 2 h with a phosphoric acid solution of 1N concentration. The waste was suspended in the acid solution until boiling under reflux at a temperature of 115 °C. At the end of this step, the powders were separated of the solution through a simple filtration without washing. The obtained material was placed in a ceramic crucible and carbonized in a muffle furnace from 300 °C to 800 °C for 1h. After carbonization, the samples were washed with distilled water many times until getting a

pH≥6 of the filtrate in order to eliminate the ashes. The activated carbon obtained was dried in the furnace at 100 °C for 24 h.

In the end, six materials were obtained, namely:

Calcined **A**ctivated **C**arbon at 300 °C (**AC₃₀₀**)
Calcined **A**ctivated **C**arbon at 400 °C (**AC₄₀₀**)
Calcined **A**ctivated **C**arbon at 500 °C (**AC₅₀₀**)
Calcined **A**ctivated **C**arbon at 600 °C (**AC₆₀₀**)
Calcined **A**ctivated **C**arbon at 700 °C (**AC₇₀₀**)
Calcined **A**ctivated **C**arbon at 800 °C (**AC₈₀₀**)

CHOICE OF THE BEST ADSORBENT

The activated carbon's adsorption of BPA is tested.

The BPA adsorption rate has been determined through adding a mass of 0.3 g of each prepared activated carbon in a series of beakers of 50 ml of BPA solution of an initial concentration of 20 mg·L⁻¹. The assays have been carried out under constant agitation during 24 h. The samples were filtered in order to determine the residual concentrations of BPA at a maximal wavelength λ_{max}= 276 nm through spectrophotometer UV-visible (PerkinElmer Lambda 45).
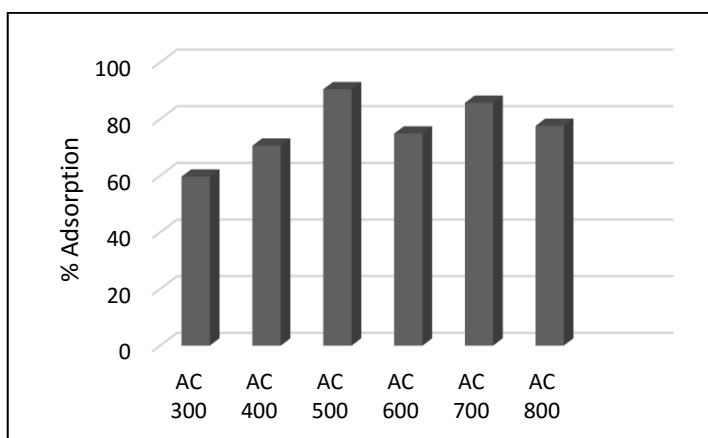

Figure 1. BPA adsorption rate by different types of AC

According to Figure 1, the most important elimination rate (91%) of Bisphenol A is obtained for the (AC₅₀₀). Based on these adsorption tests, (AC₅₀₀) will be chosen for the next assays of this study.

CHARACTERIZATION OF THE PREPARED ACTIVATED CARBON (AC₅₀₀)

Zero-point charge pH (pH$_{pzc}$)

The pH$_{pzc}$ refers to the pH value at which the net charge of the adsorbent surface is null. A rapid and simple way to determine the zero-point charge is through putting 50 ml of

distilled water in a beaker and adjusting the pH of each (values between 2 and 12) through adding the NaOH or HCl solutions (0.1 M). Then, 0.5g of the material is added to each er-lenmeyer to be characterized. The suspensions must be maintained under agitation at an ambient temperature during 24 h; thus, the final pH is measured. In tracing the curve $\Delta pH = f(pH_i)$, the value of pH_{pzc} results from the intersection of the curve with the x-axis (10).

Measuring the zeta potential

It allows the determination of the electric charge of a particle. Therefore, we measured the zeta potential of the synthesized carbon AC_{500} to be able to determine the surface charge and, thus, predict the type of interaction between the carbon particles and the adsorbed molecules. These measures have been conducted by using zeta-potential analyzer Malvern Zetasizer.

Boehm titration

A mass of 0.15 g of each sample has been mixed with 50 ml of a water solution of 0.1 N of the reagent (NaOH, or Na_2CO_3, or $NaHCO_3$, or HCl). The dispersions were agitated for 72 h at a speed of 300 rpm and 25 °C. Then, they were filtered. To determine the rates of the oxygenated groups and the basic groups, titrations in the return of the filtrate (30 mL) were made respectively with the solutions HCl (0.1 mol·L^{-1}) and NaOH (0.1 mol·L^{-1}).

Iodine number

Iodine number allows measuring the microscopic contents of an adsorbing material. The iodine adsorption capacity of each material has been determined according to the operatory mode that follows (10): 10 ml of the iodine solution at 0.01 N has been titrated using a solution of sodium thiosulfate 0.1 N in the presence of a starch solution as an indicator until the disappearance of the color. The reading volume corresponding to V_b. 0.05 g of the acti-vated carbon had been mixed at 15 ml of an iodine water solution (0.1 N) and vigorously agitated for 5 min. The mixture was titrated with a standard solution of sodium thiosulfate using a starch solution as an indicator and maintaining the volume of the burette at V_S. The iodine number is calculated through the following formula:

$$I.\,N. = \frac{(V_b - V_s)N.\,(126.9).\,\left(\frac{15}{10}\right)}{M} \qquad [1]$$

- I.N: iodine number (mg. g^{-1})
- V_b and V_S: volume of sodium thiosulfate solution required for blank and sample titrations respectively (mL)
- N: normality of sodium thiosulfate solution (N)
- 126.9: Atomic weight of iodine (g·mol^{-1}).
- M: mass of AC_{500} used (g).

Methylene Blue number

The methylene blue number (mg. g^{-1}) is an indicator of the carbon's capacity of adsor-bing the average and big organic molecules. It characterizes the carbon mesopores. In order

to determine this number, we used the method of the European Center of the Chemical Industry Federations as used by Al-Eraky et al (11). In an Erlenmeyer of 250 ml, 0.1 g of the AC_{500} and 10 ml of the blue methylene solution at a concentration of $1.944 \cdot 10^{-5}$ M are introduced. The mixture is agitated for 20 min and is, then, filtered. The residual concentration in the methylene blue is determined with a UV-visible spectrophotometer at a wavelength of 620 nm. Besides, the methylene blue number is given by the following relation:

$$M.B. = \frac{V \times M \times (C_i - C_r)}{m_c} \times 100 \qquad [2]$$

- V: Volume of methylene blue solution (ml)
- M: Atomic weight of methylene blue (g.mol^{-1})
- C_i: initial concentration of methylene blue (mol. L^{-1})
- C_r: residual concentration of methylene blue (mol. L^{-1})
- m_c: Mass of AC_{500} used (g).

Ash rate

The ash rate determines the inorganic, inert, amorph, and unused part present inside the activated carbon. The ash rates are determined with the method described in the literature (12). A sample of 0.5 g of the AC_{500} is dried in a furnace at 80 °C for 24h and, then, is put in a ceramic crucible which is put in a muffle furnace at a temperature of 650 °C for 3 hours. After cooling in an ambient temperature, the ceramic crucible is weighted. The ash rate is measured as follows:

$$Ash\% = \frac{M_3 - M_2}{M_1} \times 100 \qquad [3]$$

- M_1: initial mass of AC_{500} used (g).
- M_2: mass of crucible before carbonization (g).
- M_3: mass of the filled crucible after carbonization (g).

The moisture rate

The moisture rate is a relation expressed in percentage and calculated with equation [4] (12). A dose of 0.5 g of the AC_{500} was put in a ceramic crucible and weighted. This sample is dried and put in a furnace at 110 °C until the weight becomes constant. When taking it out of the furnace, the crucible is cooled at an ambient temperature and, then, weighted. The moisture rate is calculated as follows:

$$moisture\ \% = \frac{M_1 - M_2}{M_1} \times 100 \qquad [4]$$

- M_1: initial mass of AC_{500} used (g).
- M_2: mass of the filled crucible after drying (g).
- M_3: mass of the filled crucible before drying (g).

TGA/DTA Analysis

The thermogravimetric analysis and differential thermal analysis consist of measuring the variation of the mass of a sample according to the increase of the temperature. TGA allows understanding the behavior of the adsorbent and evaluating the quantity of the surface functions and their proportions based on the characteristic temperatures of decomposition (13). This analysis is made by simultaneous thermal analyzer PERKINELMER STA 8000 in the center of the physio-chemical analyses in Bejaïa (Algeria). The thermal evaluation of the materials (10 mg) is made at 50 °C till 1000 °C following a ramp of 10 °C·min^{-1}.

X-ray Fluorescence

It is an elementary analysis technique that allows the determination of the thermal species contained in a sample.

In this work, we used it to determine the chemical composition of the pomegranate peel and AC_{500}. The analysis is made with ZSX Primus II de Rigaku.

FTIR analysis

The surface functional groups were studied with FTIR (Perkin Elmer Universal ATR Sampling Accessory). The FTIR specters of pomegranate peel and of the resulting raw material (AC_{500}) are between 650 and 4000 cm^{-1}.

XRD analysis

The XRD diffractograms were registered with a panalytical x'pert pro diffractometer in the set 2θ between 10-920° with a step of 0.02° and a counting time of 1s, using K_{α} ray of the copper (λ = 1,5406 Å).

SEM analysis

The morphology of the adsorbent material is given in luminous images at different magnifications by the scanning electron microscope (Quanta 250 of FEI Company).

Adsorbate

The endocrine disturber of this study is the Bisphenol A (BPA) with the chemical formula $C_{15}H_{16}O_2$ (M=228.28 g·mol^{-1}), which is in the form of soluble crystals in water. The pollutant was used without any preliminary purification.
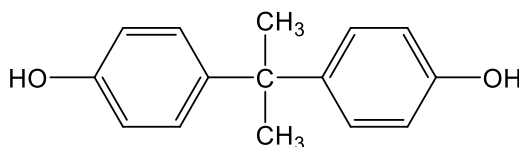

Figure 2. Molecular structure of Bisphenol A

RESULTS AND DISCUSSION

CHARACTERIZATION OF THE ADSORBENT

The pH_{pzc} of AC_{500} is 5.1 which shows that the surface is positively charged (high content of acid groups) (Figure 3a).

Undoubtedly, this is due to the fact that the solution used in the chemical activation is acid (activation with H_3PO_4). This result agrees with those obtained by the zetametry (Figure 3b) and Boehm titration (Table 1). It shows that AC_{500} has acid functions and that there are oxygenated groups that allow an important adsorption of the cationic pollutants. In fact, H_3PO_4 is a strong oxidant that can oxidize the surface carbon atoms and make them lose electrons to be positively charged (14).

The activated carbon surface may acquire a negative or positive charge according to the pH of the medium. When the pH of the solution is less than the pH_{pzc} of AC_{500} ($pH < pH_{zpc}$), this has a basic behavior that encourages the adsorption of the anionic species. Contrarily, if the pH of the medium is more than the pH_{pzc} of the AC_{500} ($pH > pH_{zpc}$), the surface of the activated carbon presents a negative charge that encourages the adsorption of the cationic species (15).

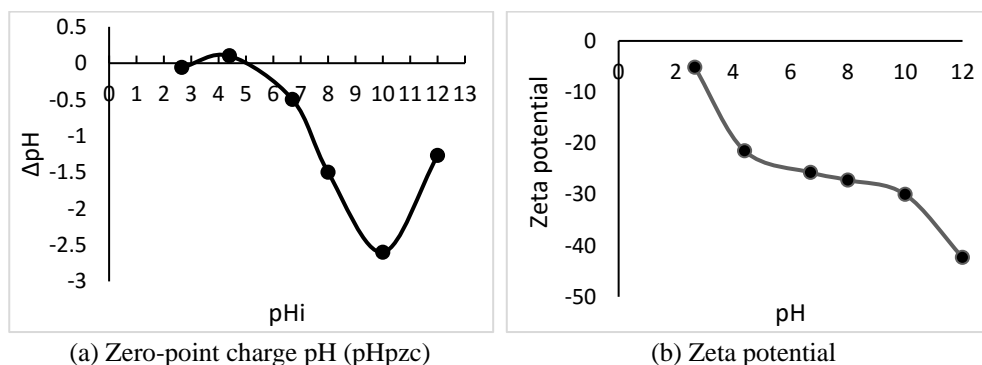(a) Zero-point charge pH (pHpzc)   (b) Zeta potential

Figure 3. Surface charge of the AC_{500}

The main chemical and textural properties of the prepared activated carbon are grouped in Table 1.

**Table 1.** Physico-chemical parameters of AC_{500}

Characteristics	Values
pH_{zpc}	5.1
Acid functions (%)	75.3
Basic functions (%)	24.7
Iodine number (mg·g^{-1})	842.45
Methylene Blue number (mg·g^{-1})	476.23
Ash content (%)	3.9
Moisture content (%)	2.69

The value of the iodine number of the AC_{500} that is superior to 842.45 mg·g^{-1} indicates that the adsorbent possesses a very developed microporosity. The value of the methylene blue number of AC_{500} (476.23 mg·g^{-1}) shows the presence of mesopores.

The rates of the moisture and ashes are 2.69% and 3.9%, respectively. According to the results, the low ashes content indicates that the precursor may resist the high temperature treatment during the carbonization and the chemical activation (16). This parameter has a significant effect on the quality of the activated carbon. Thus, the high rate of ash reduces the specific surface. In fact, the inorganic nature of the ashes makes the activation process difficult because they clog the pores of the carbonized structure (17).

Thanks to the thermogravimetric analysis, the loss of the mass of the raw pomegranate powder and of AC_{500} (Figure 4) according to the heating temperature can be tracked.

Figure 4 represent TGA and DTA curves of the mass losses by the thermal decomposition made at a heating speed of 10 °C/min for the pomegranate peel and AC_{500}. The thermal degradation of the two samples has four (04) steps.
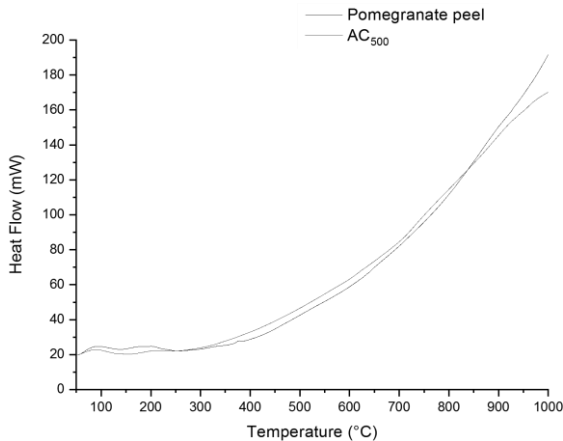
(a) Thermogravimetric analysis (TGA)
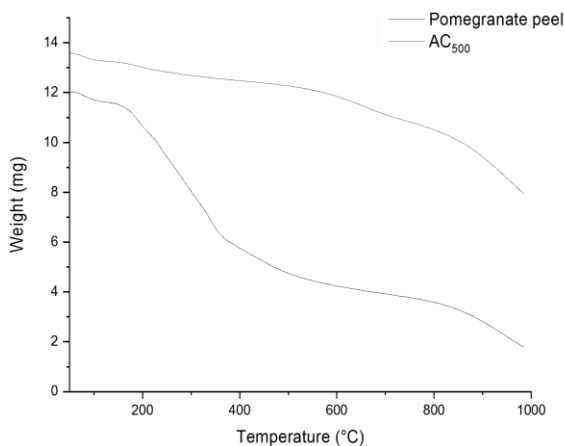
b) Differential thermal analysis (DTA)

Figure 4. Thermal analysis of pomegranate peel and AC_{500}

The first step of the loss of the mass is made at about 110 °C. This loss corresponds to physiosorbed water.

The second step takes place at about 200-325 °C for the pomegranate peel. This loss is due to the liberation of gaseous components (CH_4, CO_2, CO, H_2) and the degradation of the hemicellulose.

The third step is due to the degradation of the cellulose which is observed at about 325-390 °C. The lignin, due to its complex structure, undergoes the last step of the thermal degradation and takes place in a large set of temperatures between 100-900 °C (18).

The results of the XRF analysis of the pomegranate peel and the AC_{500} allow having the major composition of the chemical elements. The analysis shows that the two samples are majorly constructed of carbon. The highest rate is that of the carbon. This result confirms that the activated carbon AC_{500} is a strongly carbonized material. The other minerals: phosphor, potassium, and chlorine result from the composition of the start precursors or the activating agent.

The presence of phosphor may be due to the reaction of the phosphate ions with the precursor of the pomegranate peel. The rates of the different elements are given in Table 2.

Table 2. XRF results of pomegranate peel and AC_{500} prepared

Element (%)	C	O	P	K	Cl
Pomegranate peel	63	33	0.04	1.07	0.69
AC_{500}	93	0	4.07	0.65	0.07

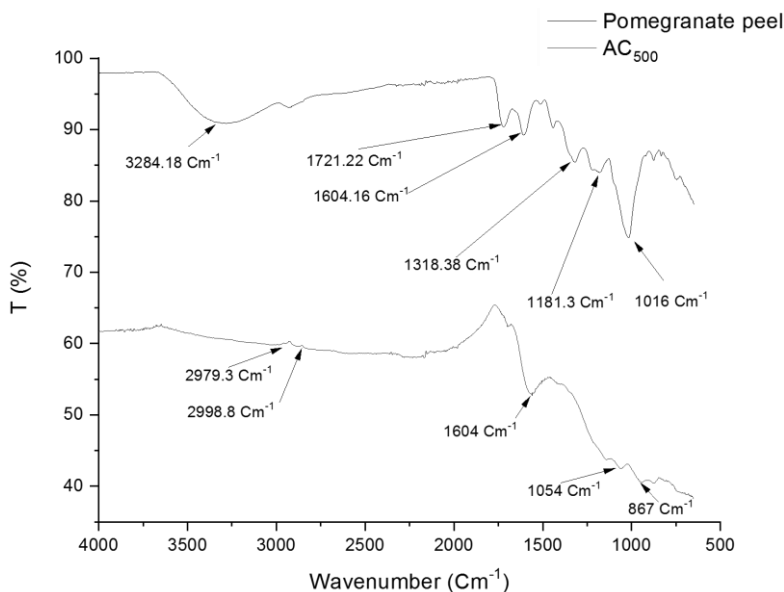Examination of the FTIR spectra (Figure 5) shows different absorption bands which are collected in Table 3.

Figure 5. FTIR spectra of pomegranate peel and AC_{500}

Table 3. Spectral characteristics of pomegranate peel and AC$_{500}$

Wavenumbers (cm^{-1})	Attribution
Pomegranate peel	
3200-3400	the elongation vibrations of the hydrogen of the hydroxyls groups O-H (of the carboxyls, phenols, or alcohol) and the adsorbed water (19)
1721	the liaisons C=O of the carboxylic acid functions of hemicellulose and lignine (20)
1604	the liaisons C=C of the aromatic cycles (20,21).
1318.38	the band is attributed to the methoxy groups C-O of the lignin (22).
1181.3	C-O (alcohols, carboxylic acids, ester, and ethers) (20)
1016	the elongation vibration C-O-C of cellulose and hemicellulose (23)
AC$_{500}$	
	A change in the intensity and the width of the peaks is noticed: There is an increase in the intensity and the width of the vibration band due to the grouping of O-H (3284 cm^{-1} for the natural pomegranate and of 3671 cm^{-1} for the AC$_{500}$). We notice a disappearance of some groupings and the appearance of others such as:
2979 and 2998	- Appearance of weak bands (C-H) at 2979 and 2998 cm^{-1} (20). - Disappearance of the functions C=O (1721 cm^{-1}) - The functions C=C of the aromatic cycles [20].
1604	- Decrease of the intensity of the bands between 1000 and 1350 cm^{-1} (C-O) of the synthesized material.
1054	- The band at 1054 cm^{-1} is attributed to the C-O functions (23).
867	- Appearance of a band at 867 cm^{-1} corresponding to the aromatic liaisons C-H (22).

The X rays diffraction studies can determine the degree of the crystalline or the amorph nature of the activated carbon. XRD profile of the pomegranate peel and the prepared activated carbon AC$_{500}$ are shown in Figure 6.
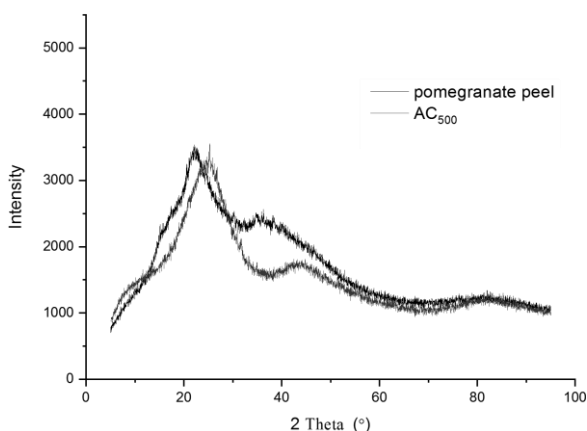
**Figure 6.** X-ray diffraction spectra of pomegranate peel and AC$_{500}$

The Figure 6, generally shows the amorph structure of both materials and a weak crystallinity of the samples in the domain between 10° and 43°.

The diffraction diagram of the raw pomegranate peel presents a peak at 22° due to the presence of native cellulose that is present in the composition of the pomegranate peel.

The diffraction diagram of the activated carbon shows certain patterns and presents the diffraction intense peak at 25° due to the presence of the carbon/graphite.

A small peak at 43° is due to the presence of dehydrated hemicellulose. The appearance of this peak shows that the activation process has been well made. The same was observed in many works (24, 25, 26).

A morphological study was carried out through observation by SEM in order to analyze the structure of the pomegranate peel particles and of the synthesized activated carbon AC_{500} and their texture. The observations at different magnifications of the pomegranate peel and AC_{500} before and after BPA adsorption are shown in Figure 7a-c, respectively.
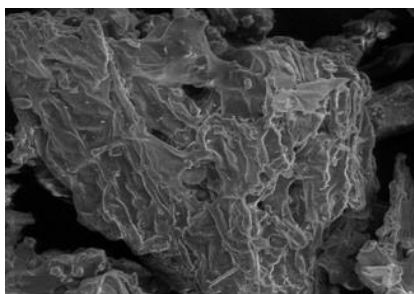
(a) Pomegranate peel
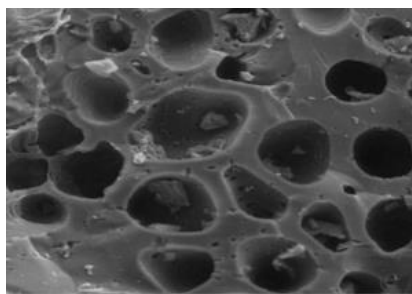
(b) AC_{500} before adsorption
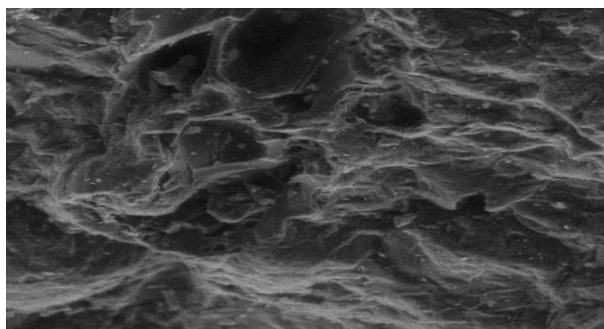
(c) AC_{500} after adsorption

Figure 7. SEM images

The images show a heterogeneous distribution of the pores on the surface of the materials analyzed. In fact, the aim of the examination with SEM is to illustrate the porosity, mainly the one created by the activation. A developed porosity allows increasing the specific surface of the adsorbent material and, thus, the number of the active sites on which the molecules may eventually be fixed (11). In addition, an observation at a strong magnification reveals the presence of an internal porosity with micrometers pore sizes (Figure 7b).

This internal porosity shall contribute to increasing the specific surface and the adsorption capacity. Regarding the morphological aspect of activated carbon after bisphenol A adsorption, SEM image reveal a modification of activated carbon morphology and the pores filling by bisphenol A (Figure 7c). A radical change in the surface texture of activated carbon was observed.

CONCLUSION

In conclusion, pomegranate peel, after chemical treatment with H_3PO_4 followed by carbonization at 500 °C, gives rise to a highly efficient adsorbent material with a Bisphenol A (BPA) removal rate exceeding 91%. Comparing this adsorption percentage to that of untreated pomegranate peel, which is 0%, allows us to infer a significant modification to the material's structure through chemical and thermal activation. This has been confirmed through physicochemical characterizations.

The obtained results indicate that after activation, several organic functions have disappeared, giving way to C-C bonds. This implies that the carbonaceous skeleton becomes predominant in the composition of the developed activated carbon. According to scanning electron microscopy (SEM) images, the formation of pores is clearly visible. By comparing the two SEM images of pomegranate peel and activated carbon, a radical change in the surface texture was observed. Finally, pomegranate powder can be classified as an economical precursor for activated carbon production, exhibiting excellent adsorptive characteristics for the removal of BPA from aqueous solutions. This confirms the potential of activated carbon derived from pomegranate peel for commercial applications.

Acknowledgements

REFERENCES

1. Marzougui, Z.; Chaabouni, A.; Elleuch, B.; Elaissari, A. Removal of bisphenol A and some heavy metal ions by polydivinylbenzene magnetic latex particles. *Environ Sci Pollut Res*. **2016**, *23*(16), 15807-15819. doi:10.1007/s11356-015-5407-5

2. Liu ,G.; Ma, J.; Li, X.; Qin, Q. Adsorption of bisphenol A from aqueous solution onto activated carbons with different modification treatments. *J Hazard Mater*. **2009**, *164*(2-3), 1275-1280. doi:10.1016/j.jhazmat.2008.09.038

3. Frankowski, R.; Zgoła-Grześkowiak, A.; Smułek, W.; Grześkowiak, T. Removal of Bisphenol A and Its Potential Substitutes by Biodegradation. *Appl Biochem Biotechnol*. **2020**;*191*(3), 1100-1110. doi:10.1007/s12010-020-03247-4

4. Cardona, Y.; Węgrzyn, A.; Miśkowiec, P.; Korili, S.A.; Gil, A. Catalytic photodegradation of organic compounds using TiO2/pillared clays synthesized using a nonconventional aluminum source. *Chem Eng J*. **2022**, *446*(March). doi:10.1016/j.cej.2022.136908

5. Lugo-Bueno, S.F.; García-Morales, R.; Coronel, R.; et al. Biocatalysis assisted by electrochemical processes for the removal of bisphenol A and triclosan in wastewater. *Environ Technol Innov*. **2022**, *28*, 102921. doi:10.1016/j.eti.2022.102921

6. Zhou, Q., Li, N.; Chen, D.; et al. Efficient removal of Bisphenol A in water via piezocatalytic degradation by equivalent-vanadium-doped SrTiO3 nanofibers. *Chem Eng Sci*. **2022**, *247*, 116707. doi:10.1016/j.ces.2021.116707

7. Meneses, I.P.; Novaes, S.D.; Dezotti, R.S.; Oliveira, P.V.; Petri, D.F.S. CTAB-modified carboxymethyl cellulose/bagasse cryogels for the efficient removal of bisphenol A, methylene blue and Cr(VI) ions: Batch and column adsorption studies. *J Hazard Mater*. **2022**, *421,* 0-3. doi:10.1016/j.jhazmat.2021.126804

8. Naganathan, K.K.; Faizal, A.N.M.; Zaini, MAA.; Ali, A. Adsorptive removal of Bisphenol a from aqueous solution using activated carbon from coffee residue. *Mater Today Proc*. **2020,** *47,* 1307-1312. doi:10.1016/j.matpr.2021.02.802

9. Bautista-Toledo, I.; Ferro-García, M.A.; Rivera-Utrilla, J.; Moreno-Castilla, C.; Fernández, F.J.V. Bisphenol A removal from water by activated carbon. Effects of carbon characteristics and solution chemistry. *Environ Sci Technol*. **2005**, *39*(16), 6246-6250. doi:10.1021/es0481169

10. Boudia, R.; Mimanne, G.; Benhabib, K.; Pirault-Roy, L. Preparation of mesoporous activated carbon from date stones for the adsorption of Bemacid Red. *Water Sci Technol*. **2019**, *79*(7), 1357-1366. doi:10.2166/wst.2019.135

11. Al-Eraky, M.M.; Mohamed, N.; Kamel, F.; et al. of Advanced Research Teaching Professiona-lism By Vignettes in Psychiatry for Nursing Students. *Int J Adv Res*. **2016**, *4*(6), 625-634. doi:10.21474/IJAR01

12. Ahmed, M.J,; Dhedan, S.K. Equilibrium isotherms and kinetics modeling of methylene blue adsorption on agricultural wastes-based activated carbons. *Fluid Phase Equilib*. **2012**, *317*, 9-14. doi:10.1016/j.fluid.2011.12.026

13. Bounaas, M.; Bouguettoucha, A.; Chebli, D.; et al. High efficiency of methylene blue removal using a novel low-cost acid treated forest wastes, Cupressus semperirens cones: Experimental results and modeling. *Part Sci Technol*. **2019**, *37*(4), 500-509. doi:10.1080/02726351.2017.1401569

14. Léonce Kouadio, D.; Diarra, M.; Djassou, A.C.; et al. Etude expérimentale de l'adsorption du bleu 16 et du méthyle rouge sur du charbon issu de la coque de la cabosse de cacao. *J Soc Ouest-Afr Chim*. Published online **2022**, 51.

15. Abba, A.; Danga, R. Removal Of Purple Of Bromocresol From Aqueous Solutions By Biosorp-tion On A Tropical Biomass: The Triplochiton Scleroxylon (ayus) Saw. *Journal des Sciences Hydrauliques*, **2019**, *16*(3), 215-232.

16. Garba, Z.N.; Rahim, A.A. *Evaluation of Optimal Activated Carbon from an Agricultural Waste for the Removal of Para-Chlorophenol and 2,4-Dichlorophenol*. Vol 102. Institution of Chemical Engineers; **2016**. doi:10.1016/j.psep.2016.02.006

17. Mamane, O.S., Zanguina, A.; Daou, I.; Natatou, I.; De, J. Chimie SO africaine De. Préparation et caractérisation de charbons actifs à base de coques de noyaux de Balanites Eagyptiaca et de Zizyphus Mauritiana. *J. Soc. Ouest-Afr Chim*. **2016,** *41,* 59-67.

18. Aziri, S. Utilisation des déchets agro-industriels pour l'élimination du chrome hexavalent en solution aqueuse. Ph.D.Thesis, University of Mouloud Mammeri, 2018.

19. Belala, Z.; Jeguirim, M.; Belhachemi, M.; Addoun, F.; Trouvé, G. Biosorption of basic dye from aqueous solutions by Date Stones and Palm-Trees Waste: Kinetic, equilibrium and thermodyna-mic studies. *Desalination*. **2011**, *271*(1-3), 80-87. doi:10.1016/j.desal.2010.12.009

20. El Messaoudi, N.; El Khomri, M.; Bentahar, S.; Dbik, A.; Lacherai, A.; Bakiz, B. Evaluation of performance of chemically treated date stones: Application for the removal of cationic dyes from aqueous solutions. *J Taiwan Inst Chem Eng*. **2016**, *67* (January 2018), 244-253. doi:10.1016/j.jtice.2016.07.024

21. Bouchelta, C.; Medjram, M. S.; Bertrand, O.; and Bellat, J. P. Preparation and characterization of activated carbon from date stones by physical activation with steam, *J. Anal. Appl. Pyrolysis*, **2008**, *82*(1), 70–77. doi: 10.1016/j.jaap.2007.12.009.

22. Al-Ghouti, M.A.; Hawari, A.; Khraisheh, M. A solid-phase extractant based on microemulsion modified date pits for toxic pollutants. *J Environ Manage*. **2013**, *130*, 80-89. doi:10.1016/j.jenvman.2013.08.045

23. Janković, B.; Manić, N.; Dodevski, V.; Radović, I.; Pijović, M.; Katnić, Đ.; Tasić, G. Physico-chemical characterization of carbonized apricot kernel shell as precursor for activated carbon preparation in clean technology utilization. *J Clean Prod.* **2019**, *236*, 117614. doi:10.1016/j.jclepro.2019.117614

24. Djeziri, S.; Taleb, Z.; Djellouli, H.M. Kinetic Study of Adsorption of Phenolic Compounds From Olive Oil Mill Wastewater on Activated Carbon. *Acta Period Technol*. **2023**, *54,* 197-208. doi:10.2298/apt2354197d

25. Mekhalef Benhafsa, F. Fixation de certaines molécules organiques polluantes des eaux (colorant Victoria Bleu Basique) par divers adsorbants. Ph.D. Thesis, University of Djilali Liabes, Sidi BEL Abbes, Algeria. **2019.**

26. Supong, A.; Bhomick, P.C.; Baruah, M.; Pongener, C.; Sinha, U.B.; Sinha, D. Adsorptive removal of Bisphenol A by biomass activated carbon and insights into the adsorption mechanism through density functional theory calculations. *Sustain Chem Pharm*. **2019**, *13*(April), 100159. doi:10.1016/j.scp.2019.100159

CHEMOMETRIC MODELING OF BIOCONCENTRATION FACTOR OF 6-CHLORO-1,3,5-TRIAZINE DERIVATIVES BASED ON MLR-QSPR APPROACH

Milica KARADŽIĆ BANJAC [ID], *Strahinja KOVAČEVIĆ** [ID],
Sanja PODUNAVAC-KUZMANOVIĆ [ID], *Lidija JEVRIĆ* [ID]

Faculty of Technology Novi Sad, University of Novi Sad, Bulevar Cara Lazara 1, Novi Sad, Serbia

Pesticides have an important role in agriculture since they can prevent large crop losses which is crucial in order to keep pace with population growth that is estimated to be 9.7 billion people by the year 2050. The use of pesticides is not always in accordance with good agricultural practice so the human and environmental exposure to pesticides are a continuing concern. Some triazine derivatives are well-known commercially available pesticides with proven activity. The researchers have task to design and develop new pesticides with diminished negative influence on environment and humans together with a good crop protection ability. In order to achieve this, many computational and artificial intelligence tools have been used along with extensive experimental work. A group of twenty-one 6-chloro-1,3,5-triazine derivatives was investigated in the domain of bioconcentration factor, as an indicator of the bioaccumulation potential of a substance, and multiple linear regression (MLR)-quantitative structure-property relationship (QSPR) modeling was conducted. The proposed MLR-QSPR model was extensively statistically validated in order to provide reliable model for further research work. All conducted procedures, internal and external validation as well as normality test of residuals indicated good fitness, absence of systematic error in model development and high predictive ability of the proposed model.

Keywords: chemometrics, ecotoxicity, multiple linear regression, pesticides.

INTRODUCTION

Considering today's fast-growing population, agricultural and food industry have to ensure enough food supplies. Since it is necessary to maintain good quality with the highest possible crop yield, the use of various pesticides is widespread. Pesticides affect weed, insect, bacteria, fungi, etc. but also contribute to the environmental (water, soil and crops) pollution (1-3). One of the many derivative groups used in agricultural purposes are triazine derivatives (4). The first use of triazine herbicides was in 1957 when simazine was approved for commercial use (5). Triazines are effective in weed control and they are used as pesticides (6), herbicides (7) and antifungal compounds (8). In today's modern society and agriculture, new pesticides have to meet toxicological, ecological, environmental and economical requirements.

In silico approach can have a great contribution regarding the estimation of the influence of compounds on the environment since pesticides can have high toxic effect on water, soil and crops as well as on human health (9, 10). Quantitative structure-activity relationship (QSAR) mathematical models together with in silico methods are commonly used for prediction of: toxicity towards aquatic organisms (11, 12), bioconcentration factor (BCF) (13, 14) and biodegradability (15, 16). The bioconcentration factor (BCF) represents an indicator of the bioaccumulation potential of a substance and it is a key parameter when environmental risk assessment is considered (17, 18). The use of chemometric tools with

aim to obtain models for BCF prediction is useful for the cost reduction (number of animals used in the experiments which are of expensive nature) and for the environmental risk assessment (aquatic toxicology). There are many ways for BCF prediction including various physicochemical properties expressed as molecular descriptors (19-21). Nowadays, different software solutions such as VegaNIC (Virtual models for property evaluation of chemicals within a global architecture) (22), Toxicity Estimation Software Tool (TEST) (23), Chemical Properties Estimation Software System (ChemProp) (24), etc are being used. The maximum and limit values when it comes to the bioconcentration are regulated by legislation of individual region or country. If focusing on the European Union, regulatory framework refers to the European Chemical Agency of the European Union, REACH – Registration, Evaluation, Authorization and Restriction of Chemicals Regulation, Regulation (EC) No 1907/2006 (25). The BCF has a great roll in life cycle and environmental risk assessment and it was extensively researched when it comes to triazine derivatives and their residues. Researchers investigated triazine herbicides in terms of environmental risk assessment and toxicity in the Yellow Sea and Bohai Sea of China (26), risk assessment of triazine herbicides in surface waters in Southeast Florida (27), thermal and metabolic factors affecting bioaccumulation of triazine herbicides by rainbow trout (28), etc.

This study represents the continued research regarding the triazine derivatives, particularly the derivatives of 6-chloro-1,3,5-triazine derivatives, after our previously published researches (29-33). In this paper, BCF was the central point of interest. Multiple linear relationship (MLR) modeling was used to correlate selected molecular descriptors (maxsCl, LipoaffinityIndex and ATSp5) with the bioconcentration factor (BCFmeylan) in order to obtain statistically meaningful and valid model. The justifiability of the presented quantitative structure-property relationship (QSPR) model was evaluated through internal and external validation procedures and the model was confirmed to be of high statistical quality and significant predictive ability.

MATERIAL AND METHODS

THE SERIES OF 6-CHLORO-1,3,5-TRIAZINE DERIVATIVES

The set of the studied compounds included twenty-one 6-chloro-N^2,N^4-, 6-dichloro-N- and 6-chloro-N^2,N^4-bis(1-methylcyclopentyl) triazine derivatives. The IUPAC names of the studied compounds are listed in Table 1. The compounds were synthesized at the Faculty of Technology and Metallurgy, University of Belgrade, according to the procedures given previously in the literature (34, 35).

Table 1. The IUPAC names of the analyzed triazine derivatives

Compound	IUPAC name
1	6-chloro-N^2,N^4-dipropyl-1,3,5-triazine-2,4-diamine
2	6-chloro-N^2,N^4-bis(propan-2-yl)-1,3,5-triazine-2,4-diamine (propazine)
3	N^2,N^4-bis(butan-2-yl)-6-chloro-1,3,5-triazine-2,4-diamine
4	6-chloro-N^2,N^4-bis(2-methylpropyl)-1,3,5-triazine-2,4-diamine
5	6-chloro-N^2,N^4-dicyclopentyl-1,3,5-triazine-2,4-diamine
6	6-chloro-N^2,N^4-dicyclohexyl-1,3,5-triazine-2,4-diamine
7	6-chloro-N^2,N^4-dicycloheptyl-1,3,5-triazine-2,4-diamine

Table 1. Continuation

Compound	IUPAC name
8	6-chloro-N^2,N^4-dicyclooctyl-1,3,5-triazine-2,4-diamine
9	6-chloro-N^2,N^4-bis(1-phenylethyl)-1,3,5-triazine-2,4-diamine
10	6-chloro-N^2,N^4-bis(1-(*p*-tolyl)ethyl)-1,3,5-triazine-2,4-diamine
11	6-chloro-N^2,N^4-bis(1-(4-chlorophenyl)ethyl)-1,3,5-triazine-2,4-diamine
12	N^2,N^4-bis(1-(4-bromophenyl)ethyl)-6-chloro-1,3,5-triazine-2,4-diamine
13	6-chloro-N^2,N^4-dicyclohexyl-N^2,N^4-dimethyl-1,3,5-triazine-2,4-diamine
14	6-chloro-N^2,N^4-dicyclohexyl-N^2-phenyl-1,3,5-triazine-2,4-diamine
15	6-chloro-N^2,N^4-dicyclohexyl-N^2,N^4-diphenyl-1,3,5-triazine-2,4-diamine
16	6-chloro-N^2,N^4-bis(1-methylcyclopentyl)-1,3,5-triazine-2,4-diamine
17	6-chloro-N^2,N^4-bis(1-methylcyclohexyl)-1,3,5-triazine-2,4-diamine
18	6-chloro-N^2,N^4-bis(1-methylcycloheptyl)-1,3,5-triazine-2,4-diamine
19	4,6-dichloro-*N*-(1-methylcyclopentyl)-1,3,5-triazine-2-amine
20	4,6-dichloro-*N*-(1-methylcyclohexyl)-1,3,5-triazine-2-amine
21	4,6-dichloro-*N*-(1-methylcycloheptyl)-1,3,5-triazine-2-amine

MULTIPLE LINEAR REGRESSION MODELING

The MLR modeling was carried out using NCSS 2023 program (36). The variable selection from the pool of various molecular descriptors was done by forward selection with switching algorithm. The search was stopped when the number of terms reached 3. The selected and considered molecular descriptors were calculated by PaDEL program (37) on the basis of two-dimensional molecular structures that were previously drawn and presented to the PaDEL program. The MLR model was selected based on the statistical parameters and predictive performance of the MLR model. The predictive ability was estimated applying internal and external validation procedures. The input parameters of the MLR model included the following molecular descriptors: maxsCl (atom type electrotopological state, maximum atom-type E-State: -Cl), LipoaffinityIndex (index of lipoaffinity) and ATSp5 (autocorrelation descriptor weighted by polarizability). The logarithm of bioconcentration factor (logBCF), estimated by VegaNIC software (BCFmeylan, version 1.0.2, based on Meylan approach), was the output variable in the MLR modeling procedure (22). All the data used in the modeling are presented in Table 2. Values for maxsCl varied from 0.5696 (compound **10**) to 0.8939 (compound **11**), for LipoaffinityIndex varied from 4.3972 (compound **1**) to 14.0103 (compound **15**) and for ATSp5 varied from 865.41 (compound **1**) to 50.8953 (compound **15**). Regarding the BCFmeylan values ranged from 1.08 (compound **2**) to 3.74 (compound **11**). Bioconcentration factor represents the absorption of pollutants from the dissolved phase. It can be calculated applying the following equation:

$$BCF = c \,/\, c_w \qquad [1]$$

where c represents the equilibrium concentration of pollutant in the organisms (μg/kg), whilst c_w is the concentration of pollutant in the water phase (μg/L). The BCF plays a crucial role as an initial screening parameter for bioaccumulative and toxic substances in environmental risk assessment cycle. It provides quantitative insights into a contaminant's uptake by organisms from water (38).

Table 2. The input and output parameters used in the MLR modeling

Compound No.	BCFmeylan	maxsCl	LipoaffinityIndex	ATSp5
Training set:				
1	1.38	0.6638	4.3972	865.41
2	1.08	0.6464	4.4934	988.84
4	1.93	0.6502	5.7406	1070.31
5	2.43	0.6776	6.1413	1442.43
6	3.08	0.6738	7.4564	1637.08
7	3.73	0.6700	8.7716	1851.33
8	3.16	0.6669	10.1187	2416.19
9	2.89	0.5737	9.1508	2182.26
10	3.61	0.5696	10.4107	2392.94
11	3.74	0.8939	9.4198	2449.47
13	3.58	0.6774	9.5055	2349.55
14	2.80	0.6296	10.7158	3292.75
15	1.49	0.5855	14.0103	5089.53
16	3.03	0.6555	7.5715	1856.53
17	3.68	0.6517	8.8914	2177.11
18	3.19	0.6479	10.2114	2534.50
19	1.66	0.7235	4.4942	1010.39
21	2.31	0.7197	5.8260	1335.49
External test set:				
3	1.93	0.6464	5.6838	1191.73
12	3.39	0.5851	9.5588	2562.89
20	1.99	0.7216	5.1601	1164.06

VALIDATION OF THE REGRESSION MODEL

The validity of the formed MLR model was estimated by internal and external validation procedures. The internal validation included the calculation of the following parameters: determination coefficient (R^2), adjusted determination coefficient (R^2_{adj}), variation coefficient (*VC*), mean square error (*MSE*), average percent error (*APE*) and Fischer's test (*F*). The internal validation included the application of cross-validation and calculation of corresponding parameters: leave-one-out (LOO) cross-validation determination coefficient (R^2_{cv}) and predicted residuals sum of squares (*PRESS*). The external validation was carried out in the way that compounds **3**, **12** and **20** were omitted from the training set and used as external test set. The compounds for the external test set were randomly chosen. The predictive power of the established MLR model was estimated by comparison of the observed and predicted logBCF values as well as by the analysis of randomness of residuals distribution. The multicollinearity of the model was estimated by variance inflation factor (*VIF*). If the *VIF* is less than 10, the multicollinearity is limited (39).

RESULTS AND DISCUSSION

MULTIVARIATE LINEAR REGRESSION MODEL

The descriptors selection was carried out so the number of the independent variables meets the criteria known as Topliss-Costello rule according to which the ratio of the number of objects (compounds) and the number of molecular descriptors included in model is equal or less than five (40). The MLR modeling resulted in the following mathematical model:

$$\textbf{logBCFmeylan} = -3.12 \ (\pm1.02) + 3.78 \ (\pm1.31) \ \textbf{maxsCl} +$$

$$+ \ 0.89 \ (\pm0.1) \ \text{LipoaffinityIndex} - 0.002 \ (\pm0.000) \ \text{ATSp5} \qquad [2]$$

The bioconcentration factor of the investigated molecules is best correlated with maxsCl, LipoaffinityIndex and ATSp5. From the presented MLR model it can be observed that atom type electrotopological state, maximum atom-type E-State and index of lipoaffinity descriptors contribute positively to the value of logarithm of bioconcentration factor while negative value in front of autocorrelation descriptor weighted by polarizability indicate that the greater the value of descriptor, the lower the value of logBCFmeylan is. The modeling was done based on raw data (non-scaled data), considering the fact that the data normalization was not resulted in any acceptable model.

VALIDATION AND APPLICABILITY DOMAIN OF THE MLR MODEL

The usefulness of the established MLR model was validated using the plots showing observed *versus* predicted logBCF values (Figure 1).
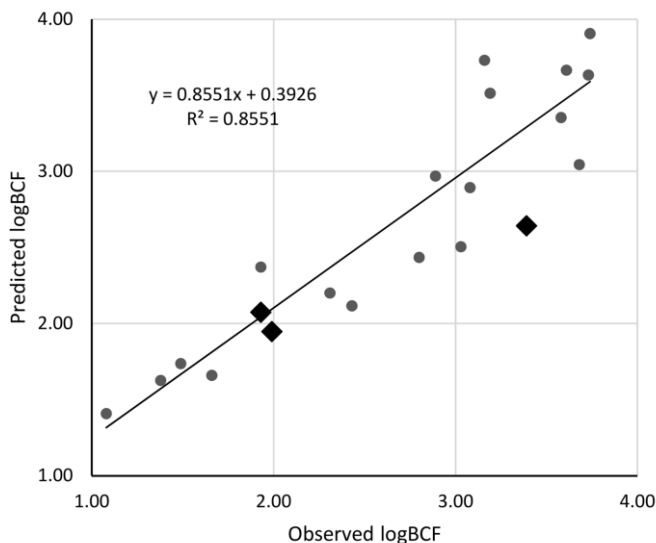

Figure 1. The linear relationship between observed bioconcentration factor and bioconcentration factor predicted by the established MLR model (● – training set, ◆ – external test set)

The significant value of the slope (0.8551) and acceptable intercept value (0.3926) validate the proposed model. Since the comparison of the observed and predicted data can indicate how the data are correlated, it can be concluded that presented model correlates the data well. In order to investigate the existence of a systematic error in development of the QSPR model the observed values of logBCF were plotted *versus* residuals (Figure 2). Presented graph shows that the residuals are randomly distributed on both sides of the zero axis. This leads to the conclusion that there is the absence of systematic error in the development of the presented MLR-QSPR model. Compounds used for training and external test set (compounds **3**, **12** and **20**) were separated and marked differently in both presented graphs.
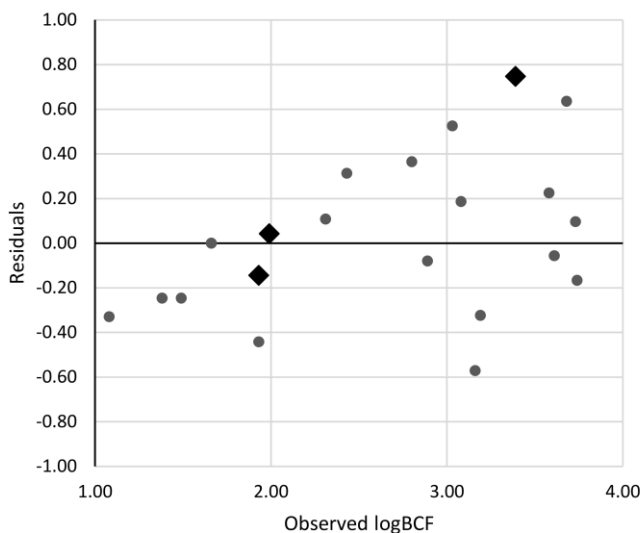

Figure 2. The distribution of the residuals for the established MLR model (● – training set, ◆ – external test set)

In Figure 3 histogram and normal probability plot of the residuals of logBCF parameter are presented. The obtained results indicate that there are not any substantive departures from normality either outliers among data. It can be concluded that observed data are normally distributed. The histogram shows that the majority of the residuals is concentrated around zero. Small number of the residuals crosses the value of +0.6. Table 3 shows the conducted normality tests of residuals as a measure of the goodness of fit. The used tests and statistic values were as follows: Shapiro-Wilk (0.982), Anderson-Darling (0.144), D'Agostino Skewness (0.434), D'Agostino Kurtosis (-0.584) and D'Agostino Omnibus (0.529). For all presented test *p*-value ranged from 0.5593 to 0.9707. It can be concluded that the observed residuals are normally distributed according to all five conducted tests.
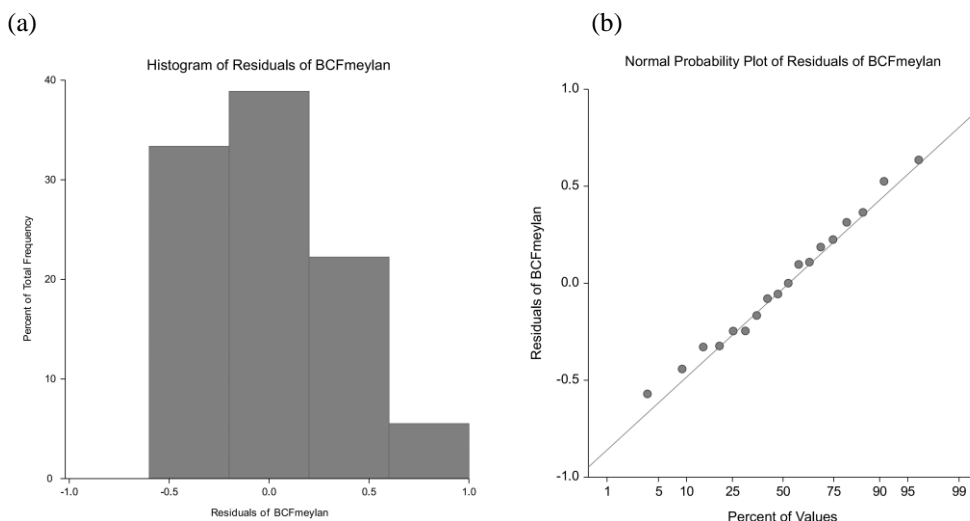
(a)

(b)

Figure 3. Histogram (a) and normal probability plot (b) of the residuals of logBCF
parameter

Table 3. Normality tests of residuals

Test of H$_0$: Residuals Normally Distributed			
Test	**Test statistic value**	***p*-value**	**Reject H$_0$ at α = 0.02?**
Shapiro-Wilk	0.982	0.9676	No
Anderson-Darling	0.144	0.9707	No
D'Agostino Skewness	0.434	0.6643	No
D'Agostino Kurtosis	-0.584	0.5593	No
D'Agostino Omnibus	0.529	0.7675	No

The *VIF* values of the independent variables are shown in Table 4. As one of the most important features, while building MLR model, is to avoid multicollinearity so this requirement was also fulfilled. There is no significant influence of multicollinearity since all the *VIF* values are lower than 10.

Table 4. The *VIF* values of the independent variables

Independent variable	*VIF*
maxsCl	1.08
LipoaffinityIndex	9.15
ATSp5	9.11

Table 5 gives insight regarding the internal and external validation parameters together with their optimal values. The quality of the predictive power of the presented model was tested using the leave-one-out (*LOO*) method. Parameters used for model assessment were:

correlation coefficient (R^2), adjusted correlation coefficient (R^2_{adj}), coefficient of variation (*CV*), mean square error (*MSE*), average percentage error (*APE*), Fisher's test (*F*), cross-validation correlation coefficient (R^2_{cv}) and predicted residual error sum of squares (*PRESS*). All presented parameters were in accordance with stated optimal values which indicate the high predictive ability of the presented MLR-QSPR model.

Table 5. The internal and external validation parameters of the MLR model

Parameter	Value	Optimal value
R^2	0.8551	> 0.80
R^2_{adj}	0.8241	> 0.70
CV	0.1363	Lower the CV implies smaller residuals relative to the predicted value
MSE	0.1365	< 0.2
APE	11.4%	< 20%
F	27.5	Higher *F* means better fitting of the data
R^2_{cv}	0.6507	> 0.60
PRESS	4.6054	It depends on the nature of the data

The applicability domain of the presented model is defined by the values of the used molecular descriptors and output variable. This implies the following values: maxsCl (0.5696-0.8939), LipoaffinityIndex (4.3972-14.0103), ATSp5 (865.41-5089.53) and BCFmeylan (1.08-3.74).

CONCLUSION

In the present study, data set comprising of twenty-one 6-chloro-1,3,5-triazine derivatives was investigated concerning the bioconcentration factor as a key parameter when environmental risk assessment is perceived. Using *in silico* approach, suitable molecular descriptors were chosen (maxsCl, LipoaffinityIndex and ATSp5) and logBCFmeylan was predicted using QSPR-MLR mathematical modeling. The proposed model was statistically assessed using internal and external validation and resulted in: *VIF* < 9.15 for all three molecular descriptors, $R^2 = 0.8551$, $R^2_{adj} = 0.8241$, $R^2_{cv} = 0.6507$ and *PRESS* = 4.6054. The observed versus predicted values and observed values versus residuals were graphically evaluated indicating the absence of systematic error. Normal probability of the residuals and normality test of residuals indicated normal distribution. The presented study of the modeling of bioconcentration factor provides valuable MLR model that could be used for prediction of bioconcentration factor of novel triazine derivatives, structurally similar to the compounds used in the modeling.

Acknowledgement

REFERENCES

1. Akash, S.; Sivaprakash, B.; Rajamohan, N.; Muruga Pandiyan, C.; Vo, D.V.N. Pesticide pollutants in the environment – A critical review on remediation techniques, mechanism and toxicological impact. *Chemosphere*. **2022**, *301*, 134754.

2. Rajmohan, K.S.; Chandrasekaran, R.; Varjani, S. A review on occurrence of pesticides in environment and current technologies for their remediation and management. *Indian J. Microbiol*. **2020**, *60*, 125-138.

3. Leoci, R.; Ruberti, M. Pesticides: An overview of the current health problems of their use. *J. Geosci. Environ. Prot*. **2021**, *9*, 1-20.

4. Sharma, A.; Sheyi, R.; de la Torre, B.G.; El-Faham, A.; Albericio, F. *s*-Triazine: A privileged structure for drug discovery and bioconjugation. *Molecules*. **2021**, *26 (4)*, 864.

5. LeBaron, H.M.; McFarland, J.E.; Burnside, O.C. The triazine herbicides: A milestone in the development of weed control technology. In The triazine herbicides, 50 years revolutionizing agriculture; LeBaron, H.M.; McFarland, J.E.; Burnside, O.C., Eds.; Elsevier: Amsterdam, **2008**, 1-12.

6. Gupta, A.K.S.; Bhattaharya, T.; Hajela, K.; Shankar, K.; Ahmad, S. Synthesis and pesticidal activities of some substituted 1,2,4-triazines. *Pest. Sci*. **1985**, *16 (1)*, 65-72.

7. Koizumi, K.; Kuboyama, N.; Tomono, K., Tanaka, A.; Ohkl, A.; Kohno, H.; Wakabayashi, K.; Böger, P. Novel 1,3,5-triazine derivatives with herbicidal activity. Pest. Sci. **1999**, *55 (6)*, 642-645.

8. Mekheimer, R.A.; Abuo-Rahma, G.E-D,; Abd-Elmonem, M.; Yahia, R.; Hisham, M.; Hayallah, A.M.; Mostafa, S.M.; Abo-Elsoud, F.A.; Sadek, K.U. New *s*-triazine/tetrazole conjugates as potent antifungal and antibacterial agents: Design, molecular docking and mechanistic study. *J. Mol. Struct*. **2022**, *1267*, 133615.

9. Su, R.; Li, D.; Wu, L.; Han, J.; Lian, W.; Wang, K.; Yang, H. Determination of triazine herbicides in juice samples by microwave-assisted ionic liquid/ionic liquid dispersive liquid-liquid microextraction coupled with high performance liquid chromatography. *J. Sep. Sci*. **2017**, *40 (14)*, 2950-2958.

10. Narenderan, S.T.; Meyyanathan, S.N.; Babu, B. Review of pesticide residue analysis in fruits and vegetables. Pre-treatment, extraction and detection techniques. *Food Res. Int*. **2020**, *133*, 109141.

11. Chatterjee, M.; Roy, K. Prediction of aquatic toxicity of chemical mixtures by the QSAR approach using 2D structural descriptors. *J. Hazard. Mater*. **2021**, *408*, 124936.

12. Toma, C.; Cappelli, C.I; Manganaro, A.; Lombardo, A.; Aening, J.; Benfenati, E. New models to predict the acute and chronic toxicities of representative species of the main trophic levels of aquatic environments. *Molecules*. **2021**, *26 (22)*, 6983.

13. Xu, J-Y.; Wang, K.; Men, S-H.; Yang, Y.; Zhou, Q.; Yan, Y-G. QSAR-QSIIR-based prediction of bioconcentration factor using machine learning and preliminary application. *Environ. Int*. **2023**, *177*, 108003.

14. Bertato, L.; Chirico, N.; Papa, E. Predicting the bioconcentration factor in fish from molecular structures. *Toxics*, **2022**, *10 (10)*, 581.

15. Lee, M.; Min, K. A comparative study of the performance for predicting biodegradability classification: The quantitative structure–activity relationship model vs the graph convolutional network. *ACS Omega*, **2022**, *7 (4)*, 3649-3655.

16. Jiang, S.; Liang, Y.; Shi, S.; Wu, C.; Shi, Z. Improving predictions and understanding of primary and ultimate biodegradation rates with machine learning models. *Sci. Total Enivron*. **2023**, *904*, 166623.

17. Petoumenou, M.; Pizzo, F.; Cester, J.; Fernández, A.; Benfenati, E. Comparison between bioconcentration factor (BCF) data provided by industry to the European Chemicals Agency (ECHA) and data derived from QSAR models. *Environ. Res*. **2015**, *142*, 529-534.

18. Lunghini, F.; Marcou, G.; Azam, P.; Patoux, R.; Enrici, M.H.; Bonachera, F.; Horvath, D.; Varnek, A. QSPR models for bioconcentration factor (BCF): are they able to predict data of industrial interest? *SAR QSAR Environ. Res*. **2019**, *30 (7)*, 507-524.

19. Dearden, J.C.; Hewitt, M. QSAR modelling of bioconcentration factor using hydrophobicity, hydrogen bonding and topological descriptors, *SAR QSAR Environ. Res*. **2010**, *21*, 671-680.

20. Aranda, J.F.; Bacelo, D.E.; Leguizamón Aparicio, M.S.; Ocsachoque, M.A.; Castro, E.A.; Duchowicz, P.R. Predicting the bioconcentration factor through a conformation-independent QSPR study. *SAR QSAR Environ. Res*. **2017**, *28*, 749-763.

21. Mansouri, K.; Grulke, C.M.; Judson, R.S.; Williams, A.J. OPERA models for predicting physicochemical properties and environmental fate endpoints. *J. Cheminformatics*. **2018**, *10*, 1-19.

22. VegaNIC application, Laboratory of Environmental Chemistry and Toxicology of Mario Negri Institute of Pharmacological Research, http://vega-qsar.eu.

23. Martin, T.; Harten, P.; Young, D. TEST (Toxicity Estimation Software Tool), US Environmental Protection Agency, Washington, USA, **2012**, https://www.epa.gov/chemical-research/toxicity-estimation-software-tool-test.

24. UFZ, ChemProp, Helmholtz Centre for Environmental Research – UFZ, Leipzig, DE, **2018**, http://www.ufz.de/ecochem/chemprop.

25. European Chemicals Agency ECHA, https://echa.europa.eu/home.

26. Yang, L.; Li, H.; Zhang, Y.; Jiao, N. Environmental risk assessment of triazine herbicides in the Bohai Sea and the Yellow Sea and their toxicity to phytoplankton at environmental concentrations. *Environ. Int*. **2019**, *133 (A)*, 105175.

27. Fernandez, M.V.; Gardinali, P.G. Risk assessment of triazine herbicides in surface waters and bioaccumulation of Irgarol and M1 by submerged aquatic vegetation in Southeast Florida. *Sci. Total Environ*. **2016**, *541*, 1556-571.

28. Tarja, N.; Kirsti, E.; Marja, L.; Kari, E. Thermal and metabolic factors affecting bioaccumulation of triazine herbicides by rainbow trout (*Oncorhynchus mykiss*). *Environ. Toxicol*. **2003**, *18 (4)*, 219-226.

29. Salaković, B.; Kovačević S.; Karadžić Banjac M.; Jevrić. L.; Podunavac-Kuzmanović, S.; Antonović, D. Comparative chemometric analysis, ranking and selection of lipophilicity parameters of 6-chloro-1,3,5-triazine derivatives with acyclic and cyclic substituents. *APTEFF*. **2022**, *53*, 88-99.

30. Karadžić Banjac, M.; Kovačević, S.; Jevrić, L.; Podunavac-Kuzmanović, S. Artificial intelligence in prediction of ecotoxicity of a series of *s*-triazine compounds as potential pesticides. *APTEFF*. **2023**, *54*, 245-253.

31. Kovačević, S.; Karadžić Banjac, M.; Anojčić, J.; Banjac, V.; Ilić, P.; Salaković, B.; Podunavac-Kuzmanović, S.; Jevrić, L. Comparative analysis of anisotropic lipophilicity of a series of 6-chloro-1,3,5-triazines determined in reversed phase ultra high performance liquid chromatography system. *Agriculture*, **2023**, *13*, 2212.

32. Kovačević, S.; Karadžić Banjac, M.; Jevrić, L.; Podunavac-Kuzmanović, S. Linear quantitative structure-ecotoxicity relationship modeling of a series of symmetrical triazine derivatives based on physicochemical parameters. *APTEFF*. **2023**, *54*, 255-264.

33. Salaković, B.; Kovačević S.; Karadžić Banjac M.; Podunavac-Kuzmanović, S.; Jevrić. L.; Pajčin, I.; Grahovac, J. New perspective on comparative chemometric and molecular modeling of antifungal activity and herbicidal potential of alkyl and cycloalkyl *s*-triazine derivatives. *Processes*. **2023**, *11*, 358.

34. Bončić-Caričić, G.A.; Tadić, Ž.D.; Jeremić, D.S. Electron impact mass spectrometry of some 2,4,6-substituted *s*-triazines. Effect of the ring size. *Int. J. Mass Spectrom. Ion Phys*. **1983**, *47*, 451-454.

35. Antonović, D.; Bončić-Caričić, G.A. Gas chromatographic retention indices for *N*-substituted amino s-triazines on DB-1 and DB-5 capillary columns. *J. Serb. Chem. Soc*. **1994**, *59 (12)*, 993-996.

36. NCSS Statistical Software (2023). NCSS, LLC. Kaysville, Utah, USA, ncss.com/software/ncss.

37. Yap, C.W. PaDEL-descriptor: An open source software to calculate molecular descriptors and fingerprints. *J. Comput. Chem*. **2011**, *32 (7)*, 1466-1474.

38. Wang, W.-X. Chapter 4 – Bioaccumulation and Biomonitoring, Editor(s): Julián Blasco, Peter M. Chapman, Olivia Campana, Miriam Hampel, Marine Ecotoxicology, Academic Press, **2016**, 99-119.

39. O'Brien, R.M. A caution regarding rules of thumb for variance inflation factor. *Qual. Quant*. **2007**, *41*, 673-690.
40. Topliss, J.G.; Costello, R.J. Chance correlations in structure-activity studies using multiple regression analysis. *J. Med. Chem*. **1972**, *15*, 1066-1068.

THE APPLICATION OF HYDRODYNAMIC CAVITATION METHODS TO INCREASE THE EFFICIENCY OF THE PROCESS OF EXTRACTING BIOLOGICALLY ACTIVE SUBSTANCES FROM THE WALNUT SEPTUMS

Liubov P. HOZHENKO[1]*, Georgiy K. IVANITSKY[1,2], Bogdan Ya. TSELEN[1], Natalia L. RADCHENKO[1], Anna Ye. NEDBAILO[1]

[1] Institute of Engineering Thermophysics of the National Academy of Sciences of Ukraine, Maria Kapnist Str. 2a, Kyiv, Ukraine

[2] National Technical University of Ukraine "Igor Sikorsky Kyiv Polytechnic Institute", Beresteiska Avenue 37, Kyiv, Ukraine

The article presents experimental studies of the intensification of the process of extracting biologically active substances from the walnut septum using the mechanisms of the method of discrete-pulse energy input (DPEI) in pulsating dispersers. On the basis of the obtained results of studies of the effects of the shock action of the liquid flow and hydrodynamic cavitation on the physicochemical parameters of the aqueous extract of walnut septum, the effectiveness of the application of the most rigid mechanism of the method of DPEI is shown. In the course of experimental studies, it was established that the amount of dry substances released during the extraction process in a cavitation-type pulsating disperser is approximately 2 times greater than in an impact-type pulsating disperser. The use of hydrodynamic cavitation made it possible to maximally extract biologically active substances from walnut partitions in 20 minutes of cavitation treatment, which proportionally exceeds the shock effect of hydrodynamic impact by 57 %. It has been established that the cavitation effect is the most effective mode of the method of DPEI when applied in the extraction processes from plant raw materials, which is currently one of the most effective ways to achieve high-energy indicators in food and chemical technologies for obtaining thermolabile substances.

Keywords: Method of discrete-pulse energy input, Hydrodynamic cavitation, Extraction, Walnut septum.

INTRODUCTION

The main task in the development of energy-efficient technologies is always aim at increasing the technical and economic indicators of production. Therefore, increasing the productivity of equipment and reducing energy consumption for technological operations requires the creation and implementation of efficient devices with low specific energy and material capacity, a high degree of influence on processed substances. At the same time, the economic, rational, resource-saving and energy-efficient production of biologically active components of natural origin for further use in various industries always remains an urgent problem. The article presents the results of a complex study of the technological modes of obtaining biologically active components from the plant raw materials when the cavitation mechanism is initiate. The walnut septum with a specific structure consists of unique useful elements. Extract from walnut membranes has immunoprotective, antimicrobial, phagocytic, mitotic and antioxidant activity and is widely used in the pharmaceutical, food, and chemical industries (1-5).

In the Institute of Engineering Thermophysics of the National Academy of Sciences of Ukraine, on the basis of the concept of discrete-pulse energy input (DPEI), for many years, the development of highly efficient mass transfer devices, in particular jet pulsating dispersers (extractors) of various types for extraction from plant raw materials (6). These devices, such as impact type pulsating dispersers (extractors), have found wide application in industry (7, 8). The intensification of the extraction processes in these jet pulsation devices is based on such mechanisms of DPEI, as periodic acceleration and deceleration of the flow, the action of shear stresses of developed turbulence. On the basis of mathematical modeling of hydrodynamic and heat-mass exchange processes in the liquid and gas tracts of pulsating dispersers, analytical methods and calculations were developed, and rational designs and optimal modes of operation of such devices were proposed (7-9).

The application of traditional extraction methods is limited by the fact that they accelerate only the external hydrodynamic transfer processes in the extractant in the vicinity of the plant particle, while the rate of the extraction process is limited by the rate of internal transfer. To accelerate the internal diffusion transfer of the target component from the plant cell through the complex capillary structure of the plant particle to the surface of the particle in the extractant, it is necessary to use cavitation methods (10, 11). Unlike the abovementioned references, where extraction is carried out by traditional infusion methods at high temperatures and with the use of alcohol as a solvent, cavitation methods allow the extraction process to be carried out at low or moderate temperatures and without the addition of alcohol (12-14).

Pulsation dispersers (extractors) created at the Institute of Engineering Thermophysics of the NAS of Ukraine work based on the principle of DPEI, including impact type pulsation dispersers (extractors) and our proposed modification – a cavitation type pulsating disperser, in which cavitation mechanisms are used. As you know (6), cavitation is one of the most rigid mechanisms of the DPEI principle and therefore it is advisable to apply it in extraction processes.

The purpose of the work study of the influence of hydrodynamic cavitation mechanisms on the efficiency and productivity of the extraction process from raw materials using the example of walnut septums in pulsation extractors created on the basis of the DPEI principle.

On the example of the extraction of bioactive substances from the walnut septum, to compare cavitation extraction methods with other dynamic extraction methods as a further development of the DPEI concept (6, 13, 15).

Experimental studies of the process of extracting walnut septum were carried out in parallel in impact and cavitation type pulsating dispersers developed at the Institute of Engineering Thermophysics of the NAS of Ukraine.

EXPERIMENTAL

The extraction process with intensive mixing provides the condition for the growth of the convective diffusion coefficient to infinity, that is, the convective mass transfer is carried out instantaneously, and the mass transfer coefficient is determined only by the diffusion coefficient in the pores of the plant material. Initiation of the cavitation mechanism during processing in a cavitation reactor leads to a significant acceleration of the process at its slowest stage, that is, it allows influencing the internal diffusion coefficient. Due to the intense oscillation of the particles of the "solid-liquid" system, there is a local increase in

temperature in places of friction, a decrease in the viscosity of the extractant, and, therefore, an increase in the internal diffusion coefficient.

The schematic diagram of the impact type pulsating disperser is presented in Figure 1.

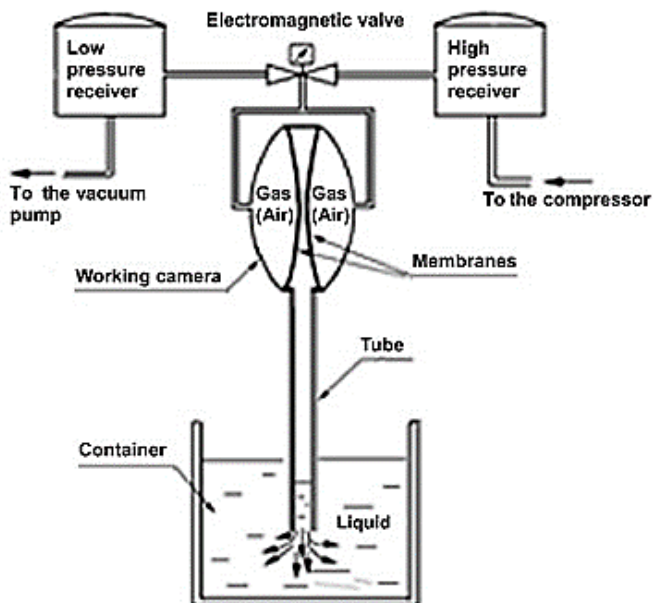The principle of operation and operating parameters are previously described (7-9).

Figure 1. Schematic diagram of an impact type pulsating disperser

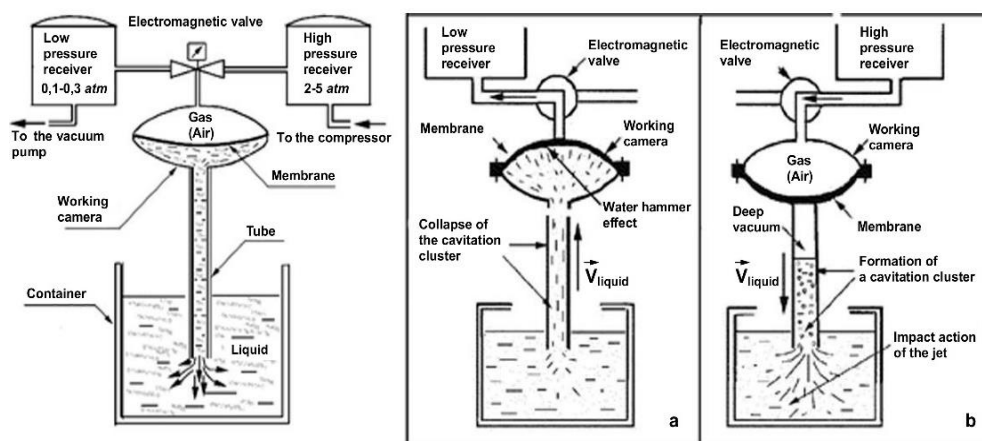The schematic diagram of the cavitation type pulsating disperser is presented in Figure 2.

Figure 2. Schematic diagram of a cavitation type pulsating disperser and the main dynamic effects of the DPEI method that are implemented: a) stage of liquid intake into the working chamber; b) the stage of liquid ejection from the chamber

The extractant mixture with crushed plant material is in the loading tank under atmospheric pressure p_a at temperature T_1. During the operation of the extractor, the liquid mixture enters the working chamber from the tank or flows out of the chamber into the tank through a cylindrical pipe that is hermetically connected to the lower surface of the chamber. The upper and lower surfaces of the working chamber have the shape of a spherical segment, between which there is an elastic membrane that separates the liquid and gas tracts of the device. Through a hole on the upper surface, the working chamber is connected to the gas path. A three-way solenoid valve periodically connects the chamber to a high-pressure receiver (HPR) connected to the compressor, or to a low-pressure receiver (LPR) connected to a vacuum pump, at set time intervals. Pressure values in HPR can be set in the interval p_{comp}=0,2÷0,5 MPa, and in LPR - in the interval p_{vac}=0,001÷0,003 MPa.

At the stage of connecting the chamber to the HPR, the membrane intensively pushes the liquid out of the chamber through the pipe into the tank under the action of high pressure. When the membrane covers the hole on the lower surface of the chamber, all the liquid leaves the chamber. At this moment, the flow velocity in the pipe reaches its maximum value (about 10 m/s) and the liquid continues to move down the pipe by inertia (without contact with the membrane). After the separation of the liquid mixture from the membrane in the upper part of the pipe, a cavity is formed under vacuum with a continuously growing volume, which is gradually filled with steam. It was established that due to the rapid movement of the liquid column, the vapor pressure in the cavity is significantly lower than the saturated vapor pressure $p_{sat}(T_1)$. The pressure in the liquid at the boundary with the cavity instantly drops from p_{comp}=0,3 MPa to $p_1<p_{sat}(T_1)$=0,002 MPa, which leads to boiling of the liquid mixture near the free surface.

The pressure difference p_a-$p_{sat}(T_1)$ and the action of the frictional force against the wall cause a sharp braking of the liquid mixture in the pipe, which then changes direction and moves with increasing speed towards the chamber until it reaches the entrance to the chamber. If by this point the chamber is still connected to the HPR, then the entrance to the chamber is blocked, and the moving liquid mixture immediately stops. If the chamber is already connected to the LPR, then the liquid mixture from the pipe quickly fills the chamber and stops on the membrane adjacent to the upper surface of the chamber. In both cases, a momentary stoppage of flow initiates the phenomenon of hydraulic shock. The next time the camera is connected to the HPR, the cycle is repeated. The frequency of cycle repetitions, depending on the mode, is in the range of 0,5 to 1,5 Hz.

Figure 2 also shows the main dynamic effects of the method of DPEI, implemented in a cavitation-type pulsating disperser. These include: the dynamic effect of the jet flowing from the pipe into the tank and contributing to intensive turbulent mixing of the mixture; the effect of hydraulic shock resulting from the inhibition of the reverse flow on the surface of the membrane, which is accompanied by high-frequency changes in compression and rarefaction in the chamber and pipe and, as a result, the occurrence of secondary cavitation effects. But the most powerful cavitation effects occur after the exit of the liquid from the chamber into the pipe.

Since the research was carried out using an apparatus in which the processes of dispersion, mixing and extraction are implemented at the same time, in order to obtain an uncontaminated extract of walnut septums, the raw materials were loaded chopped on a mechanical manual extruder to optimal sizes l=5÷10 mm (2-5, 13). The determined dimensions of the raw material depend on the geometrical parameters of the working tube of the device, so that during processing the raw material does not compact in the cross-section of the tube. In the course of research, it was established that further grinding to obtain the smaller par-

ticle sizes is impractical. As a result of the conducted experimental studies, water systems of a brown color without crushed particles after filtering were obtained. On the basis of the analysis of economic and technological aspects, the development of technological regimes of the process of extraction from the walnut septums was carried out at a temperature 22 °C and hydraulic modules 1:10. Samples of the liquid were taken during the processing at five-minute intervals for further determination of the content of dry substances according to the State Standard of Ukraine (DSTU 804:2015). For research of physical and chemical properties used a measuring complex EZODO PCT-407. Study of the microstructure were carried out by the method of optical microscopy on a light microscope Axio Imager Z1m production by Carl Zeiss.

RESULTS AND DISCUSSION

The obtained results shown in Figure 3 testify that 15 min processing in a cavitation reactor ensures the equilibrium of concentrations of target substances in the raw material and extract. However, the significance of the salt content in the samples obtained in the impact type disperser has a stable character (Figure 4). This can be explained by the unsaturation of the solution at temperature 22 °C, because during the extraction process under the influence of the cavitation mechanism, a significant local increase in temperature is observed (up to 40 °C) and, accordingly, the growth of the internal diffusion coefficient.
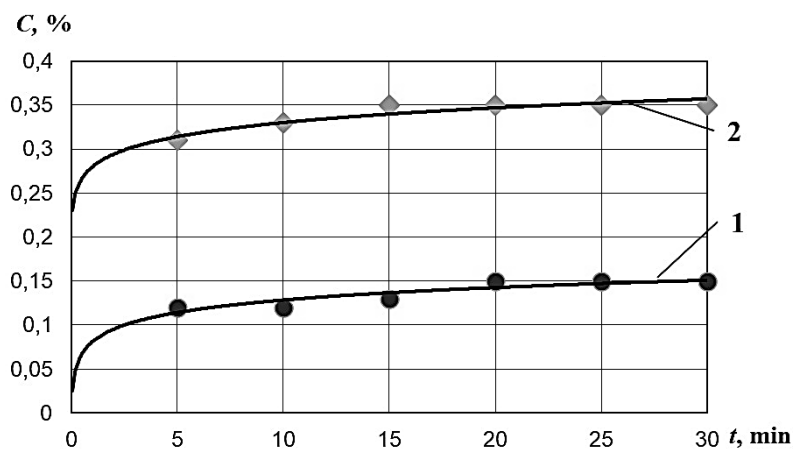
Figure 3. Dependence of the amount of dry substances in the aqueous extract of walnut septums on the duration of processing: 1 – impact type pulsating disperser; 2 – cavitation type pulsating disperser

Although in both cases, there was a place for the use of devices that using the DPEI method but the implementation of its most powerful cavitation influence takes place in a cavitation type disperser. It should be noted that during the research, the temperature of 22°C was not maintained in the cavitation-type disperser, unlike the shock-type disperser where temperature of the liquid was a constant. However, the relatively maximum yield of

the amount of dry substances (0,35%) can be achieved at a constant temperature of the processed medium of 22 °C in a cavitation type disperser. Therefore, comparing Figures 3 and 4 it is possible to substantiate the obtained indicators of physicochemical parameters against the background of the quantitative composition of the target substances in the system depending on the duration and intensity of the effect of the cavitation mechanism in pulsation-type reactors.
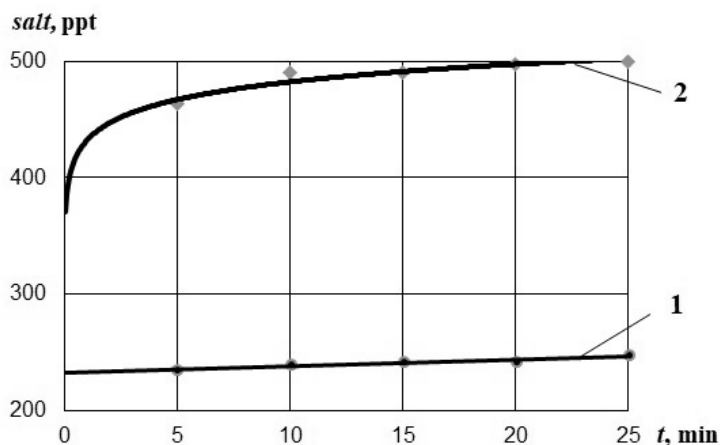

Figure 4. Dependence of the salt content in the aqueous extract of walnut septums on the duration of processing: 1 – impact type pulsating disperser; 2 – cavitation type pulsating disperser

The measured redox potential (ORP) values differ by an order of magnitude depending on the temperature effect on the environment during the initiation of the cavitation mechanism. However, to describe the quality of the obtained liquid saturated with target substances, it is necessary to have data on biological and chemical parameters during oxidation reactions. Commonly known that the oxygen content in water is an inversely related to temperature, i.e. it always decreases with its increase. A local increase in temperature due to the implementation of the cavitation mechanism in the system leads to the release of oxygen. A decrease the ORP indicates an increase in renewable substances in the system, and an increase the ORP an increase in oxidizing substances. Accordingly, it is possible to influence on the relaxation of ORP through cavitation processing. Because of the cavitation effect on the liquid medium, the decrease in the ORP value is proportional to the decrease in pressure pulses. In all selected samples, the value of the hydrogen index was within the limits pH=6,5÷6,78.

Before loading, walnut membranes were crushed on a manual extruder to the specified sizes, related to the geometry of the working nodes of the pulsating disperser and subsequent filtering of the mixture.

Appearance of particles of walnut septums for processing in devices and in water mixture, depending on the treatment, is presented in Figure 5. Particles of crushed raw materials for processing in devices are presented in Figure 5a. As a result of optical microscopy, it became clear that in the process of extraction on the impact type pulsating disperser, the particles were still crushed to a size of about 150-200 μm (Figure 5b). When processing on

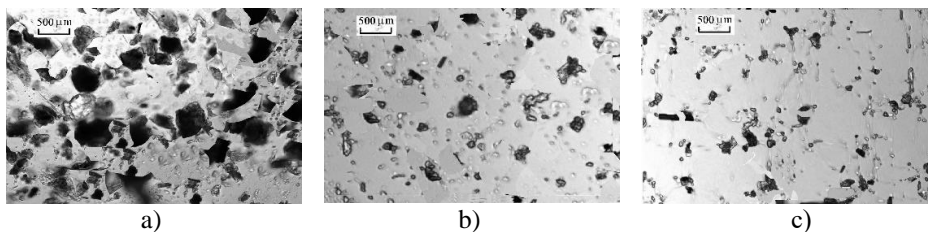the cavitation type pulsating disperser, the particles were crushed more strongly up to 50-100 μm (Figure 5c).

a)   b)   c)

Figure 5. Image of the structure of the received samples of walnut septum particles: a) – before processing; b) – after 20 min of processing in an impact type pulsating disperser; c) – after 20 min of processing in a cavitation type pulsating disperser.

In the course of conducting experimental research, it was established that due to the cavitation effect on the processed medium, the equilibrium concentration in the "solid-liquid" system is reached faster than due to the impact of the shock action by mixing. This explained by the uniform distribution of pressure pulses during the cavitation effect on the processed medium in the cavitation type disperser.

The application of the cavitation method for the extraction of biologically active substances from walnut septum with other extractants besides water at other temperatures, the analysis of the biochemical composition of the extract, etc. will be the next topic of our research.

CONCLUSION

The dynamic effects of hydrodynamic cavitation, which are characteristic of pulsation type reactors, have different effects on water systems during the extraction process, depending on the duration of processing and temperature regimes. The obtained values of physicochemical parameters (pH and salt content) allow evaluating the efficiency of the extraction process using a complex of mechanisms of the DPEI method. The pH value of the aqueous extract of the partitions of walnut septums for 25 minutes at a temperature of 22 °C was within the range of pH=6,5÷6,78. The salt content did not change significantly when processed in an impact type pulsating disperser. The use of the cavitation mechanism makes it possible to remove the target components approximately 2 times more than with pulsating hydrodynamic impact. The determination of the amount of dry substances released from the duration of processing showed that 15 min of cavitation effect on the liquid medium during the extraction of walnut septums ensures the balance of mass concentrations of the "solid-liquid" system. Therefore, it is leads to a reduction in the duration of the process of extracting target substances without additional heating to the boiling temperature. The results of optical microscopy to confirm a uniform powerful effect of pressure pulses on the particles of plant material in the processed environment. When comparing the use of impact and cavitation type pulsating dispersers for the strong rough structure of walnut septums, the efficiency of the extraction process under the influence of the cavitation mechanism is 2 times greater. Therefore, the use of the more powerful cavitation mechanism of the method of DPEI leads to a 2-fold increase in the yield of biologically active substances. At the same

time, the maximum removal from the walnut septums (0,35 %) is achieved after 20 minutes of cavitation processing, which is 57 % proportionally more than the shock effect of hydro-dynamic impact.

The technology of obtaining biologically active substances from plant raw materials is important for the extraction of thermolabile substances, which ensures the optimal application of cavitation mechanisms of the DPEI method in mass transfer devices.

REFERENCES

1. Mates, L.; Rusu, M.E.; Popa, D.-S. Phytochemicals and Biological Activities of Walnut Septum: A Systematic Review. *Antioxidants*, **2023**, *12*(3), 604. https://doi.org/10.3390/antiox12030604.

2. Mehdizadeh, T.; Mohammadipour, N.; Langroodi, A.M.; Raeisi, M. Effect of walnut kernel septum membranes hydroalcoholic extract on the shelf life of traditional butter. *Heliyon*, **2019**, *5*(3), E01296. https://doi.org/10.1016/j.heliyon.2019.e01296

3. Jaćimović, V.; Adakalić, M.; Ercisli, S.; Božović, D.; Bujdoso, G. Fruit Quality Properties of Walnut (*Juglans regia* L.) Genetic Resources in Montenegro. *Sustainability*, **2020,** *12*(23), 9963. https://doi.org/10.3390/su12239963

4. Aghapour, S.K.F.; Sisakhtnezhad, S. Effect of the Internal Septum Extract of the Walnut Kernel on the Mesenchymal Stem Cells Cycle and MSCs-derived Insulin-Producing B-cells Differentiation and Glucose Uptake. *Jentashapir J Cell Mol Biol*. **2021**, *12*(2), e115014. https://doi.org/10.5812/jjcmb.115014

5. Sultanova, M.; Dalabayev, A.; Saduakas, A.; Nurysh, A.; Akzhanov, N.; Yakiyayeva, M. The potential of non-traditional walnut shells waste for the production of antioxidant reach extracts intended for the food industry. *Potravinarstvo Slovak Journal of Food Sciences*, **2023,** 17, 391-404. https://doi.org/10.5219/1862

6. Dolinskyi, A. A.; Ivanitskyi, G. K., *Teplomassoobmen i hidrodinamika v parozhidkostnykh dispersnykh sistemakh. Teplofizicheskie osnovy diskretno-impulsnoho vvoda enerhii* [Heat and mass transfer and hydrodynamics in vapour-liquid disperse systems. Thermophysical basics of the method of discrete-pulse energy input.], Naukova dumka, Kyiv, Ukraine, 2008, p. 381.

7. Basok, B. I.; Novitskaia, M. P.; Chayka, O. I. *Hidrodynamika i teploobmen pri pnevmopulsatsionnom vozdeystvii na zhydkie sistemy* [Hydrodynamics and heat transfer in case of pneumatic pulsation action on liquid systems], Kalyta, Kyiv, 2014, p. 140.

8. Nakorchevskyi, A. I.; Basok, B. I. *Hidrodynamika i massoperenos v heterohennykh sistemakh i pulsiruiushchikh potokakh* [Hydrodynamics and heat and mass transfer in heterogeneous systems and pulsating flows], Naukova dumka, Kyiv, Ukraine, 2001, p. 345.

9. Ivanitskyi, G. K.; Korchynskyi, A. A.; Matiushkin, M. V. *Matematicheskoe modelirovanie protsessov v pulsatsionnom disperhatore udarnoho tipa* [The mathematical modeling of processes in pulsating dispersant of impact type]. *Prom. teplotekhnika* [Industrial heat engineering], Kyiv: **2003**, *25* (1), 29-34. http://ittf.kiev.ua/vidavnicha-diyalnist/

10. Rostagno, M. A.; Prado, J. M.; *Natural Product Extraction: Principles and Applications;* Royal Society of Chemistry, Cambridge, UK, **2013**; pp. 500.

11. Fowsiya, J.; Gunalaban, M. *A Hand Book on: Semi Micro Technique for Extraction of Alkaloids.* International E-Publication, Indore, India, **2015;** pp. 36. https://www.researchgate.net/publication/281113568_A_HAND_BOOK_ON_SEMI_MICRO_T ECHNIQUE_FOR_EXTRACTION_OF_ALKALOIDS

12. Vitenko, T. M. *Hidrodynamichna kavitatsia u masoobminnykh, chimichnykh i biolohichnykh protsessakh* [The hydrodynamic cavitation in mass transfer, chemical and biological processes]. Ternopil Ivan Puliuy National Technical University, Ternopil, Ukraine, 2009, p. 220.

13. Ivanitskyi, G. K.; Chayka, O.I.; Gozhenko, L. P. Zastosuvannia kavitatsiynoho reaktora pulsatsionnoho typu dlia ekstrahuvannia z roslynnoi syrovyny [The use of pulsating cavitation reactor type for extraction of plant raw material]. *Naukovi pratsi ONAKHT* [Scientific Works]. **2017**, *47*, 138-142.

14. Ivanitskiy, G.K.; Gozhenko, L.P. Analiticheskoye issledovaniye usloviy vozniknoveniya kavitatsii v trubie pulsatsionnogo dispergatora udarnogo tipa. *Prom. teplotechnika*, **2014,** 36(6), 49–56.

15. Droździel, P.; Vitenko, T.; Voroshchuk, V.; Narizhnyy, S.; Snizhko, O. Discrete-Impulse Energy Supply in Milk and Dairy Product Processing. *Materials*, **2021**, *14*(15), 4181. https://doi.org/10.3390/ma14154181

ANTIFUNGAL POTENTIAL OF CLOUD-POINT EXTRACT OBTAINED FROM HORNED MELON (*CUCUMIS METULIFERUS*) WASTE

Teodora R. CVANIĆ* ⓘ *, Olja Lj. ŠOVLJANSKI* ⓘ *, Ana M. TOMIĆ* ⓘ *, Aleksandra S. RANITOVIĆ* ⓘ *,*
Dragoljub D. CVETKOVIĆ ⓘ *, Gordana S. ĆETKOVIĆ* ⓘ *, Vanja N. TRAVIČIĆ* ⓘ

Faculty of Technology Novi Sad, University of Novi Sad, Bulevar Cara Lazara 1, Novi Sad, Serbia

In this study, the antimicrobial efficacy of a cloud-point extract (CPE) derived from the peels of horned melon (Cucumis metuliferus) was evaluated. By employing cloud-point extraction, a cutting-edge extraction technique, bioactive phytochemicals were effectively isolated from the peels, yielding a rich concentration of antioxidants and antimicrobial agents. The antifungal activities of the extract, including growth inhibition, minimal inhibitory concentration (MIC), and time-kill kinetics, were tested against phytopathogenic fungal species isolated from fruits, namely Aspergillus sp., Penicillium sp., Trichoderma sp., and Geotrichum sp. The extract exhibited notable antimicrobial properties, with inhibition zones measuring between 16 and 31 mm, and MIC values ranging from 3.75 to 60 mg/mL. High-performance liquid chromatography (HPLC) analysis identified several phenolic compounds within the CPE, including p-hydroxybenzoic acid, gallic acid, protocatechuic acid, caffeic acid, catechin, syringic acid, and vanillic acid. These findings suggest that the CPE of horned melon peels holds noteworthy promise as a natural antimicrobial agent, with potential applications in food preservation and safety. Furthermore, this research indicates the potential of suppressing fungal growth on fresh fruit samples as well, since the work included monitoring the development of fungal contamination on grape samples coated with CPE extract, encouraging the sustainable extraction and application of natural bioactive compounds.

Keywords: Cloud-point extraction, Horned melon peels, Antifungal activity, Phytochemical analysis.

INTRODUCTION

Antimicrobial resistance (AMR) poses a global threat to human health and economic stability, significantly affecting agricultural productivity, food security, and contributing to food waste (1, 2). The growing resistance of microorganisms underscores the urgent need for the discovery and development of new antimicrobial agents. Plants are well-known sources of abundant metabolites with antimicrobial properties, capable of inhibiting the growth of a variety of microorganisms (3). While many synthetic antimicrobial compounds are available, their high production costs and adverse side effects, when compared to plant-derived compounds, highlight the necessity of replacing them with natural alternatives. Natural compounds are favoured for their low toxicity, biodegradability, and eco-friendly nature (4). Moreover, plant-based bioactive compounds often exhibit unique biocidal mechanisms distinct from conventional antibiotics, which may have a profound impact on managing resistant pathogens (5). Among the most widely used natural antimicrobial agents are essential oils and plant extracts obtained from different parts of the plant, such as roots, seeds, leaves, pulp, and flowers (6). The presence of secondary metabolites, including tannins, terpenoids, alkaloids, phenolics, and flavonoids, makes these extracts promising candidates for combating viral, bacterial, fungal, and protozoan infections (7). The

distinct mechanisms of action exhibited by plant-derived bioactive compounds offer a substantial advantage over traditional antibiotics, particularly in the treatment of resistant microorganisms. As a result, these compounds have broad applications in both pharmaceuticals and traditional medicine (5). Recent interest has focused on the extraction of valuable secondary metabolites and evaluating their antimicrobial potential, with particular attention to extraction methods that minimize environmental impact. Green extraction technologies, such as cloud-point extraction (CPE), ultrasound-assisted extraction (UAE), and microwave-assisted extraction (MAE), are gaining traction due to their ability to reduce energy consumption, lower environmental pollution, and produce high-quality extracts (8). CPE, in particular, is a novel solid-liquid extraction technique that offers a cost-effective, non-toxic, and efficient method for concentrating a wide range of analytes (9). CPE operates based on the principle of separating compounds by exploiting the cloud point of non-ionic surfactants, which leads to the partitioning of hydrophobic and hydrophilic molecules into distinct phases. This technique is particularly advantageous for isolating thermally sensitive compounds, as it requires mild conditions and minimal use of organic solvents, making it an environmentally friendly and sustainable approach (10).

In the present study, the peels of horned melon (*Cucumis metuliferus*), a globally cultivated exotic fruit rich in flavonoids, phenolic compounds, glycosides, and carotenoids, were selected as the source material (11). This fruit is native to Africa and recognized for its unique appearance and potential health benefits, such as antidiabetic, antihypertensive, antimicrobial and antioxidant effects (11). The primary objective of this research was to assess the antimicrobial potential of horned melon peel extracts against a range of fungi. Additionally, an applicability test was conducted to evaluate the fungal growth control of the CPE extract on fresh grape samples, focusing on its efficacy against the most resistant fungal strain.

EXPERIMENTAL

PLANT MATERIAL AND CHEMICALS

Horned melon fruits were organically grown in the Pannonia Plain, Novi Sad, Serbia, on the Fruška Gora Mountain (45°12′ N, 19°45′ E). The peel was manually separated under aseptic conditions and freeze-dried using a Martin Crist Alpha 2-4 freeze-drier (Osterode, Germany) for 2 hours at -40 °C. Primary drying occurred at 0.01 mbar and temperatures between -40 °C and 20 °C for 48 hours, followed by ultimate drying at 20 °C to 30 °C and 0.005 mbar for 4 hours. The freeze-dried peel was stored at -20 °C, manually milled into a coarse powder, and kept in a freezer at -20 °C until extraction. Tween 80 was obtained from Alfa Aesar (Karlsruhe, Germany), and all other chemicals were of analytical grade.

Cloud-Point Extraction

The extraction followed the method of Travičić et al. (9). In brief, the horned melon peel sample was mixed with water at a 1:50 ratio, with 10% Tween 80 added. The pH was adjusted to 3, and the mixture was stirred for 20 minutes on a magnetic stirrer, followed by centrifugation at 4000 rpm for 10 minutes. NaCl (18%) was added to the supernatant, and the mixture was incubated at 45 °C for 20 minutes to allow micelle formation. A second centrifugation at 4000 rpm for 10 minutes yielded the targeted surfactant-rich phase as the top layer.

CHEMICAL ANALYSIS

Polyphenolic compounds were identified and quantified using high-performance liquid chromatography (HPLC) on a Shimadzu Prominence system (Shimadzu, Kyoto, Japan), equipped with an LC-20AT binary pump, CTO-20A thermostat, and SIL-20A autosampler, connected to a DAAD detector. Separation was carried out on a Luna C18 RP column (250 mm × 4.6 mm, 5 µm particle size; Phenomenex, Torrance, CA, USA), with a C18 pre-column (4 × 30 mm, Phenomenex). Standards were dissolved in 50% methanol, and chromatograms were recorded from 190 to 800 nm, with identification and quantification at absorption maximums. Concentrations were calculated based on chromatograms and calibration curves of standard solutions.

ANTIFUNGAL ACTIVITY ASSESSMENT

The antifungal potential of the CPE is evaluated through a series of *in vitro* assays growth inhibition assays. The CPE is tested against four fungal species which are isolated from fruit samples: *Aspergillus* sp., *Penicillium* sp., *Trichoderma* sp., and *Geotrichum* sp. Inhibition zones are measured to assess the effectiveness of the extract using the disk-diffusion method (12), while minimal fungicidal concentration (MFC) is determined using microtiter assay described in detail by Šovljanski et al (13). The time-dependent fungicidal potential is studied to understand the rate at which it kills the fungal cells during contact between CPE extract and sensitive fungi by applying a test-kill kinetics study (14).

APPLICABILITY TEST

Fresh grapes were purchased from a local market, thoroughly washed with distilled water, and air-dried in a laminar flow chamber at room temperature. *Aspergillus* sp. was cultured on potato dextrose agar (PDA, HiMedia, Mumbai, India) at 25 °C for 5 days, harvested, and filtered to create a spore suspension at 6 log spores/mL. All grape samples are measured and divided into sterile containers to obtain two sets of samples: uncontaminated samples (controls) and contaminated samples (artificially contaminated samples with fungal suspension). In each set, samples are additionally separated into following groups: Group A (control, no treatment, sprayed with water), Group B (control treated with extraction solvent, sprayed with surfactant-rich phase without horned melon extract), and Group C (treated with CPE extract from horned melon peels). All contaminated samples are treated with 100 µL of the fungal suspension, while the control received the same volume of sterilized water. All samples were aerobically stored at 21 °C and 85% relative humidity for 8 days. Digital images of each grape were captured under consistent lighting and distance to document fungal growth.

RESULTS AND DISCUSSION

The cloud-point extract (CPE) from horned melon peels exhibited a rich profile of polyphenolic compounds, as identified by HPLC analysis (Table 1). Catechin was the most abundant polyphenol, with a concentration of 42.19 mg/100g, followed by vanillic acid (5.55 mg/100g) and gallic acid (3.72 mg/100g). Other phenolic compounds, including protocatechic acid (2.81 mg/100g), syringic acid (2.49 mg/100g), caffeic acid (0.52 mg/100g), and *p*-hydroxybenzoic acid (0.37 mg/100g), were present in smaller amounts. The presence

of catechin as the dominant polyphenol is notable, given its well-documented antioxidant and antimicrobial properties. Previous studies have highlighted catechin's significant role in various plant extracts, contributing to their biological activities, particularly antimicrobial and antioxidant effects (15). The high catechin content in the CPE from horned melon peels suggests a potential for strong bioactivity, aligning with findings from catechin-rich sources such as green tea (16). Gallic acid, the second most abundant polyphenol, is also known for its potent antimicrobial and antioxidant effects. Studies on gallic acid have shown its ability to inhibit the growth of various microorganisms (17), supporting its role in the antifungal activity observed in the current study.

The antifungal potential of the CPE was evaluated against four fungal species: *Aspergillus* sp., *Penicillium* sp., *Trichoderma* sp., and *Geotrichum* sp. The extract exhibited notable antifungal activity, with inhibition zones ranging from 16.00 mm to 31.00 mm. The largest inhibition zone was observed for *Penicillium* sp. (31.00 mm), followed closely by *Trichoderma* sp. (30.33 mm) and *Geotrichum* sp. (26.67 mm). *Aspergillus* sp. showed the smallest inhibition zone at 16.00 mm (Table 1). Regarding the minimal fungicidal concentration (MFC), *Trichoderma* sp. displayed the greatest susceptibility, with an MFC of 3.75 mg/mL. Further, *Penicillium* sp. and *Geotrichum* sp. also showed significant susceptibility, with MFC values of 7.50 mg/mL and 30.00 mg/mL, respectively, while *Aspergillus* sp. required a much higher concentration (60.00 mg/mL) for fungicidal action. These results align with existing literature on plant-derived polyphenols, which are known to exhibit antimicrobial properties by disrupting fungal cell membranes and inhibiting growth (18). The strong antifungal activity of the CPE, particularly against *Penicillium* sp., suggests its potential as a natural antifungal agent. Comparable studies have demonstrated similar efficacy in polyphenol-rich plant extracts, supporting their use in agricultural and food preservation applications (19).

Table 1. Evaluation of dominant polyphenolic compounds and antifungal potential of the CPE extract

HPLC analysis of polyphenolic compounds		
The identified compound	Concentration (mg/100g)	Total content (mg/100g dw)
p-hydroxybenzenic acid	0.37	
Gallic acid	3.72	
Protocatechic acid	2.81	
Caffeic acid	0.52	57.65
Catechin	42.19	
Syringic acid	2.49	
Vanillic acid	5.55	
Antifungal potential		
Test fungi	Inhibition zones (mm)	Minimal fungicidal concentration (mg/mL)
Aspergillus sp.	16.00±0.00	60.00±0.00
Penicillium sp.	31.00±1.00	7.50±0.00
Trichoderma sp.	30.33±0.56	3.75±0.00
Geotrichum sp.	26.67±0.56	30.00±0.00

Since the cloud-point extract from horned melon peels contains significant amounts of catechin and other polyphenolic compounds, which contribute to its observed antifungal properties, the time-kill kinetics was conducted to make additional view of the pharmaco-dynamic potential of the fungicide effect. Figure 1 demonstrates the effectiveness of the cloud-point extract (CPE) of horned melon peels against tested fungal species. For *Aspergillus* sp., the extract shows moderate fungicidal activity which are additionally confirmed that this specie is the most resistant one using in this study (Figure 1a). At MIC, there is a steady reduction in fungal concentration over time, with significant inhibition observed by 48 hours and almost complete kill at 96 hours. At 0.5 MIC, the CPE extract shows less inhibition, and the fungal load remains relatively stable, suggesting that higher concentrations are necessary for effective control of *Aspergillus* growth. Since the MIC concentration for *Aspergillus* sp. is the initial concentration of CPE extract, multiple MICs were unable to test.
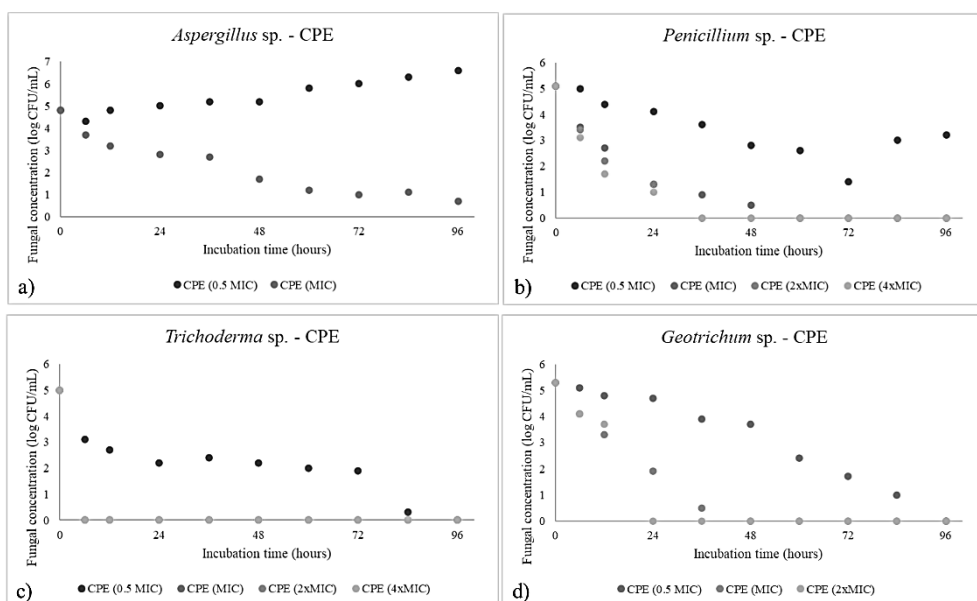

Figure 1. Time-kill kinetics study for CPE extract

For *Penicillium* sp., the CPE extract exhibits potent antifungal activity even at lower concentrations (Figure 1b). The MIC and 2xMIC concentrations demonstrate a rapid decline in fungal load within the first 24 hours, with near-complete elimination by 48 hours. The 4x MIC shows complete inhibition much earlier, at 24 hours, emphasizing its efficiency. At 0.5 MIC, the reduction is slower, but there is still significant inhibition observed over time. The pronounced response to CPE in *Penicillium* sp. further supports the high susceptibility of this fungal strain, which aligns with previous reports of Penicillium being highly sensitive to polyphenolic compounds (19). In the case of *Trichoderma* sp., the extract shows rapid and effective antifungal action (Figure 1c). At MIC, the fungal load decreases to undetectable levels within the first 24 hours, and this effect is maintained through 96 hours. The killing effect is equally pronounced at 2x and 4x MIC concentrations, where fungal eradication occurs within 24 hours. Even at 0.5 MIC, the extract significantly reduces

fungal growth, indicating strong efficacy of the CPE against this fungal strain. This confirms the susceptibility of *Trichoderma* sp. to the polyphenolic compounds in the extract, particularly catechin, which is known to disrupt fungal cell walls (18). *Geotrichum* sp. shows a dose-dependent response to the CPE extract (Figure 1d). At MIC, there is a clear reduction in fungal load, although the effect is not as immediate as seen with *Penicillium* or *Trichoderma.* The 2x and 4x MIC concentrations display stronger inhibitory effects, with significant fungal reduction by 48 hours. However, at 0.5 MIC, there is only a moderate decrease in fungal concentration, suggesting that higher doses are necessary for effective fungicidal activity. The time-kill kinetics data reveals that the CPE extract of horned melon peels exhibits a strong antifungal effect across all tested fungal species, even though the degree of effectiveness varies between species. *Penicillium* sp. and *Trichoderma* sp. show the highest susceptibility, with rapid fungal kill even at MIC concentrations. *Aspergillus* sp. and *Geotrichum* sp. require higher initial concentrations for similar levels of inhibition, indicating more moderate susceptibility.

Based on the results shown in Table 1 and Figure 1, it is clear that the CPE of horned melon peels possesses significant antifungal potential. However, the study also reveals that *Aspergillus* sp. is the most resistant fungal species, requiring the highest concentration of CPE extract for effective growth inhibition. *Aspergillus* is a well-known phytopathogen, which poses challenges in both agricultural and food preservation settings due to its ability to survive and thrive under various conditions. Given this resistance, *Aspergillus* sp. was chosen for further *in vivo* evaluation of the CPE extract's applicability. The *in vivo* assessment involved testing the CPE extract on grapes, a highly perishable fruit prone to fungal contamination during storage. The experiment monitored fungal growth and the effectiveness of the CPE extract in inhibiting fungal development on grape samples over an 8-day storage period. This test is critical in determining whether the CPE extract can be applied in practical settings, such as food preservation, where controlling fungal spoilage is paramount.

Figure 2 demonstrates the *in vivo* antifungal assessment of the CPE extract on grape samples over an 8-day storage period.

The study aimed to evaluate the potential of the CPE extract in preventing fungal growth, specifically *Aspergillus* sp., a known phytopathogen. The experiment involved both uncontaminated and contaminated samples treated with water (Control A), extraction solvent (Control B), and CPE extract (Test C).

Based on the obtained results, the uncontaminated grape samples treated with water (control A) showed no significant fungal growth across the 8-day storage period. However, by day 8, the samples began to show slight degradation, with minor shriveling and color changes, indicating organoleptic unacceptability. Grape samples treated with the extraction solvent (control B) exhibited slightly better preservation than those treated with water, but the overall trend of spoilage remained similar by day 8, where the samples showed slight yellowing and shriveling, indicating the limited protective effect of the solvent. The samples treated with the CPE extract (control C) remained in notably better condition throughout the 8 days. Minimal visual degradation was observed, and no fungal growth was detected. The grapes maintained their color and texture better than the other controls, suggesting that the polyphenolic compounds in the CPE extract provided protective effects against spoilage and oxidative degradation, likely due to the extract's antioxidant properties.

Given contamination samples with *Aspergillus* sp., the contaminated samples treated with water (sample A) showed rapid fungal growth, with visible mold development by day 3. By day 5, extensive fungal colonization was observed, and by day 8, the grapes were

heavily deteriorated, indicating that water alone had no inhibitory effect on *Aspergillus* sp. growth which was expected. Grape samples treated with the extraction solvent (sample B) showed a slightly delayed onset of fungal growth compared to water-treated samples. However, by day 5, fungal growth became more prominent, and by day 8, the samples were almost entirely colonized by *Aspergillus* sp., indicating that the extraction solvent had minimal antifungal activity on its own. In stark contrast to the control groups, the samples treated with the CPE extract demonstrated significant resistance to fungal colonization. By day 8, the samples treated with the CPE extract displayed no fungal development, maintaining a better overall appearance and minimal deterioration than the untreated and solvent-treated controls. This suggests that the CPE extract possesses potent antifungal potential, effectively inhibiting the growth of *Aspergillus* sp. over the storage period. The *in vivo* results clearly demonstrate the antifungal efficacy of the CPE extract in both preventing fungal growth and preserving the quality of grape samples. The extract showed notable protective effects on uncontaminated samples, likely due to its polyphenolic content, which is known for its antioxidant and antimicrobial properties.
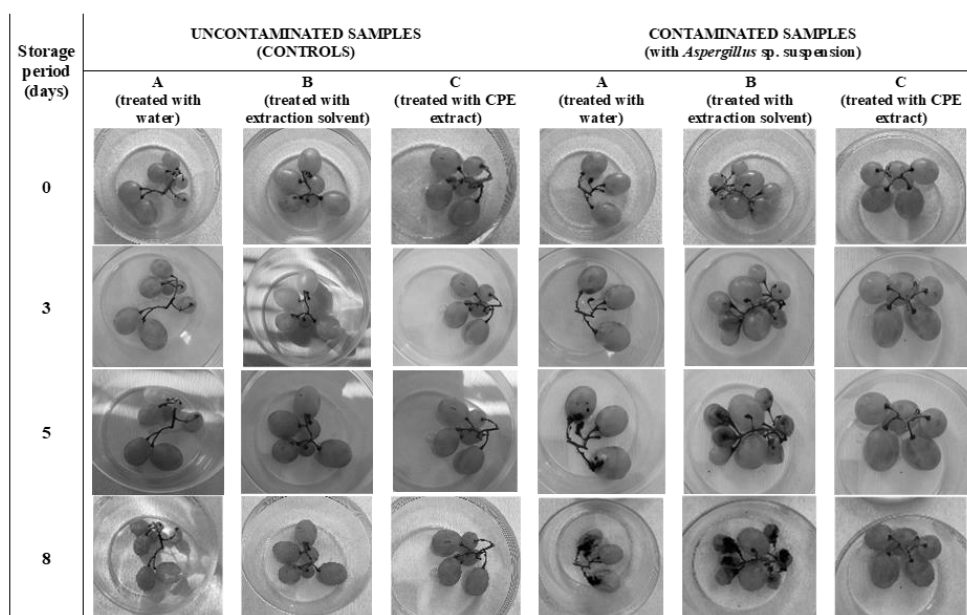

Figure 2. Evaluation of CPE potential during storage of grapes

CONCLUSION

The present study demonstrates the potent antifungal properties of the cloud-point extract (CPE) from horned melon peels. The extract was rich in polyphenolic compounds, with catechin being the most abundant, contributing to its strong biological activity. The antifungal assays revealed significant inhibition of fungal growth, with *Penicillium* sp. and *Trichoderma* sp. showing the highest susceptibility. However, *Aspergillus* sp. exhibited greater resistance, requiring higher concentrations of the CPE extract for effective inhibition. The *in vivo* experiments on grape samples further validated the antifungal efficacy of

the CPE extract. The CPE-treated grapes demonstrated marked resistance to fungal growth, particularly against *Aspergillus* sp., and showed better preservation in terms of texture and color over the 8-day storage period compared to control samples. These results highlight the potential of the CPE extract as a natural preservative, capable of mitigating fungal contamination and spoilage in post-harvest storage, especially in perishable fruits like grapes. Overall, the obtained results suggest that the CPE extract can serve as a promising alternative to synthetic fungicides and preservatives in the agricultural and food industries. Its natural composition, coupled with effective antifungal activity, presents an eco-friendly and sustainable solution for enhancing the shelf life of fruits and controlling fungal pathogens. Further research is recommended to optimize the extraction process and investigate the application of the CPE extract in other fruits and food systems.

Acknowledgement

REFERENCES

1. Šovljanski, O.; Ranitović, A.; Tomić, A.; Ćetković, N.; Miljković A.; Saveljić, A.; Cvetković D. Synergistic Strategies of Heat and Peroxyacetic Acid Disinfection Treatments for *Salmonella* Control. *Processes*, **2023**, *12*(11), 1336. https://doi.org/10.3390/pathogens12111336

2. Salam, M.A.; Al-Amin, M.Y.; Salam, M.T.; Pawar, J.S.; Akhter, N.; Rabaan, A.A.; Alqumber, M.A.A. Antimicrobial Resistance: A Growing Serious Threat for Global Public Health. *Healthcare*, **2023**, *11*(13), 1946. https://doi.org/10.3390/healthcare11131946

3. Abdallah, E.M.; Alhatlani, B.Y.; de Paula Menezes, R.; Martins, C.H.G. Back to Nature: Medicinal Plants as Promising Sources for Antibacterial Drugs in the Post-Antibiotic Era. *Plants,* **2023**, *12*(17), 3077. https://doi.org/10.3390/plants12173077

4. Vaou, N.; Stavropoulou, E.; Voidarou, C.; Tsigalou, C.; Bezirtzoglou, E. Towards Advances in Medicinal Plant Antimicrobial Activity: A Review Study on Challenges and Future Perspectives. *Microorganisms*, **2021**, *9*(10), 2041.

5. Arip, M.; Selvaraja, M.; R, M.; Tan Lee, F.; Leong Mun Y.; Tan Puay, L.; Yap Vi, L.; Chinnapan, S.; Tat Ng, C.; Abdullah, M.; K, D.; Jubair, N. Review on Plant-Based Management in Combating Antimicrobial Resistance - Mechanistic Perspective. *Frontiers in Pharmacology*, **2022**, *13,* 879495. https://doi.org/10.3389/fphar.2022.879495

6. Bolouri, P.; Salami, R.; Kouhi, S.; Kordi, M.; Asgari Lajayer, B.; Hadian, J.; Astatkie, T. Applications of Essential Oils and Plant Extracts in Different Industries. *Molecules*, **2022**, *27*(24), 8999. https://doi.org/10.3390/molecules27248999

7. Roy, A.; Khan, A.; Ahmad, I.; Alghamdi, S.; Rajab, B.S.; Babalghith, A.O.; Alshahrani, M.Y.; Islam, S.; Islam, M.R. Flavonoids a Bioactive Compound from Medicinal Plants and Its Therapeutic Applications. *BioMed research international*, **2022**, *2022*, 5445291. https://doi.org/10.1155/2022/5445291

8. Martins, R.; Barbosa, A.; Advinha, B.; Sales, H.; Pontes, R.; Nunes, J. Green Extraction Techniques of Bioactive Compounds: A State-of-the-Art Review. *Processes*, **2023**, *11*, 2255. https://doi.org/10.3390/pr11082255

9. Travičić, V.; Cvanić, T.; Šovljanski, O.; Erceg, T.; Perović, M.; Stupar, A.; Ćetković, G. Updating the Status quo on the Eco-Friendly Approach for Antioxidants Recovered from Plant Matrices Using Cloud Point Extraction. *Antioxidants*, **2024**, *13*, 280. https://doi.org/10.3390/antiox13030280

10. Giovanoudis, I.; Athanasiadis, V.; Chatzimitakos, T.; Kalompatsios, D.; Bozinou, E.; Gortzi, O.; Nanos, G.D.; Lalas, S.I. Implementation of Cloud Point Extraction Using Surfactants in the Recovery of Polyphenols from Apricot Cannery Waste. *Eng*, **2023**, *4*, 1225-1235.

11. Šovljanski, O.; Šeregelj, V.; Pezo, L.; Tumbas Šaponjac, V.; Vulić, J.; Cvanić, T.; Markov, S.; Ćetković, G.; Čanadanović-Brunet, J. Horned Melon Pulp, Peel, and Seed: New Insight into Phytochemical and Biological Properties. *Antioxidants,* **2022**, *11*, 825. https://doi.org/10.3390/antiox11050825

12. Tomić, A.; Šovljanski, O.; Nikolić, V.; Pezo, L.; Aćimović, M.; Cvetković, M.; Stanojev, J.; Kuzmanović, N.; Markov, S. Screening of Antifungal Activity of Essential Oils in Controlling Biocontamination of Historical Papers in Archives. *Antibiotics*, **2023**, *12*, 103. https://doi.org/10.3390/antibiotics12010103

13. Aćimović, M.; Zeremski, T.; Šovljanski, O.; Lončar, B.; Pezo, L.; Zheljazkov, V.D.; Pezo, M.; Šuput, D., Kurunci, Z. Seasonal Variations in Essential Oil Composition of Immortelle Cultivated in Serbia. *Horticulturae*, **2022**, *8*, 1183.

14. Šovljanski, O.; Saveljić, A.; Aćimović, M.; Šeregelj, V.; Pezo, L.; Tomić, A.; Ćetković, G.; Tešević, V. Biological Profiling of Essential Oils and Hydrolates of *Ocimum basilicum* var. *Genovese* and var. *Minimum* Originated from Serbia. *Processes*, **2022**, *10*, 1893. https://doi.org/10.3390/pr10091893

15. Kim, S.; Yang, Y.; Choi, I. Catechin content and antioxidant activity of green tea by various extraction methods. *Journal of Functional Foods*, **2016**, *23*, 167–173.

16. Yang, R., Zhang, Z.: Antimicrobial activity of catechins from green tea: A mechanistic approach. *Biochemical and Biophysical Research Communications*, **2019**, *518*(2), 1092-1097.

17. Moo-Huchin, V.; Estrada-León, R.; Sauri-Duch, E. Gallic acid and its role in antimicrobial properties of tropical fruit extracts. *Food Chemistry*, **2014,** *164*, 82-87.

18. Falcão, D.; Lima, C.;Almeida, J. Antimicrobial and antifungal properties of plant-derived polyphenols: A review. *Molecules,* **2019**, *24*(3), 565. https://doi.org/10.3390/antibiotics11010046

19. Hussain, M.; Rana, I.; Shafique, M.; Rehman, M. Antifungal efficacy of polyphenolic extracts from plant sources against common foodborne fungi. *Food Control,* **2021,** *121*, 107387. https://doi.org/10.3390/molecules25163748

INVESTIGATION OF MICROBIAL BIOCONTROL AGENTS AND ESSENTIAL OILS SYNERGISM IN SUPPRESSION OF AFLATOXIGENIC
Aspergillus flavus

Tatjana D. DUJKOVIĆ, Ivana S. DANILOV, Vanja R. VLAJKOV*,
Nevena B. GLADIKOSTIĆ, Selena Ž. DMITROVIĆ, Nataša Lj. LUKIĆ,
Aleksandar I. JOKIĆ, Jovana A. GRAHOVAC

Faculty of Technology Novi Sad, University of Novi Sad, Bulevar Cara Lazara 1, Novi Sad, Serbia

Confectionery industry wastewater contains substantial amounts of organic and inorganic matter, posing a significant environmental burden. Microbial bioconversion offers a promising solution by utilizing these nutrients to produce value-added products, such as microbial biocontrol agents. Bacillus spp. in combination with essential oils, are particularly promising for fungicidal applications. The aim of this study was to investigate the potential of confectionery industry wastewater as a medium for producing the Bacillus sp. BioSol021-based biocontrol agent and to assess the effects of incorporating essential oils into the cultivation medium on bacterial growth and antimicrobial activity against the aflatoxigenic fungal pathogen Aspergillus flavus. Biomass content of Bacillus sp. BioSol021 was measured using the plate count method, while antifungal activity was evaluated using the well-diffusion method. The biomass content of Bacillus sp. BioSol021 during cultivation suggests the potential for utilizing this waste as suitable substrate for microbial growth, as no inhibition was observed. However, the addition of essential nutrients' sources could be considered to enhance biomass proliferation. The applied essential oils did not inhibit bacterial growth; rather, thyme and fennel oils increased biomass content compared to medium without essential oils. The highest antimicrobial activity against Aspergillus flavus was observed using oregano oil, followed by basil oil, with maximum activity at 72 hours of cultivation, which also corresponded with the highest biomass content. Future research should focus on further investigating wastewater seasonal characteristics, optimizing bioprocess parameters, and exploring the specific mechanisms of biocontrol action of both the Bacillus isolate and essential oils, as well as their interactions.

Keywords: confectionery industry wastewater, biocontrol, *Bacillus amyloliquefaciens*, essential oils, *Aspergillus flavus*.

INTRODUCTION

The rapid growth of the global population, followed by the economic development in emerging countries, is significantly increasing global food demand. As efforts intensify to enhance food production and prevent supply disruptions, the large volumes of wastewater generated during food manufacturing processes across various sectors are becoming a major environmental concern (1). The confectionery industry, an important sector in the food industry, produces a variety of products such as chocolates, cereals, starch-based confections, dairy products, canned fruits, jams, and sweets (2), generating substantial volumes of wastewater with high levels of contaminants. While confectionery industry wastewater (CIW) generally lacks toxic substances like heavy metals and is considered less toxic compared to other industrial effluents, it contains significant amounts of biodegradable or-

ganic matter (3). CIW is primarily composed of organic compounds and suspended solids, resulting in high chemical oxygen demand (COD) and biological oxygen demand (BOD) values. Typically, COD values range from 1,000 to 12,000 mg O_2/L, while BOD_5 values range from 500 to 8,000 mg O_2/L. This wastewater contains organic substances such as sugars, fats, and dyes, as well as residues from cleaning and disinfecting agents, which can alter pH levels and increase nitrogen and phosphorus concentrations (4). Such composition is especially critical for industries located in small municipalities, where the low dilution factor can lead to increased environmental impact (3).

The most commonly used methods for treating confectionery wastewater include mechanical pre-treatment, anaerobic and aerobic biological treatments, followed by coagulation/flocculation (5). Considering the presence of inorganic and organic contaminants in confectionery wastewater, which can provide nutrients for microbial growth, a viable treatment approach could involve microbial bioconversion. This method leverages the available nutrients to generate value-added products, such as microbial biocontrol agents (3).

Biological control represents an innovative strategy in agriculture that relays on biological agents usage to protect plants from pathogens, providing an alternative to conventional agrochemicals such as synthetic pesticides. This approach leverages microbial biocontrol agents, including microbial biomass and metabolites, which are effective in managing plant diseases (6). These agents are characterised by their high efficacy, selective biocontrol activity, and diverse mechanisms of action, which contribute to antimicrobial resistance risk minimization. They produce a range of bioactive compounds, such as antibiotics, endotoxins, bacteriocins, siderophores, hydrolytic enzymes, hydrogen cyanide (HCN), phenazine-1-carboxylic acid (PCA), and 2,4-diacetylphloroglucinol (DAPG), included in the pathogen suppression and disease prevention. Additionally, these agents support soil quality and biodiversity (7).

Bacillus spp. are widely recognized as effective biocontrol agents (BCAs) due to their effectiveness in managing plant diseases. These bacteria are highly competitive in their natural environments and capable of colonizing the roots of various monocot and dicot species. Root colonization is crucial for biocontrol efficacy, enabling the secretion of antimicrobial compounds and plant resistance elicitors (8). *Bacillus* spp. employ several mechanisms to inhibit the development of phytopathogenic organisms and plant disease occurrence. They produce antibiotics that target and suppress pathogen growth, secrete siderophores to chelate iron and deprive pathogens of this essential nutrient, and release lytic enzymes that degrade pathogen cell wall. Additionally, these bacteria generate toxins that directly damage or kill pathogens and induce systemic resistance in plants, enhancing their own defense mechanisms against pathogen attacks (9).

On the other hand, essential oils are also effective for protecting plants from various pathogens. These oils, derived from various plant parts, have shown promising effects in eco-friendly pest management. They are aromatic, volatile organic compounds with antibacterial, insecticidal, and antimicrobial properties, and have demonstrated significant potential in reducing damage caused by phytopathogenic fungi (10).

The *Aspergillus* genus, known for its ability to produce secondary metabolites with potent toxic effects, is recognized as one of the most significant and widespread fungal pathogens threatening crops (11). *Aspergillus flavus* is a well-known opportunistic pathogen that infects a variety of economically important crops, including corn, oilseeds, rice, and nuts, and a major producer of aflatoxins. The International Agency for Research on Cancer (IARC) has classified aflatoxin B1 (AFB1) as a Group 1 carcinogen, indicating it poses a serious carcinogenic risk to both humans and animals (12). Chemical control of

fungal pathogens, including *Aspergillus flavus*, typically involves synthetic fungicides with distinct modes of action. Integrated Pest Management (IPM) strategies often recommend using fungicides with different modes of action either in mixtures or alternately on the same crop. Recent fungicides include succinate dehydrogenase inhibitors (SDHIs), phenyl-pyr-roles (PP fungicides), which disrupt fungal osmotic signal transduction and osmoregulation (e.g., fludioxonil), as well as benzimidazole carbamates and demethylation inhibitors (DMIs), which interfere with sterol biosynthesis in fungal cell membranes (13). In addition to chemical control, significant efforts are being made to develop effective biological control methods for managing these pathogens. One of the leading candidates among bio-based fungicides are representatives of the *Bacillus* genus, followed by essential oils with a considerable potential in this area (6, 11, 14-17).

The objective of this study was to investigate the potential of microbial biocontrol agent production using the *Bacillus* sp. isolate BioSol021 as a producing microorganism, and confectionery industry wastewater as an alternative medium. Additionally, the study aimed to assess the effects of incorporating essential oils into the cultivation medium on both, the growth of the microorganism and its antimicrobial activity against the aflatoxigenic fungal pathogen *Aspergillus flavus*.

EXPERIMENTAL

MICROORGANISMS

The microorganism utilized in this study was *Bacillus* sp. strain BioSol021, isolated from the rhizosphere of common beans (*Phaseolus vulgaris*). This strain was identified as a member of the *Bacillus amyloliquefaciens* operational group based on 16S rRNA gene sequencing (GenBank accession number ON569805) and biochemical characterization using VITEK2 BCL cards (Biomerieux, Marcy-l'Étoile, France) (18). The test microorganism, or phytopathogen, used in the study was *Aspergillus flavus* ATCC 22546.

The producing microorganism, *Bacillus* sp. strain BioSol021, was kept on a semi-solid commercial nutrient agar medium (HiMedia Laboratories, India). The fungal test microorganism, *Aspergillus flavus* ATCC 22546, was preserved on a semi-solid synthetic medium, SMA (Sabouraud maltose agar). Both microorganisms were stored at 4 °C. To reactivate their metabolic activity and reproductive capability, the microorganisms were refreshed on the same nutrient media used for storage under the following conditions: *Bacillus* sp. BioSol021 at 28 °C for 48 hours; *Aspergillus flavus* ATCC 22546 at 26 °C for 120 hours.

MEDIA AND CULTIVATION CONDITIONS

The inoculum of the producing microorganism was prepared by transferring a loopful of the refreshed biomass into a synthetic liquid medium, nutrient broth (HiMedia Laboratories, India), and cultivating it on a laboratory rotary shaker at 28 °C and 150 rpm with spontaneous aeration for 48 hours. Ten percent (v/v) of the inoculum was used for inoculation of the cultivation medium.

Cultivation of the producing microorganism was performed using confectionary industry wastewater (CIW) both with and without the addition of the selected essential oils. The confectionery industry wastewater was acquired from one of the largest industrial producers in the Republic of Serbia and collected as a mixture of effluents from all production faci-

lities. The internal wastewater quality control parameters obtained from the industrial partner are given in Table 1. The essential oils were commercially acquired from the agricultural holding from Bačko Novo Selo, Republic of Serbia, and were produced from organically grown aromatic plants. In each of the 10 Erlenmeyer flasks (300 mL), 100 mL of CIW was added. All cultivation media were sterilized by autoclaving at 121 °C and 2.1 bar for 20 min. Subsequently, 5 drops (0.05 mL) of different essential oils were introduced into each flask as follows: cumin in the first flask, fennel in the second, basil in the third, followed by thyme, sage, German chamomile, dill, savory, and oregano. CIW without added essential oil was used as a control. Cultivation of the producing microorganism was carried out on a laboratory shaker at 28 ℃, with an external agitation rate of 150 rpm and spontaneous aeration for 96 hours. Daily sampling was conducted to assess biomass growth and antimicrobial activity against *Aspergillus flavus* ATCC 22546.

Table 1. Quality parameters of the confectionery industry wastewater used as media basis for production of microbial biocontrol agents.

Parameter/Effluent	pH value	Dry matter (mg/L)	COD (mg O_2/L)	BOD (mg O_2/L)
CIW	5.26	2500	4950	1641

BIOMASS CONTENT DETERMINATION

The biomass content of *Bacillus* sp. BioSol021 in daily samples of cultivation broth was determined using the plate count method. Seven dilutions were prepared for each sample to achieve a dilution range from 10^{-1} to 10^{-7}. The plating method involved mixing 0.5 mL of the prepared dilutions (-5, -6, and -7) with previously melted and tempered (50±1 °C) nutrient agar, vortexing, and then pouring the mixture into Petri dishes. The plates were incubated at 28 °C for 48 hours, after which the number of individual colonies was counted, and colony-forming units per mL were calculated using the following equation:

$$CFU/mL = \frac{number\ of\ colonies * dilution\ factor}{volume\ of\ specimen\ used} \quad [1]$$

IN VITRO BIOCONTROL EXPERIMENTS

Antifungal activity of *Bacillus* sp. BioSol021 cultivation broth samples collected at different cultivation time points was tested using the well-diffusion method against the test fungal pathogen *Aspergillus flavus* ATCC 22546. The suspension of the test microorganism was prepared by adding the fungal biomass in sterile saline to achieve the final concentration of 10^5 CFU/mL. One milliliter of this fungal suspension was mixed with melted and tempered (50±1 °C) SMA medium and spread in 90 mm Petri plates. After solidification of the medium, three wells, each 10 mm in diameter, were made in each plate, and 100 μL volume of the cultivation broth sample was added to each well. The plates were incubated at 26 °C for 96 hours, after which the diameters of the inhibition zones were measured.

EXPERIMENTAL DATA ANALYSIS

Statistical analysis of the experimental data was performed using Statistica 13.3 software (Dell Technologies, TX, USA). Duncan's multiple range test was employed to identify homogeneous groups of variances among the independent variables. Microsoft Excel (Microsoft Corporation, Washington DC, USA) was used for calculation of mean values and standard deviations and for graphical representation of the experimental results. All statistical analyses were conducted at a 95% significance level.

RESULTS AND DISCUSSION

BIOMASS CONTENT OF *Bacillus* sp. BIOSOL021 DURING CULTIVATION ON CONFECTIONERY INDUSTRY WASTEWATER WITH AND WITHOUT THE ADDITION OF ESSENTIAL OILS

The growth of *Bacillus* sp. isolate BioSol021 in the wastewater confectionery industry wastewater-based medium, with the addition of various essential oils, was monitored over 96 hours and compared to growth in wastewater without the addition of essential oils. The addition of these essential oils in most cases did not have a significant impact on the bacterial growth of the tested isolate as shown in Figures 1 and 2. All samples, with the exception of samples EO1 and EO2 exhibited maximum growth at 72 hours, followed by a decline in the number of viable cells, indicating the onset of the death phase. In contrast, samples EO1 and EO2 demonstrated maximum growth at 96 hours, suggesting that the death phase was absent in these media. Notably, sample EO2, which included the addition of fennel essential oil, exhibited the highest microbial growth, with a maximum biomass concentration reaching 8.5 log CFU/mL at 96 h. Conversely, the cultivation medium containing sage essential oil exhibited the lowest microbial growth, indicating an inhibitory effect of this essential oil on the growth of the investigated *Bacillus* isolate. Although there was an initial increase in the growth during the first 24 hours, a rapid decline was observed thereafter. When examining the growth curve of *Bacillus* sp. BioSol021 in confectionery industry wastewater, standard kinetic patterns were observed. However, the growth is less pronounced than what would be expected in a medium with all the necessary nutrients, showing an increase of just under 1 log unit over 72 hours. These results suggest that the medium lacks sufficient nutrient sources for substantial biomass proliferation. Therefore, it is necessary to consider adding primarily a suitable carbon source, followed by investigation of providing additional amounts of other essential nutrients, such as nitrogen and phosphorus sources.
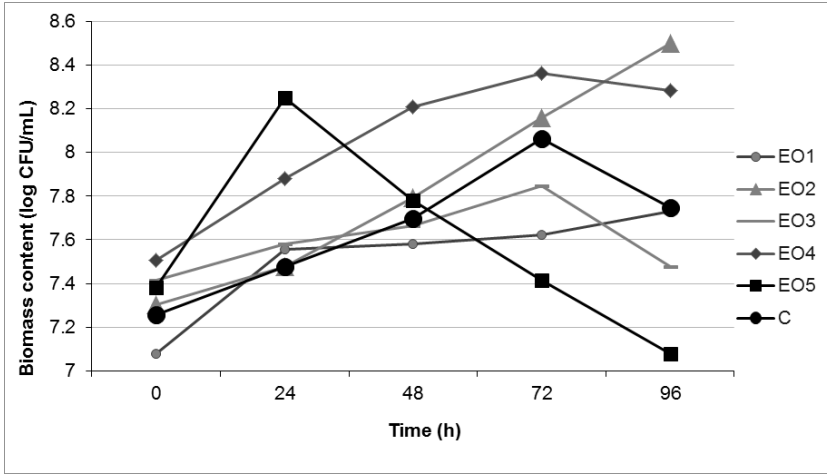
Figure 1. Biomass content of *Bacillus* sp. BioSol021 during cultivation using confectionery industry wastewater with and without addition of essential oils (EO1-cumin; EO2-fennel; EO3-basil; EO4-thyme; EO5-sage; C-CIW without essential oils)
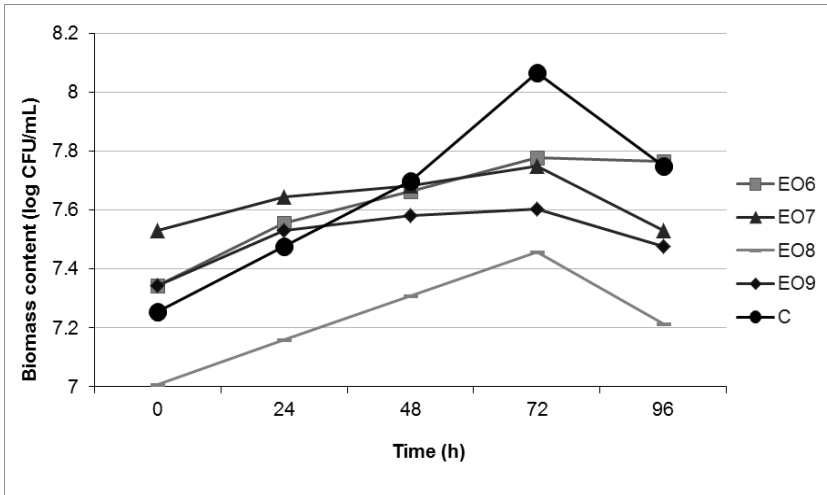

Figure 2. Biomass content of *Bacillus* sp. BioSol021 during cultivation using confectionery industry wastewater with and without addition of essential oils (EO6-German chamomile; EO7-dill; EO8-savory; EO9-oregano; C-CIW without essential oils)

While existing research indicates that essential oils can inhibit *Bacillus* species, particularly those associated with food spoilage, such as *Bacillus cereus* (19, 20), our study did not observe a substantial inhibitory effect. On the contrary, the presence of certain essential oils, such as EO2 and EO4, promoted the growth of the *Bacillus* isolate. The other isolates exhibited similar bacterial growth trend comparable to the one observed in the medium without the addition of these oils, with cell counts consistently remaining above 10^7 CFU/mL.

BIOCONTROL ACTIVITY OF *Bacillus* sp. BIOSOL021 AGAINST *Aspergillus flavus*

To investigate the biocontrol activity of *Bacillus* sp. BioSol021 cultivated using CIW with or without the addition of essential oils, the well diffusion method was used with cultivation broth samples collected at different time points. The greatest inhibitory activity against *Aspergillus flavus* ATCC 22546 was observed at 72nd hour of cultivation. Table 2 presents the mean values of the inhibition zone diameters obtained from the 72-hour samples, which directly indicate the suppressive effects of the cultivation broth samples against the investigated fungal pathogen.

Table 1. Mean values and standard deviations of inhibition zone diameters obtained using 72-hour samples of cultivation broths against *Aspergillus flavus* ATCC 22546.

Sample	Inhibition zone diameter (mm)
EO2	44.00±2.00[a]
EO7	45.00±1.00[a]
EO1	47.33±1.52[b]
EO4	48.00±2.00[b]
EO6	50.66±1.15[c]
EO5	52.00±1.73[cd]
C	52.66±1.15[cd]
EO8	53.66±1.15[d]
EO3	60.00±2.00[e]
EO9	60.33±1.52[e]

* EO1 - cumin; EO2 - fennel; EO3 - basil; EO4 - thyme; EO5 - sage; C - CIW without essential oils; EO6 - German chamomile; EO7 - dill; EO8 - savory; EO9 - oregano. Different letters next to the values indicate different homogeneous groups based on Duncan's multiple range test.

The lowest antimicrobial activity against *Aspergillus flavus* ATCC 22546 was observed in sample EO2, which used fennel essential oil, resulting in the inhibition zone diameter of 44±2 mm, and in sample EO7, which used caraway essential oil, with an inhibition zone of 45±1 mm. The highest antimicrobial activity was observed in sample EO9, with a mean inhibition zone diameter of 60.33±1.52 mm. This was achieved by cultivating the *Bacillus* isolate in CIW supplemented with oregano essential oil. A slightly lower antimicrobial activity was recorded for sample EO3, with a mean inhibition zone diameter of 60±2 mm, using basil essential oil, but the both values were at the same level of statistical significance. The inhibition zone diameters achieved using the 72-hour cultivation broth sample without essential oils addition were 52.66±1.15 mm. The antimicrobial activity of samples EO3 and EO9 over 96 hours, as well as the control sample without the essential oils, i.e. the complete cultivation course in terms of biocontrol activity, is presented in Figure 3 for the selected samples with the highest observed level of antifungal activity.
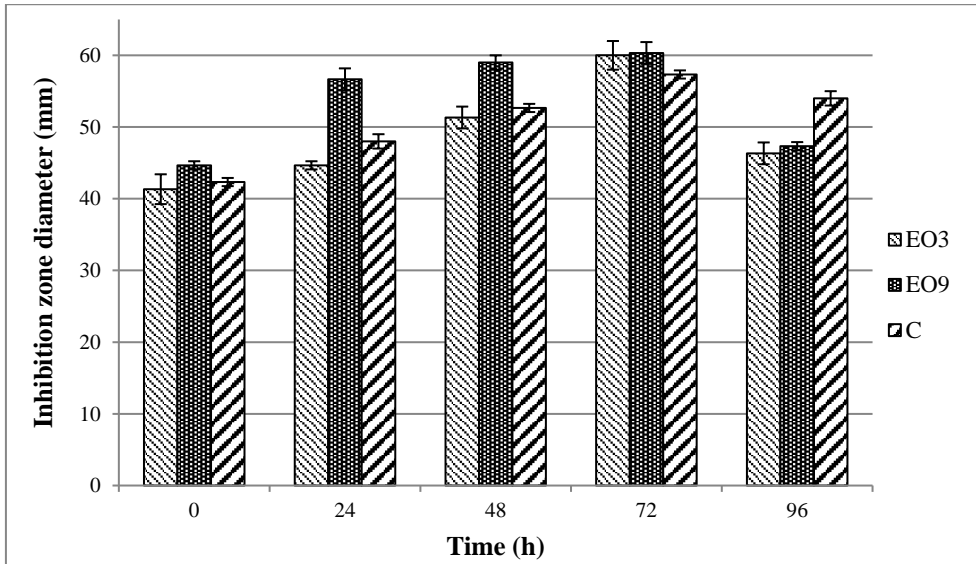
Figure 3. Antimicrobial activity of *Bacillus sp.* BioSol021-based biocontrol agents cultivated in confectionery industry wastewater with the addition of basil (EO3) and oregano (EO9) essential oils, as well as without essential oil (C), against *Aspergillus flavus* ATCC 22546.

The use of industrial waste streams as potential media for production of biocontrol agents has not been extensively explored in the literature. The production of biocontrol agents based on *Trichoderma viride* has been tested using various effluents, including soluble starch-based synthetic medium, dewatered municipal sludge, cheese industry wastewater sludge, pre-treated and untreated pulp and paper industry wastewater, and slaughterhouse wastewater, with the highest production observed using the soluble starch-based medium (21). Pajčin et al. demonstrated the successful use of whey and meat processing wastewater for the production of biocontrol agents based on *Bacillus velezensis,* with bacterial content increasing by almost 3 log units after 72 hours of cultivation (22). Whey and winery flotation wastewater have also been successfully used to produce biocontrol agents based on *Bacillus amyloliquefaciens* for controlling *Aspergillus* spp. In that study, the highest inhibition zone diameter was about 50 mm, which is 10 mm lower than in this study. This suggests that essential oils, in combination with the *Bacillus* sp. BioSol021 isolate, exhibit enhanced antimicrobial activity against *Aspergillus* spp. (6). Yezza et al. demonstrated that secondary sludges from three different wastewater treatment plants and starch industry wastewater are effective raw materials for the production of high-potency *Bacillus thuringiensis* biopesticides (23). Kumar et al. examined the techno-economic aspects of biopesticide production using starch industry wastewater and demonstrated that this process not only offers an alternative for disposal of industrial wastewater, but also effectively utilizes it as an inexpensive carbon source, significantly reducing raw material costs for fermentation process (24).

Plant extracts and essential oils exhibit a wide range of biological activities, including antifungal, antibacterial, antiviral, and antioxidant properties, making them valuable in the search for new antimicrobial compounds and alternatives for treating infectious diseases. These natural substances have been extensively studied for their potential as antiseptics and

disinfectants, showing significant effectiveness against bacteria, fungi, viruses, and parasites. Furthermore, their application in healthcare and food safety highlights their role as protective agents against pathogens, offering a promising strategy to combat bacterial resistance and improve food preservation (25). The antifungal activity of aromatic compounds in essential oils is influenced by their specific biochemical functions based on chemical structure variations. Phenols, such as eugenol, chavicol, and 4-allyl-2-6-dimethoxyphenol, show the highest antifungal activity, while cinnamic and hydrocinnamic acids also display significant fungistatic properties. Methoxy groups, however, do not substantially enhance the fungistatic effects of components like eugenol and 4-allyl-2-6-dimethoxyphenol. Based on their antifungal potential, these aromatic components can be ranked as follows: phenols > cinnamic aldehydes > alcohols > aldehydes ≥ ketones > ethers > hydrocarbons. This ranking is determined by the duration of fungal growth inhibition observed through macroscopic analysis (26). Plant-derived natural compounds and essential oils commonly investigated for their efficacy against *Aspergillus flavus* and aflatoxin contamination in food are those derived from food-flavoring plants, including clove (*Syzygium aromaticum*), cinnamon (*Cinnamomum zeylanicum*, *C. verum*), oregano (*Origanum vulgare*), and thyme (*Thymus vulgaris*). These plants and their essential oils or extracts have been used in food preparation for centuries and are classified as 'generally recognized as safe' (GRAS) by the U.S. FDA (United States Food and Drug Administration). Their beneficial effects on human health further support their potential as safe, natural antifungal and antiaflatoxigenic agents. Among the plant essential oils tested, thyme essential oil was one of the most effective antifungals, demonstrating significant activity against *Aspergillus flavus*, *Aspergillus parasiticus*, *Aspergillus ochraceus*, and *Fusarium moniliforme* (27, 28). However, in this study, the combination of thyme essential oil with the *Bacillus* sp. BioSol021 isolate exhibited only moderate activity, contrary to basil and oregano essential oils whose addition synergistically increased biocontrol action of the investigated microbial active component.

CONCLUSION

The biomass content of *Bacillus* sp. BioSol021 during 96 h of cultivation using the confectionery industry wastewater suggest the suitability of this food industry effluent for microbial growth of the selected microbial active component since no inhibition of microbial growth was observed. Microbial biomass content could be potentially further increased by adding the additional essential nutrients to the investigated waste-based medium basis, presenting a novel research path to be explored. The impact of adding essential oils to the wastewater was also examined, focusing on their effects on bacterial growth and the combined antifungal activity of the isolate and the essential oils. It was found that essential oils did not significantly inhibit bacterial growth; in fact, biomass content was higher in the presence of thyme and fennel oils compared to wastewater without the essential oils. As for antifungal activity against *Aspergillus flavus* ATCC 22546, the highest activity was observed with oregano oil, followed by basil oil, with maximum activity at 72 hours of cultivation correlating with the highest biomass content. This study supports circular economy principles by investigating the food industry waste potential for advancement of the secondary production technologies and promotes further investigation of biocontrol agents as viable alternatives to conventional chemical pesticides and fungicides. Future research should focus on further investigating wastewater characteristics and batch/seasonal variations, assessing its feasibility, optimizing bioprocess/cultivation parameters, and exploring

the specific mechanisms of action and interactions/synergism of both the *Bacillus* isolate and the essential oils.

REFERENCES

1. Lee, S. Y.; Stuckey, D. C. Separation and biosynthesis of value-added compounds from food-processing wastewater: Towards sustainable wastewater resource recovery. *J. Cleaner Prod.* **2022**, *357*, 131975.

2. Kora, E.; Antonopoulou, G.; Zhang, Y.; Yan, Q.; Lyberatos, G.; Ntaikou, I. Investigating the efficiency of a two-stage anaerobic-aerobic process for the treatment of confectionery industry wastewaters with simultaneous production of biohydrogen and polyhydroxyalkanoates. *Environ. Res.* **2024**, *248*, 118526.

3. Patsialou, S.; Politou, E.; Nousis, S.; Liakopoulou, P.; Vayenas, D. V.; Tekerlekopoulou, A. G. Hybrid treatment of confectionery wastewater using a biofilter and a cyanobacteria-based system with simultaneous valuable metabolic compounds production. *Algal Research.* **2024**, *79*, 103483.

4. Zajda, M.; Aleksander-Kwaterczak, U. Wastewater treatment methods for effluents from the confectionery industry–an overview. *J. Ecol. Eng.* **2019**, *20*(9), 293-304.

5. Bouchareb, R.; Derbal, K.; Yelfouf, A.; Diaf, D. B.; Mahfouf Bouchareb, E.; Dizge, N. Effective Treatment of Chocolate Industry Effluent Using Waste from Biocosmetic Industry. *CLEAN–Soil, Air, Water.* **2021**, *49*(12), 2100033.

6. Dmitrović, S.; Pajčin, I.; Vlajkov, V.; Grahovac, M.; Jokić, A.; Grahovac, J. Dairy and wine industry effluents as alternative media for the production of *Bacillus*-based biocontrol agents. *Bioengineering.* **2022**, *9*(11), 663

7. Lahlali, R.; Ezrari, S.; Radouane, N.; Kenfaoui, J.; Esmaeel, Q.; El Hamss, H.; Belabess, Z.; Barka, E.A. Biological Control of Plant Pathogens: A Global Perspective. *Microorganisms.* **2022***, 10*(3), 596*.

8. Anckaert, A.; Arias, A.A.; Hoff, G. The use of *Bacillus* spp. as bacterial biocontrol agents to control plant diseases. In *Microbial Bioprotectants for Plant Disease Management*; Köhl, J., Ravensberg, W., Eds.; Burleigh Dodds Science Publishing: Cambridge, UK, **2022**; pp. 1–54.

9. Villarreal-Delgado, M. F.; Villa-Rodríguez, E. D.; Cira-Chávez, L. A.; Estrada-Alvarado, M. I.; Parra-Cota, F. I.; Santos-Villalobos, S. D. L. The genus *Bacillus* as a biological control agent and its implications in the agricultural biosecurity. *Mex. J. Phytopathol.* **2018**, *36*(1), 95-130.

10. Sil, A.; Pramanik, K.; Samantaray, P.; Firoz, M.; Yadav, V. Essential oils: A boon towards eco-friendly management of phytopathogenic fungi. *J. Entomol. Zool. Stud.* **2020**, *8*(4), 1884-1891.

11. Vlajkov, V.; Pajčin, I.; Loc, M.; Budakov, D.; Dodić, J.; Grahovac, M.; Grahovac, J. The Effect of Cultivation Conditions on Antifungal and Maize Seed Germination Activity of *Bacillus*-Based Biocontrol Agent. *Bioengineering.* **2022**, *9*(12), 797.

12. Khan, R.; Ghazali, F. M.; Mahyudin, N. A.; Samsudin, N. I. P. Biocontrol of aflatoxins using non-aflatoxigenic *Aspergillus flavus*: A literature review. *J. Fungi.* **2021**, *7*(5), 381.

13. Masiello, M.; Somma, S.; Ghionna, V.; Logrieco, A. F.; Moretti, A. *In vitro* and in field response of different fungicides against *Aspergillus flavus* and *Fusarium* species causing ear rot disease of maize. *Toxins.* **2019**, *11*(1), 11.

14. Moyne, A. L.; Shelby, R.; Cleveland, T. E.; Tuzun, S. A. D. I. K. Bacillomycin D: an iturin with antifungal activity against *Aspergillus flavus*. *J. Appl. Microbiol.* **2001**, *90*(4), 622-629.

15. Farzaneh, M.; Shi, Z. Q.; Ahmadzadeh, M.; Hu, L. B.; Ghassempour, A. Inhibition of the *Aspergillus flavus* growth and aflatoxin B1 contamination on pistachio nut by fengycin and surfactin-producing *Bacillus subtilis* UTBSP1. *Plant Pathol. J.* **2016**, *32*(3), 209.

16. Tian, F.; Woo, S. Y.; Lee, S. Y.; Park, S. B.; Zheng, Y.; Chun, H. S. Antifungal activity of essential oil and plant-derived natural compounds against *Aspergillus flavus*. *Antibiotics*. **2022**, *11*(12), 1727.

17. da Silva Bomfim, N.; Kohiyama, C.Y.; Nakasugi, L.P.; Nerilo, S.B.; Mossini, S.A.; Romoli, J.C.; Graton Mikcha, J.M.; Abreu Filho, B.A.; Machinski, M. Antifungal and antiaflatoxigenic activity of rosemary essential oil (*Rosmarinus officinalis L.*) against *Aspergillus flavus*. *Food Addit. Contam.: Part A*. **2019**, *37*(1), 153 - 161.

18. Dmitrović, S.; Pajčin, I.; Lukić, N.; Vlajkov, V.; Grahovac, M.; Grahovac, J.; Jokić, A. Taguchi grey relational analysis for multi-response optimization of *Bacillus* bacteria flocculation recovery from fermented broth by chitosan to enhance biocontrol efficiency. *Polymers*. **2022**, *14*(16), 3282.

19. Valero, M.; Salmeron, M. C. Antibacterial activity of 11 essential oils against *Bacillus* cereus in tyndallized carrot broth. *Int. J. Food Microbiol.* **2003**, *85*(1-2), 73-81.

20. Valero, M.: Giner, M. J. Effects of antimicrobial components of essential oils on growth of *Bacillus cereus* INRA L2104 in and the sensory qualities of carrot broth. *Int. J. Food Microbiol.* **2006**, *106*(1), 90-94.

21. Verma, M.; Brar, S. K.; Tyagi, R. D.; Surampalli, R. Y.; Valero, J. R. Industrial wastewaters and dewatered sludge: rich nutrient source for production and formulation of biocontrol agent, *Trichoderma viride*. *World J. Microbiol. Biotechnol.* **2007**, *23*, 1695-1703.

22. Pajčin, I. S.; Vlajkov, V.; Dujković, T.; Grahovac, J. Effluents from industrial processing of the food of animal origin as media for biocontrol agents production. *J. Process. Energy Agric.* **2023**, *27*(1). 16-21.

23. Yezza, A.; Tyagi, R. D.; Valero, J. R.; Surampalli, R. Y. Bioconversion of industrial wastewater and wastewater sludge into *Bacillus thuringiensis* based biopesticides in pilot fermentor. *Bioresour. Technol.* **2006**, *97*(15), 1850-1857.

24. Kumar, L. R.; Ndao, A.; Valéro, J.; Tyagi, R. D. Production of *Bacillus thuringiensis* based biopesticide formulation using starch industry wastewater (SIW) as substrate: a techno-economic evaluation. *Bioresour. Technol.* **2019**, *294*, 122144.

25. Chouhan, S.; Sharma, K.; Guleria, S. Antimicrobial activity of some essential oils - present status and future perspectives. *Medicines*. **2017**, *4*(3), 58.

26. Saad, N. Y.; Muller, C. D.; Lobstein, A. Major bioactivities and mechanism of action of essential oils and their components. *Flavour Fragrance J.* **2013**, *28*(5), 269-279.

27. Sakkas, H.; Papadopoulou, C. Antimicrobial activity of basil, oregano, and thyme essential oils. *J. Microbiol. Biotechnol.* **2017**, *27*(3), 429-438.

28. Pinto, E.; Gonçalves, M.J.; Hrimpeng, K.; Pinto, J.; Vaz, S.N.; Vale-Silva, L.A.; Cavaleiro, C.; Salgueiro, L. Antifungal activity of the essential oil of *Thymus villosus* subsp. *lusitanicus* against *Candida*, *Cryptococcus*, *Aspergillus* and dermatophyte species. *Ind. Crops Prod.* **2013**, *51*, 93-99.

INSTRUCTION FOR MANUSCRIPT PREPARATION

Acta Periodica Technologica publishes reviews and scientific papers covering all branches of food, chemical, biochemical, and pharmaceutical technologies, as well as process engineering and related scientific fields.

Acta Periodica Technologica is published in English. The journal may include supplements from congresses, meetings or symposiums.

SUBMISSION OF PAPERS

The manuscript submission deadline is the July 31ˢᵗ of the current year. This deadline can be shortened depending on the number of manuscripts received.

All correspondence, including submission of the manuscript, notification of the Editor's decision and requests for revision, takes place by e-mail apteff@tf.uns.ac.rs or apteff.tf.uns@gmail.com.

Authors are expected to propose the category of manuscript (review or original scientific paper) and three potential reviewers. Reviewers should be experts in the field of the paper, and not associated with the institution with which the authors are affiliated. The final choice of referees will remain entirely with the Editor. Also, optionally, the authors should state any person that is not desired as a reviewer.

Submission of paper implies that:
- it is prepared according to this Instructions,
- it has not been published previously (except in the form of an abstract or as a whole in the proceedings of papers of a scientific meeting, or as part of a published lecture or academic thesis),
- it is not under consideration for publication elsewhere, and
- it will not be published elsewhere in the same form, in English or any other language, without the written consent of the publisher.

PREPARATION OF MANUSCRIPT

Language: Manuscript should be written in English.

Typing: Manuscript must be written in Word with a font size 10 pt., 1.5 lines spaced, with 2.5 cm margins, on A4 pages (maximum 15 pages for scientific papers and 25 pages for review papers). All lines of the manuscript should be numbered restarting on each page. Also, all pages must be numbered. Tables, figures and schemes must be imported into the text. Abbreviations and symbols-notation should be explained at first appearing, or on a separate list at the end of the manuscript.

General format. The manuscript should contain the following in this order: PAPER TITLE, Author(s) full name(s), Affiliation, ABSTRACT, KEYWORDS, INTRODUCTION, EXPERIMEN-TAL, RESULTS and DISCUSSION, CONCLUSIONS, ACKNOWLEDGEMENTS and REFE-RENCES.

The paper title should be written in capital bold characters on the first page, without any symbols, formulas, or abbreviations. The title should be concise and explanatory of the content of the paper. The authors' full names (name, middle name, and surname) and Orcid ID in round brackets should appear italicized under the title. Also, indicate with an asterisk who is in charge of correspondence throughout the refereeing and publication process. Ensure that an e-mail address and a complete postal address are provided. The author's affiliation should be stated after their name. Indicate all associations with a superscript number directly after the author's name and in front of the relevant address. If the paper was given, wholly or in part, at a scientific meeting, this should be stated in a footnote on the title page.

Abstract (100 - 300 words, italicized) should to be placed below the paper title, author's name, and affiliations. Abstract should contain the aim of the research, the methodology, the findings, and the conclusion.

Keywords (normal letters, max. 5 keywords) should be listed afterward.

Introduction should state previous relevant work with appropriate references, the problem investigated and the aim of work.

Experimental. The materials and procedures used should be explained clearly and in sufficient detail so that others can replicate the work. Only novel techniques should be presented in full. Existing methods must include relevant references.

Results and Discussion. Results should be presented concisely, with tables or illustrations for clarity. The significance of the findings should be discussed without repetition of the material in the Introduction. The adequate number of illustrations, graphs and chemical formulae used must be kept on a minimum.

Conclusions. This section should present the main conclusions of the study. Also, conclusions should indicate the significance of contribution and application possibilities of the obtained results.

Acknowledgements: These should be kept to a minimum.

References should be indicated in the text with Arabic numerals in round brackets ( ), in the order they appear. All publications cited in the text should be presented in a list of references given on a separate page. Abbreviations of journal titles should be given according to the Chemical Abstracts Service (CASSI Search Tool; http://cassi.cas.org). The list of references should be prepared in accordance with the ACS citation style and their appearance in the text. Give names of all authors (do not use „et al.“), with their initials after respective surnames. Include the paper title, the abbreviated or full journal name, **the year** (in bold), *volume* (italicized), number (in round brackets if available), the first and last page numbers, and the DOI number.

Examples:

Journals: Pascual, E.C.; Goodman, B.A; Yeretzian, C. Characterisation of Free Radicals in Soluble Coffee by Electron Paramagnetic Resonance Spectroscopy. *J. Agric. Food Chem.* **2002**, *50* (21), 6114-6122. https://doi.org/10.1021/jf020352k

Books: Morris, R. *The Last Sorcerers: The Path from Alchemy to the Periodic Table*; Joseph Henry Press: Washington, DC, 2003; pp 145-158.

Book with more chapters: Puls, J.; Saake, B. Industrially Isolated Hemicelluloses. In *Hemicelluloses: Science and Technology*; Gatenholm, P., Tenkanen, M., Eds.; ACS Symposium Series 864; American Chemical Society: Washington, DC, 2004; pp 24-37.

Book of Abstracts: Noe, W.; Howaldt, M.; Ulber, R.; Scheper, T. Immunobase elution assay for process control, 8th European Congress on Biotechnology, Budapest, 17-21 August 1997, Book of Abstracts WE 163, p. 246.

Thesis: Linstead, J.B. Effects of adding natural antioxidants on colour stability of paprika. Ph.D. (or M.S.) Thesis, University of Glasgow, November 2006.

Patent: Lenssen, K. C.; Jantscheff, P.; Kiedrowski, G.; Massing, U. Cationic Lipids with Serine Backbone for Transfecting Biological Molecules. Eur. Pat. Appl. 1457483, 2004.

Unpublished data: Should be cited with one of the following comments: in press, unpublished work or personal communication.

Online citations: Should include the author, title, website and date of access.
   Example: Wright, N.A. The Standing of UK Histopathology Research 1997-2002.
   http://pathsoc.org.uk (accessed 7 October 2004).

Chemical nomenclature and units. Authors are requested to use SI units and chemical nomenclature following the rules of Chemical Abstracts whenever possible.

Tables. Each Table is numbered with an Arabic numeral, followed by the title (**Table 1.** The result...). The table width must be 13 cm max.

Figures. Each drawing or figure should also be numbered with Arabic numerals followed by the title (**Figure 1.** Chromatogram of...).

Schemes and figures must be submitted as separate files in their original extension (xls, xlsx, tiff, bmp, jpg…).

Formulae and Equations. Type formulas and mathematical equations clearly, accurately placing superscripts and subscripts. Equations should be indicated in the text using Arabic numbers in square brackets [ ].

Review process. All papers submitted to the journal will be reviewed by at least two independent referees who will be asked to complete the refereeing job within 4-6 weeks. The final decision on publication will be made by the Editorial Board. Manuscripts may be sent back to authors for revision if necessary. Revised manuscript submissions should be made as soon as possible (within 2 weeks) after the receipt of the referees' comments.

Proofs. The corresponding author will receive via email an uncorrected proof of the manuscript. This proof should only be used to check for spelling errors in the manuscript. After receiving the email with uncorrected proof, authors have 48 hours to submit a list of corrections. Another alternative is to mark changes to the pdf file with sticky note option and return it to the Editor's office.

Author service. For inquiries relating to the submission of the manuscript, please send an email to the Editor's office at one of the addresses listed: apteff@tf.uns.ac.rs or apteff.tf.uns@gmail.com.

Editorial board postal address:

University of Novi Sad

Faculty of Technology Novi Sad
Journal *Acta Periodica Technologica*

PO Box 6, 21125 Novi Sad, Serbia.